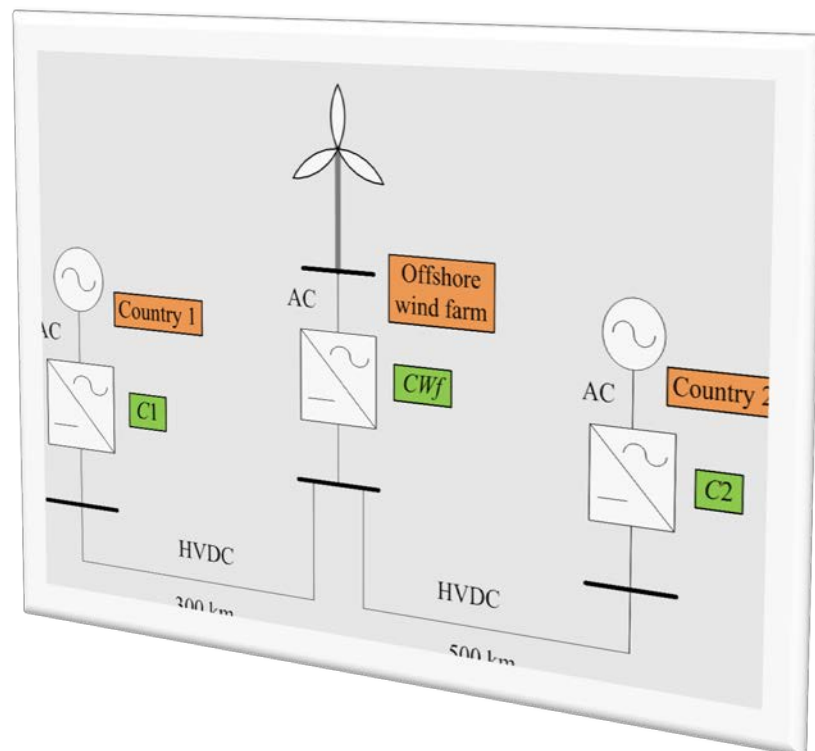# Report

Report on deep offshore wind farm grid integration aspects including a case study

HiPRwind WP5 – deliverable D5.2

Author(s)
Harald G. Svendsen, Jorun I. Marvik – SINTEF Energy Research, Norway
Salvador Ceballos Recio – Tecnalia, Spain

This report constitutes deliverable D5.2 of the HiPRwind project funded by the European Union's 7th Framework Programme under Grant Agreement no. 256812.

The report is written by authors affiliated to SINTEF Energy Research (Norway) and Tecnalia (Spain)

SINTEF

tecnalia Inspiring Business

KEYWORDS:
Offshore wind, grid integration, HVDC, PSCAD, square wave rectifier, power electronics

Report

Report on deep offshore wind farm grid integration aspects including a case study

HiPRwind WP5 – deliverable D5.2

VERSION	DATE
1.0	2015-05-29

AUTHOR(S)
Harald G. Svendsen, Jorun I. Marvik – SINTEF Energy Research, Norway
Salvador Ceballos Recio – Tecnalia, Spain

CLIENT(S)	CLIENT'S REF.
HiPRwind consortium	D5.2

PROJECT NO.	NUMBER OF PAGES/APPENDICES:
502000064	133

ABSTRACT

This document present results from the European collaboration project *HiPRwind* related to Task 5.2 *Power transmission system and grid connection control*. This task has addressed technical solutions for grid connection of large and far offshore wind farms, with emphasis on design of the electrical power transmission system and control of power electronic components.

It gives an overview of current status regarding grid connection of offshore wind farms, and presents detailed analyses of case studies related to 1) Square Wave High Frequency converter technology for a novel DC transmission architecture where each wind turbine is directly connected to a DC grid, and 2) high voltage transmission system of a 1 GW wind farm connected to two separate onshore grid points via a 3-terminal HVDC grid.

The report describes modelling approaches, results from numerical simulations and experimental tests in laboratory environments.

PREPARED BY	SIGNATURE
Harald G Svendsen	

CHECKED BY	SIGNATURE
Iver Bakken Sperstad	

APPROVED BY	SIGNATURE
John O Tande	

REPORT NO.	ISBN	CLASSIFICATION	CLASSIFICATION THIS PAGE
TR A7482	978-82-594-3622-1	Unrestricted	Unrestricted

Document history

VERSION	DATE	VERSION DESCRIPTION
1.0	2015-05-29	Final version

Summary

This report provides an overview of grid connection options for large offshore wind farms, and presents detailed investigations of case studies addressing novel solutions for wind turbine converter systems and HVDC transmission systems.

Regarding wind turbine and collection grids, Square Wave High Frequency converters have been analysed as a promising alternative to get medium voltage DC power output from wind turbines. The main benefit of such solutions is the potential cost saving promoted by the use of simpler and cheaper DC cables in the collector system, smaller and lighter high frequency transformers and the possibility of removing the offshore substation in those wind farms where this is feasible.

The behaviour of such converters has been analysed. The voltage and current waveforms were described in detail, and the relation between input and output voltage dependency on converter parameters was studied. Four converter prototypes have been implemented and different configurations have been tested in a laboratory setup to validate the concept. The use of the leakage inductance of the transformer as an inherent element of the converter to shape the current waveforms was discussed. The analytical expression of the relation between the converter input voltage and the output current was developed, as a function of the main converter parameters. The converter has no control parameters and the input converter DC bus voltage varies with the HVDC line voltage and the output current. With conveniently chosen parameters the converter can operate in open loop.

The power losses of the proposed Square Wave High Frequency architectures were also analysed, finding reduction in power losses of direct connection of wind turbines to DC transmission lines, or by using an intermediate wind farm DC grid.

Regarding high voltage transmission to shore, HVDC systems have been analysed, in particular a case study of a 1 GW wind farm connected to onshore connection points in two different countries via a multi-terminal HVDC grid. Emphasis was on modelling and analysis of fault detection and fault-ride-through capability for short circuit and ground faults in the wind farm collection grid, in the DC transmission grid and on AC-sides of the two onshore HVDC terminals.

For faults in the onshore AC grids, simulations showed that the HVDC-transmission system can operate through such faults if the HVDC terminals have either DC-voltage control or active power control with DC-voltage droop. The short circuits caused very small disturbances in the wind farm voltage, and are therefore assumed to also have negligible impact on operation of the wind turbines.

For faults in the HVDC grid, small required clearing times may be a critical issue for fault ride-through of the healthy part of the system. In order to assure fault ride-through of the un-faulted parts of the system, DC-breakers are required. For faults located on the branch between the wind farm HVDC-terminal and the terminal with constant DC-voltage control, the required disconnection time was found to be very short and critical for DC breaker choice. Another issue is that faults close to the converter stations were seen to cause very large currents in the anti-parallel diodes of the semiconductor switches. To prevent damage, the required disconnection times for phase-to-phase faults were found to be less than 1 ms. for the worst cases, and a few milliseconds for phase-to-ground faults. This appears very difficult to achieve in practice. However, with other topologies, especially the modular multilevel converter, the large current due to discharge of the capacitor in the phase-to-phase fault cases could probably be avoided.

Distance protection appears suited for use in the wind farm collection grid, despite the low short-circuit levels of the converter interfaced generators. However, there could potentially be problems with this type of protection in smaller wind farms with converter interfaced turbines. The solution would then be to use differential protection.

Table of contents

APPENDICES

PROJECT NO.
502000064

REPORT NO.
TR A7482

VERSION
1.0

6 of 133

1 Introduction

This document present results from the European collaboration project *HiPRwind* related to Task 5.2 Power *transmission system and grid connection control*. This task has addressed technical solutions for grid connection of large and far offshore wind farms, with emphasis is on design of the electrical power transmission system and control of power electronic components.

Larger and larger offshore wind farms are currently being built and the 1 GW capacity milestone is likely to be reached within a few years. At the same time, distances from onshore connection points are being stretched, making standard high voltage AC (HVAC) transmission by subsea cables infeasible. These two factors, i.e. higher power and longer distances, are therefore pushing the development of new and robust solutions, such as high voltage DC (HVDC) transmission.

Currently, the onshore wind power industry is a much bigger business than the offshore wind industry. Special designs for offshore applications are therefore avoided, and 50 Hz collection grids are preferred. With a bigger offshore wind industry in the future, standard dedicated offshore solutions are likely to emerge.

To set the scene, a general layout which is expected to become a standard grid connection solution for a large and far offshore wind farm is shown in Figure 1.1. The wind turbine consists of a mechanical drive-train connecting the rotating blades via a gearbox to a generator. Power output from the generator is then converted to 50 (or 60) Hz frequency and transformed up to about 30 kV, which is the voltage level of the collection grid. All the wind turbines are connected at an offshore transformer station, which increases the voltage to transmission level, typically about 130 kV. A converter station contains the HVDC converter system for the HVDC transmission grid to shore. On the other end of the transmission cable(s) is the onshore substation, where power is again converted to 50 Hz AC, and transformed to the voltage level of the mainland transmission grid.
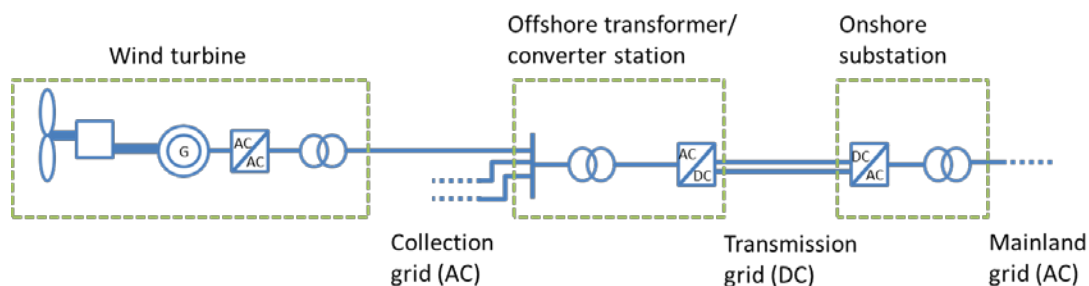
Figure 1.1: Schematic overview of offshore wind farm grid connection

The focus of his report is the medium voltage collection grid and the high voltage transmission system. This is addressed through case studies. The report has three main parts.

The first part (Chapter 2) of the report gives an overview of current status regarding grid connection of offshore wind farms, including high voltage AC (HVAC) and DC (HVDC) transmission options, power electronics, wind turbine technologies, controls, and some comments on emerging technologies with high cost saving potential.

The second part (Chapter 3) considers a novel DC transmission architecture where each wind turbine is directly connected to a DC grid. The report describes and analyses in detail square wave high frequency DC/DC converter technology for application in a wind turbine. The design is tested in numerical simulations and in laboratory experiments.

The third part considers the HVDC transmission systems, with emphasis on controls and fault handling. This part is split in three chapters. Chapter 4 describes the modelling of a case study consisting of a 1 GW wind farm connected to two separate onshore grid points via a 3-terminal HVDC

grid. Chapter 5 describes the HVDC converter modelling and parameter tuning in detail. Chapter 6 then follows this up with results from numerical simulations.

1.1 Context

The main aim of the HiPRwind project has been to develop and demonstrate technology for floating wind turbines. At present a small number of pilot projects for floating wind turbines exist, but the technology is not yet mature. However, the potential is very large. Many areas for wind power harnessing can be exploited if floating wind turbines become commercially viable. From the electrical point of view, the question whether the turbines are floating or bottom-fixed is not the most essential. As noted above, transmission distances and high power rating are the main technical challenges. And of course the challenge of bringing down the costs, investment costs and lost income due to power losses and equipment failures.

From the technical point of view, it is necessary for wind farms to obey stringent grid connection requirements, specified by transmission system operators to ensure efficient, safe and economic operation of the power system. These grid codes define requirements for generators regarding e.g. fault ride-through capability, frequency and voltage control, and power quality [1.1], [1.2]. For the design of the electrical connection for wind farms it is important to ensure that these requirements are guaranteed. The application of power electronic converters with their high degree of controllability makes this possible. In fact, the control capabilities of modern wind farms are not fully exploited as typically operated and integrated into the power systems today. It should also be emphasised that a large wind farm is essentially a power plant where the grid code applies at a single or multiple connection points where it interfaces with the rest of the grid. In other words, the issue of grid code compliance is not fundamentally a wind turbine concern, but a wind farm concern.

It is expected that many future offshore wind farms will be in relatively near proximity to each other compared to the distance to shore. In such situations it is likely to be beneficial to have a common grid connection for the wind farms. Combined solutions involving offshore wind farms and HVDC interconnectors should also be considered [1.3]. Clustering of offshore wind farms has already been decided in Germany, and offshore HVDC platforms with transmission cables to land are already built. In the German model, these are owned and operated by the Transmission System Operator (TSO), so the wind farm grid connection point is in fact the offshore converter station. Finding the optimal grid layout and control scheme for a wind cluster grid and transmission system is not easy, as wind farms are likely to be developed step-wise and have different owners. For example, the economic considerations should take into account the risk that a planned wind farm may be delayed or not built at all.

Wind energy is a variable source of power and large wind farms and clusters have a significant impact on power prices and power flow in the grid. For this reason they affect the power exchange (both trading and balancing) between different price areas and countries. In areas where offshore wind farms and offshore interconnectors are planned in the proximity of each other, it is therefore highly relevant to consider combined grid solutions [1.3][1.4]. So far, grid connection of offshore wind farms has been achieved by dedicated cables, bringing the power directly to shore before transporting it to where the demand is. The cost-reducing alternatives mentioned above include some level of multi-terminal or meshed grid, where power from wind farms is allowed to flow in more than one direction. An example where such connection options have already been considered is the planned *Kriegers Flak* wind farms in the Baltic Sea.

1.2 Bibliography

[1.1]   National Grid, GB Grid code - Connection Conditions. Issue 4, Revision 6. 2011. http://www2.nationalgrid.com/UK/Industry-information/Electricity-codes/Grid-code/The-Grid-code/ (accessed Apr 2015).

[1.2]   ENTSO-E, Network Code on Requirements for Grid Connection Applicable to all Generators, https://www.entsoe.eu/major-projects/network-code-development/requirements-for-generators/Pages/default.aspx (accessed Apr 2015).

[1.3]   De-Decker, J., et al., OffshoreGrid - Final Report: Offshore Electricity Grid Infrastructure in Europe. 2011. http://www.offshoregrid.eu/ .

[1.4]   Hueartas Hernando, D., M. Korpås, and S. van Dyken, Windspeed D6.3 - Grid Implications: Optimal design of a subsea power grid in the North Sea. 2011, SINTEF Energy Research / Windspeed project. http://www.windspeed.eu .

2 Grid connection of offshore wind

This chapter gives an outline of the current status and trends of concepts and technologies relevant for the grid connection of offshore wind farms.

2.1 Overview of grid connection solutions

This section gives a high-level overview of grid connection design that may be suitable for future large offshore wind farms. The aim is to give a brief overview from existing literature, and no further assessment of the different options is given here.

The typical grid connection solution for offshore wind farms today consists of a synchronous AC grid all the way from the wind turbine to mainland AC grid connection point. Of the three examples in Section 2.1.2, both Horns Rev and Thanet have pure AC collection and transmission grids. In the usual setup, wind turbines are installed along feeders connected to a collection point at an offshore substation platform, which contains the step-up transformer that increases the voltage to transmission level. In addition to the transformer(s), the offshore platform also includes necessary protection (switchgear). From the transformer station, high voltage AC (HVAC) transmission cables transport the power to the mainland AC grid. A typical grid layout is illustrated in Figure 2.1a.

For long transmission distances, the HVAC option is not feasible and high voltage DC transmission is used instead. At present (2015), there are a few German wind farms with HVDC transmission to shore. One example is the Bard Offshore 1, as described in Section 2.1.2.3. Regarding the collection grid, this solution is identical to the pure AC solution. A typical grid layout is illustrated in Figure 2.1b. With future wind farms being installed farther and farther away from shore, it is expected that this solution will become increasingly common. With DC transmission, the collection grid frequency is decoupled from the mainland AC frequency, meaning that both voltage and frequency can be fully controlled with the offshore converter station. There are two main technologies for high voltage DC (HVDC) transmission, depending on the conversion technologies applied. One is based on line-commutated converter (LCC) technology, and the other is based on voltage-sourced converter (VSC) technology. These are described in more detail in Section 2.2.

a) AC wind farm with HVAC transmission to shore

b) AC wind farm with HVDC transmission to shore
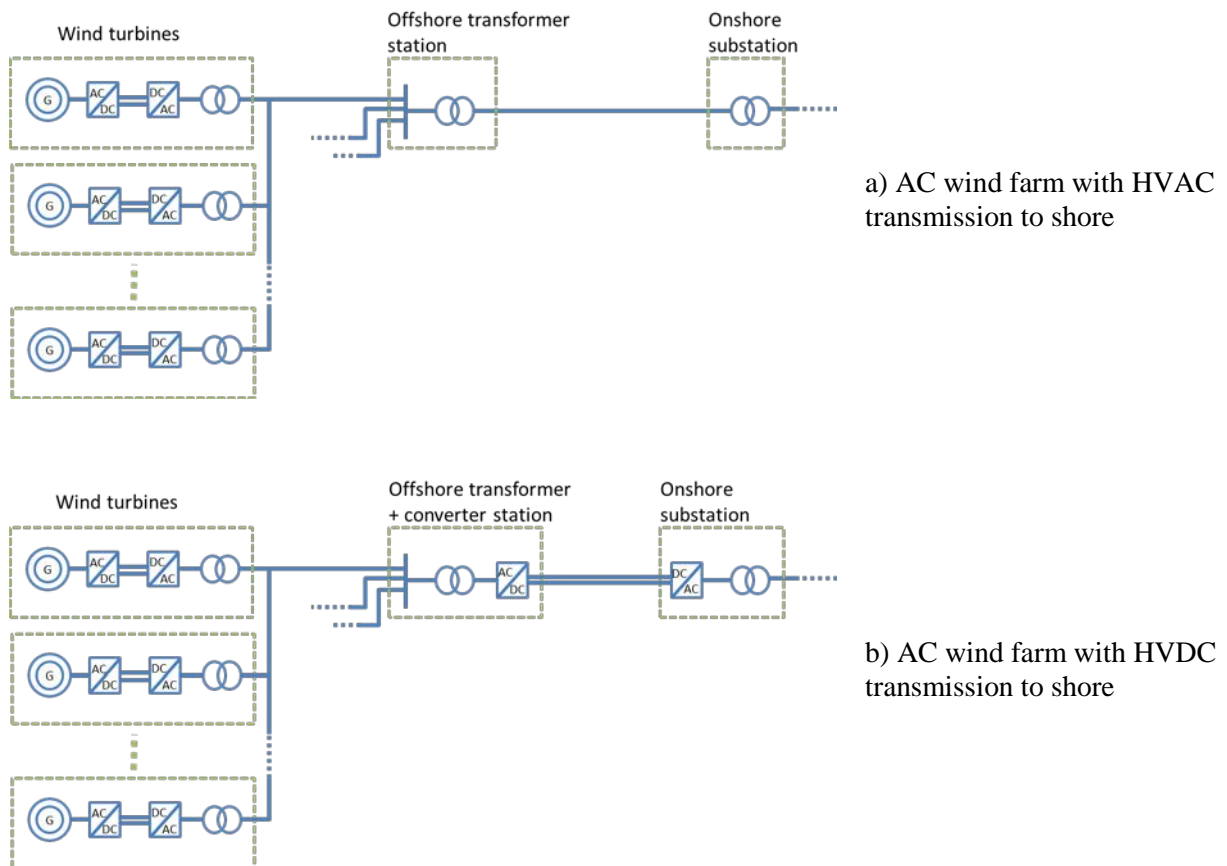
Figure 2.1: Present day wind farm connection alternatives

Table 2.1 summarises the possible combinations of AC and DC grid connection of wind farms, with an indication of which combinations are existing solutions or future solutions. Another overview of alternative technologies for grid connection technology for future offshore wind farms is found e.g. in ref. [2.1], and different wind farm layouts are discussed e.g. in ref. [2.2]. A 2020 scenario for German grid connection of offshore wind is discussed in ref. [2.3].

Table 2.1: Grid connection – AC/DC options

		Collection	
		AC	**DC**
Transmission	**AC**	Common today	Unlikely option
	DC	One exists, likely to become common	Possible future option

Offshore wind power farms in operation today are located close to shore, and rely on AC-transmission through subsea cables. AC transmission is and will remain the preferred choice, but limitations makes it infeasible for large and far offshore wind farms, as discussed below.

PROJECT NO.
502000064

REPORT NO.
TR A7482

VERSION
1.0

11 of 133

Power converters play an important role for most modern wind turbines, and for HVDC transmission systems that are likely to be applied for the grid connection of future large offshore wind farms. These two applications are quite different:

Wind turbine converters
- Low voltage (typically 0.69 kV)
- Modest power (6 MW for state-of-the art offshore turbine)

HVDC transmission system converters
- High voltage (150 kV+)
- High power (hundreds of MW)

2.1.1 AC vs. DC

Power transmission for offshore wind farms rely on subsea cables. Due to shorter distance between conductor and ground, cables have higher capacitance than overhead lines. This capacitance cannot be reduced significantly by changing dimensions. Because of this high capacitance, AC cables have charging currents which are proportional to the cable length. At 50–150 km, the charging current approaches the cable's rated current, which means that the transfer capacity will be limited by the cable's thermal limit. Reactive compensation units can be installed to mitigate the problem to some extent. At one point however, the active power transmission capacity will be limited by voltage stability rather than thermal limit, which means that AC transmission is no longer feasible. Gas Insulated Line (GIL) has been proposed to extend the possible length of submarine AC transmission.

Cables for DC transmission have no capacitive charging current, thus there is no flow of reactive current in the cable. However, due to switching losses in the power electronics converters, the total losses are larger than for HVAC. So far market demand has motivated development of cables up to ±320 kV. Qualifying a cable for a new, higher voltage level is costly. Higher levels are possible, but will not be developed before there is a project that requires higher transfer and voltage levels. Ref. [2.4] gives an overview of wind farm grid connection with emphasis on VSC-HVDC.

A comparison of suitability of high voltage AC (HVAC) versus high voltage DC (HVDC) is shown in Figure 2.2. It indicates that AC transmission is not possible over longer distances (AC favourable for distances less than 120 km for power levels below 200 MW, for higher power levels the possible distance is decreased). In short, the AC vs. DC transmission status is:

- AC: suitable for low power or high power at short distances
- DC: suitable for high power at long distances

Existing HVDC connections are connected to AC grid via converters at both ends and protection on the AC side of the converters. This is partly due to the unavailability of DC protection equipment. Ref. [2.5] evaluates the benefits and drawbacks of DC transmission for offshore wind farms. Ref. [2.6] describes HVDC systems for wind farms consisting of doubly fed induction generators.

PROJECT NO.
502000064

REPORT NO.
TR A7482

VERSION
1.0

12 of 133
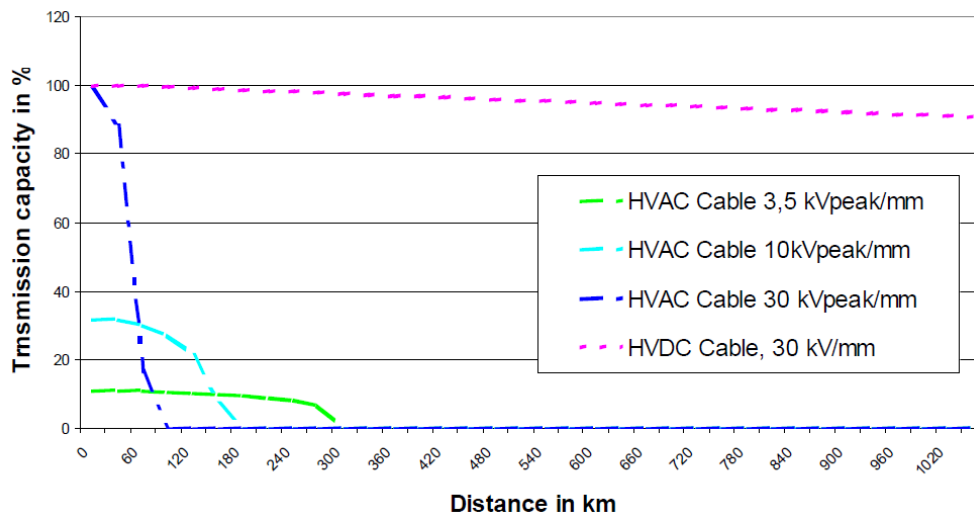
Figure 2.2: Power transmission for AC and DC cables. Source: [2.7]

2.1.2 Examples of existing grid connection solutions for offshore wind farms

Here, three examples of recently developed offshore wind farms are presented, illustrating the state-of-the-art for the offshore wind power industry. Commercial actors, of course, tend to favour trusted and well proven technology. Due to the time it takes from decision making to commissioning of a large wind farm, this naturally means that there is a gap of several years between what is at the forefront technologically versus commercially.

2.1.2.1 Horns Rev 2

Horns Rev 2 is a 209 MW offshore wind farm on the western coast of Denmark, consisting of 91 Siemens SWP 2.3 MW turbines. The wind turbine power conversion topology is a squirrel cage induction generator plus full scale converter, as described in Section 2.3. The distance to shore is 27–41 km, and water depth is 9–17 m. The wind farm grid consists of 13 feeders connected to an offshore transformer station, where the voltage is increased from 33 kV to 150 kV. The onshore connection point is to the 400 kV mainland transmission grid, via another step-up transformer. An overview of the grid connection is shown in Figure 2.3, and the collection grid is shown in Figure 2.4. Further information about the wind farm can be found in ref. [2.8].
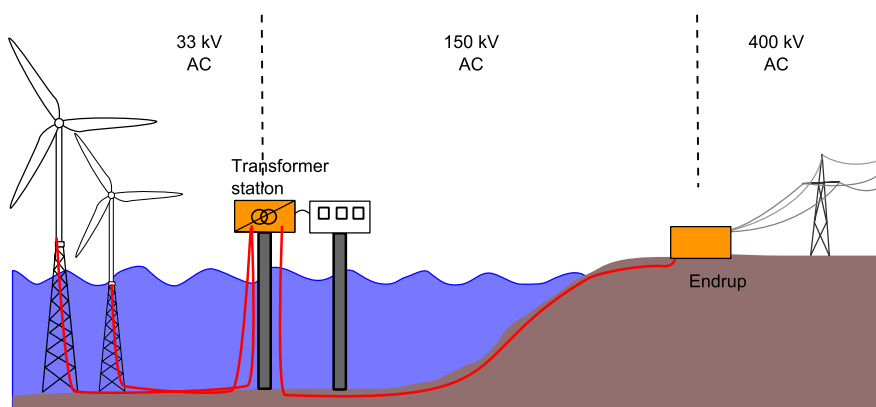
Figure 2.3: Horns Rev 2 grid connection

PROJECT NO.
502000064

REPORT NO.
TR A7482

VERSION
1.0

13 of 133
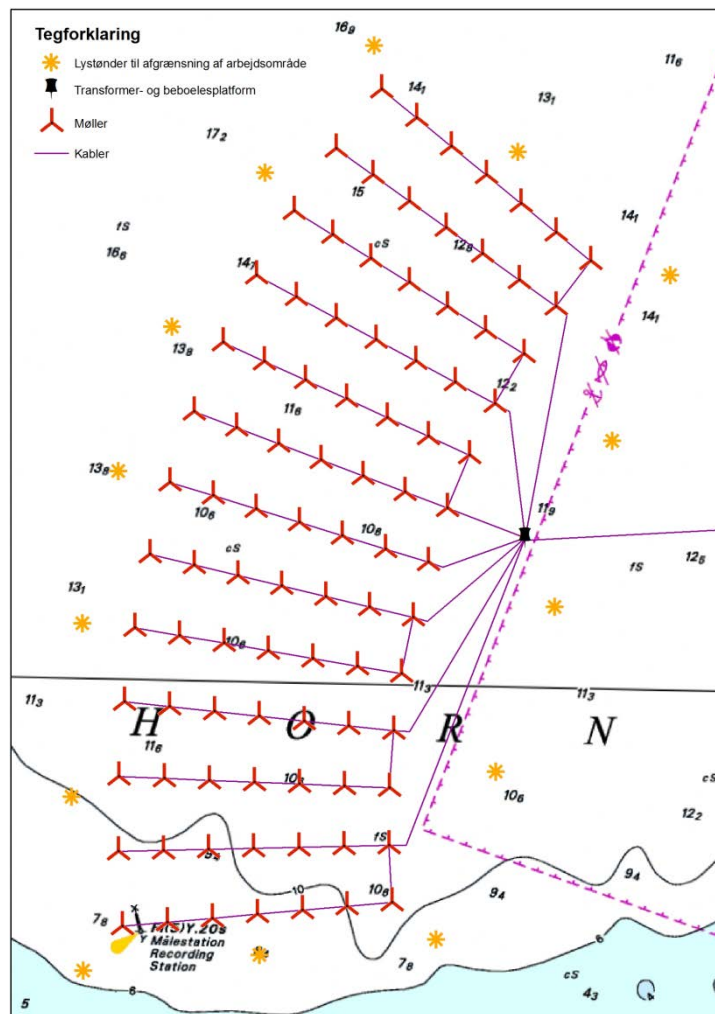
Figure 2.4: Horns Rev 2 collection grid

The transmission system consists of a 42 km long submarine cable (170 kV XLPE 3-core power cable including a fibre-optic element), a cable substation connecting submarine and land cables, and a 56 km long land cable (150 kV).

2.1.2.2 Thanet

Thanet [2.9] is a 300 MW offshore wind farm outside the south-east coast of Great Britain. When it was built in 2010, it was the world's largest offshore wind farm. The overall grid connection concept is similar to the Horns Rev 2 case, except that voltage levels are 33 kV for the collection grid, and 132 for the transmission grid. Power transmission to shore is done with two three-phase 132 kV XLPE submarine cables. The water depth at the site is 20–25 m, and the distance to shore is 12 km. The grid connection is illustrated in Figure 2.5.

The wind farm consists of 100 Vestas V90 3 MW wind turbines, each with a doubly fed induction generator as described in Section 2.3. The collection grid consists of 10 radial feeders with 10 turbines per circuit. The onshore connection point is the 132 kV Richborough substation. This substation includes two Siemens SVC Plus reactive power compensation systems that assist in ensuring grid code compliance of the wind farm.

PROJECT NO.
502000064

REPORT NO.
TR A7482

VERSION
1.0

14 of 133
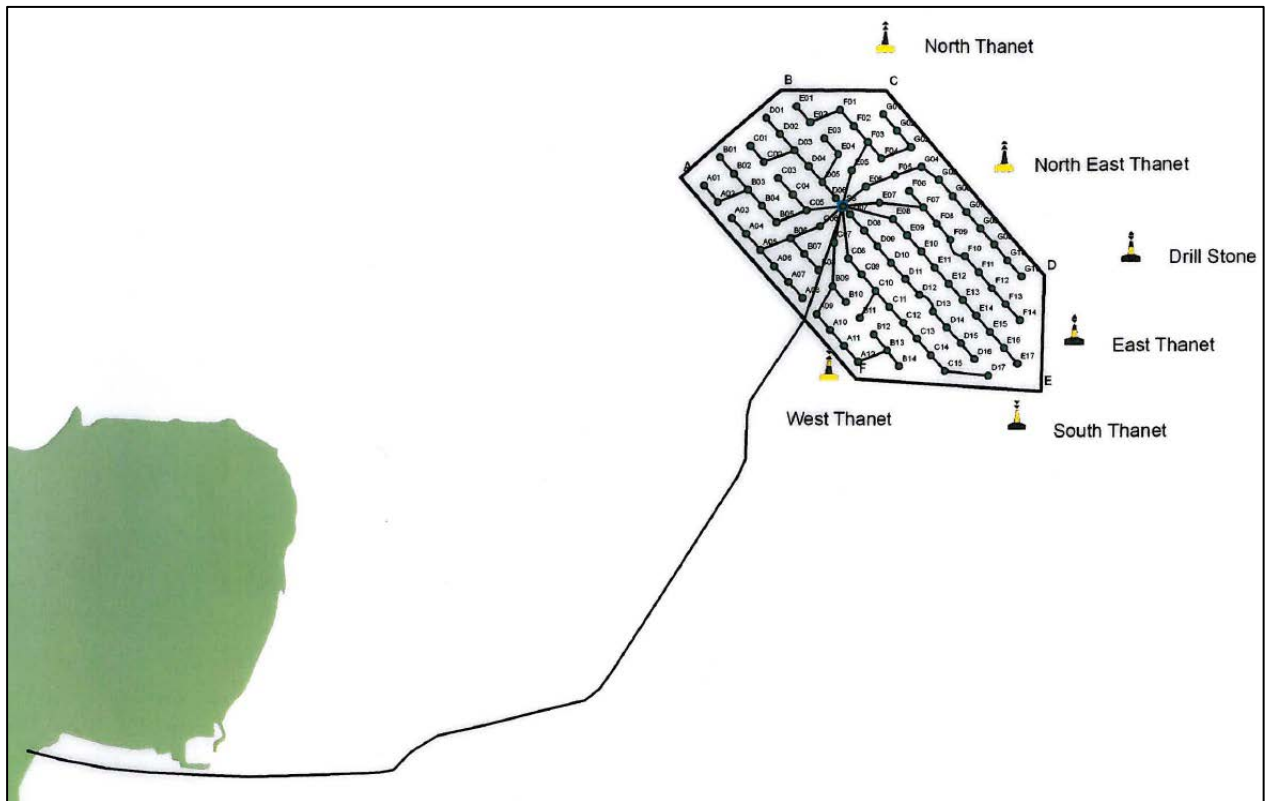
Figure 2.5: Thanet collection and transmission grid layout

2.1.2.3 BARD Offshore 1

The BARD Offshore 1 wind farm belongs to the BorWin cluster in the German North Sea, and was finished in 2013. At the time of completion, the wind farm was the largest offshore wind farm in the world (400 MW), with the longest distance to shore (128 km). The water depth is about 40 m. Further information about the wind farm can be found in ref. [2.10].

An overview of the grid connection is shown in Figure 2.6. The wind farm consists of 80 BARD wind turbines of 5 MW, with doubly fed induction generators. These feed power into a 36 kV AC collection grid which will be connected to an offshore transformer station. At the transformer station the voltage is transformed to 155 kV for the supply of the offshore HVDC converter station (BorWin Alpha), based on ABB HVDC Light technology, and further transmission by ±150 kV DC to shore (HVDC BorWin1). At the onshore receiving station at Diele the power will be injected into the mainland 380 kV transmission grid.
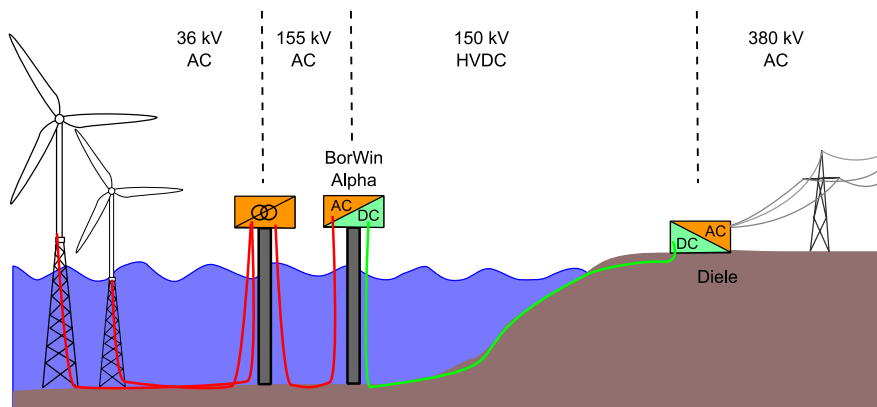
Figure 2.6: BARD Offshore 1 grid connection

2.2 Power transmission

This section considers power transmission systems for offshore wind farms. A good reference with a more comprehensive overview of power electronics and grid solutions for offshore wind farms is ref. [2.11].

2.2.1 HVAC

Most of the electrical power in the world is transmitted using High Voltage Alternating Current (HVAC) transmission lines. This is also true in offshore transmission systems installed between mainland and stations located on (or under) the sea. It is a well-established technology.

An HVAC offshore wind farm contains the following main components (Figure 2.7):

- AC Collecting system where the generated power in the wind turbine is collected in medium voltage cables and sent to the transforming station.
- Offshore transforming substation with transformers and reactive power compensation.
- Three-phase submarine cables (generally a single three core cable). Due to their construction, distributed capacitance in submarine cables is much higher than the capacitance in overhead lines. Thus the feasible transmission length is reduced for marine applications. Reactive power increases with the voltage and length of the cable, and long transmission distances require big reactive compensation equipment at both ends of the line.
- Onshore transforming substation with transformers and reactive power compensation.
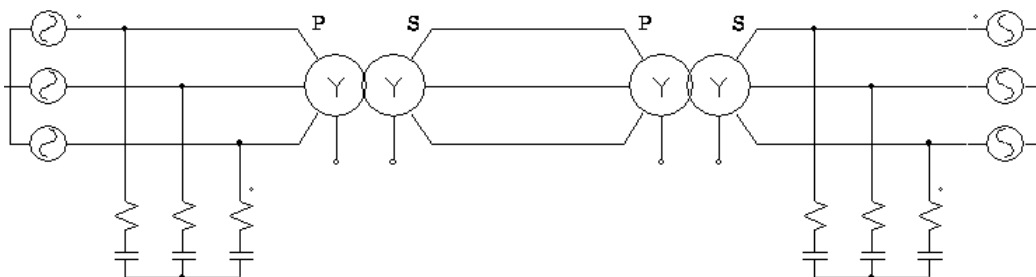
Figure 2.7: HVAC transmission system

Due to the high capacitance, AC cables will have charging currents, which are proportional to the cable length. At 50–150 km the charging current approaches the cable's rated current, which means

that the transfer capacity will be limited by the cable's thermal limit. Reactive compensation units can be installed to mitigate the problem to some extent. At one point however, the active power transmission capacity will be limited by stability limit rather than thermal limit, which means that AC transmission is no longer feasible. Gas Insulated Line (GIL) has been proposed to extend the possible length of submarine AC-transmission.

Offshore wind power farms in operation today are located close to shore, and thus AC-transmission is used. AC transmission is and will remain the preferred choice, but limitations makes it infeasible for large and far offshore wind farms. Horns Rev 1, with a power of 160 MW and a transmission distance of 21 km, was the first offshore wind farm using HVAC.

If the transmission voltage is the same as the onshore grid voltage, the onshore transforming station may not be necessary. For example, the Cape Wind project (420 MW) has been planned with a 115 kV marine transmission line equal to the onshore grid and the onshore transforming station is eliminated.

Some features regarding the transmission and collector system of HVAC offshore wind farms are shown in Table 2.2 [2.12].

Table 2.2: HVAC offshore wind farms. Collector and transmission system features

Name	CS				OS	TS			
	N_{clu} [a]	V_{cs} [b] (kV)	D_{wt} [c]	L_{cs} [d] (km)		V_{ts} [b] (kV)	N_{cab} [e]	L_{lf} [f] (km)	L_{cpss} [f] (km)
Huaneng Roncheng	–	–	–	–	–	–	–	–	–
Walney 1	5	33	–	–	1	132	1	45	1
Baltic 1	–	33	–	–	1	150	–	61	–
Belwind 1	6	33	5.6–7.2	50	1	150	1	52	3
Chenjagang Xiangshui	–	–	–	–	–	–	–	–	–
Thanet	10	33	5.6–8.8	55	1	132	2	26	3
Robin Rigg	–	–	–	–	2	–	–	–	–
Longyuan Rudong 1	–	–	–	–	–	–	–	–	–
Rodsand 2	–	33	–	–	1	132	–	–	–
Donghai Bridge	–	–	–	–	–	–	–	–	–
Gunfleet Sands	–	33	–	–	1	132	–	8.5	–[g]
Rhyl Flats	3	33	–	–	0[h]	33	3	–	2
Gäslingergrund	1	20	–	–	–	–	–	–	–
Alpha Ventus	2	33	6.6	16	1	110	1	61	5
Horns Rev 2	7	–	–	70	1[i]	–	–	–	–
Thorntonbank I	1	36	7.0	50.8	1[j]	150	2	36	3.3
Lynn-Inner Dowsing	6	36	–	32	0[j]	36	6	40	–
Kemi Ajos	–	–	–	–	–	110	–	0	–
Prinses Amalia	10	22	–	45	1	150	1	28	7[g]
Egmond aan Zee	3	34	–	–	0	34	3	–	7
Lillgrund	5	33	–	22	1	130	1	7	2
Burbo Bank	3	33	5.0–6.7	5	0	33	3	8	3.5
Barrow	4	33	5.6–8.3	–	1	132	–	27	3
Kentish Flats	3	33	7.8–7.8	18.9	0	33	3	10	2.6
Scroby Sands	–	–	–	–	0	–	–	–	–
Arklow Bank 1	–	–	–	–	–	–	–	–	–
Rodsand 1 (Nysted)	8	33	5.9–10.4	48	1	132	–	11	18
North Hoyle	2	–	–	16	0	–	2	22	–
Horns Rev	5	33	7.0	–	1	150	1	21	–
Middlegrunden	1	30	2.4	3.5	0	30	2	2	1.5

[a] Number of clusters of turbines according to their electrical arrangement, not to their geometrical disposition.

[b] Vcs and Vts stand for the voltages of the CS (also known as internal grid) and the TS, respectively.

[c] Separation among the turbines factorized by the turbine diameter. When two values are given, they account for the geometrical distances between turbines in a row and between rows, respectively.

[d] Total length of the MVAC collector system of the farm.

[e] Number of cables for the TS. Three phase high voltage alternating current (HVAC) submarine cable with optic fibre for communications is the general case.

[f] The length of the TS is the length of the submarine cable (L_{lf}), in most cases between the OS and the landfall, plus the length of the onshore transmission line (L_{cpss}), between the landfall and the CPS.

[g] A three phase submarine cable is connected in the landfall to three single phase and communication cables.

[h] Data corresponding to ongoing second and third phases of Thorntonbank OWPP.

[i] It is the first OS to offer accommodation facilities for O&M staff and visitors.

[j] When there is no OS, each cluster of OWTs has its own transmission cable, at least as far as the landfall, the voltages of the collection and transmission systems being the same.

2.2.2 HVDC LCC

Classical High Voltage Direct Current (HVDC) systems are based on Line Commutated Converters (LCC) using thyristors as the switching element [2.13]. The origin of the name of the converter is the need of an existing AC network in order to achieve proper commutation of the current between thyristors. Figure 2.8 shows a typical 12 pulse HVDC LCC system.

PROJECT NO.
502000064

REPORT NO.
TR A7482

VERSION
1.0

18 of 133
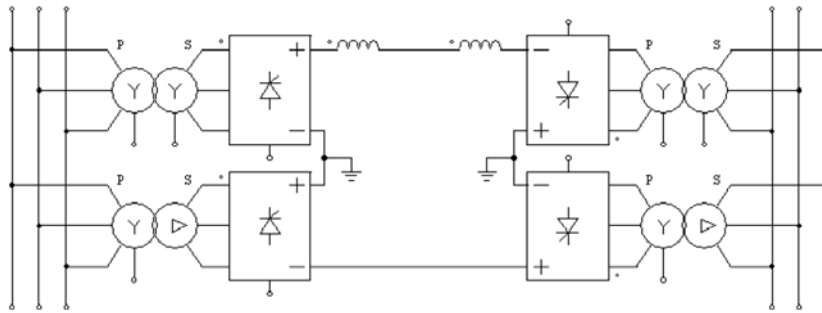
Figure 2.8: HVDC LCC transmission system

HVDC LCC systems allow for flexible and fast active power control and there is no limit in the transmission distance unlike HVAC because there is no capacitive current. The current in the line can only flow in one direction, but power can flow in both directions reversing the voltage polarities through the firing angle control. HVDC LCC converters have a lagging current and they draw reactive power around 60 % of their rated active power. Large capacitive filters must be used at both ends of the line to compensate this reactive power.

Normally each LCC converter is made up of two converters connected in series forming a 12 pulse rectifier. This converter operates with switching frequencies of 50-60 Hz and the power losses are low (0.7 % at 100% load and 0.1 % at no load). These losses can be reduced with the use of a STATCOM [2.14]. Additionally the STATCOM can be used to meet grid code requirements. This kind of transmission system can only transfer power between active grids, and an auxiliary generator for system start-up would be necessary in the offshore marine farm.

HVDC LCC systems have the following main components at each end of the transmission line:

- Transformers: Substations at both ends need transformers in order to raise the voltage to the necessary level for the transmission line. Usually both, star and delta, connections are required for a 12 pulse converter (see Figure 2.8). 12 pulse converters cancel harmonics and the filter size is reduced. HVDC LCC transformer design is challenging because they must provide isolation at the AC plus DC voltages and tapings must be included for the proper control of the system [2.13].

- LCC power converter based on thyristors: The LCC power converter is the heart of a HVDC LCC system because it is the element that obtains the AC to DC conversion and vice versa. Today thyristors with silicon wafers of 125 mm exist capable of standing 8 kV and currents up to 4 kA DC. HVDC LCC systems of 1000 MW onshore and 500 MW offshore are feasible with state of the art technology. LCC converters need reactive power for proper operation because the current is out of phase with the line voltage due to the control angle of the thyristors. Also the reactance of the line and the transformers affect the control characteristics of the system and Constant Extinction Angle control is necessary [2.13].

- AC and DC filters: LCC converters generate a high content of low order harmonics in the line currents and AC and DC filters are necessary. These AC filters supply part of the reactive power needed by the LCC converter as well. The DC filter avoid the generation of circulating AC currents in the cable.

- DC current filtering reactance: Each DC cable needs a reactance to avoid current interruption with minimum load, limit DC fault currents, and reduce current harmonics in the cable.

PROJECT NO.
502000064

REPORT NO.
TR A7482

VERSION
1.0

19 of 133

- Capacitors or STATCOM for reactive power compensation: As mentioned above, LCC converters require reactive power for proper operation. Capacitors or STATCOM are needed to compensate for reactive power demand in the grid.

HVLC LCC is a mature technology, and it could be an alternative for wind farms generating more than 500 MW and with transmission distances of more than about 100 km [2.15], as discussed in the previous section. However application of HVDC LCC submarine transmission has only been used for power transfer between high voltage grids on the mainland, and there is no existing LCC converter station located in the sea for the connection of offshore wind farms, gas or oil extracting platforms. Several universities and manufacturers are studying the viability of HVDC LCC in these applications [2.16, 17].

In Table 2.3 some existing HVDC LCC installations are shown.

Table 2.3: Marine HVDC LCC installations

Project	Power (MW)	Transmission system (km)	Voltage (kV)
Basslink (Australia-Tasmania)	500	290	400
Italy-Greece HVDC link	500	163	400
Rómulo (Península-Baleares)	400	237	$\pm$ 250

Connection of HVDC LCC converters with weak grids is problematic because it may cause commutation failure of the thyristors. The reactive power consumption and the problems with commutation failures can be reduced using Capacitor Commutated Converter (CCC) or alternatively the Controlled Series Capacitor Converter (CSCC) (Figure 2.13 a and b). These are a special type of HVDC LCC with series capacitors between the converter transformer and the thyristor bridge.

In the CCC, the reactive power compensation capacitors are connected in series between the valves and converter transformer. In CSCC, the capacitor current can be controlled using parallel thyristors. The capacitor in series with the converter transformer reduces the commutation impedance of the converter, which in turn reduces the reactive power requirement of the converter. The risk of commutation failure following disturbances is also reduced.

Some other topologies for improvement of HVDC LCC converters have been proposed in the last years, such as a bipolar configuration with a 12-pulse bridge [2.15] or a 36-pulse operation (Figure 2.13c [2.18]). A LCC HVDC transmission system based on a new inductive filtering method is presented in [2.19]. It includes a new converter transformer and the related full-tuned branches, resulting in a stable solution with enhanced fault-recovery performance.

Since the voltage is reversed with direction of power flow for HVDC LCC, mass-impregnated cables have to be used as XLPE is not suited. These require water-tight lead shields at both ends of the cable.

PROJECT NO.
502000064

REPORT NO.
TR A7482

VERSION
1.0

20 of 133
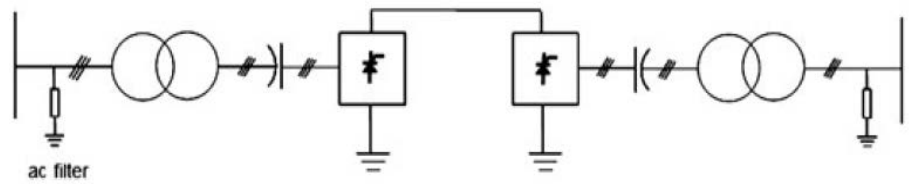
(a) CCC.
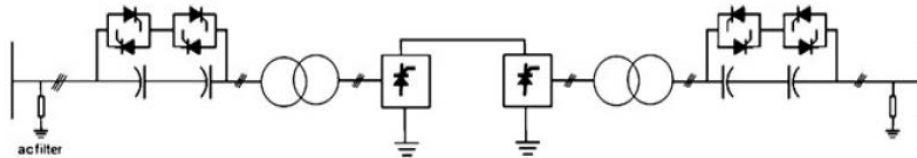
(b) CSCC.
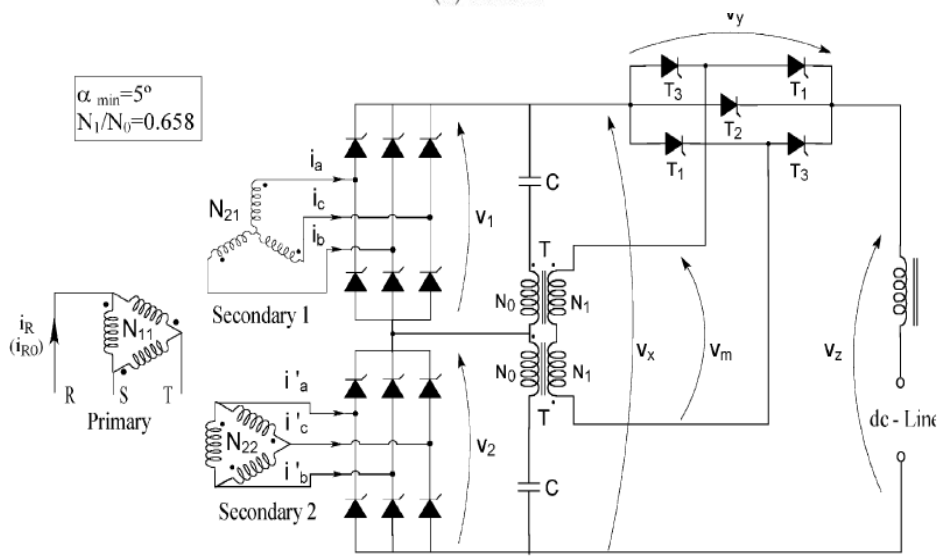
(c) 36 pulse converter.

Figure 2.9: Alternative HVDC LCC systems

2.2.3 HVDC VSC

Voltage-sourced converters (VSC) rely on the integrated gate-commutated thyristor (IGBT), a valve that can be switched both on and off by a control signal. These converters operate by controlling both the amplitude and phase angle of the voltages and thus behaves as voltage sources in the AC grid (hence the name). Due to high switching frequency, the harmonic content is low. Thus the filter requirements are less than for HVDC LCC, which allows for compact converter stations.

Characteristics for VSC HVDC are described in for instance refs.[2.1, 7]. An important feature is that active and reactive power exchange can be controlled independently, and the converter can both produce and consume reactive power. A fast dynamic response can be achieved, to comply with grid code requirements. The AC voltage can be controlled at both stations, so that the converter can operate in a weak network (provided the phase lock loop (PLL) is intended for operation in a weak network). Communication between the stations is not required.

PROJECT NO.
502000064

REPORT NO.
TR A7482

VERSION
1.0

21 of 133

As opposed to HVDC LCC, there is no change of voltage polarity when the direction of power flow is reversed. The fixed polarity of the DC voltage allows for the use of XLPE cables. It also makes it easier to build multi terminal schemes. DC-voltage will be a measure of power balance (corresponding to frequency for AC-system), and voltage droop for the DC-voltage controller can be used to share power between the terminals in a multi-terminal solution.

High power IGBT development allows the use of VSC in HVDC systems in the frequency range of 1–2 kHz with much lower harmonic distortion than HVDC LCC systems although with higher power losses [2.20, 21]. This technology is reaching power transmission capability of 1100 MW. Today 100-400 MW class VSC HVDC systems are in operation [2.15, 22]. Figure 2.10 shows the schematic of a HVDC VSC transmission system.
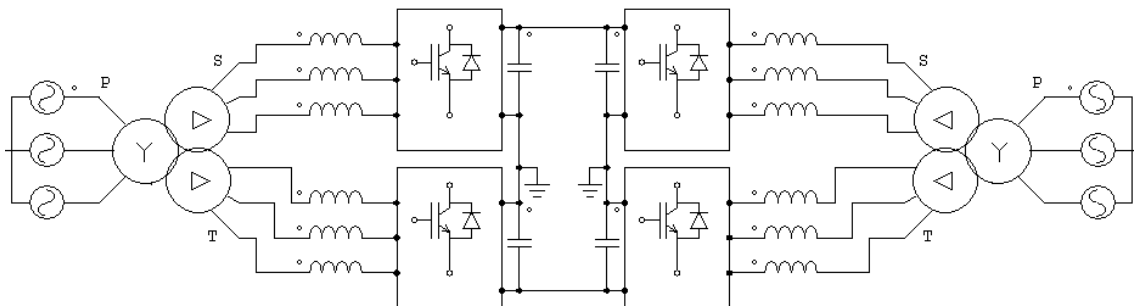
Figure 2.10: HVDC VSC transmission system

An HVDC VSC system has the following main components:

- Transformers: The transformers in HVDC VSC stations are similar to HVDC LCC transformers, but special attention for the higher switching frequency harmonics is necessary.
- VSC converter based on IGBTs: The VSC power converter is the heart of a HVDC VSC system. It is a three phase IGBT inverter operating at 1–2 kHz. Multilevel converters are very well suited in this application because their high voltage capacity, lower harmonic content and high efficiency. Today HVDC VSC systems of 1100 MW and 300 kV are feasible with state of the art technology.
- AC and DC filters: VSC converters generate lower content of harmonics, and the AC and DC filters are smaller than in LCC stations.
- DC current filtering reactance: each DC cable needs a reactance to limit DC fault currents and reduce current harmonics in the cable.

HVDC VSC overcomes most of the HVDC LCC problems at increased converter cost and higher power losses. In the case of HVDC VSC, as in HVDC LCC, the power can flow in both directions but the voltage polarity cannot be reversed. The VSC converters can control instantaneously the reactive power as well as the active power and they can help start the AC system at which they are connected. The installation of this type of converters does not increase the short circuit current at the PCC (Point of Common Coupling) and they increase the reliability of the grid.

The first VSC systems had a power loss in the converters of 2.8–3.2 % of the transmitted power (1.4–1.6 % per converter station). As an example, total losses in the Cross Sound Transmission system, including converter loss and resistive loss in the cable, were 14 MW, that is, 4.2 % of the transmitted power. Modern multilevel IGBT VSC converters have lower losses and ABB estimates that losses with new generation IGBTs will be almost equal to HVDC LCC converters, around 0.7 %.

PROJECT NO.
502000064

REPORT NO.
TR A7482

VERSION
1.0

22 of 133

HVDC VSC systems allow independent control of active and reactive power at each end of the line and power transmission can be controlled with high flexibility. At the offshore station reactive power can be supplied for the marine generators and at the onshore substation reactive power can be used to regulate voltage at the Point of Common Coupling, PCC. Active power control can be used to regulate frequency in the grid, which can be very helpful if the grid onshore is weak. Even when no active power is available from the marine farm, the onshore station can operate as reactive power regulator to sustain the grid voltage. HVDC VSC converter stations are more compact than HVDC LCC and the offshore platform size can be smaller and less expensive.

VSC converters can start even with a dead grid, thus no additional start-up mechanism is necessary offshore. Even when the onshore grid has collapsed, the system may start by itself.

HVDC VSC is not such a mature technology as HVDC LCC, but operational experience is showing that it is reliable. Today at least three manufacturers are able to build HVDC VSC systems, Siemens, ABB and Alstom. The first HVDC VSC system was installed in 1997 by ABB, to connect mainland Sweden to the island of Gotland, with a power rating of 3 MW and 10 kV voltage, aiming to study the viability of the technology [2.23]. Since then, several VSC HVDC systems have been built worldwide, including submarine transmission lines. Table 2.4 includes a summary of the worldwide VSC HVDC projects and their basic parameters [2.24]. Whereas several installations of power transmission between onshore grids exist, only a few HVDC VSC stations are located offshore. These are the Troll A platform in the North sea, the wind park cluster BorWin 1, which is the first grid connected offshore wind farm using HVDC, and the Valhall platform in Norway.

Table 2.4: Main data of offshore HVDC VSC installations

Project	In service	Power (MW)	Transmission system (km)	Voltage (kV)
Hellsjön (Sweden)	1997	3	10	± 10
Gotland Light (Sweden)	1999	50	98	± 80
Tjaereborg Light (Denmark)	2000	7,2	4,3	± 9
Directlink (Australia)	2000	180	65	± 80
Eagle Pass (U.S.A.)	2000	36	†	± 15.9
MurrayLink (Australia)	2002	220	180	± 150
Cross Sound (U.S.A.)	2002	330	40	± 150
Troll A Gas platform (Norway)	2005	80	68	± 60
Estlink (Estonia-Findland)	2006	350	105	± 150
Borkum 2 (Germany)	2009	400	203	± 150
Caprivi Link (Namibia)	2009	300	970	350
Valhall (Norway)	2010	78	292	150

†: Back to Back connection without cable

HVDC VSC is the preferred HVDC technology for offshore wind farms [2.25-28]. Table 2.5 includes a summary of the main features of planned wind farms operating with HVDC VSC.

PROJECT NO.
502000064

REPORT NO.
TR A7482

VERSION
1.0

23 of 133

Table 2.5: Main data of offshore wind farms operating with HVDC VSC

Project name	Owner Companies	Commiss. Year[1]	Converter technology	Rated power (MW)	HVAC voltage (kV)	HVDC voltage (kV)	Cable length offshore (km)	onshore (km)
BorWin1	TenneT/Mitsubishi	2012	LIGHT	400	170/380	±150	125	75
BorWin2	TenneT/Mitsubishi	2013	PLUS	800	155/300/400	300	125	75
DolWin1	TenneT	2013	LIGHT	800	155/380	±320	75	90
HelWin1	TenneT	2013	PLUS	576	155/250	259	85	45
SylWin1	TenneT	2014	PLUS	864	155/300/380	±320	160	45
DolWin2	TenneT[2]	2015	LIGHT[3]	900	155/380	±320	45	90
HelWin2	TenneT	2015	PLUS	690	155/300/380	±320	85	45

Most of the latest development in HVDC VSC converters is based on multilevel topologies, such as the Modular Multilevel Converters (MMC) of Siemens, the Cascaded Two Level converters (CTL) of ABB and the Chain-Link Converters (CLC) of Alstom. MMC converters and derived topologies are scalable and simple, and the operational power losses are lower than conventional HVDC VSC [2.29-31].

Regarding grid layouts, several VSC HVDC configurations have been investigated in the last years for grid connection of large-scale offshore wind farms. Two-terminal VSC HVDC system is a typical and well-known solution. Multi-terminal solutions are also under analysis. In this case, several offshore/onshore converter stations and HVDC cables can be arranged in different ways, having this configuration a significant impact on the economic and technical aspect of the system [2.32, 33]. Several HVDC layouts including point-to-point, ring or star configurations among others are presented in [2.34].

A present barrier in applying such topologies is suitable DC circuit breakers, as bringing the whole system voltage to zero in case of a fault would result in a significant loss of power. Fast DC circuit breakers suitable for multi-terminal HVDC systems are not commercially available yet. Nevertheless some developments based on solid state devices are under study [2.35, 36]. Ref. [2.37] proposes a DC grid management for a VSC based multi-terminal HVDC system, seemingly with satisfactory results.

Some alternative topologies to the conventional HVDC VSC architecture have been proposed recently. For instance [2.38] introduces an alternative topology clustering several wind turbines that share a common Current Source Inverter (CSI) (Figure 2.11). The CSI is directly connected to the DC cable. The wind turbines operate at a variable speed which is common for all generators in the same group and the reference speed is the optimal average speed for the group. The authors consider that the inability to operate each wind turbine at its optimum speed is not a great loss in efficiency, since it is likely that the wind profile will be largely similar for a group of closely located turbines. In this topology the generator converters are not needed since the CSI facilitates the variable speed operation of each cluster of wind turbines.

PROJECT NO.
502000064

REPORT NO.
TR A7482

VERSION
1.0

24 of 133
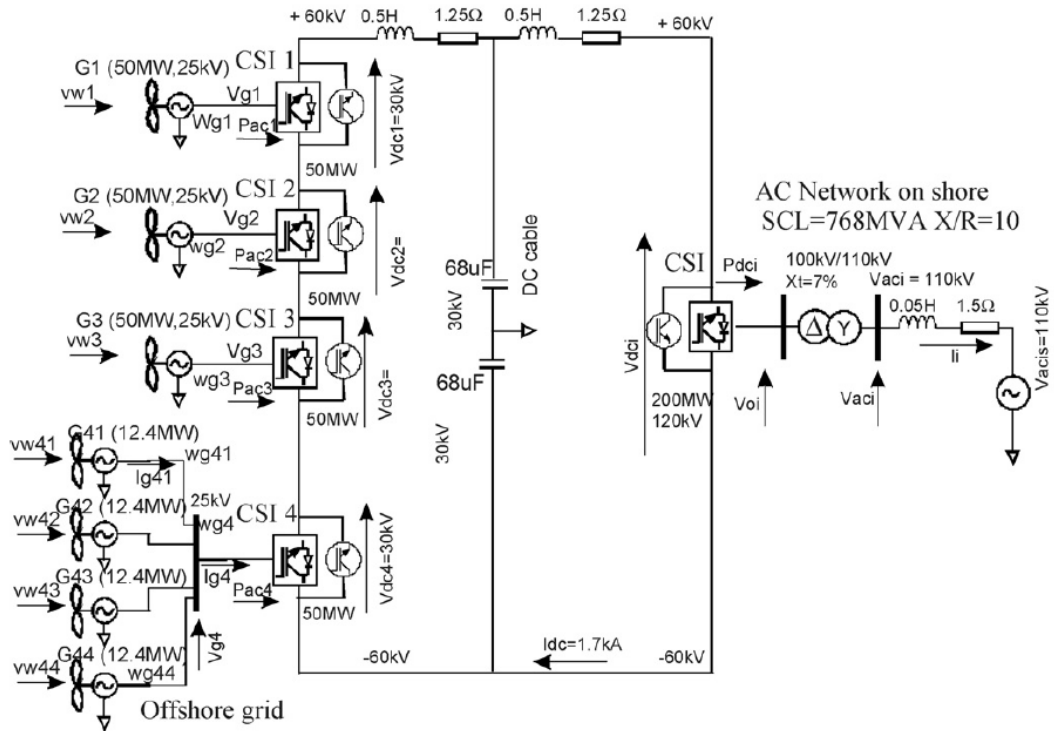
Figure 2.11: Common Current Source Inverter topology

In [2.39] a new topology is proposed for a 300 MW offshore wind farm based on parallel connection of several VSC converters (Figure 2.12). As in the previous case several wind turbines are clustered sharing the same VSC converter, thus they operate at the same speed. The main benefit of this concept is that individual converters are not required in the wind turbines.
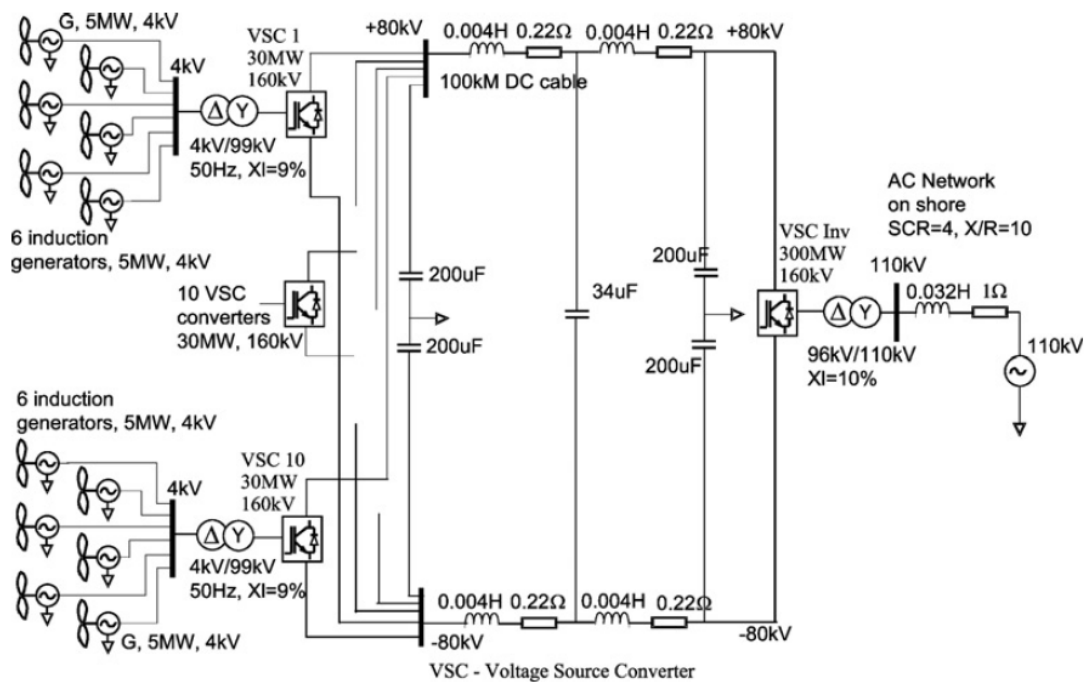
Figure 2.12: Common Voltage Source Converter topology

PROJECT NO.
502000064

REPORT NO.
TR A7482

VERSION
1.0

25 of 133

2.2.4 Cable types

There are different cable types suitable for transmission of large amounts of power over large distances. The differences are mainly related to the insulation systems, which give the cables different characteristics. The main cable types are *cross-linked polyethylene* (XLPE) cables and *mass-impregnated* cables.

XLPE cables are generally the choice of preference for AC transmission and for VSC HVDC transmission. They are lighter than mass-impregnated cables and allow higher temperature. XLPE cables exist up to (approximately) 420 kV for land cables, and up to 245 kV for submarine cables. These values are likely to increase in the future, allowing perhaps 800 kV and 3000 MW.

XLPE cables build up space charges when used for DC transmission. This is problematic for LCC schemes which use reversed polarity to change direction of the power, flow, hence they cannot be used as LCC HVDC transmission cables. For VSC HVDC, on the other hand, the voltage polarity does not reverse and XLPE is a good choice.

Mass-impregnated cables are presently suitable for voltages of up to 45 kV AC and 500 kV DC. The insulation typically consists of high-density paper tapes impregnated with a high-viscosity compound which does not require fluid pressure feeding, thus allowing these cables to be installed in HVDC links in very long lengths, up to several hundreds of kilometres.

2.3 Wind turbines

This section presents a survey of the different existing electrical systems for wind turbines. The survey focuses on high power wind turbines. A good general reference for current wind turbine technology is *Wind Energy – The Facts* [2.40]. Another good reference is the *UpWind* project reports [2.41, 42]. The solutions included in this section are solutions that are common or expected to be suitable for *large offshore turbine* applications.
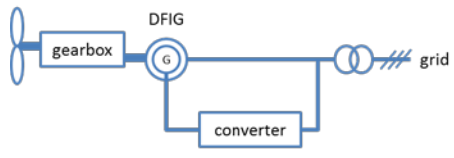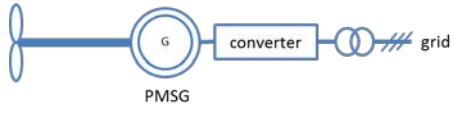
Variable speed turbines with a gearbox that transforms the low speed rotation of the blades to high speed rotation in the generator are by far the most common system in modern wind turbines sold in the last decade. Variable speed (as opposed to fixed speed) is essential in order to extract maximum energy from the wind. Moreover, cheaper and simpler fixed speed turbines have difficulty in satisfying tightened grid codes.

Since variable speed operation of the generator translates directly into electric power with variable frequency, some form of frequency converter is needed to ensure that the power supplied to the main grid has the desired frequency (50 or 60 Hz). This adds extra costs, but also controllability that is essential for grid code compliance.

There is presently a trend towards direct-drive turbines with a low-speed generator. The big advantage of direct drive generators is that they omit the gearbox, making them more reliable. The drawbacks are weight, size and cost. The generator can be electrically excited (rotor windings) or permanent magnet synchronous generator, which is assumed most suitable due to less size.

The most common variable speed turbine concepts are summarised in Table 2.6.

Table 2.6: Variable speed turbine concepts

Description	Illustration
Doubly fed induction generator (DFIG) These are the most common generator concepts in large wind turbines sold today. The DFIG offers variable speed operation with a reduced converter cost (about 30% of full converter costs **[2.41]**).	
Squirrel cage induction generator (SCIG) with converter Variable speed operation using a standard SCIG can be achieved by inserting a full-scale converter between the generator and the grid. The main drawback of this system is the cost of the converter. This is a less common solution, but exists in some Siemens designs.	
Permanent magnet synchronous generator (PMSG) This system relies on permanent magnets in the generator rotor to set up the rotating magnetic field, and a full scale converter to allow variable speed. The main advantages are no electrical excitation system and slip rings (brushless), and better efficiency and simpler fault-ride-through capabilities compared to the DFIG. The disadvantages are higher costs than for wound-rotor synchronous generators, and losses in the converter.	
Direct-drive (gearless) turbine with converter Direct-drive generators have a rotor that is directly connected to the hub of rotor blades, so the generator speed is identical to the rotational speed of the blades, which is a low speed. The low speed is associated with a high torque in the generator, and a large size which is necessary to fit all the electromagnetic poles. The big advantage of direct drive generators is that they omit the gearbox, making them more reliable. The drawbacks are weight, size and cost. The generator can be electrically excited (rotor windings) or permanent magnet synchronous generator, which is assumed most suitable due to smaller size.	

One of the main benefits of variable speed wind turbines compared to fixed speed ones is the maximum power extraction capability. Despite this, there is no commonly agreed data as to how much the power extraction is increased with variable speed operation, we can say that an energy increase between 10 and 15 % is obtained [2.43].

Another important benefit of variable speed solutions is the reduction of the mechanical loads on the blades, the drive train and the tower. Also, power oscillations which generate flicker are reduced when variable speed solutions are used power [2.44, 45].

The main drawback in variable speed wind turbines is the need of additional electrical equipment, mainly power converters, to control the rotational speed of the generator. Nevertheless, studies by the EWEA show that, in a group of 52 wind turbines with rated power above 1 MW from 20 manufacturers, only 3 still use fixed speed concepts, 12 models use two speed concepts and 37 models use limited or full speed variable systems [2.40].

Table 2.7 shows some features of wind turbines already operating in offshore wind farms [2.12]. About half of them use doubly fed induction generators, whereas the other half is based on squirrel cage induction generators with full converter. Table 2.8 shows some general characteristics of oncoming offshore wind turbines [2.46]. It is remarkable that although half of the already operating wind turbines are based on squirrel cage induction generators, none of the oncoming designs follow this strategy. In the SWT-6.0-120 turbine Siemens has shifted to permanent magnet generators. A more detailed discussion of some common generator concepts is given below.

Table 2.7: Wind turbines already operating in commissioned offshore wind farms

Manufacturer	Model	Years	Rated power (MW)	Generator	Gearbox	Total installed (MW)	Quota (%)
Repower	5M	2009	5.0	DFIG	3	60	2.0
Areva	M5000	2009	5.0	PMSG	2	30	1.0
Siemens	SWT-3.6-107	2007–2011	3.6	SCIG	3	731	23.5
Vestas	V90/3.0-Off	2006–2011	3.0	DFIG	3	933	29.2
Sinovel	SL 3000/90	2010–2011	3.0	DFIG	3	204	6.6
Winwind	WWD-3-100	2008–2009	3.0	PMSG	0	30	1.0
Siemens	SWT-2.3-82/93	2004–2011	2.3	SCIG	3	740	23.7
Vestas	V80/2000	2002–2008	2.0	DFIG	3	400	12.9

Table 2.8: Oncoming offshore wind turbines

Manufacturer	Model	Full-scale prototype	Power (MW)	Diameter (m)	Generator Type	Voltage	Gearbox[1]
Bard	Bard 6.5	2011	6.5	120	PMSG	LV[5]	3
Siemens	SWT-6.0-120	2011	6.0	120/154[6]	PMSG	LV	0
Sinovel	SL 6000	2011	6.0	128	DFIG	–	3
XEMC-Darwind	XE/DD	2011	5.0	115	PMSG	–	0
GE Energy	4.1-113	2011	4.1	113	PMSG	–	0
Guodian UP	UP-6000	2012	6.0	128	DFIG	–	3
2B-Energy	2B6[7]	2012	6.0	130	DFIG	–	3
AMSC-Hyundai HI	HQ5500	2012	5.5	127/140	–	MV[8]	0
Gamesa	G11X-5.0	2012	5.0	128	PMSG	LV	2
Dewind	DSME 7.0	2013	7.0	160	PMSG	–	2
Mitsubishi PSE	SeaAngel	2013	7.0	165	PMSG	MV	0[9]
Vestas	V164/7.0	2013	7.0	164	PMSG	–	2
Alstom Power	Haliade 150	2013	6.0	150	PMSG	–	0
Nordex	N150/6000	2013	6.0	150	PMSG	MV	0
Mingyang WPIG	SCD 6.0	2013	6.0	140	PMSG	–	0
Gamesa	G14X	2014	7.0	140	PMSG	–	2
Sway	Sway	2015	10.0	145	–	–	0
AMSC	Sea Titan	2015	10.0		PMSG	MV[10]	0

2.3.1 Squirrel cage induction generator

The Squirrel Cage Asynchronous Generator can be used for variable speed operation if a power converter is included in the design. As in the fixed speed design, a gearbox is needed to increase the rotational speed of the blades. The power converter overrides the use of the soft starter and the

PROJECT NO.
502000064

REPORT NO.
TR A7482

VERSION
1.0

28 of 133

capacitor bank. A back-to-back power converter with rated power around 120 % and 150 % of the generator is needed. In most of the designs the back-to-back converter is built as two voltage source converters with 6 IGBTs with a common DC bus (Figure 2.13). This full power converter controls the generator rotational speed and the system can operate at the optimum efficiency point. Sometimes, a lower rating power converter (20-30 %) is used to reduce the cost of the system. The power converter is used only at low wind speeds. When the wind speed increases, the power converter is bypassed, the stator is directly connected to the grid and the wind turbine operates at fixed speed.

Although the squirrel cage machine is robust and economical, this system presents several drawbacks. The main problem is the cost of the power converter and filters because they must be rated very high, around 120-150 % of the wind turbine power in order to provide the necessary reactive current [2.47]. In spite of the previously mentioned drawbacks, this type of wind turbine is being built by Siemens for offshore applications with rated power up to 3.6 MW.
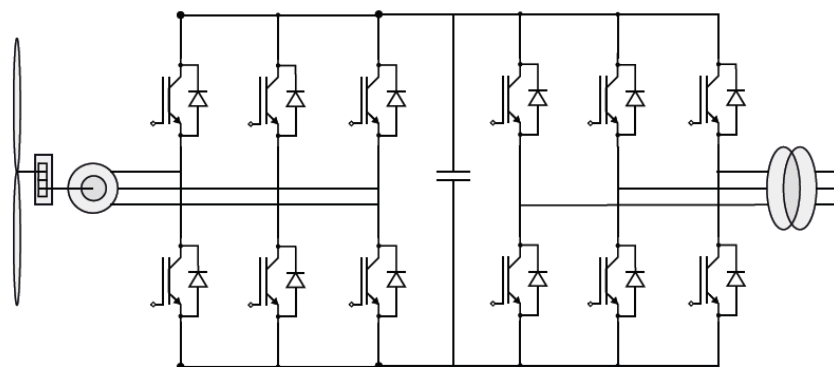
Figure 2.13: Squirrel cage asynchronous generator with full power back-to-back converter

2.3.2 Wound rotor induction generator

The Wound Rotor Induction Generator was first used in a wind turbine in the GROWIAN [2.48] project in Germany. As in the case with squirrel cage machines, a gearbox must be used to adapt the low speed blades to the high speed generator. In this design the stator is directly connected to the grid. The rotor can be connected either to a set of variable resistances (Figure 2.14a) or to a back-to-back power converter connected to the grid (Figure 2.14b)

When a set of variable resistances are connected to the rotor, the speed of the machine can be controlled within a limited range around ±10 % of its nominal speed reducing the mechanical load and improving the efficiency of the turbine. Vestas used this concept with the commercial name of OptiSlipTM. Nordic Windpower also used this idea in wind turbines with rated power of 3 MW with a speed variation range of 5 %. The power in the rotor is wasted in the resistances. This is a drawback because a considerable amount of energy is lost.

The second configuration, with a power converter connected to the rotor (doubly fed induction generator) (Figure 2.14b) is more widely spread among manufacturers and it is the workhorse of the onshore wind power industry.

The back-to-back converter controls the rotor voltage to set the optimum speed. The active and reactive power of the stator can be controlled independently with this topology and the rotor power is not lost as heat. Speed variations of ±33 % around its nominal value can be achieved with a power converter rating of 25 % of the rated power. Vestas used this topology with the trademark OptiSpeedTM and many other manufacturers use this system in their wind turbines.

The system, despite its popularity because of its low cost, presents several disadvantages. One of the main problems is the use of brushes and slip rings in the rotor. Periodical maintenance and monitoring

within 6 and 12 months must be programmed for the brushes [2.49]. The brushes and slip ring system can be eliminated using a second asynchronous machine with sharing the same rotor as the wound rotor machine. The windings in both machines are connected and the control is applied in the secondary machine stator. WEIER Elektrik has delivered such systems to Vestas and Enercon. The NREL (National Renewable Energy Laboratory) in the USA studied the substitution of the brushes and slip rings with a rotating transformer. The rotor power would be delivered without any contact [2.50].

2.3.3 Synchronous generator

The synchronous generator uses a *wound rotor* fed with direct current (Figure 2.15) or *permanent magnets* in the rotor to develop a rotating magnetic field. The stator feeds the external load through three phase windings. The main advantage of synchronous generators is the possibility of building very low rotational speed machines using a high number of poles. Low speed machines can be directly coupled to the blades, thus eliminating the use of a gearbox, which is a common cause of failure in wind turbines. The resulting design is more robust and the space requirements in the nacelle are significantly reduced. However a generator with high number of poles and power rating in the order of several megawatts requires a very high diameter machine which is difficult to transport and install. Sometimes a half-way alternative, with medium speed synchronous generators and simple single stage gearbox is preferred. The speed conversion ratio between the generator and the blades in this case is around 6:1. The generator diameter is not excessive and the resulting gearbox is more simple and robust.

The synchronous generator uses a full power back-to-back converter to control the speed of the machine. Synchronous generators with wound rotor also require an AC/DC converter and slip rings to magnetize the rotor.
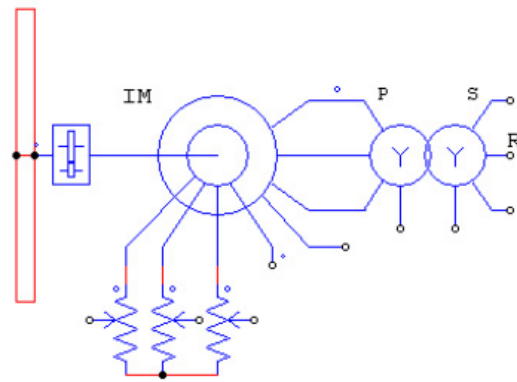
(a) Rotor resistance control
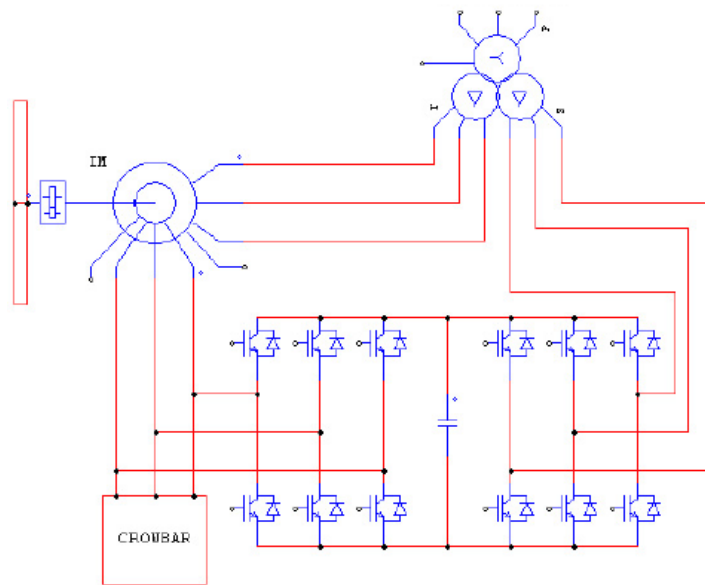
(b) Reduced power *back-to-back* converter

Figure 2.14: Wound rotor asynchronous generator topologies
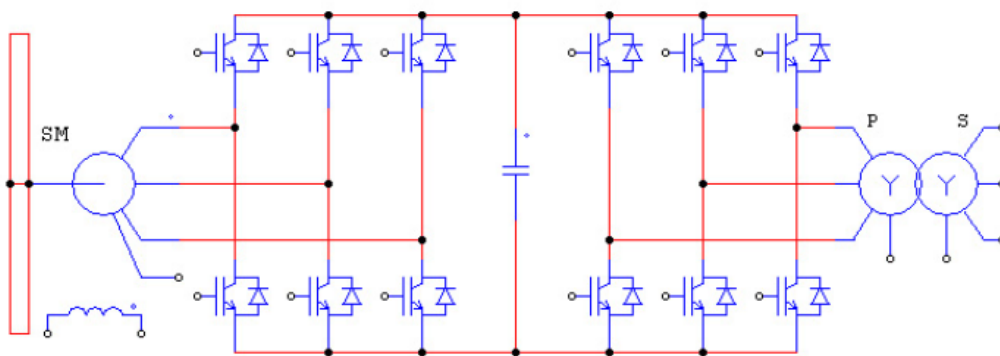
Figure 2.15: Wound rotor synchronous generator

PROJECT NO.
502000064

REPORT NO.
TR A7482

VERSION
1.0

31 of 133

The wound rotor synchronous generator is the most extended among the synchronous generators in the wind industry. Enercon uses this type of generator in its high power wind turbines. The wound rotor synchronous generator presents a very high efficiency because all the stator power is used for power production. The power factor of the machine is easily controlled by the field winding in the rotor and the stator current is minimized for every operating point.

The main drawback of wound rotor synchronous generator is the use of slip rings and brushes, and the need of a secondary converter to generate the rotor field.

Permanent magnet synchronous generators have been used in low power wind turbines below 50 kW rated power without a gearbox in battery charging applications or in hybrid systems with diesel generators. In the last years, high power wind turbines are introducing this type of generators. Mitsubishi manufactures the MWT-S300 300 kW and MWT-S600 600 kW with permanent magnet synchronous generators and the MWT-S2000 2 MW wind turbine is in the test stage before mass production. WinWinD has installed the first 5 MW turbines in Bremerhaven, Germany, with a 3 kV Alstom permanent magnet synchronous generator. Zephyros also used this concept in the Z72 2 MW wind turbine.

Although the permanent magnet synchronous generator is technologically appealing, it has several drawbacks. The cost of the permanent magnets is high, thus the resulting generator is expensive, and the permanent magnets can suffer demagnetization [2.51]. In addition the design of this type of generator is complex and the necessary rotor diameter is high. This is a problem for land transport of the generator.

2.3.4 Medium voltage electrical systems in wind turbines

The continuous increase in the rated power of wind turbines makes it logical to ask the next question: is it be better to keep the wind turbine generator and power converter voltages in the low voltage (LV) range below 1000 V, or is it better to start using medium voltage (MV) generators between 1000 V and 35 kV, and power converters to reduce the current rating and the conductor section?

It is very illustrative to look at the catalogue of the main drive manufacturers and observing the power rating and the voltage range of their products. Figure 2.16a shows the power and voltage range of the drive families of three important manufacturers [2.52] and Figure 2.16b shows the LV and MV drive types used in the naval industry [2.53]. It is obvious that the drive market for power above 1-2 MW has opted to use MV equipment. The reason for this is the reduction of the currents and the cost of the conductors.

As the power of wind turbine increases, LV systems will meet design problems with very high currents. As an example, a 5 MW generator operating at 690 V has a rated current of 4.2 kA, which is a very high value. The most likely evolution will be the adoption of 3.3 kV, 4.2 kV, 6.3 kV or even higher MV generators. This will reduce the current, the conductor sizes and maybe the transformer can be eliminated. Some wind turbine manufacturers are introducing MV equipment in their designs [2.54-56]. For instance Alstom uses the Multibrid concept with a 3 kV permanent magnet synchronous generator in the 5 MW WinWinD M5000 wind turbine, Acciona uses a 12 kV generator in its 1.5 and 3 MW models and Zephiros uses a 4 kV generator. Medium voltage power converters are also already in the market such as the ACS5000 and PCS6000 from ABB, the MV7000 from Converteam or the MV 500 from Ingeteam. Most of these converters use three level topologies (Figure 2.17) that are better suited than conventional 6 IGBT VSC converters to work at medium voltages. In addition they generate current with less harmonic content and have a higher efficiency.

The NREL studies predict a reduction of the cost of energy of 2.5-3.5% if the wind turbines are designed with MV equipment [2.52]. The study is based on information and data provided by manufacturers, including the material, installation and labour costs (MV requires higher skilled

PROJECT NO.
502000064

REPORT NO.
TR A7482

VERSION
1.0

32 of 133

workers and more complicated maintenance operations). The low currents in MV generators allow the location of converters and transformers at the base of the tower demanding less space and weight requirements for the design of the nacelle.
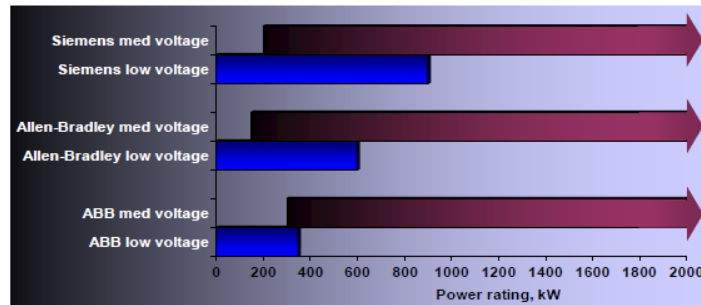
(a) Motor Drive families.
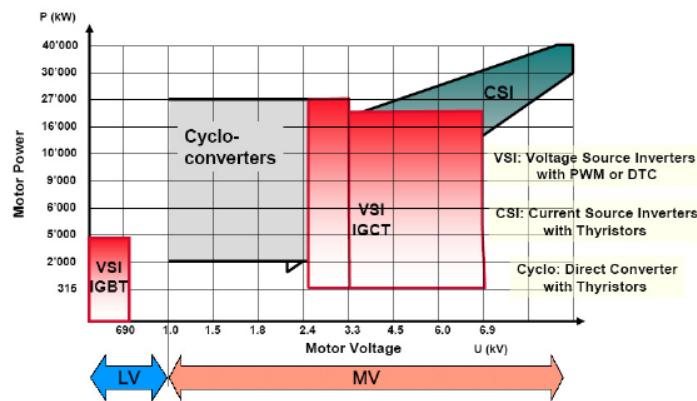
(b) Drive types in naval applications

Figure 2.16: High power drives
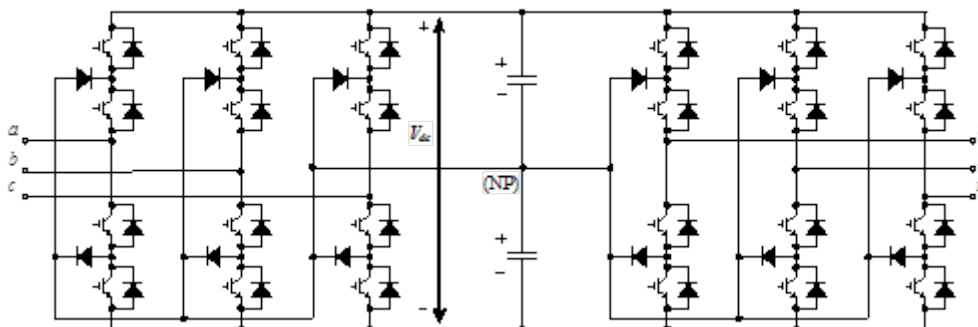
Figure 2.17: Back-to-back three level NPC converter

2.4 Control systems

As illustrated in Figure 2.18, the control systems for a wind farm grid connection system can schematically be separated in three levels, 1) turbine level control; 2) wind farm level control; 3)

PROJECT NO.
502000064

REPORT NO.
TR A7482

VERSION
1.0

33 of 133

transmission level control. A schematic overview of major control objectives and their boundaries in time and impact level is shown in Figure 2.19 [2.57].
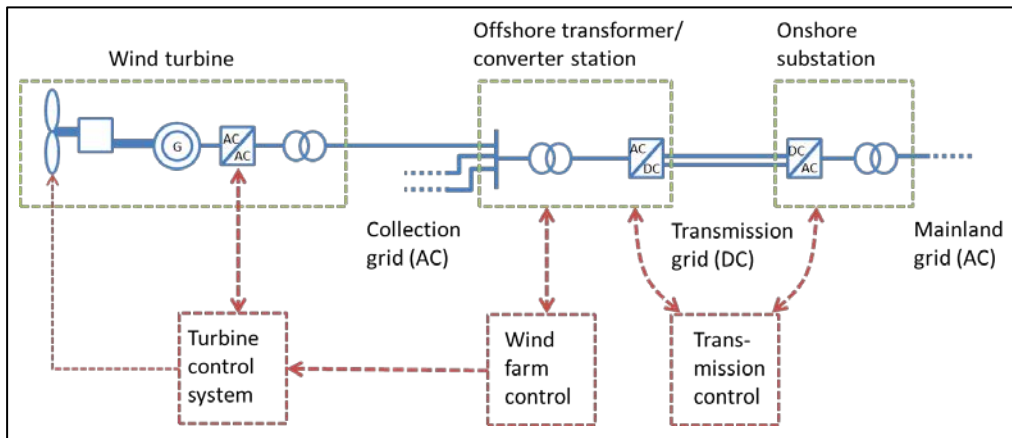
Figure 2.18: Schematic overview of control systems for wind farm and grid connection
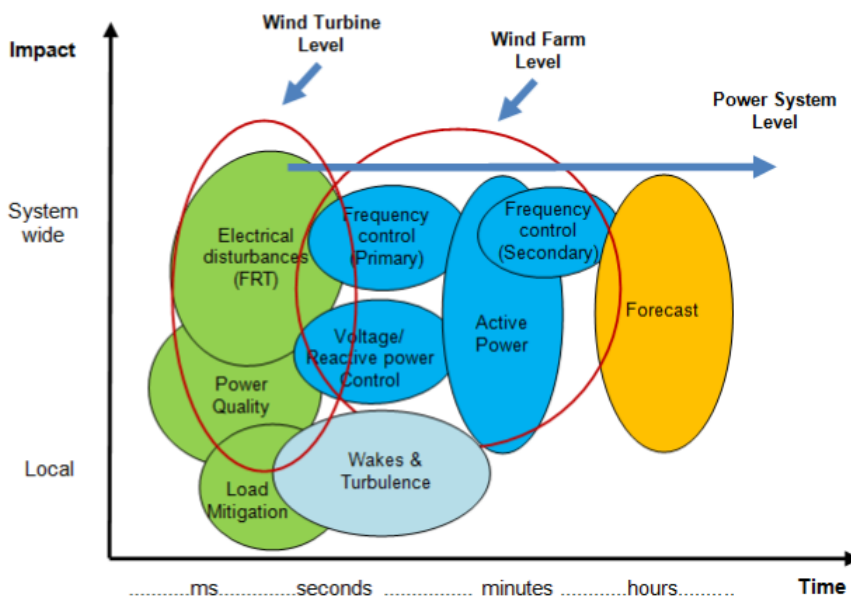
Figure 2.19: Schematic of wind farm control sub systems. Source: [2.57].

2.4.1 Turbine control

With the development of ever larger wind turbines and offshore installations, an increasing importance is put on the control system, and its contribution to a reliable operation. Traditional wind turbine control has primarily been designed to maximise the power output for wind speeds up to the rated speed, and to limit the output for higher speeds in order to avoid damage to the turbine. However, modern, very large turbines are relatively more flexible than traditional ones, and reduction of fatigue related dynamic loads is becoming more important, in particular tower loads. It is also important to avoid excitation of any structural natural frequencies. Due to the high overall cost of a large turbine, including the cost of maintenance and downtime, the cost of an advanced control system is relatively

PROJECT NO.
502000064

REPORT NO.
TR A7482

VERSION
1.0

34 of 133

small. This is even more so for offshore wind farms, where installation and maintenance costs in particular are much higher.

Floating turbines pose additional challenges for the control system since these are, naturally, much more influenced by wave driven motions, and a stronger coupling between aerodynamics (wind driven) and hydro-dynamics (wave driven). For example, low-frequency oscillatory forwards–backwards motions of the floating tower are negatively damped by traditional pitch control. Stabilisation of this motion is therefore an important control objective. Side–to–side motions may also need to be damped actively by the control system. An overview of engineering challenges for floating wind turbines is given in ref. [2.58].

Wind generators use power electronic converters which allow them to operate at variable speed. This feature has its pros and cons. An advantage is the additional control flexibility to condition the power output; but a disadvantage is the vulnerability of the power converters to withstand large fault currents (for long period of time), in the event of a disturbance.

As stated in ref. [2.57], it has become standard practice in modern MW-size machines to introduce controllers that provide active damping of turbine components to reduce blade, tower and drive-train loads, whilst optimising energy capture and maintaining power quality. However, as wind turbines become larger and more flexible, these controllers have to be designed with great care as the coupling between flexible modes increases and so does the potential to destabilise the turbine.

2.4.2 Wind farm level control

From the wind farm level perspective, the objective is to maximise total power capture and ensure satisfactory power quality. This implies *coordinated* control of the wind turbines. In other words, the performance of each individual wind turbine is less important than the overall performance. Coordinated control may for example reduce wake effects and improve storm shutdown behaviour.

Minimisation of wake effects is of high concern when designing the wind farm layout, but since the wind direction is not constant, operational control may also be important to reduce wake losses. For example, using the yaw degree of freedom, the wake of wind turbines can be directed away from wind turbines placed behind it. This is an active field of research and development. Wake losses can easily be reduced by increasing the distance between each turbine, but then power cable lengths are also increased, giving both increased capital expenses and increased power losses. Also, increased distances means that fewer turbines will fit within a given area.

In order to develop a wind farm grid design and a wind farm level control system that fully exploits the control flexibility offered by the power electronics in variable-speed wind turbines, it is necessary to have suitable wind farm models. Development of such models is an on-going research activity.

2.4.3 Transmission level control

The offshore transmission system for a future, large and far-ashore wind farm will likely be based on HVDC technology, probably a VSC-HVDC system. VSC-HVDC transmission can control the active and reactive power independently, provide reactive power control, transmit the power without distance restrictions, and provide additional functionality such as frequency control and oscillations damping.

Connection of very large offshore wind farms requires new approaches to a number of areas related to HVDC control, such as coordination of HVDC terminal behaviour, robust control of inverter interactions and protection against faults [2.59].

Importantly, enhanced controllers for the front-end converter of the HVDC link are needed in order to allow wind farms to contribute to network operation as required by grid codes [2.57]. As the DC link screens the wind farm(s) from the onshore network, such control capability becomes very important since control requirements will be directly imposed on the HVDC connection, such as the provision of short-term frequency support to the network (primary response).

PROJECT NO.
502000064

REPORT NO.
TR A7482

VERSION
1.0

35 of 133

Other control possibilities should also be investigated further, such as the coordinated control of energy storage technologies available in the system with the wind farm connection; capabilities that may be further enhanced by the inter-connections among different regional AC networks.

Special devices, such as *Static Var Compensators* (SVC) and *Static Synchronous Compensators* (STATCOM) may be used to provide the dynamic reactive power control required to keep the AC voltage within the grid connection agreement (grid code) limits. The rapid response of the SVC/STATCOM can also reduce the voltage drop experienced by the wind farm during remote AC system faults, thus increasing the fault ride-through capability of the wind farm.

Multi-terminal HVDC transmission systems require special control philosophies, and this topic is an active area of research. See e.g. refs. [2.34, 60-62].

2.5 Novel DC and low frequency AC solutions

In the last years some alternatives to directly tap the wind turbines to a medium voltage DC collector grid have been proposed. Their main objective is to reduce the cost of the whole transmission system using cheaper DC cables for the collector grid and avoiding, if possible, the offshore substation.

Pure DC grids for offshore wind farms is an active topic for research and development, but no such solutions have yet been implemented in any wind farm that exists or is under construction. There are outstanding technical difficulties that need to be resolved before DC grids will become a viable option for offshore wind farms. Thorough discussions of DC wind farm options are found e.g. in refs. [2.2, 63] . Two main types of DC systems can be envisaged, with wind turbines connected in parallel or in series respectively, see Figure 2.20.

Parallel coupled wind turbines with a DC collection grid are the direct DC analogy to the above options with AC collection grid. A typical layout is illustrated in Figure 2.20. In order to achieve desired voltage level for power collection and transmission one or more voltage step-ups may be needed, depending on the output DC voltage of the wind turbines. As discussed in ref. [2.2], if the voltage from the wind turbines is about 20–40kV only one step is required. If the output voltage of the wind turbine is lower (~5kV), and two steps are required, the wind turbines could be divided into groups where the first voltage step-up is done group-by-group, and the high-voltage side of the first DC transformer is connected to the second transformer. If only one transformation step is used, the wind turbines can be connected in radials directly to the main DC transformer, similarly as for the large AC wind farm. Increasing the DC voltage can be done with or without a transformer. If a transformer is used, the topology is in principle like an inverter + transformer + rectifier, except the transformer frequency does not have to be 50 Hz. Since the voltage step-up can be done at increased frequencies, e.g. 500 Hz, the transformer weight can be drastically reduced compared to standard 50 Hz transformers. With this solution, more or less any voltage ratio can be achieved. If no transformer is used (DC boost converter), the voltage ratio is limited to relatively small values with current technology. In the low to medium power area DC/DC converters are widely used and are a standard component, which could easily be adapted for low voltage grid application. In contrast to this, no feasible concepts exist, so far, for transforming DC voltages at higher power levels.

Series coupled wind turbines will give a voltage build-up that may allow direct transmission to shore without a substation. A major advantage of such a system is that it avoids any offshore converter or transformation platforms. The number of turbines needed in series in order to achieve the desired transmission voltage depends on the voltage output of each single turbine. With standard technology today, a generator voltage of 0.69 kV and DC voltage of about 3 kV would be reasonable. Since the turbines are connected in series, the voltage to earth increases for each connected turbine. Although the voltage difference at the DC terminals may be only 3 kV, the voltage to earth will for the last turbine equal the transmission voltage (to earth), that is, hundreds of kilovolts. Hence, electrical insulation is a serious challenge for these types of configurations. Insulation has to be incorporated somewhere. One possibility is to use a transformer (inside the turbine AC/DC converter topology);

PROJECT NO.
502000064

REPORT NO.
TR A7482

VERSION
1.0

36 of 133

other options are to include the insulation in the generator or the entire nacelle. Besides the electrical issues themselves, there is also a question of maintenance at such high voltages. These, and other technical challenges related to DC wind farms are active topics of research.

a) DC wind farm with parallel connected turbines

b) DC wind farm with series connected wind turbines and no offshore substation
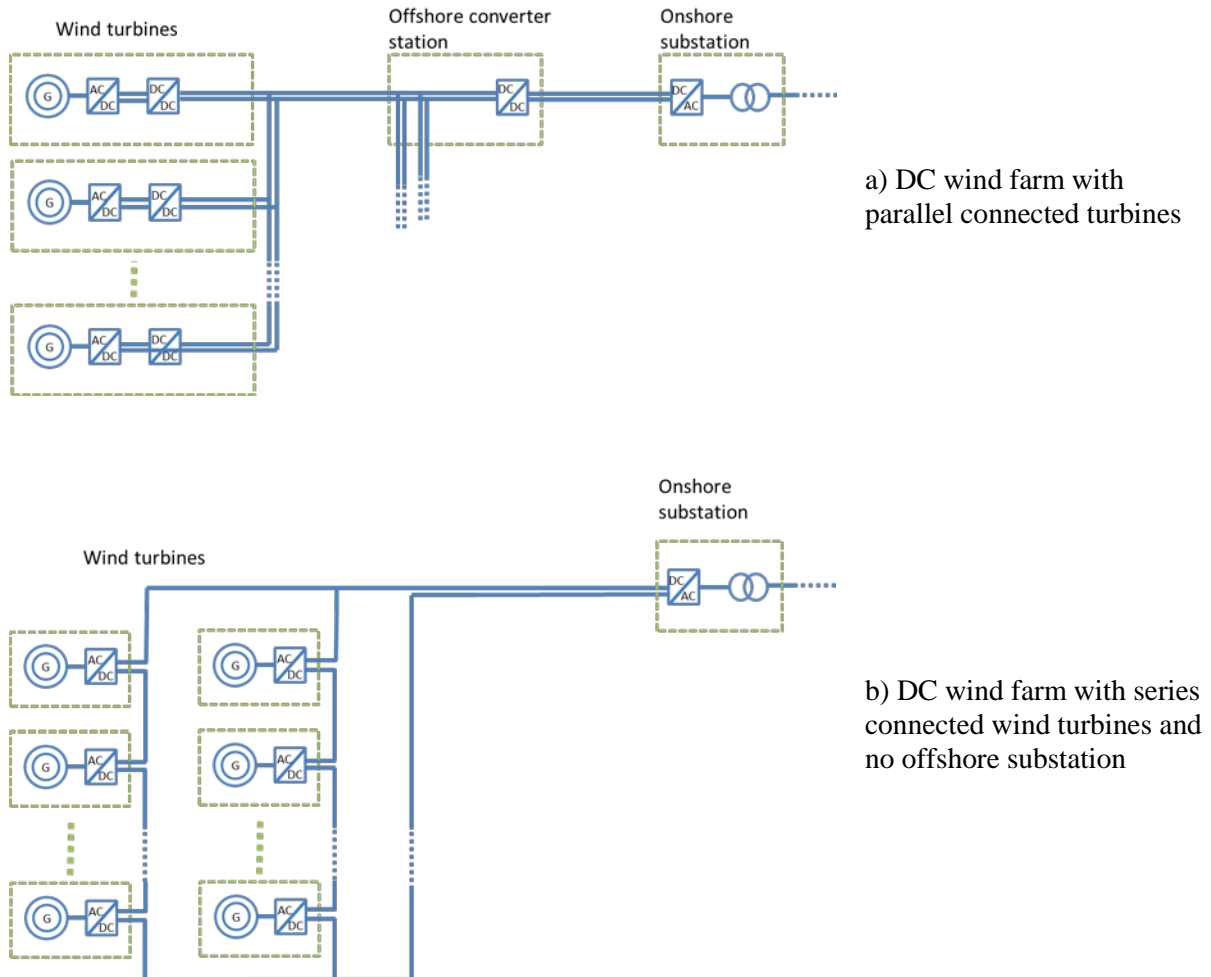
Figure 2.20: DC wind farm with wind turbines connected in parallel (a) and series (b)

Multi-terminal DC transmission

The term *multi-terminal DC grid* refers to DC grids with three or more terminals connected to a common DC bus. For a cluster of wind farms, or in situations where it may be desirable to combine the grid connection of one or more wind farms with an offshore HVDC transmission corridor, multi-terminal HVDC grids are widely thought of as a possible future choice of preference. The main obstacle for the emergence of such solutions today is the lack of proven technology, in particular related to the protection against faults in the DC grid, i.e. DC circuit breakers for high voltages and high power ratings. Current technologies rely on power electronics and are costly. (AC protection is inherently easier since the current alternates between a positive and a negative value and is therefore instantaneously zero twice per period. These zero crossings are the points when the circuit breaker breaks the current.) More discussion of DC grids and protection is found in ref. [2.64].

Different multi-terminal HVDC-VSC topologies for large offshore wind farms are investigated in Ref. [2.34], which includes a description of system requirements and a review of control schemes and

PROJECT NO.
502000064

REPORT NO.
TR A7482

VERSION
1.0

37 of 133

HVDC circuit topologies. An analysis of DC-side faults, their transients and resulting protection issues is presented in Ref. [2.64]. The study includes short-circuit faults and cable ground faults, and a protection design and relay coordination method is proposed for a small-scale DC wind farm. Ref. [2.1] includes a discussion on multi-terminal DC grids and points out that DC-voltage droop characteristics can be used to control the amount of power exchange to the AC-networks.

2.5.1 Transmission systems with a DC collector grid for offshore wind farms

In order to tap the wind turbines to a medium voltage DC grid some modifications of the power electronics inside the turbine should be done. Most of the proposed topologies are based on permanent magnet synchronous generators followed by a rectifier and a DC/DC converter. The main difference amongst these topologies lies in the DC/DC converter that is used. DC/DC single phase full bridge converters with a high frequency transformer to increase the voltage level and a passive or active medium voltage rectifier (Figure 2.21) have been proposed in [2.65-67]. Ref. [2.68] proposes a resonant DC/DC converter (Figure 2.22) with very low switching losses. Ref. [2.69] proposes a configuration with diode rectifiers connected to the generator and buck converters. Ref. [2.70] adopts an interesting DC/DC topology based on a 3-phase/1-phase AC/AC converter, a high frequency transformer and a controlled rectifier. Finally, a completely new concept is proposed in [2.71]; this topology includes permanent magnet generators, medium frequency transformers and simple power converters to realize a compact and light system (Figure 2.23).

(a) (b)
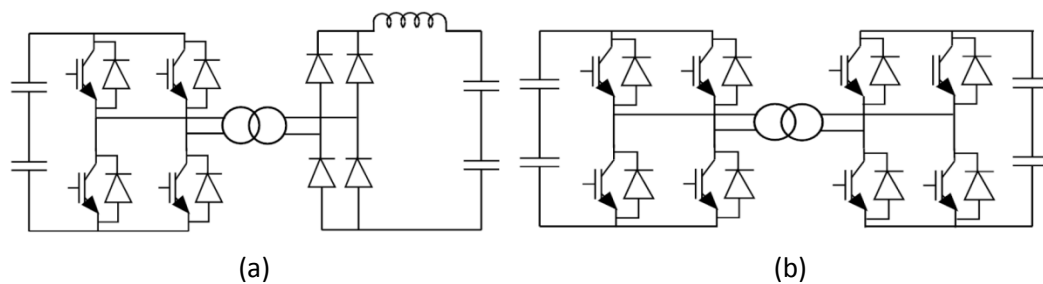
Figure 2.21: Full bridge converter topologies with (a) passive filter, and (b) active rectifier
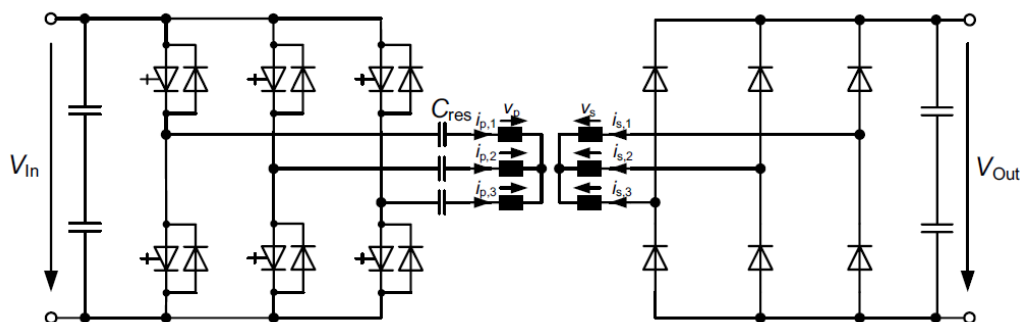
Figure 2.22: Resonant converter

Although solutions considering DC collector grids have been proposed by the scientific community, and some manufacturers, such as Converteam, are developing this technology [2.66], it is not mature enough and some technical challenges still need to be addressed. Consequently there is not any commercial installation using this technology. In addition, feasibility of such solutions is still a matter

PROJECT NO.
502000064

REPORT NO.
TR A7482

VERSION
1.0

38 of 133

of debate, with some authors being of the view that DC collection grids are not going to find a widespread acceptation in the future [2.72].
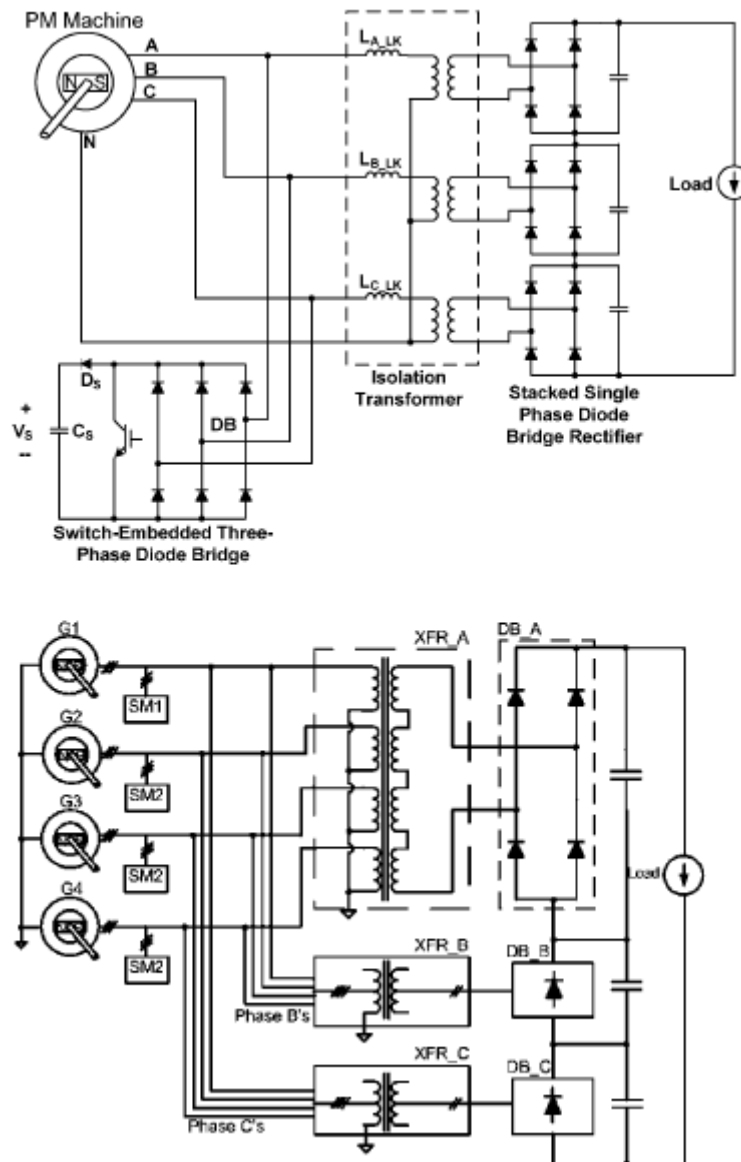
Figure 2.23: Permanent magnet generator and medium frequency transformers

2.5.2 Collection grid with AC frequency different from 50 Hz

An intriguing possibility that arises when a decoupling of wind farm grid and consumer (mainland) grid frequency is considered is to have a collection grid (and transmission grid) that is AC, but with a lower than 50 Hz frequency. This would in a sense be a compromise between AC and DC, as it could benefit from the advantages of AC power associated with protection, transformation and control, and at the same time have DC-like advantages associated with reduced charging currents and therefore losses and need for reactive power compensation.

PROJECT NO.
502000064

REPORT NO.
TR A7482

VERSION
1.0

39 of 133

The main disadvantage of low frequency AC concepts is probably the lack of proven technology and therefore the uncertainties of how well such systems would work in practice at the desired voltage and power rating levels. There exist AC systems with lower frequency, e.g. the 15 kV 16.7 Hz AC railway power supply in parts of Europe, but these systems are quite different from an offshore wind farm. Ref. [2.73] investigates the use of low frequency AC for offshore wind farm grid connection. An additional relevant reference is ref. [2.74], which includes experimental results.

For shorter distances where losses and reactive power are not critical, there is also the alternative to have *high frequency* AC grids (e.g. 500 Hz). Some advantages to such wind farm collection systems may be [2.75] that higher frequency components (transformers) are smaller and lighter and that the costs for the power electronics are lower. A disadvantage may be that AC/AC conversion using pulse-width modulation (PWM) requires large filters to smooth the output to get a "nice" sinusoidal voltage. This represents additional costs and losses, but may not be necessary when there are no load customers are connected. Such systems are not suitable for very large wind farms since a medium frequency distribution network is needed within the wind farm.

2.6 Bibliography

[2.1] Kling, W.L., R.L. Hendriks, and J.H. Boon. *Advanced transmission solutions for offshore wind farms*. in *IEEE Power and Energy Society General Meeting - Conversion and Delivery of Electrical Energy in the 21st Century*. 2008. Pittsburgh, USA.http://dx.doi.org/10.1109/PES.2008.4596257

[2.2] Lundberg, S., *Wind Farm Configuration and Energy Efficiency Studies - Series DC versus AC Layouts*, in *Department of Energy and Environment*. 2006, Chalmers University of Technology: Gothenburg, Sweden. p. 141. http://webfiles.portal.chalmers.se/et/PhD/LundbergStefanPhD.pdf (accessed Nov 2011).

[2.3] Erlich, I. and H. Brakelmann. *Integration of wind power into the German high voltage transmission grid*. in *2007 IEEE Power Engineering Society General Meeting*. 2007.http://dx.doi.org/10.1109/PES.2007.385790

[2.4] Chaudhary, S.K., R. Teodorescu, and P. Rodriguez, *Wind Farm Grid Integration Using VSC Based HVDC Transmission - An Overview.* 2008 Ieee Energy 2030 Conference, 2008: p. 493-499.http://dx.doi.org/10.1109/ENERGY.2008.4781061

[2.5] Bresesti, P., et al., *HVDC connection of offshore wind farms to the transmission system.* Ieee Transactions on Energy Conversion, 2007. **22**(1): p. 37-43.http://dx.doi.org/10.1109/TEC.2006.889624

[2.6] Xu, L. and B.R. Andersen, *Grid connection of large offshore wind farms using HVDC.* Wind Energy, 2006. **9**(4): p. 371-382.http://dx.doi.org/10.1002/we.185

[2.7] Asplund, G. *Sustainable energy systems with HVDC transmission*. in *IEEE PES General meeting*. 2004. Denver, USA.http://dx.doi.org/10.1109/PES.2004.1373296

[2.8] DONG Energy (website). *Horns Rev 2*. Available from: http://www.dongenergy.com/Hornsrev2/DA (accessed Oct 2011).

[2.9] Vattenfall. *Thanet Offshore Wind Farm*. Available from: http://www.vattenfall.co.uk/en/thanet-offshore-wind-farm.htm (accessed Jan 2012).

[2.10] BARD Engineering (website). Available from: http://www.bard-offshore.de/en/projects/offshore/bard-offshore-1 (accessed Nov 2009).

[2.11] Nee, H.-P. and L. Angquist, *Perspectives on Power Electronics and Grid Solutions for Offshore Wind Farms*, in *Elforsk rapport 10:96*. 2010, Elforsk. http://www.elforsk.se/rapporter/?rid=10_96 (accessed Nov 2011).

PROJECT NO.
502000064

REPORT NO.
TR A7482

VERSION
1.0

40 of 133

[2.12] Madariaga, A., et al., *Current facts about offshore wind farms.* Renewable & Sustainable Energy Reviews, 2012. **16**(5): p. 3105-3116.http://dx.doi.org/10.1016/j.rser.2012.02.022

[2.13] Arrillaga, J., *High voltage direct current transmission*. 1998: Institution of Electrical Engineers (IEE).

[2.14] Weber, T., et al. *Grid integration of Sand-bank 24 offshore windfarm using LCC HVDC connection*. in *CIGRE Session B4, no. 302*. 2008

[2.15] Montilla-DJesus, M.E., et al., *Optimal Operation of Offshore Wind Farms With Line-Commutated HVDC Link Connection.* Ieee Transactions on Energy Conversion, 2010. **25**(2): p. 504-513.<Go to ISI>://000278063800027

[2.16] Cartwright, P., L. Xu, and C. Sasse. *"Grid integration of large offshore wind farms using hybrid HVDC transmission*. in *Nordic Wind Power Conference*. 2004

[2.17] Xu, J., et al. *Grid integration of large offshore wind energy and oil gas installations using LCC HVDC transmission system*. in *International Symposium on Power Electronics, Electrical Drives, Automation and Motion (SPEEDAM 2010)*. 2010

[2.18] Villablanca, M., et al., *Point-to-point HVdc systems using 36-pulse operation.* Electric Power Systems Research, 2004. **69**(1): p. 43-50.http://dx.doi.org/10.1016/j.epsr.2003.07.008

[2.19] Li, Y., et al., *Study on Steady- and Transient-State Characteristics of a New HVDC Transmission System Based on an Inductive Filtering Method.* Ieee Transactions on Power Electronics, 2011. **26**(7): p. 1976-1986.http://dx.doi.org/10.1109/Tpel.2010.2098888

[2.20] Asplund, G., et al. *DC transmission based on voltage source converters*. in *International Conference on Large High Voltage Electric Systems. CIGRE'98,*. 1998

[2.21] Meier, S., *Novel voltage source converter based HVDC transmission system for offshore wind farms*. 2005, Royal Institute of Technology: Stockholm, Sweden.

[2.22] Muyeen, S.M., R. Takahashi, and J. Tamura, *Operation and Control of HVDC-Connected Offshore Wind Farm.* Sustainable Energy, IEEE Transactions on, 2010. **1**(1): p. 30-37.http://dx.doi.org/10.1109/tste.2010.2041561

[2.23] da Silva, F. and R. Castro, *Power flow analysis of HVAC and HVDC transmission systems for offshore wind parks.* International Journal of Emerging Electric Power Systems, 2009. **10**(3): p. 1-13

[2.24] Flourentzou, N., V.G. Agelidis, and G.D. Demetriades, *VSC-Based HVDC Power Transmission Systems: An Overview.* Ieee Transactions on Power Electronics, 2009. **24**(3-4): p. 592-602.http://dx.doi.org/10.1109/Tpel.2008.2008441

[2.25] Chaudhary, S.K., R. Teodorescu, and P. Rodriguez. *Wind Farm Grid Integration Using VSC Based HVDC Transmission - An Overview*. in *2008 Ieee Energy 2030 Conference*. 2008

[2.26] Koutiva, X.T., et al., *Optimal integration of an offshore wind farm to a weak AC grid.* Ieee Transactions on Power Delivery, 2006. **21**(2): p. 987-994.http://dx.doi.org/10.1109/Tpwrd.2005.859275

[2.27] Xu, L., L.Z. Yao, and C. Sasse, *Grid integration of large DFIG-based wind farms using VSC transmission.* Ieee Transactions on Power Systems, 2007. **22**(3): p. 976-984.http://dx.doi.org/10.1109/Tpwrs.2007.901306

[2.28] Bozhko, S., et al., *Large offshore DFIG-based wind farm with line-commutated HVDC connection to the main grid: Engineering studies.* Ieee Transactions on Energy Conversion, 2008. **23**(1): p. 119-127.http://dx.doi.org/10.1109/Tec.2007.914155

[2.29] Saeedifard, M. and R. Iravani, *Dynamic Performance of a Modular Multilevel Back-to-Back HVDC System.* Ieee Transactions on Power Delivery, 2010. **25**(4): p. 2903-2912.http://dx.doi.org/10.1109/Tpwrd.2010.2050787

[2.30] Li, K. and C. Zhao. *New Technologies of Modular Multilevel Converter for VSC-HVDC Application*. in *Asia-Pacific Power and Energy Engineering Conference (APPEEC 2010)*. 2010

PROJECT NO.
502000064

REPORT NO.
TR A7482

VERSION
1.0

41 of 133

[2.31] Marquardt, R. *Modular multilevel converter: An universal concept for hvdc-networks and extended dc-bus-applications*. in *International Power Electronics Conference (IPEC)*. 2010. Sapporo

[2.32] Zhou, K., et al. *Topologies and control of VSC-HVDC systems for grid connection of large-scale offshore wind farms*. in *11th International Conference on Electrical Machines and Systems (ICEMS 2008)*. 2008

[2.33] Xu, L., et al. *The role of multiterminal HVDC for wind power transmission and AC network support*. in *Asia-Pacific Power and Energy Engineering Conference (APPEEC 2010)*. 2010

[2.34] Gomis-Bellmunt, O., et al., *Topologies of multiterminal HVDC-VSC transmission for large offshore wind farms.* Electric Power Systems Research, 2011. **81**(2): p. 271-281.http://dx.doi.org/10.1016/j.epsr.2010.09.006

[2.35] Häfner, J. and B. Jacobson, *Proactive Hybrid HVDC Breakers - A key innovation for reliable HVDC grids*, in *The electric power system of the future - Integrating supergrids and microgrids International Symposium,*. 2011: Bologna.

[2.36] Jocvic, D., et al. *Feasibility of DC Transmission Networks*. in *2nd IEEE PES International Conference and Exhibition on Innovative Smart Grid Technologies (ISGT Europe)*. 2011

[2.37] Xu, L., L. Yao, and M. Bazargan. *DC grid management of a multi-terminal HVDC transmission system for large offshore wind farms*. in *International Conference on Sustainable Power Generation and Supply. SUPERGEN*. 2009

[2.38] Jovcic, D., *Offshore wind farm with a series multiterminal CSI HVDC.* Electric Power Systems Research, 2008. **78**(4): p. 747-755.http://dx.doi.org/10.1016/j.epsr.2007.05.023

[2.39] Jovcic, D. and N. Strachan, *Offshore wind farm with centralised power conversion and DC interconnection.* Iet Generation Transmission & Distribution, 2009. **3**(6): p. 586-595.http://dx.doi.org/10.1049/iet-gtd.2008.0372

[2.40] EWEA, et al., *Wind Energy - The Facts*. 2009, EWEA. http://www.wind-energy-the-facts.org/.

[2.41] Polinder, H., et al., *UpWind Deliverable 1B2 B1 - Concept report on generator topologies, mechanical & electromagnetic optimization*. 2007, Delft University of Technology / Aalborg University / University of Edinburgh. http://www.upwind.eu/publications/1b2-transmission-and-conversion (accessed Nov 2011).

[2.42] Greedy, L., *UpWind - Review of electrical drive-train topologies*. 2007, Garrad Hassan. http://www.upwind.eu/publications/5-control-systems (accessed Nov 2011).

[2.43] Milborrow, D., *Does variable speed mean more energy?* WindStats Newsletter, 2000. **13**(1): p. 4-7

[2.44] Hoffmann, R. and P. Mutschler. *The influence of control strategies on the energy capture of wind turbine*. in *IEEE World Conference on Industrial Applications of Electrical Energy*. 2000. Rome

[2.45] Carlson, O., J. Hylander, and K. Thorborg. *Survey of variable speed operation of wind turbines*. in *European Union Wind Energy Conference*. 1996. Göteborg

[2.46] Madariaga, A., et al., *Technological Trends in Electric Topologies for Offshore Wind Power Plants.* Renewable and Sustainable Energy Reviews (under revision),

[2.47] Nicolas, C., et al. *Guidelines for the design and control of electrical generator systems for new grid connected wind turbine generators*. in *28th Annual Conference of the IEEE Industrial Electronics Society*. 2002

[2.48] Warnecke, O., *Einsatz einer doppelgespeisten asynchronmachine in der grossen windenergieanlage growian.* Siemens Energietechnik, 1983. **5**: p. 362-367

[2.49] Würfel, M. and W. Hofmann. *Monitoring and diagnostics of the rotor slip-ring systems of three-phase current induction generators*. in *ICEM'2002*. 2002. Brujas

[2.50] Lipo, T., D. Panda, and D. Zarko, *Design and test of DC voltage link conversion system and Brushless Doubly-Fed Induction Generator for variable speed wind energy applications*, in *Tech. Rep. NREL subcontractor report NREL/SR-500-34583*. November 2005.

[2.51] Carlin, P., A. Laxson, and E. Muljadi, *The history and state of the art of variable-speed wind turbines technology*, in *Tech. Rep. NREL/TP-500-28607*. 2001, NREL.

[2.52] Erdman, W. and M. Behnke, *Application of medium voltage electrical apparatus of the class of variable speed multi-megawatt low wind speed turbines*, in *Subcontract report NREL/SR-500-38686*. 2005, NREL.

[2.53] Adnaness, A. *A survey of concepts for electric propulsion in conventional ice breaking osvs*. in *30th propulsion and emissions conference*. 2008

[2.54] Versteegh, J. *Design of the Zephyros Z72 wind turbine with emphasys on the direct drive PM generator*. in *Nordic Workshop on Power and Industrial Electronics (NORPIE)*. 2004. Trondheim, Norway

[2.55] Faulstich, A., J. Stinke, and F. Wittwer. *Medium voltage converter for permanent magnet wind power generators up to 5 MW*. in *European Conference on Power Electronics and Applications*. 2005

[2.56] Eichler, M., P. Maibach, and A. Faulstich. *Full size voltage converter for 5 MW wind power generators*. in *European Wind Energy Conference*. 2008

[2.57] Anaya-Lara, O., et al., *Control Challenges and Possibilities for Large Offshore Wind Farms*, in *EPE Joint Wind Energy and T&D Chapters Seminar, Trondheim, Norway, 9-11 May*. 2011. http://www.epe-association.org/epe/seminars/Wind2011/ (accessed Nov 2011).

[2.58] Butterfield, S., W. Musial, and J. Jonkman, *Engineering Challenges for Floating Offshore Wind Turbines*, in *Copenhagen Offshore Wind Conference*. 2005: Copenhagen, Denmark.

[2.59] Xiang, D.W., et al., *Coordinated control of an HVDC link and doubly fed induction generators in a large offshore wind farm.* Ieee Transactions on Power Delivery, 2006. **21**(1): p. 463-471.http://dx.doi.org/10.1109/TPWRD.2005.858785

[2.60] Liang, J., et al., *Control of multi-terminal VSC-HVDC transmission for offshore wind power*, in *Power Electronics and Applications, 2009. EPE '09. 13th European Conference on* 2009: Barcelona. http://ieeexplore.ieee.org/xpls/abs_all.jsp?arnumber=5279067.

[2.61] Xu, L., B.W. Williams, and L. Yao, *Multi-terminal DC transmission systems for connecting large offshore wind farms*, in *Power and Energy Society General Meeting - Conversion and Delivery of Electrical Energy in the 21st Century, 2008 IEEE*. 2008: Pittsburgh, PA, USA. http://dx.doi.org/10.1109/PES.2008.4596508.

[2.62] Haileselassie, T.M., et al., *Connection scheme for north sea offshore wind integration to UK and Norway: Power balancing and transient stability analysis*, in *PowerTech, 2011 IEEE Trondheim* 2011. http://dx.doi.org/10.1109/PTC.2011.6019351

[2.63] Meyer, C., *Key Components for Future Offshore DC Grids*. 2007, Technical University of Aachen: Aachen, Germany. p. 98.

[2.64] Yang, J., J.E. Fletcher, and J. O'Reilly, *Multiterminal DC Wind Farm Collection Grid Internal Fault Analysis and Protection Design.* Ieee Transactions on Power Delivery, 2010. **25**(4): p. 2308-2318.http://dx.doi.org/10.1109/Tpwrd.2010.2044813

[2.65] Lundberg, S., *Performance comparison of wind park configurations*, in *Dept. Electric Power Engineering, Chalmers University of Technology*. 2003.

[2.66] Monjean, P., et al. *Control Strategies of DC-Based Offshore Wind Farm*. in *14th European Conference on Power Electronics and Applications (EPE 2011)*. 2011

[2.67] Max, L. and T. Thiringer. *Control method and snubber selection for an 5 MW wind turbine single active bridge DC/DC converter*. in *12th European Conference on Power Electronics and Applications (EPE 2007)*. 2007

PROJECT NO.
502000064

REPORT NO.
TR A7482

VERSION
1.0

43 of 133

[2.68] Meyer, C. and R. De Doncker. *Design of a Three-Phase Series Resonant Converter for Offshore DC Grids*. in *Industry Applications Conference & 42nd IAS Anual Meeting*. 2007

[2.69] Veilleux, E. and P. Lehn. *Interconnection of direct-drive wind turbines using a distributed HVDC converter station*. in *35th Annual Conference of IEEE Industrial Electronics (IECON 2009)*. 2009

[2.70] Mogstad, A.B. and M. Molinas. *Power Collection and Integration on the Electric Grid from Offshore Wind Parks,*. in *Nordic Workshop en Power and Industrial Electronics*. June 2008

[2.71] Prasai, A., et al. *A new architecture for offshore wind farms*. in *European Conference on Power Electronics and Applications*. May 2008

[2.72] Nee, H.-P. and L. Ängquist, *Perspectives on power Electronics and Grid Solutions for Offshore Wind Farms*, in *Elforsk rapport 10:96*. Nov. 2010.

[2.73] Qin, N., et al. *Offshore wind farm connection with low frequency AC transmission technology*. in *Power & Energy Society General Meeting. PES '09*. 2009. Calgary, Canada: IEEE

[2.74] Xifan, W., C. Chengjun, and Z. Zhichao, *Experiment on fractional frequency transmission system.* Power Systems, IEEE Transactions on, 2006. **21**(1): p. 372 - 377

[2.75] Meier, S., *System Aspects and Modulation Strategies of an HVDC-based Converter System for Wind Farms*, in *School of Electrical Engineering, Electrical Machines and Power Electronics*. 2009, Royal Institute of Technology: Stockholm.

PROJECT NO.
502000064

REPORT NO.
TR A7482

VERSION
1.0

44 of 133

3 Square Wave High Frequency Rectifier

Section 2 presented different transmission architectures for offshore applications. HVAC is the most common solution for offshore wind energy transmission due to their simplicity and robustness. However, as the size of the offshore wind farms increases and they are set further offshore, HVDC VSC systems have technical and economic benefits. There are several offshore wind farms in the planning or building stage using this technology.

Alternative solutions directly tapping the wind turbines to a medium voltage collector grid are presently under study. The main benefit of these solutions is the potential cost saving promoted by the use of simpler and cheaper DC cables in the collector system, smaller and lighter high frequency transformers and the possibility of remove the offshore substation in those wind farms where this is feasible.

This section analyses an alternative DC transmission architecture where each wind turbine is directly connected to a DC cable with minor modifications within the turbine power conversion stage. An outline of the system is shown in Figure 3.1. The focus in this section is on the DC/DC converter.
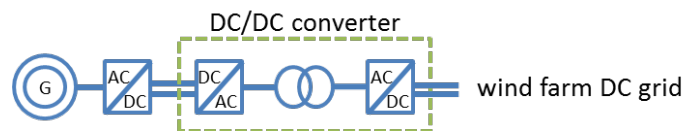
Figure 3.1: Wind turbine with high frequency DC/DC converter

The analysed system is based on the Square Wave High Frequency Rectifier (SWHFR) shown in Figure 3.2. Although the power stage is simple, the properties of the system, when controlled with a six step square voltage, make it a good choice for the connection to an HVDC line. The main difference of SWHFR in comparison with a conventional wind turbine in a HVAC or HVDC VSC system is the type of transformer, the control of the IGBT inverter and the output rectifier and filter reactance. The transformer operates with a high frequency (1-5 kHz) six pulse square wave voltage instead of the three phase sinusoidal 50-60 Hz voltage used in conventional wind turbines. This means its size and weight are smaller. An inquiry has been launched to some manufacturers in order to have real data about the dimensions and losses of a high frequency transformer suitable for a 3MW wind turbine. According to manufacturer's data it would be feasible to make a 3MW, 5 kHz, 30 kV, transformer with an approximated size of 2000x560x700 mm and estimated losses of about 3 kW. A very significant reduction in terms of size and losses in comparison with a similar 50 Hz transformer (size: 2210x770x2200, losses: 30 kW) can be achieved. At the output of the transformer, a three phase diode rectifier is connected to an output filter (a series reactance and parallel capacitor). The final result is a converter with very similar volume when compared with state of the art converters used today but with a DC output.

The proposed system, unlike a conventional HVDC VSC system, can dispense with the use of the offshore VSC converter station in those wind farms where the power is low enough to be transmitted at a medium voltage level suitable to be used inside the wind turbines. In these situations each wind turbine can be directly connected to the HVDC line. If series connection of two wind turbines in a ±80 kV bipolar configuration is considered, a power level up to 450 MW can be transmitted with state of the art cable technology and without using an offshore substation. In addition, as only two wind turbines are connected in series, problems related to series connection are minimized. Despite this solution is preferred in terms of costs, redundancy and flexibility of installation, it is also possible to use the SWHFR topology with a lower voltage collector grid and an offshore substation with a DC/DC converter. The usage of the SWHFR technology under these circumstances still allows for a reduction of the transformer size and the use of cheaper DC cables in the collector system.
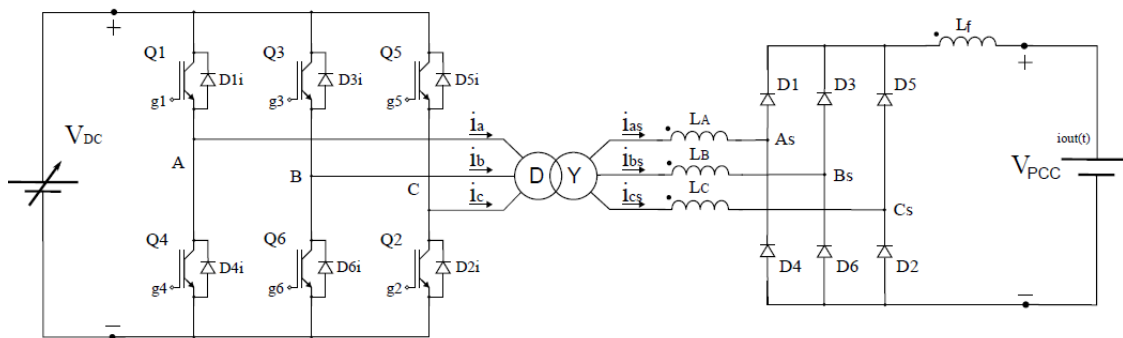
Figure 3.2: Square Wave High Frequency Converter

3.1 Analytical study

3.1.1 Three phase VSC output voltage

The output voltage of a three phase voltage source converter can take 8 different values depending on the combination of the IGBT conduction states. This is so because the upper and lower IGBTs connected to one phase cannot be simultaneously conducting in order to avoid a short circuit in the DC bus voltage. The state where the upper and lower IGBTs connected to one phase are both open will not be considered as it is not used under normal operating conditions although it takes place during the death time protection when the current is switched from the upper IGBT to the lower IGBT and vice versa.

The following switching functions are defined:

$$S_A = \begin{cases} 1 \ if \ Q_1 closed \ and \ Q_4 \ open \\ 0 \ if \ Q_1 open \ and \ Q_4 \ closed \end{cases}$$

$$S_B = \begin{cases} 1 \ if \ Q_3 closed \ and \ Q_6 \ open \\ 0 \ if \ Q_3 open \ and \ Q_6 \ closed \end{cases}$$

$$S_C = \begin{cases} 1 \ if \ Q_5 closed \ and \ Q_2 \ open \\ 0 \ if \ Q_5 open \ and \ Q_2 \ closed \end{cases}$$

The inverter state is perfectly defined by the three switching functions. The resulting 8 voltage combinations are shown in Table 3.1. The inverter output voltage is normalized using the input DC bus voltage, V_{DC}, as reference.

Table 3.1: Normalised inverter output voltage.

Switch position S_A-S_B-S_C	$\dfrac{V_{AN}}{V_{DC}}$	$\dfrac{V_{BN}}{V_{DC}}$	$\dfrac{V_{CN}}{V_{DC}}$	$\dfrac{V_{AB}}{V_{DC}}$	$\dfrac{V_{BC}}{V_{DC}}$	$\dfrac{V_{CA}}{V_{DC}}$
000	0	0	0	0	0	0
100	2/3	-1/3	-1/3	1	0	-1
110	1/3	1/3	-2/3	0	1	-1
010	-1/3	2/3	-1/3	-1	1	0
011	-2/3	1/3	1/3	-1	0	1
001	-1/3	-1/3	2/3	0	-1	1
101	1/3	-2/3	1/3	1	-1	0
111	0	0	0	0	0	0

The SWHFR system controller applies a six pulse square control to obtain a fixed pattern square wave output voltage of the converter with a fixed frequency. Figure 3.3 shows the switching function sequence and the inverter output phase to phase voltage six pulse square voltage waveform. The frequency of the six pulse square waveform f_{sw} is equal to the switching frequency of the input voltage source converter.

3.1.2 Ideal transformer and rectifier output voltage

The inverter six pulse square waveform output voltage shown in Figure 3.3 is applied to the input of the transformer. Basic three-phase transformers can have a combination of star (wye) and delta primary and secondary winding arrangements. The output voltage of the transformer varies with the winding configuration. Neglecting the reactance voltage drop, the output voltage waveform has the same shape than the input voltage waveform with a $\Delta - \Delta$ and a $Y - Y$ configuration. The ideal transformer output voltage, V_{DC}^* is defined as

$$V_{DC}^* = \frac{N_S}{N_P} V_{DC} \qquad (1)$$

Where N_S is the number of turns in the secondary, N_P is the number of turns in the primary and V_{DC} is the input DC voltage.

PROJECT NO.
502000064

REPORT NO.
TR A7482

VERSION
1.0

47 of 133
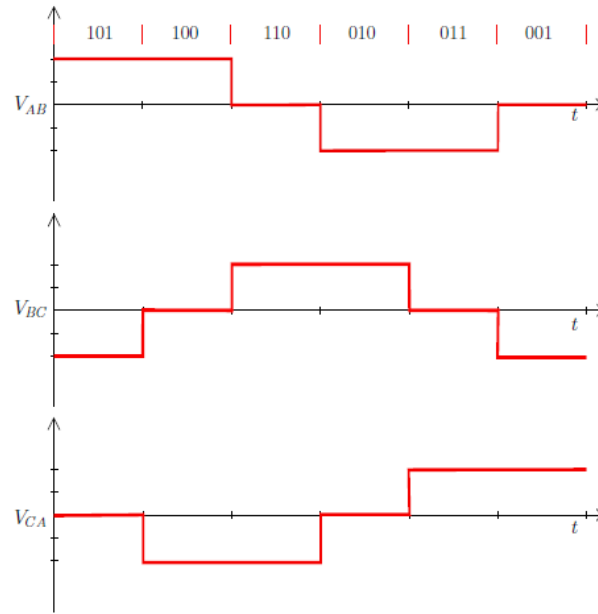
Figure 3.3: VSC output phase to phase voltage.

For the $\Delta - \Delta$ and the $Y - Y$ configuration, the transformer output line to line voltages are:

$$V_{AsBs} = \frac{N_S}{N_P} V_{AB}$$

$$V_{BsCs} = \frac{N_S}{N_P} V_{BC} \tag{2}$$

$$V_{CsAs} = \frac{N_S}{N_P} V_{CA}$$

For the $\Delta - Y$ configuration, the transformer output line to line voltages are:

$$V_{AsBs} = \frac{N_S}{N_P} (V_{AB} - V_{BC})$$

$$V_{BsCs} = \frac{N_S}{N_P} (V_{BC} - V_{CA}) \tag{3}$$

$$V_{CsAs} = \frac{N_S}{N_P} (V_{CA} - V_{AB})$$

For the $Y - \Delta$ configuration, the transformer output line to line voltages are:

$$V_{AsBs} = \frac{N_S}{N_P} V_{AN}$$

$$V_{BsCs} = \frac{N_S}{N_P} V_{BN} \tag{4}$$

$$V_{CsAs} = \frac{N_S}{N_P} V_{CN}$$

Under ideal conditions the output voltage of the rectifier is the maximum phase to phase voltage.

$$V_{out} = \max\{V_{AsBs}, V_{BsCs}, V_{CsAs}, V_{BsAs}, V_{CsBs}, V_{AsCs}\} \tag{5}$$

The output voltages of the four possible winding configurations for the 8 switch combinations are shown in Table 3.2.

PROJECT NO.
502000064

REPORT NO.
TR A7482

VERSION
1.0

48 of 133

Table 3.2: Transformer phase to phase output voltages for different switch positions and transformer winding configurations.

Switch position	Δ-Δ and Y-Y			Δ-Y			Y-Δ		
	$\frac{V_{A_sB_s}}{V^*_{DC}}$	$\frac{V_{B_sC_s}}{V^*_{DC}}$	$\frac{V_{C_sA_s}}{V^*_{DC}}$	$\frac{V_{A_sB_s}}{V^*_{DC}}$	$\frac{V_{B_sC_s}}{V^*_{DC}}$	$\frac{V_{C_sA_s}}{V^*_{DC}}$	$\frac{V_{A_sB_s}}{V^*_{DC}}$	$\frac{V_{B_sC_s}}{V^*_{DC}}$	$\frac{V_{C_sA_s}}{V^*_{DC}}$
000	0	0	0	0	0	0	0	0	0
100	1	0	-1	1	1	-2	2/3	-1/3	-1/3
110	0	1	-1	-1	2	-1	1/3	1/3	-2/3
010	-1	1	0	-2	1	1	-1/3	2/3	-1/3
011	-1	0	1	-1	-1	2	-2/3	1/3	1/3
001	0	-1	1	1	-2	1	-1/3	-1/3	2/3
101	1	-1	0	2	-1	-1	1/3	-2/3	1/3
111	0	0	0	0	0	0	0	0	0

When the input VSC is controlled to achieve a six pulse square wave voltage at the output, the resulting rectifier output voltages during steady state for the different transformer configurations are:

$$Y - \Delta \rightarrow V_{out} = \frac{2}{3} V^*_{DC}$$

$$Y - Y \text{ or} \Delta - \Delta \rightarrow V_{out} = V^*_{DC} \tag{6}$$

$$\Delta - Y \rightarrow V_{out} = 2V^*_{DC}$$

The equivalent $\Delta - Y$ transformer output circuits connected to the diode bridge are shown in Figure 3.4 for the six switching states of the VSC.

3.1.3 Transformer and rectifier output voltage during overlap

Once the ideal voltage output of the transformer has been calculated, the effect of the overlap due to the current commutation from one diode to another will be introduced. If the impedance of the transformer is neglected, the current transfers instantly from one diode to another with higher anode potential in the rectifier stage. However, due to the transformer leakage inductance and the series inductance, in practice, the current takes a finite time to fall in the diode turning off and rise in the diode turning on. The leakage inductance plus any additional inductance connected in series with the transformer output are introduced in the model in this section. The total series inductance in the three phases is considered to be equal, that is

$$L_A = L_B = L_C = L_{leak} + L_{series} = L_l \tag{7}$$
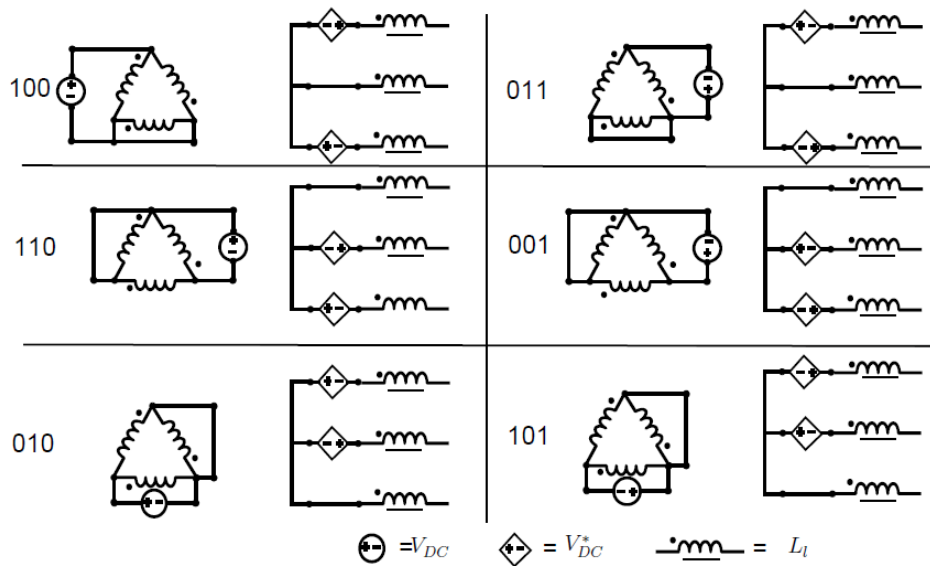
Figure 3.4: Transformer equivalent circuit for the six switching states.

The DC voltage at the point of common coupling in the HVDC line, V_{PCC}, is considered to be constant and the converter output voltage is modeled as a constant voltage source. The small voltage ripple in the DC line voltage can be neglected. The HVDC converter onshore will be in charge of maintaining this voltage constant. Regardless of the transformer connection type, when the current at the output of the rectifier is continuous, every time the state of the inverter is changed, an overlap takes place with the same duration and output voltage. The overlap effect takes place each time the controller changes the switch position and six overlaps take place each period of the six pulse square waveform. For simplicity the following new variables are defined:

$$f_{eq} = 6f_{sw} \tag{8}$$

$$T_{eq} = \frac{1}{f_{eq}} \tag{9}$$

$$D = \frac{T_{eq} - \Delta t_\mu}{T_{eq}} \tag{10}$$

where f_{eq} is the equivalent switching frequency of the output rectifier, T_{eq} is the corresponding equivalent period, f_{sw} is the switching frequency of the input voltage source converter, and Δt_μ is the overlap time.

In general terms, the overlap effect in a rectifier with series inductance and constant current at the output takes place when one diode D_x is conducting an a second diode D_y with a common cathode (or anode) is forward biased and is turned on. The leakage inductance of the transformer connected in series with each diode, L_x and L_y, limit the rate of change of current in D_x as i_x decreases from I_{DC} to 0 and in D_y as i_y increases from 0 to I_{DC}. A circulating current, i, flows between the two diodes. If the transformer leakage inductances are identical ($L_x = L_y = L_l$), the output voltage during commutation, V_{out}, is mid-way between the conducting phase voltages V_x and V_y, creating a series of notches in the output voltage waveform. This interval during which both D_x and D_y conduct is termed the overlap period and it is defined by the overlap time Δt_μ. Ignoring diode voltage drops, the overlap duration and the resulting rectifier output voltages are calculated below for different transformer connections.

The most convenient transformer connection for the application is the $\Delta - Y$ and with this type of connection the overlap process can be described as follows (Figure 3.5):

PROJECT NO.
502000064

REPORT NO.
TR A7482

VERSION
1.0

50 of 133

(a) Before overlap (100)

(b) During overlap (110)

(c) After overlap (110)
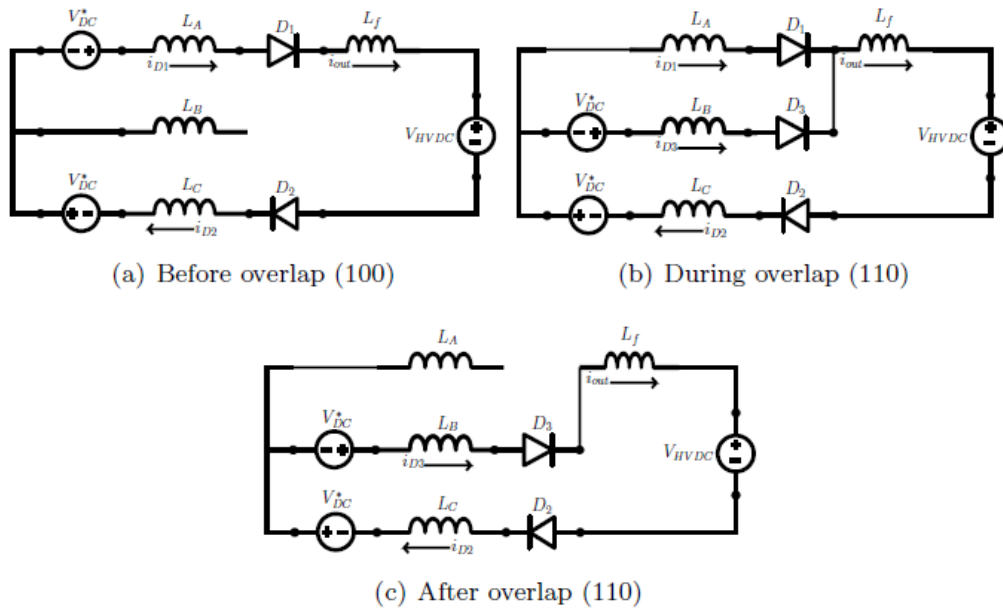
Figure 3.5: 100-110 transition with $\Delta - Y$ connected transformer.

Initially, the VSC converter state of the switches is 100 and the diode connected to the upper side of phase A, D_1, and the diode connected to the lower side of phase C, D_2, are conducting.

Then, at instant t_1, the controller changes the switches to the 110 state. The current in the diode D_1 must fall to zero and the current in the diode connected to the upper side of phase B, D_3, which is forward biased, must rise until it carries all the output current. Due to the existing inductance, this current change takes some time, and an overlap (simultaneous conduction of two upper or lower diodes) takes place. This process takes place between t_1 and t_2 with a duration of Δt_μ.

Before, during and after the overlap interval, D_2 carries the output current $i_{out}(t)$. During overlap, the voltages in the equivalent series inductances of the transformer are:

$$\frac{di_{out}(t)}{dt} \approx -\frac{\Delta I}{\Delta t_\mu} \tag{11}$$

$$V_{Lf} = -L_f \frac{\Delta I}{\Delta t_\mu} \tag{12}$$

and

$$V_{LA} = L_l \frac{di_A}{dt} = L_l \frac{di_{D1}}{dt}$$

$$V_{LB} = L_l \frac{di_B}{dt} = L_l \frac{di_{D3}}{dt} \tag{13}$$

$$V_{LC} = L_l \frac{di_{out}(t)}{dt} \approx L_l \frac{\Delta I}{\Delta t_\mu}$$

where ΔI is the change in the output current during overlap and $\Delta t_\mu = t_2 - t_1$ is the duration of the overlap process. The voltages in L_A and L_B can be obtained as follows

$$i_{D1}(t) + i_{D3}(t) = i_{out}(t) \tag{14}$$

$$V_{LA} + V_{LB} = L_l \frac{di_{out}(t)}{dt} \approx -L_l \frac{\Delta I}{\Delta t_\mu} \tag{15}$$

and

PROJECT NO.
502000064

REPORT NO.
TR A7482

VERSION
1.0

51 of 133

$$V_{LA} = -V_{DC}^* + V_{LB}$$

$$V_{LA} \approx -\frac{V_{DC}^*}{2} - L_l \frac{\Delta I}{2\Delta t_\mu} \tag{16}$$

$$V_{LB} \approx \frac{V_{DC}^*}{2} - L_l \frac{\Delta I}{2\Delta t_\mu}$$

The interval during which both D_1 and D_3 conduct, Δt_μ, can be calculated as the time that the current in D_1 falls from the maximum value of the output current, I_{outMAX}, to 0. As the derivative of the current can be considered constant then

$$\frac{di_{D1}}{dt} \approx -\frac{I_{outMAX}}{\Delta t_\mu} \approx -\frac{V_{DC}^*}{2L_l} - \frac{\Delta I}{2\Delta t_\mu} \tag{17}$$

$$I_{outMAX} = I_{DC} + \frac{\Delta I}{2} \tag{18}$$

$$\Delta t_\mu \approx \frac{2L_l I_{DC}}{V_{DC}^*} \tag{19}$$

The rectifier output voltage during overlap, V_{outMIN}, is

$$V_{outMIN} = -V_{LA} + V_{DC}^* + V_{LC} = \frac{3}{2}V_{DC}^* + \frac{3}{2}L_l \frac{\Delta I}{\Delta t_\mu} \tag{20}$$

The output current will fall with constant slope if

$$\frac{3}{2}V_{DC}^* + \frac{3}{2}L_l \frac{\Delta I}{\Delta t_\mu} < V_{PCC} \tag{21}$$

which will be the case in a properly designed converter. The output current decrease can be obtained from the voltage in the output filter inductance

$$V_{Lf} = L_f \frac{di_{out}(t)}{dt} \approx L_f \frac{-\Delta I}{\Delta t_\mu} \tag{22}$$

$$V_{Lf} = V_{outMIN} - V_{PCC} \tag{23}$$

$$\Delta I = \frac{1}{\frac{3}{2} + \frac{L_f}{L_l}}\left[\frac{2V_{PCC}}{V_{DC}^*} - 3\right]I_{DC} \tag{24}$$

If the DC bus voltage rises above the following limit

$$V_{DC}^* = \frac{2}{3}V_{PCC} \tag{25}$$

ΔI would be negative and the equation is no longer valid.

From equation 19, when $\Delta t_\mu > T_{eq}$, a maximum current value is obtained, above which, the overlap is not finished before the next switching state. This value is

$$I_{DCMAX} = \frac{1}{2}\frac{V_{DC}^*}{L_l f_{eq}} \tag{26}$$

Above this limit, the overlap process is extended to the next switching cycle and the previous results are no longer valid.

In order to have current flowing in the diodes and the overlap finished before the next switching takes place, the following conditions must be fulfilled

$$\frac{V_{PCC}}{2} \leq V_{DC}^* \leq \frac{2V_{PCC}}{3} \tag{27}$$

From equation 24 it is clear that ΔI is always lower than I_{DC} and the converter always operates with continuous current in the rectifier output inductance, L_f. The maximum ripple to DC current takes place when

PROJECT NO.
502000064

REPORT NO.
TR A7482

VERSION
1.0

52 of 133

$$L_f \ll L_l \quad \text{and} \quad V_{DC}^* = \frac{V_{PCC}}{2}, \tag{28}$$

under these conditions

$$\Delta I_{MAX} = \frac{2}{3} I_{DC} \tag{29}$$

Once the current from the diode D_1 has been transferred to the diode D_3, at instant t_2 the diode D_1 is open circuited, the overlap is finished and the final circuit configuration is that corresponding to the switch 110 position (Figure 3.5c). This state has a duration of $T_{eq} - \Delta t_\mu$, until the next switching state is selected. During this interval, the rectifier output voltage, V_{outMAX}, is

$$V_{outMAX} = 2V_{DC}^* - 2L_l \frac{\Delta I}{T_{eq} - \Delta t_\mu} \tag{30}$$

or

$$V_{outMAX} = V_{PCC} + L_f \frac{\Delta I}{T_{eq} - \Delta t_\mu} \tag{31}$$

The rectifier output voltage waveform, $V_{out}(t)$, can be written in each switching state of the voltage source converter as

$$V_{out}(t) = \begin{cases} V_{outMIN} & \text{if } 0 < t < \Delta t_\mu \\ V_{outMAX} & \text{if } \Delta t_\mu < t < T_{eq} \end{cases} \tag{32}$$

The resulting output current waveform will be a sawtooth curve with constant falling slope during overlap and raising slope when the overlap is finished, as shown in Figure 3.6.
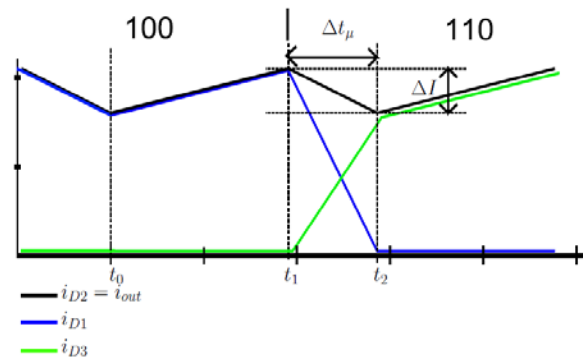
Figure 3.6: Resulting rectifier diode currents.

During steady state operation, the average voltage in the filter inductance is zero. If the resistive voltage drop from the rectifier output to the HVDC line is negligible, the average value of the current is constant and the rectifier average output voltage must be equal to the HVDC line voltage at the point of connection of the converter. The rectifier output voltage waveform, $V_{out}(t)$, is shown in Figure 3.7 together with the DC line voltage, V_{PCC}. The positive (red) and negative (green) areas in Figure 3.7 must be equal in steady state and the output current is periodical with a sawtooth waveform.

PROJECT NO.
502000064

REPORT NO.
TR A7482

VERSION
1.0

53 of 133
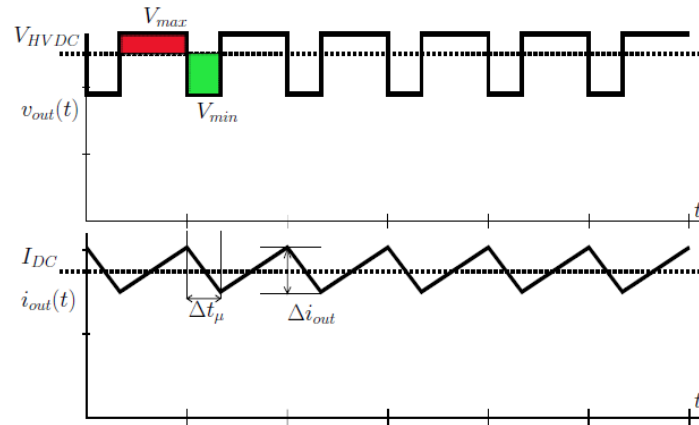
Figure 3.7: Output voltage and current waveforms.

If the series resistance of the output filter inductance is small, the average rectifier output voltage must be

$$\langle V_{out} \rangle = V_{PCC} \tag{33}$$

The average rectifier output voltage, $\langle V_{out} \rangle$, is

$$\langle V_{out} \rangle = 2V_{DC}^* - \langle V_{LB} \rangle - \langle V_{LC} \rangle \tag{34}$$

The average voltage from 0 to T_{eq} en the L_C inductance is zero (the current is periodic) and the average voltage in the series inductance connected to diode D_3 is determined by the current increase from 0 to $I_{MAX} = I_{DC} + \frac{\Delta I}{2}$ that is

$$\langle V_{LC} \rangle = 0$$

$$\langle V_{LB} \rangle = f_{eq} \int_0^{T_{eq}} V_{LB}(t)dt = f_{eq} L_l (I_{DC} + \frac{\Delta I}{2}) \tag{35}$$

$$\langle V_{out} \rangle = 2V_{DC}^* - f_{eq}L_l \left(I_{DC} + \frac{\Delta I}{2} \right) = 2V_{DC}^* - f_{eq}L_l I_{outpeak} \tag{36}$$

where $I_{outpeak} = I_{DC} + \frac{\Delta I}{2}$ is the peak of the output current.

Assuming negligible filter and cable resistances, V_{PCC} will remain constant for any value of the output current. Therefore, using (36) it is possible to estimate the maximum and minimum value that V_{DC}^* will take as a function of the output current. If the output current is 0 then $I_{outpeak}=0$ and

$$V_{DCMIN}^* = \frac{V_{PCC}}{2} \tag{37}$$

If, on the contrary, the output current is the maximum,

$$V_{DCMAX}^* = \frac{V_{PCC}}{2} + \frac{L_l f_{eq} I_{outpeak}}{2} \tag{38}$$

If adequate parameters are used in the transformer design the term $\frac{L_l f_{eq} I_{outpeak}}{2}$ will be small in comparison with $\frac{V_{PCC}}{2}$ and the DC bus voltage will keep almost constant. Therefore the SWHFR converter can be operated in open loop within its nominal operating range without experiencing critical variations in the DC bus voltage. This is a very desirable feature of the proposed converter because there is no need of control parameter tuning. The DC bus in the back-to-back converter of the SWHFR system (Figure 3.2) is fed from the generator through a conventional voltage source converter. This voltage source converter is controlled to achieve maximum power point tracking in the wind turbine and optimize power output. This control will function normally if the DC bus voltage,

PROJECT NO.
502000064

REPORT NO.
TR A7482

VERSION
1.0

54 of 133

V_{DC}, is kept within well-defined boundaries. When the generator starts generating power, current is delivered to the DC bus. If the bus voltage is below V_{DCmin}, there is not enough voltage, the SWHFR power converter will draw no current from the capacitors, and the voltage will rise until it starts delivering power. The voltage will rise and reach an equilibrium voltage when the input and output current of the capacitors are equal and the DC bus voltage is constant. The DC bus voltage will stay within the restricted range given by (37) and (38) without feedback control.

3.1.4 Current waveforms in the SWHFR

The load current determines the current waveforms in the transformer secondary windings. The secondary currents, in turn, shape the current in the primary windings of the transformer and in the VSC converter.

During the interval between t_0 and t_1 (see Figure 3.6), the inverter switching function value is 100 and the upper diode of phase A, D_1, and the lower diode of phase C, D_6, are carrying the output current. The rest of the diodes are in the off state. The transformer secondary currents are:

$$I_{Asec} = I_{D1}$$
$$I_{Bsec} = 0 \tag{39}$$
$$I_{Csec} = -I_{D2}$$

At t_1, the switching state of the inverter is changed from 100 to 110 and the current in diode D_1 must be transferred through the overlap process to diode D_3. During the overlap time between t_1 and t_2, the load current is shared between D_1 and D_3. The current in D_1 decreases linearly from $I_{outpeak}$ to 0 and the current in D2 increases linearly from zero to $I_{outpeak} - \Delta I$. The transformer secondary currents are:

$$I_{Asec} = I_{D1}$$
$$I_{Bsec} = I_{D3} \tag{40}$$
$$I_{Csec} = -I_{D2}$$

At t_2, the overlap process is finished and all the current in D_1 has been transferred to D_3. The transformer secondary currents are:

$$I_{Asec} = 0$$
$$I_{Bsec} = I_{D3} \tag{41}$$
$$I_{Csec} = -I_{D2}$$

A similar reasoning can be used throughout the rest of the intervals and the secondary phase currents of Figure 3.8 are obtained. If the magnetizing current is neglected, which is reasonable with a well constructed transformer, the primary currents in the case of a $\Delta - Y$ connected transformer are:

$$I_{Aprim} = \frac{N_S}{N_P}(I_{Asec} - I_{Csec})$$
$$I_{Bprim} = \frac{N_S}{N_P}(I_{Bsec} - I_{Asec}) \tag{42}$$
$$I_{Csec} = \frac{N_S}{N_P}(I_{Csec} - I_{Bsec})$$

Figure 3.8 shows the ideal transformer secondary currents and the corresponding primary currents.

PROJECT NO.
502000064

REPORT NO.
TR A7482

VERSION
1.0

55 of 133
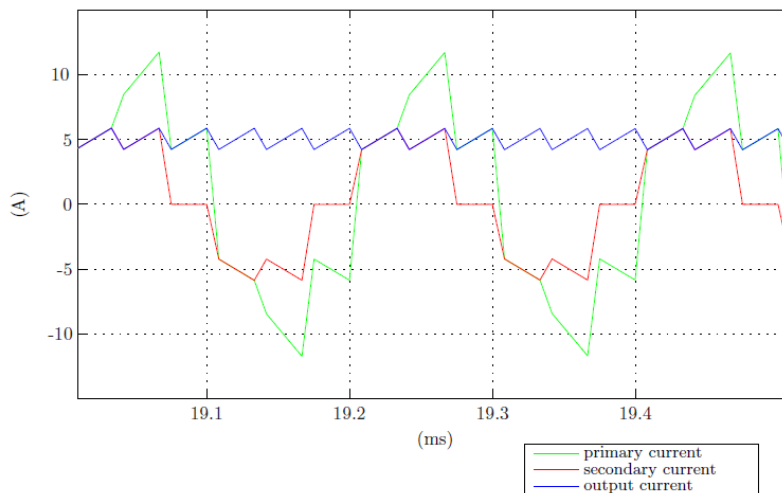
Figure 3.8: Theoretical transformer primary and secondary currents.

3.1.5 Power losses

This section analyzes the power losses of the SWFR converter. The losses of the VSC input converter, the medium voltage diode rectifier and the high frequency transformer are estimated and some conclusions are derived.

3.1.5.1 Power losses in the input VSC

The transformer primary currents determine the currents and the corresponding power losses in the inverter semiconductors (diodes and IGBTs). Figure 3.9 shows the current in phase A of the inverter and the voltage and currents waveforms in the upper IGBT and diode connected to phase A, during a commutation cycle of the upper IGBT Q1 (see Figure 3.2) .
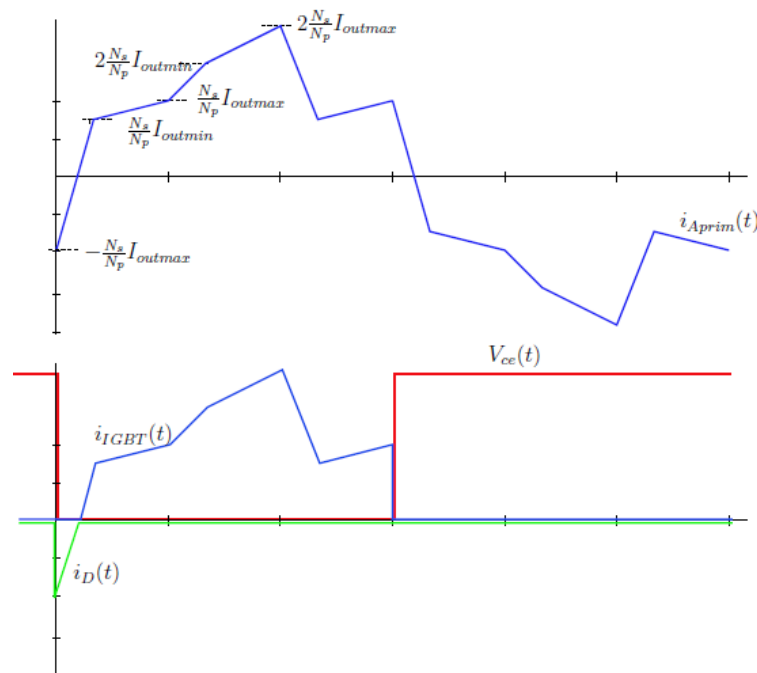
Figure 3.9: Ideal transformer primary currents, IGBT and diode currents and collector-emisor IGBT voltage.

PROJECT NO.
502000064

REPORT NO.
TR A7482

VERSION
1.0

56 of 133

When the phase current is negative, the diode must carry the phase current and when this current is positive, it flows through the IGBT. As it can be appreciated in the figure, the diode is turned off and the Q1 IGBT is turned on at zero voltage and the switching power losses are zero. When the IGBT is turned off, an inductive hard switching takes place between IGBT and diode. Thus, half of the semiconductor turn on and turn off processes are zero voltage switchings and significant power loss reduction is achieved.

A second consequence of the current waveforms is that the diodes carry a very low proportion of the current and they can be down rated and be more efficient compared to a conventional inverter.

The only switching power loss in the converter is the IGBT turn off power, that is

$$P_{switch} = P_{IGBToff} \tag{43}$$

The waveforms in the six diodes and six IGBTs in the input VSC are identical. The total power loss in the VSC converter is

$$P_{VSCloss} = 6(P_{Don} + P_{IGBTon} + P_{switch}) \tag{44}$$

where P_{Don} and P_{IGBTon} are the diode a IGBT conduction losses respectively.

The power losses of the Voltage Source Converter have been simulated and compared to a Voltage Source Converter delivering the same power to a 50 Hz AC grid (as is the case in a conventional wind turbine) for different IGBTs and power levels. The simulations have been done using the Powersim PSIM simulation tool, and more specifically, the Thermal Module available to study losses of power converters. The studied examples are:

1. 75 kW PWM sinusoidal output inverter and HFSWR converter using a sixpack Semikron 653GD176HDc SEMiX module.
2. 200 kW PWM sinusoidal output inverter and HFSWR converter using three dual Semikron 854GB176HDs SEMiX modules.
3. 500 kW PWM sinusoidal output inverter and HFSWR converter using six discrete Infineon FF1200R17KP4B2 modules.

The DC bus voltage is 1100 V and the switching frequency is 5 kHz. The power factor in the sinusoidal PWM output used is unity. The PWM sinusoidal inverter feeds the power to a 50 Hz, 690 V grid and the HFSWR delivers power to a 33 kV DC line through a high frequency transformer.

The simulation results of the power loss are shown in Figure 3.10, in the lower part of the figure as percentage of total power, and in the upper part in absolute terms in watts. In all cases there is an important reduction in power loss in the VSC using the proposed SWHFR converter instead of conventional sinusoidal PWM output. This reduction is most significant in the diode switching losses, which are almost eliminated in the case of the SWHFR.

PROJECT NO.
502000064

REPORT NO.
TR A7482

VERSION
1.0

57 of 133
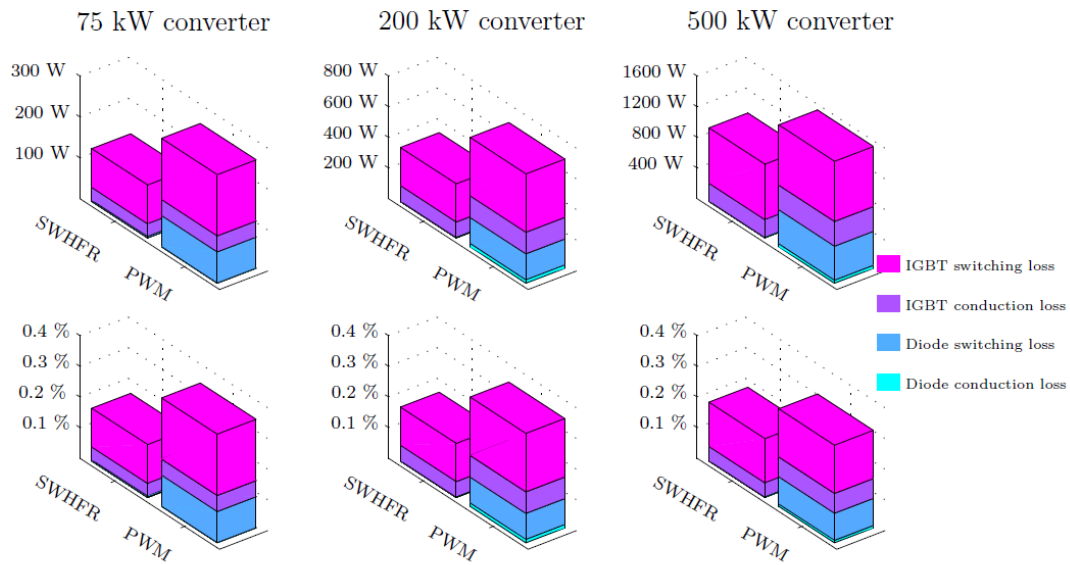
Figure 3.10: Semiconductor power losses

3.1.5.2 Power losses in the output rectifier

In a high voltage rectifier, each diode is actually formed by a series connection of n diodes. The conduction loss in each string of diodes (or series diode block) is

$$P_{string\_cond} = n\left(V_{TO}I_{aveg} + R_{don}I_{RMS}^2\right) \tag{45}$$

where V_{TO} is the diode threshold voltage, R_{don} is the diode dynamic resistor and I_{aveg} and I_{RMS} are the average and RMS values of the diode current.

Table 3.3 shows the main characteristics of several diodes that could be used for this application, depending on the desired current level.

The only considerable switching losses in the rectifier are the diode reverse recovery losses. Diode reverse recovery losses are directly proportional to $\frac{di}{dt}$ in the diode. With a transformer leakage inductance of high enough value, a low $\frac{di}{dt}$ is obtained. Consequently switching losses are negligible.

The equalizing resistors in the series diode branches introduce additional power loss. When the power converter is switching, this power loss is (see Figure 3.11a):

$$P_{Rloss} = \frac{5}{2}\frac{V_{HVDC}^2}{nR_{eq}} \tag{46}$$

Where R_{eq} is the equalizing resistor associated with each diode.

Actually, the real resistive power loss during operation is slightly lower because during overlap two diodes are carrying current instead of only one.

PROJECT NO.
502000064

REPORT NO.
TR A7482

VERSION
1.0

58 of 133

Table 3.3: Diode characteristics

Model and manufacturer	V_{rrm} (V)	I_F (A)	$I_r r$ (mA)	V_{TO} (V)	R_{don} (mΩ)
Stud Type diodes					
Westcode M0130S	2500	56	20	1.29	0.00154
SEMIKRON SKN60F	1700	75	60	1	0.004
Module Type diodes					
Powerex QRD3310001	1400	84	1	1.6	0.01
Eupec DD200S65K1	6500	200	10	0.8	0.02
Disk diodes					
Westcode M0588LC	4500	588	20	1.29	0.00154
ABB 5SDF02D6004	5500	175	20	3.35	0.0072
SiC diodes					
Eupec IDH15S120	1200	15	1.5	0.9	0.1
Cree 10kv	10000	50	0.5	3.25	0.0075
Cree C2D10120A	1200	10	1	2.5	0.26
IDY15S120	1200	7.5	0.75	0.7	0.37
Axial Lead diodes					
HVCA HVW3	3000	2	0.05	1.5	0.5
UF 600M	1000	6	0.025	0.8	0.005
VMI K100UF	10000	1.5	0.1	2.5	0.3125

When the power converter is off and the diodes are blocking the DC line voltage, the power loss in the series resistances is (see Figure 3.11b):

$$P_{\text{Rloss}} = \frac{3}{2}\frac{V_{\text{HVDC}}^2}{nR_{\text{eq}}} \qquad (47)$$
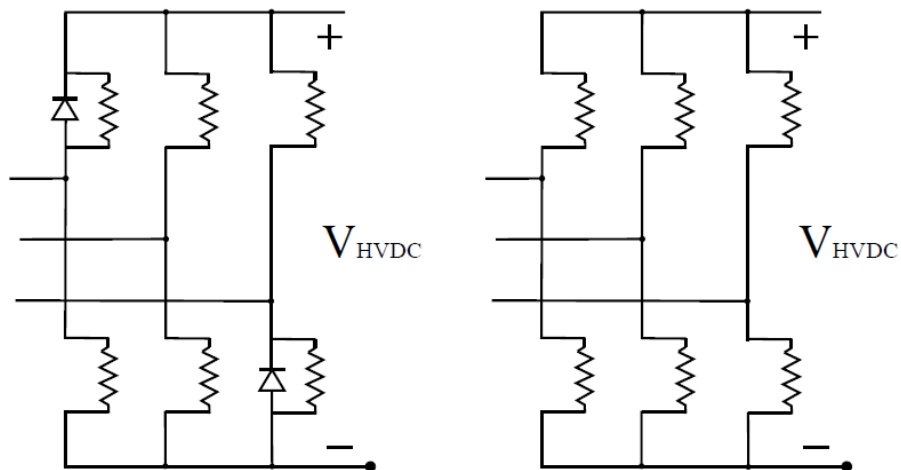
(a) Converter on. Two diodes conducting.   (b) Power off. All diodes off.

Figure 3.11: Equivalent circuit for resistive loss calculation.

The power losses in the rectifier have been calculated for different diodes. The rectifier is designed for a 33 kV DC bus. Table 3.4 shows the number of diodes, the necessary equalizing resistor and the resulting power loss for alternative 33 kV rectifiers, with different power ratings. The number of diodes, equalizing resistor values, segregated power loss values (resistive and conduction) and the percentage power loss are included in the table. The optimum choice comes from a trade of between power losses, the number and size of the diodes and the number of parallel rectifiers for a compact and simple design. The best option is the use of high voltage (10 kV) diodes. 10 kV SiC diodes have been built in research laboratories, however, there is no mass production, they are very difficult to find and they are very expensive, and only axial lead diodes are available in this voltage range.

Table 3.4: Power loss in 33 kV rectifiers.

Diode model	Output power (MW)	n	R (kΩ)	R_{loss} full load (W)	R_{loss} no load (W)	P_{on} (W)	Total loss (%)
M0130S	5.5	27	30	2504	1502	930	0.3
SKN60F	7.5	39	6	7364	4418	1100	0.6
QRD3310001	8	47	320	125	75	2150	1.2
DD200S65K1	20	10	150	1220	732	2770	0.8
M0588LC	60	15	50	2517	1510	512	0.4
5SDF02D6004	17	12	60	2544	1526	1087	0.5
IDH15S120	1.5	55	180	186	111	2747	1.8
10kv	5	7	4600	59	36	621	0.2
C2D10120A	1	55	275	124	74	7383	3.5
IDY15S120	1.5	55	400	125	75	809	5.8
HVW3	0.2	22	150000	1	0	1200	0.6
600M	0.6	66	10000	4	2	2100	0.4
K100UF	0.15	7	25000	16	9	250	0.2

In any case, power losses lower than those resulting in a HVDC VSC station (1 %) can be achieved. As an example, a 150 kW 33 kV rectifier built using Voltage Multipliers K100UF axial lead diode is formed using 7 series diodes in each rectifier arm. The parallel equalizing resistor value is 25M. The power loss generated in the equalizing resistors is very small (16 W). The conduction losses in the diodes is 250 W. The resulting power losses in the rectifier are only 0.2 % of the total power.

In addition a significant loss reduction can be achieved in the transformer. The use of a high frequency transformer allows for a reduction in the losses about an order of magnitude in comparison with a 50 Hz transformer. Conventional transformer losses are around 1% whereas the high frequency transformers present losses of about 0.1-0.2% of the nominal power.

3.2 Simulation and experimental results

For the experimental validation of the topology four SWHFR converters with a nominal power of 4 kW and an output voltage up to 700 V have been made. The high frequency transformer of each SWHFR converter has been built using three T60004-L2160-W758 cores made of VITROPERM from Vacuumschmelze with a turn ratio between primary and secondary of 1:1. The diode rectifiers have been built using SK80D12F three phase fast diode bridges from Semikron. Each SWHFR converter is controlled with a TMS320F2812 DSP from Texas Instruments. Monopolar, series and parallel configurations with up to four converters have been tested. Different leakage transformer inductances have been used in the experimental validation in order to check the effect of the overlapping process. Figure 3.12 shows a picture of the experimental platform.

PROJECT NO.
502000064

REPORT NO.
TR A7482

VERSION
1.0

60 of 133
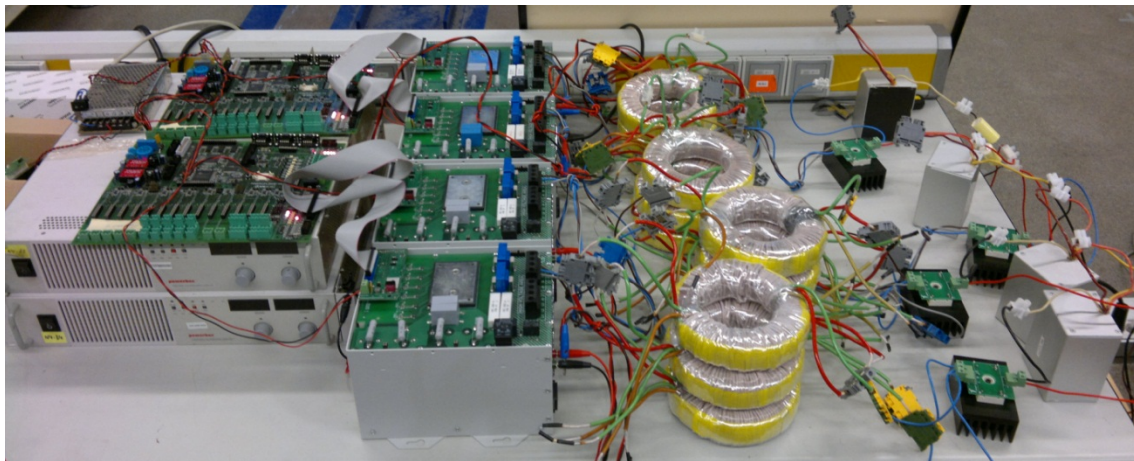
Figure 3.12: Experimental platform.

Models for the monopolar, series and parallel configurations with the same electric parameters as the experimental platform have been developed in Matlab/Simulink. As will be shown below, there is a good match between the experimental and simulated results, so it can be concluded that the simulation models represent quite precisely the performance of the real system. Based on this validation, and the assumption there are no dramatic scaling effects when considering higher power and voltage, the simulation models are expected to give accurate results also when simulating a real system with a nominal power of about 3 MW and output voltage of 80 kV.

Figure 3.14 show the experimental (blue) and simulation (dark blue) results of one converter in monopolar configuration (Figure 3.13). The DC bus is fed with a 120 V DC source. The output of the converter is connected to a 98 ohms resistive load. A 20 μH leakage inductance and a switching frequency of 2.5 kHz have been used. From top to bottom and left to right the waveforms shown in Figure 3.14 are the following: current in the transformer primary winding, current in the transformer secondary winding, voltage waveform at the transformer primary winding, voltage waveform at the transformer secondary winding, unfiltered rectifier DC output current, unfiltered rectifier DC output voltage, DC current after the output LC filter, DC voltage at the LC filter's capacitor's terminals.

Figure 3.15 shows the same current and voltage waveforms but, in this case, a transformer leakage inductance L_l=170 μH has been assumed. It can be observed how the effect of having a higher transformer leakage inductance increases the DC unfiltered current oscillations due to the overlapping effect reported in the previous section. The most significant harmonic of the unfiltered current appears at six times the switching frequency, i.e. 15 kHz. Therefore it is relatively easy to filter it. However, the higher the leakage inductance the higher the current distortion and filter requirements. Therefore the maximum transformer leakage inductance should be limited during the design stages.
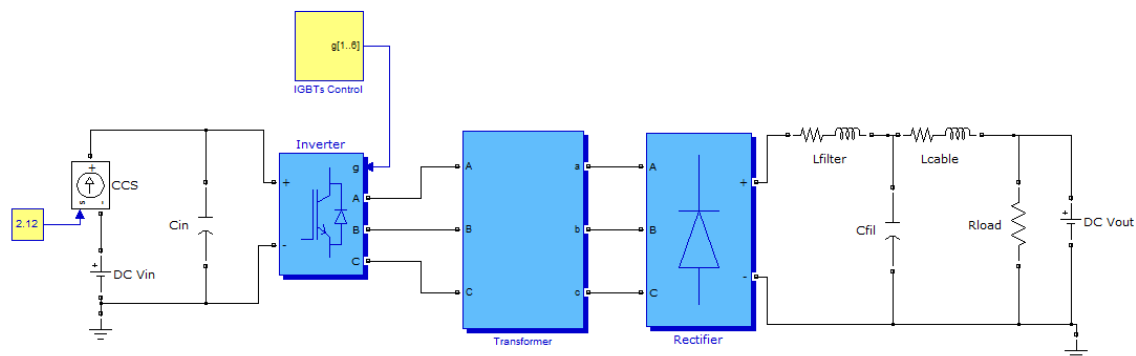
Figure 3.13: SWHFR Matlab/Simulink model.
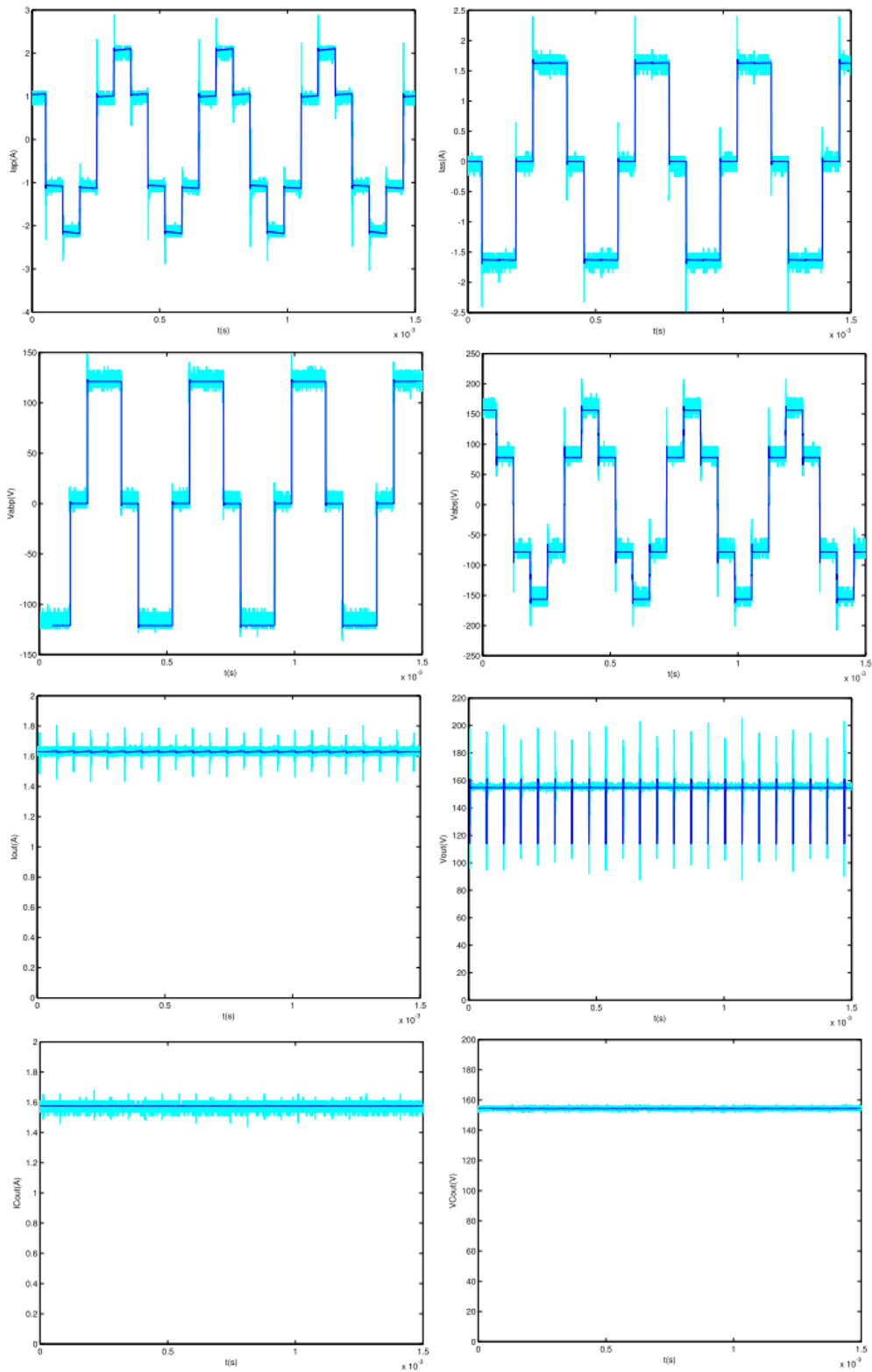
Figure 3.14: Simulation and experimental results for one converter in monopolar configuration with a leakage inductance L_l=20 µH.
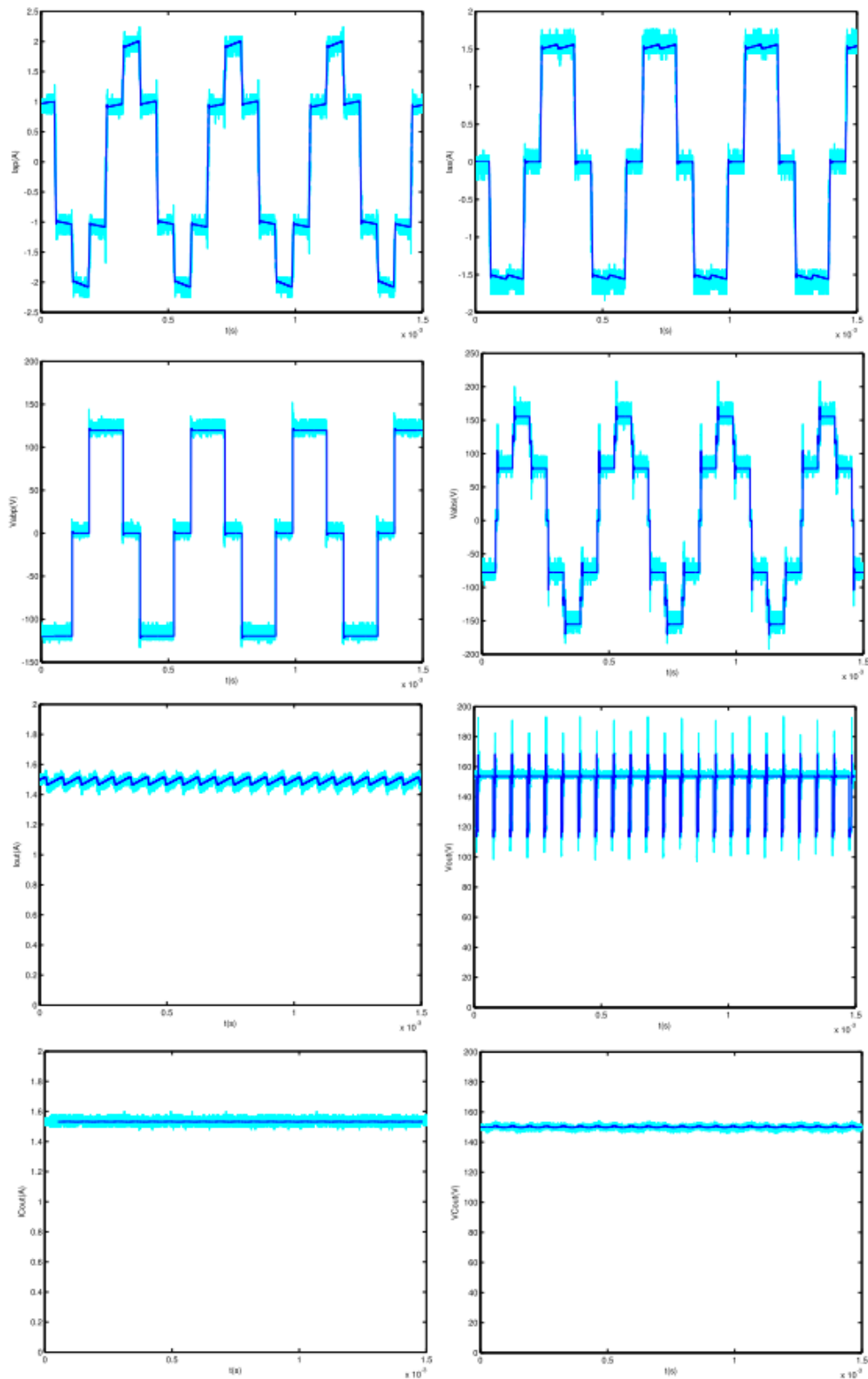
Figure 3.15: Simulation and experimental results for one converter in monopolar configuration with a leakage inductance L_l=170 µH.

Similar results have been obtained when two converters are connected in series (Figure 3.16) and in parallel (Figure 3.17). For the sake of briefness only results with a leakage inductance of 170 µH are

PROJECT NO.
502000064

REPORT NO.
TR A7482

VERSION
1.0

63 of 133

shown. The working conditions are the same that were specified previously. Figure 3.18 and Figure 3.19 show the results for the series and parallel configurations respectively. In all the cases the simulations results are confirmed quite precisely by the experimental ones.
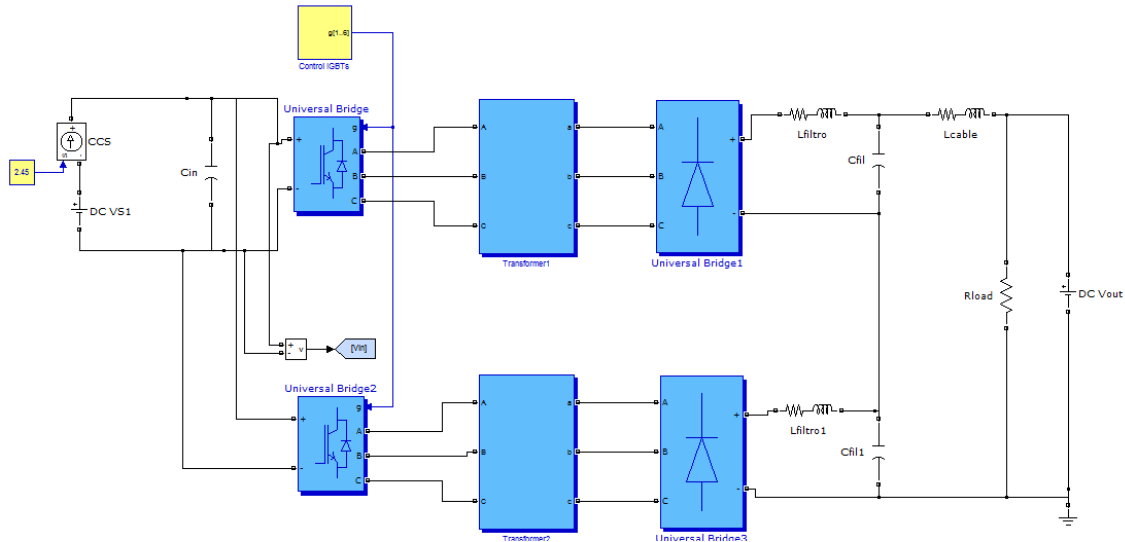
Figure 3.16: SWHFR Matlab/Simulink model in series configuration.
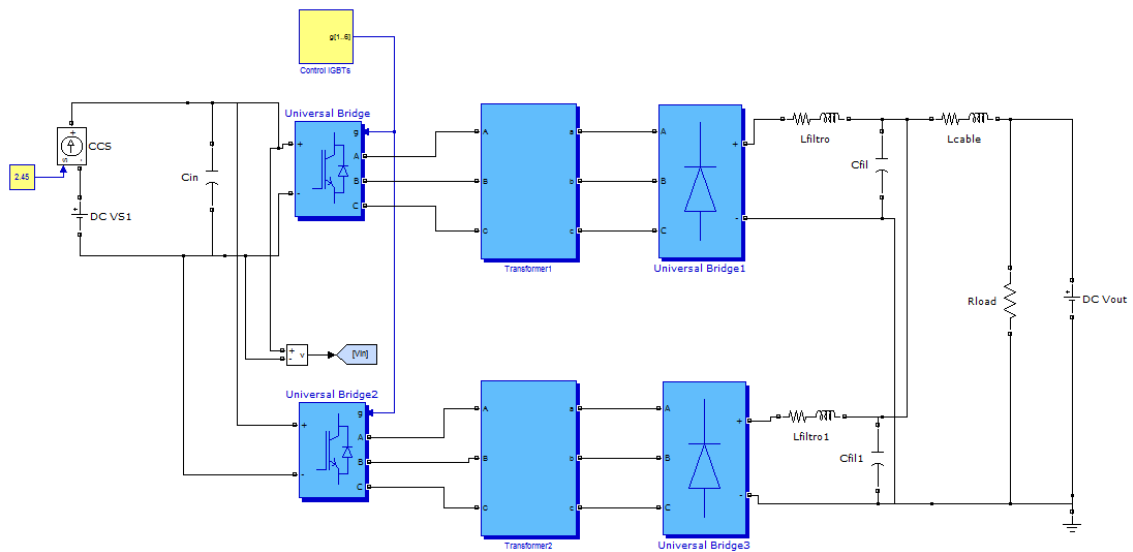
Figure 3.17: SWHFR Matlab/Simulink model in parallel configuration.

PROJECT NO.
502000064

REPORT NO.
TR A7482

VERSION
1.0

64 of 133
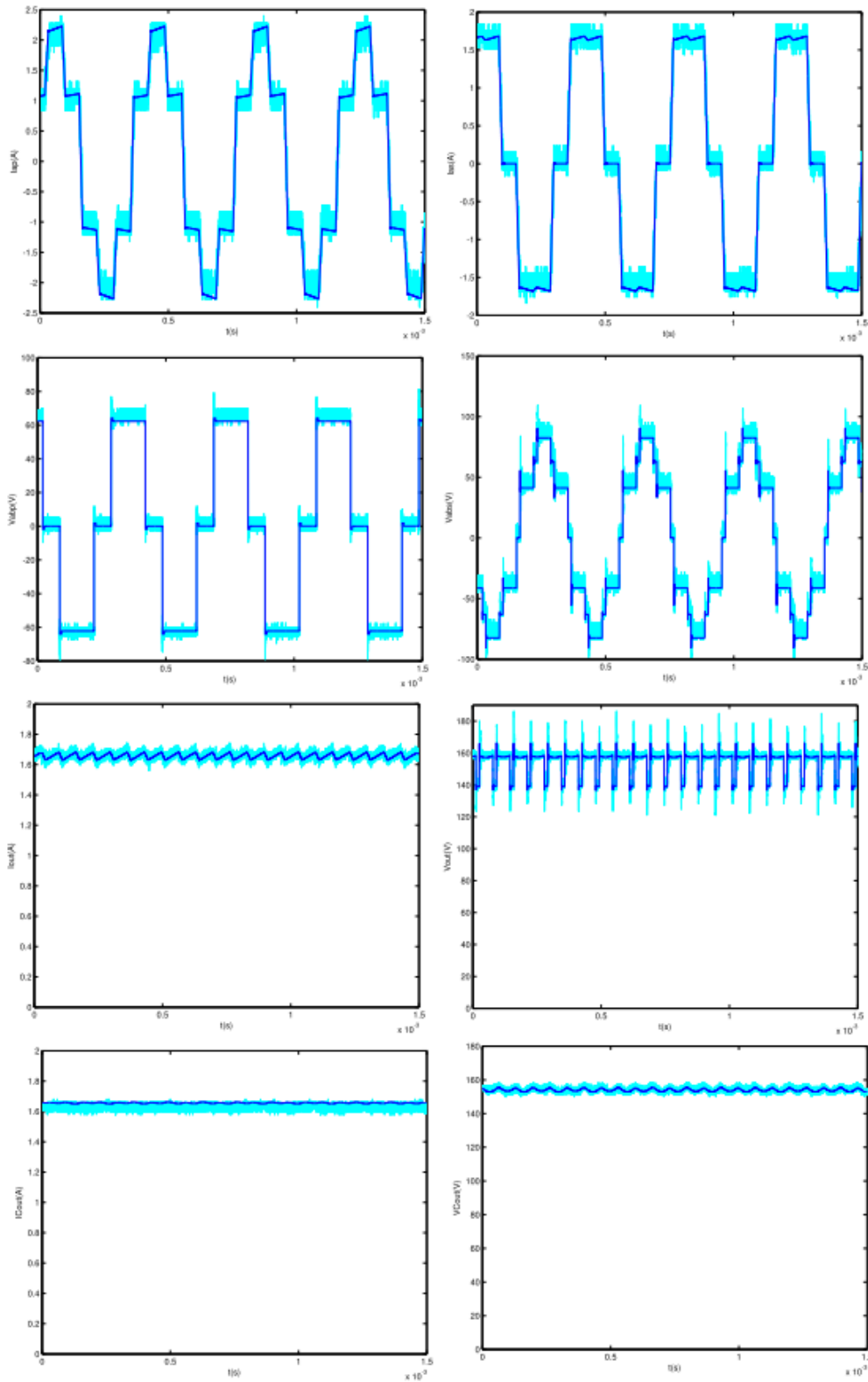
Figure 3.18: Simulation and experimental results for two converter in series configuration with a leakage inductance L_l=170 μH.

PROJECT NO.
502000064

REPORT NO.
TR A7482

VERSION
1.0

65 of 133
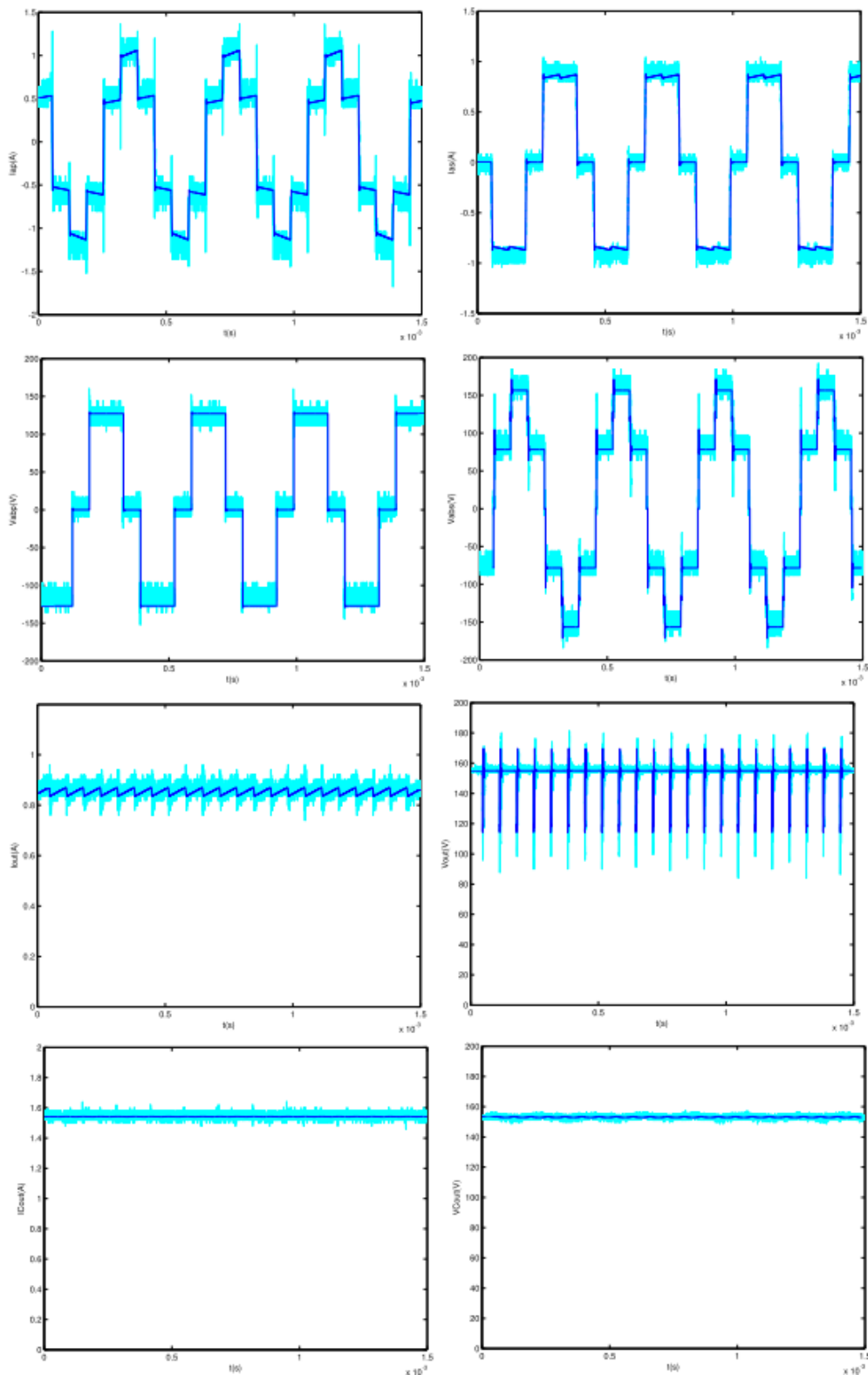
Figure 3.19: Simulation and experimental results for two converter in parallel configuration with a leakage inductance L_l=170 µH.

PROJECT NO.
502000064

REPORT NO.
TR A7482

VERSION
1.0

66 of 133

Finally a configuration with four converters has been tested. The four converters are arranged in two groups of two converters each. Converters within a group are connected in series forming a bipolar configuration. The groups of converters are connected in parallel (see Figure 3.20). This configuration aims to simulate a small wind farm with four turbines, where series connection of two wind turbines has been assumed.
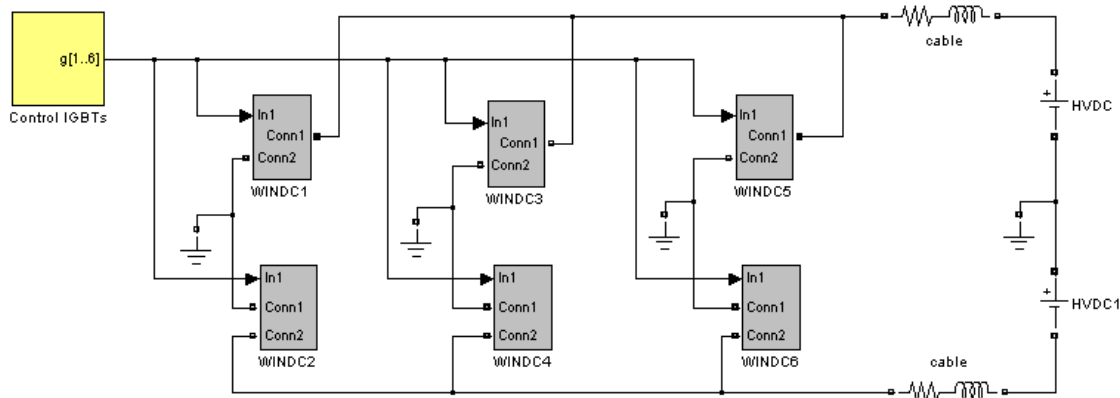
Figure 3.20: Schematic connection of four SWHFR simulating four wind turbines.

The purpose of this test is to check how the presence of strong power unbalances between the turbine groups and the dispersion on the electrical characteristics of the high frequency transformers affects the performance of the whole system. Different transformers with the leakage inductances ranging from 20 to 400 μH have been used. A strong and unbalanced power distribution between the turbine groups has been assumed. The power of one of the converter groups has been set to 1 kW while the other group is working at 4.25 kW. Figure 3.21 and Figure 3.22 shows experimental voltage and current waveforms. The waveforms of the group of converters working at 4.25 kW are displayed on the left side of the picture. The right side displays the waveforms of the converters working at 1 kW. From top to bottom the following waveforms are shown in Figure 3.21: current in the transformer primary winding, current in the transformer secondary winding, voltage waveform at the transformer primary winding, voltage waveform at the transformer secondary winding; and in Figure 3.22: rectifier DC output current, unfiltered rectifier DC output voltage, total DC current in the DC link, DC voltage at the LC filter's capacitor's terminals. The power unbalance between converter groups can be appreciated in the strong difference between the transformer currents of the left and right side of the figure. The contribution to the total current of the groups is also completely uneven. While one converter group is contributing to the total DC current with around 1.5 A the other group is supplying almost 6.5 A. These results show that the system is able to work under unbalanced conditions and with a high dispersion of the transformer leakage inductances without important problems.

PROJECT NO.
502000064

REPORT NO.
TR A7482

VERSION
1.0

67 of 133
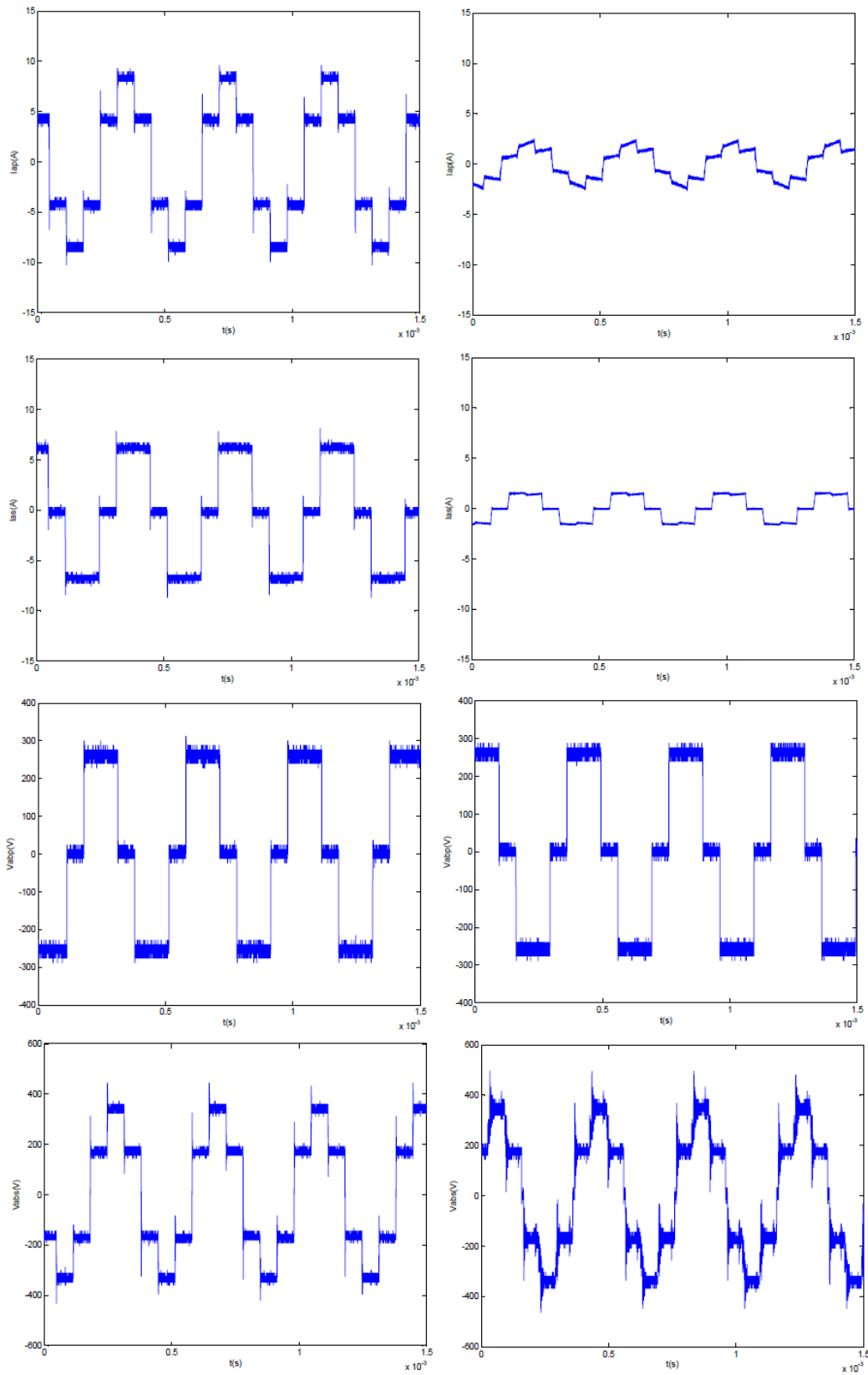
Figure 3.21: Experimental waveforms under unbalanced power distribution between converter groups and strong dispersion of the transformer leakage inductances.

PROJECT NO.
502000064

REPORT NO.
TR A7482

VERSION
1.0

68 of 133
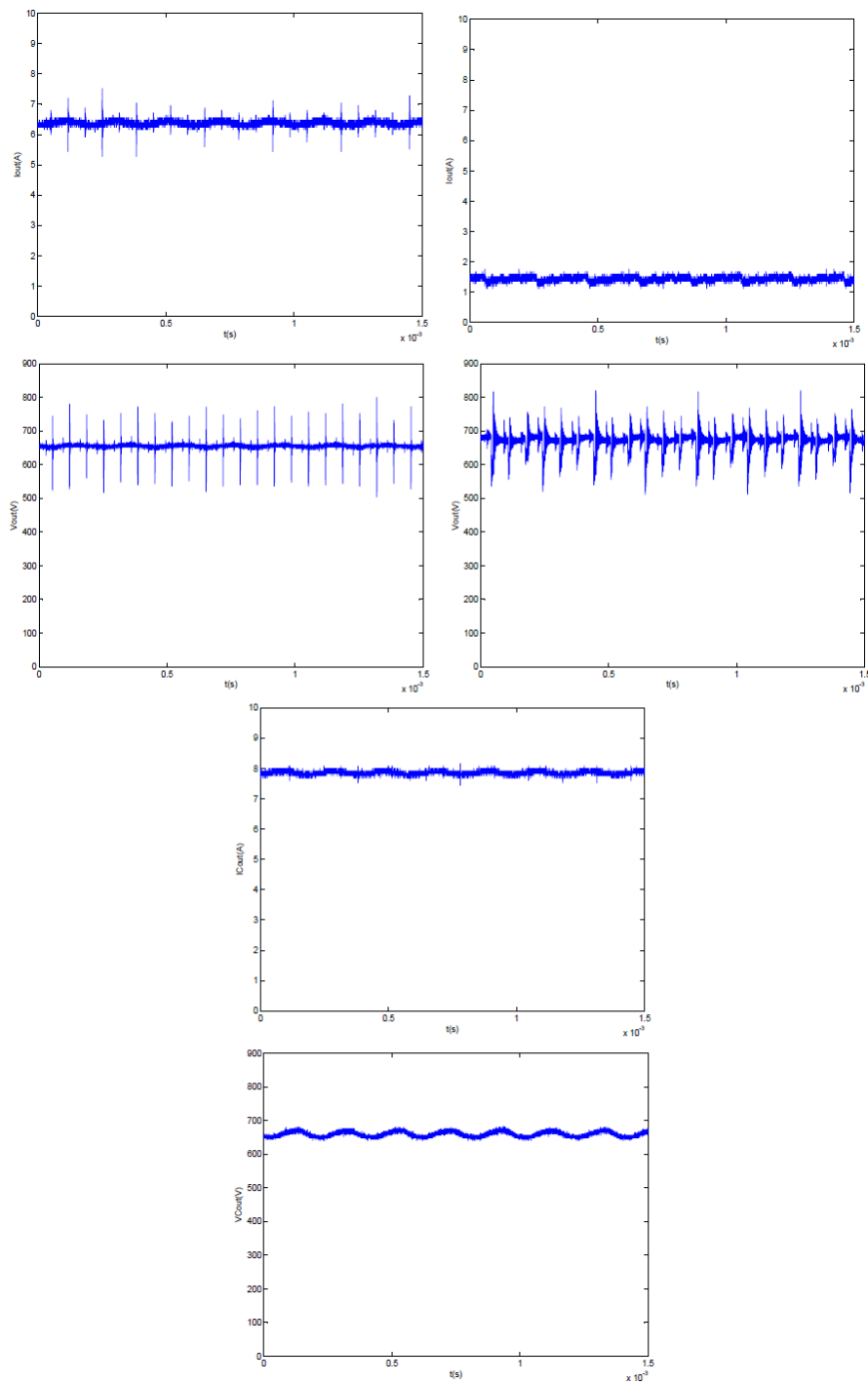
Figure 3.22: Experimental waveforms under unbalanced power distribution between converter groups and strong dispersion of the transformer leakage inductances.

3.3 Summary

The chapter has described the behavior of a Square Wave High Frequency converter. The voltage and current waveforms are described in detail, and the relation between input and output voltage dependency on converter parameters is studied. Four converter prototypes have been implemented and

PROJECT NO.
502000064

REPORT NO.
TR A7482

VERSION
1.0

69 of 133

different configurations have been tested to validate the concept. The Section described the use of the leakage inductance of the transformer as an inherent element of the converter that can be applied to shape the current waveforms. The analytical expression of the relation between the converter input voltage and the output current is developed, as a function of the main converter parameters. The converter has no control parameters and the input converter DC bus voltage will vary with the HVDC line voltage and the output current. With conveniently chosen parameters the converter can operate in open loop.

The power losses of the proposed architecture are also analyzed. An important reduction in the power losses of the SWHF converter with regard the conventional converters used in today wind turbines has been found.

PROJECT NO.
502000064

REPORT NO.
TR A7482

VERSION
1.0

70 of 133

4 Modelling of HVDC grid connection for offshore wind farm

This chapter describes the specification of layout and parameters of the grid connection of a hypothetical wind farm that is expected to be relevant in the future. Some basic specifications for the design have initially been defined:

- An offshore wind farm connected to shore through HVDC connection should be studied.
- The wind farm should have a large rating compared to existing offshore wind farms, and should be located at a distance from shore long enough to favour HVDC transmission
- The studied transmission technology should be a future solution, where topics for research still remain. The case study will therefore include a three terminal HVDC transmission system, with two terminals located onshore and one offshore. The HVDC technology will be of VSC type.

Grid connection alternatives are analysed through case studies in Chapter 6. The modelling and simulation has been performed using the power system simulation software PSCAD

The wind farm is thought to be located between two countries, and closer to country 1 than country 2, as illustrated by Figure 4.1. The distance from country 1 to the offshore wind farm should be long enough to justify HVDC transmission to the wind farm, and also long enough to justify an additional HVDC connection to country 2. There will be one HVDC terminal in each of the two countries and one at the offshore wind farm. With connection to two countries, the HVDC link can be used for direct power transmission between the two countries, in addition to transmission of wind power to the onshore power systems.
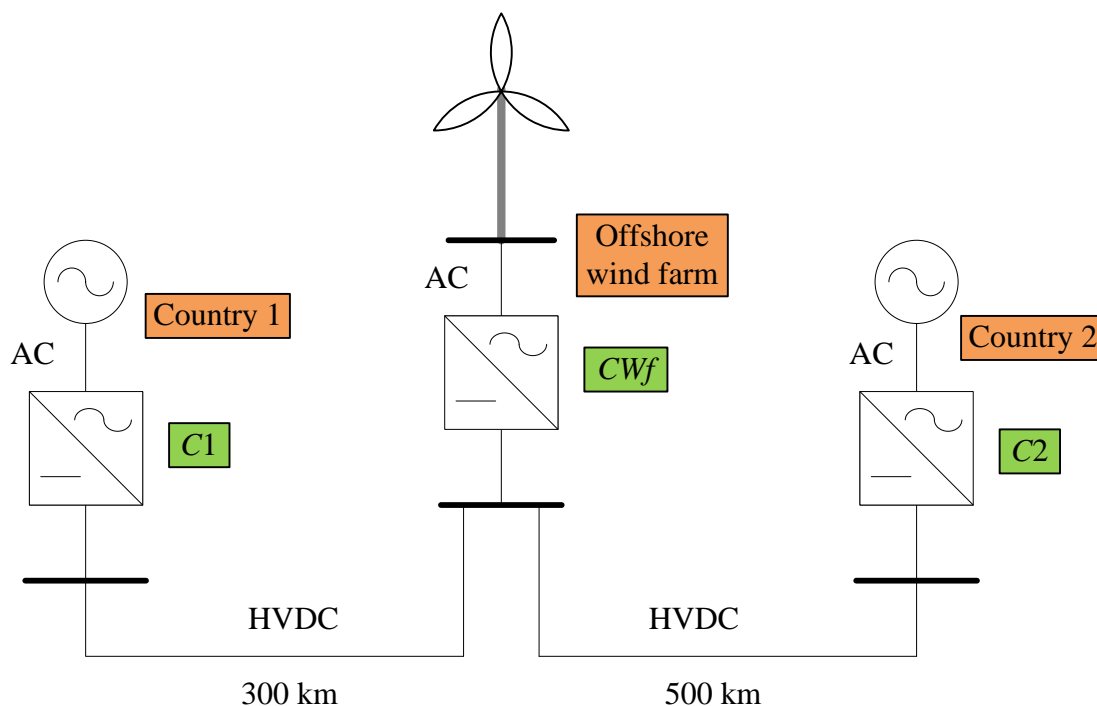
Figure 4.1 Simplified drawing of case study topology

The wind farm is assumed to be located in the North Sea between Norway and England, but could alternatively be located between e.g. Norway and Germany or Spain and France. The same principal design could be used for the other locations. In the chosen topology, the wind farm is located 300 km

PROJECT NO.
502000064

REPORT NO.
TR A7482

VERSION
1.0

71 of 133

from Norway and 500 km from England, so the total length of the HVDC link becomes 800 km. The distances are not exact, but rather very rough estimates. However, the wind farm location corresponds to an area identified as suitable for large wind farm clusters far from shore possibly using floating technology in [4.1].

4.1 Wind farm and converter ratings

The rating of the offshore wind farm is chosen to 1000 MW (1 GW). This can be the size of one single wind farm or a cluster of farms sharing the same grid connection.

1000 MW is not an unrealistic rating, as offshore wind farms of several hundred MW already are in operation, or under construction. At present, the largest offshore wind farms are located in United Kingdom, in the Irish and the North Sea. In the 504 MW Greater Gabbard project, a majority of the turbines were installed and connected to the grid by mid-2012. At present (2015), the world's largest offshore wind power plant is the 630 MW London Array.

Once the wind farm rating is chosen, the ratings of the transmission cables and the converter terminals can also be determined. The wind farm HVDC converter should as a minimum have rating equal to the wind farm rating. In order to have reactive power capability at rated active power, the converter MVA-rating could be chosen a bit larger than the active power rating. The DC transmission cables must at least have capacities to transfer rated power for the wind farm to the onshore power systems. Different options exist for the choice of ratings.

- One possibility is that the sum of the transmission capacities to the two countries equals the wind farm rating. In such a case the transfer capacity to each country could then be for instance 500 MW. Additional power transmission between the two countries would then only be possible when the wind farm is generating less than nominal power. However, it is assumed that the wind farm will generate nominal power only very few hours of the year, so that there would usually be available capacity for power transfer between the two countries.
- Alternatively, the rating of the onshore HVDC converters and the cables could be increased to allow for additional power transfer directly between the two countries. If it is assumed that the power transfer will usually be directed towards one of the countries, the converter and cable ratings from the wind farm converter to this country could be increased. Such solutions will have higher investment costs, but at the same time larger possibilities to utilize the HVDC-link.

In this work it has been chosen to have the same active power rating for the two onshore HVDC converters and corresponding DC cables as for the wind farm converter, which is 1000 MW. In order to allow for reactive power capability at rated active power, all converters have apparent power ratings of 1250 MVA.

Based on the active power rating, the DC voltage level can be determined. A high voltage level is desirable as it results in lower transmission losses, but at the same time an increased voltage level leads to higher investment costs.

Once the DC-voltage level is determined, the voltage on the converter AC-side can also be chosen. The converter AC-voltage is less than the DC-voltage, and the AC voltage can be determined from:

$$U_{AC,line-to-line} = \sqrt{3} \cdot \frac{m_a \cdot U_{DC}}{2\sqrt{2}}$$ (4.1)

Where m_a is the amplitude modulation ratio; $0 < m_a \leq 1$ [4.3].

PROJECT NO.
502000064

REPORT NO.
TR A7482

VERSION
1.0

72 of 133

4.2 DC transmission cable

Transmission between the HVDC terminals will be via subsea HVDC cables. The power is assumed to be transmitted through two parallel cables at +/- 400 kV respectively. Rated voltage on the converter DC terminals will then be 800 kV. The total transmission distance is, as stated above, 800 km.

A simple option is to model the DC cable using pi-equivalent sections. However, for a several hundred meters long cable many sections would be required; with a simulation speed of 20 µs each pi-section should not be longer than: $3 \cdot 10^5 \ km/s \cdot 20 \cdot 10^{-6} s = 6 \ km$ [4.4]. Having a large amount of pi-sections in the model would slow down the simulation speed considerably, and is therefore not a good solution for this case.

It has been chosen to model the DC transmission line by the PSCAD library cable component based on a travelling wave model. Three options are available: 1) Bergeron, 2) frequency dependent (Mode) and 3) frequency dependent (Phase). The Bergeron model is a distributed LC traveling wave model, but with lumped resistance. It represents only fundamental frequency accurately. The two frequency dependent models are both distributed RLC traveling wave models, but the phase model is stated to be the most accurate. It also has possibility for DC correction, which ensures high accuracy at the nominal frequency which is 0 Hz in this case. It should be noted that the parameter *shunt conductance* had very large impact on the result obtained using the frequency dependent phase model with DC correction. The effect of the shunt conductance has been investigated in [4.5]. Using the default value of 1e-9 mho/m resulted in large active power losses on the transmission line, also at no-load. The conductance was reduced to 1e-15 mho/m in order to eliminate these losses.

The simulation model requires cable geometry data as conductor radius and insulation thickness as inputs. In order to have realistic data, parameters for an ABB XLPE submarine cable, single core cable with lead sheath are used [4.6]. Nominal voltage for this cable is 400 kV, and the conductor cross section is 1600 mm^2. The data are most likely for AC cables, but it is assumed that a DC cable would not have very different geometry. Data are given in Table 4.1.

Table 4.1: Data for 400 kV single-core cables with lead sheath

Cross-section of conductor [mm^2]	Diameter of conductor [mm]	Insulation thickness [mm]	Diameter over insulation [mm]	Lead sheath thickness [mm]	Outer diameter of cable [mm]
1600	47.4	27.0	105.8	3.1	141.0

Only conductor, first insulation layer and sheath have been modelled here. Looking in Table 4.1, the diameter over the insulation is larger than the diameter of the conductor plus insulation thickness. This difference is assumed to be due to semiconducting layers on both sides of the insulating layer. The conductor is of copper. The geometries of the cable cross-sections are shown in Figure 4.2, copied from PSCAD.
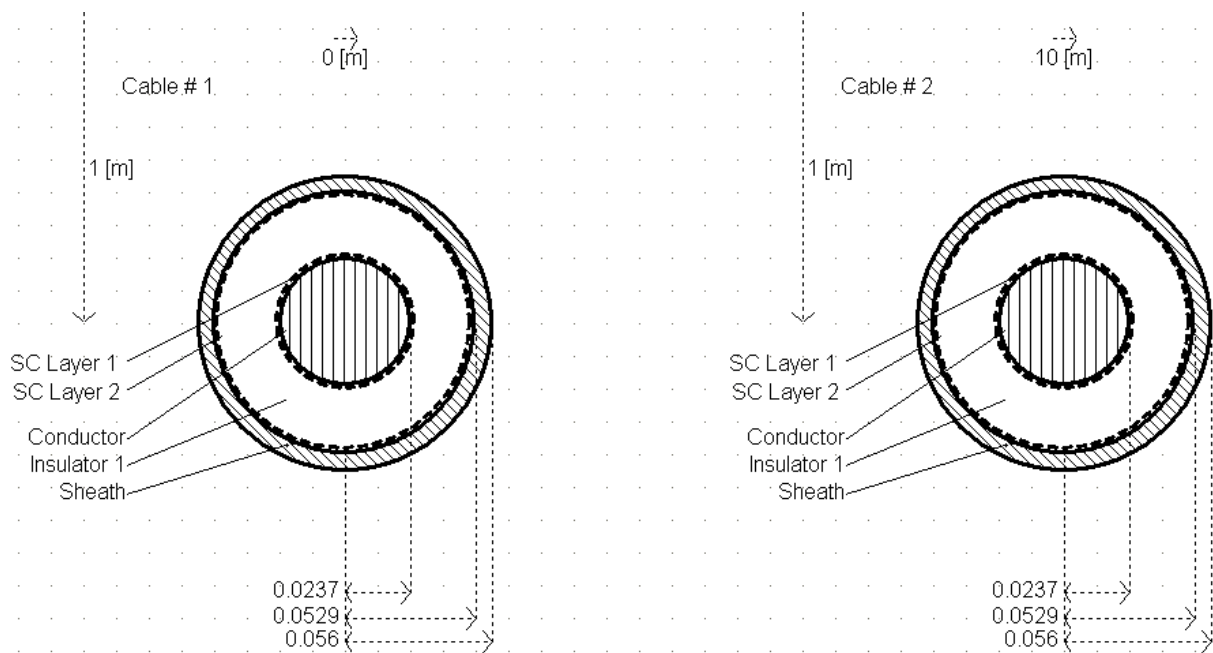
Figure 4.2 Cable geometry for 1600 mm², +/-400 kV DC cable

Some additional input parameters required for the PSCAD cable model are summarized in Table 4.2.

Table 4.2 Cable parameters

Depth below ground surface	1 m
Horizontal distance between cable centres	1 m
Conductor resistivity, ρ_{Cu}	$1.68 \cdot 10^{-8}$ Ω·m
Conductor relative permeability, $\mu_{R,Cu}$	1
Insulation relative permittivity, $\varepsilon_{R,XLPE}$	2.4
Insulation relative permeability, $\mu_{R,XLPE}$	1
Lead sheath resistivity, ρ_{Pb}	$2.2 \cdot 10^{-7}$ Ω·m
Lead sheath relative permeability, $\mu_{R,Pb}$	1

As an example, the resistance in a 800 km copper conductor is:

$$R = \frac{\rho_{Cu} \cdot l}{A} \, \Omega = \frac{1.68 \cdot 10^{-8} \, \Omega m \cdot 800 \cdot 10^{3} \, m}{1600 \cdot 10^{-6} \, m^2} = 8.4 \, \Omega \tag{4.2}$$

Nominal current is $I_{N,DC} = 1000 \, MW / 800 \, kV = 1.25 \, kA$.

The voltage drop with transmission of nominal power is $\Delta U_{DC} = 1.25 \, kA \cdot 2 \cdot 8.4 \, \Omega = 21.0 \, kV$.

The corresponding losses are: $\Delta P = 2 \cdot 8.4 \cdot 1.25^2 \, MW = 26.3 \, MW$

The simulated voltage drop and losses in an 800 km transmission line between to HVDC terminals is a bit lower than calculated according to the above expressions; about 19.2 kV and 24.5 MW

PROJECT NO.
502000064

REPORT NO.
TR A7482

VERSION
1.0

74 of 133

respectively. This gives a good overall agreement between analytical calculations and simulated results.

4.2.1 DC capacitance

The DC cable has significant capacitance, but additional capacitors can be added on the DC terminals of the converter(s) to stabilize the DC-voltage. The DC capacitance can be characterized by a time constant τ equal to the ratio of stored energy at rated voltage to rated converter power. The time constant τ corresponds to the time it takes to charge the capacitor to nominal DC voltage with rated converter power S_N. A small τ gives a DC voltage that is sensitive to changes in power, resulting in more fluctuations in the DC-voltage than with larger τ (and C). At the same time a small time constant allows for fast control of active power. According to [4.7], the time constant τ should be 5-10 ms. The DC capacitance can then be calculated:

$$\tau = \frac{C_{dc} \cdot U_{dc}^2}{2 \cdot S_N} \quad \Rightarrow \quad C_{dc} = \frac{\tau \cdot 2 \cdot S_N}{U_{dc}^2} = \frac{\tau \cdot 2 \cdot 1250}{800.0^2} \tag{4.3}$$

$$C_{dc,\tau=5ms} = 19.5\,\mu F, \quad C_{dc,\tau=10ms} = 39.1\,\mu F$$

A capacitance of $C_{dc} = 30$ µF is chosen at each converter terminal (corresponding to $\tau = 7.68$ ms). If the capacitance comes from two serially connected capacitors grounded at the junction node, each capacitor will have rating 60 µF.

4.3 AC grids in country 1 and 2

The nominal line-to-line voltage in on the AC-side of each converter is assumed to be 400 kV. This is in accordance with eq. (4.1), with $m_a = 0.8165$. As the focus of this study is the HVDC transmission from the offshore wind farm, detailed modelling of the onshore grids is out of the scope. Thus each of the two onshore grids is represented by a voltage source behind an impedance in order to limit the short circuit capacity. The HVDC terminals are assumed to be connected to stiff points of the grid in the respective countries, due to the large power ratings. A short circuit capacity of $S_{SC} = 5000$ MVA is assumed, which gives an impedance of:

$$Z_{SC} = \frac{U_N^2}{S_{SC}} = \frac{400^2}{5000}\Omega = 32\,\Omega$$

The phase angle is assumed to be 80°.

The short circuit impedance of 32 Ω includes the impedance in series with the ideal voltage source and the transformer leakage impedance

4.4 Wind farm

The main focus of this work on transmission, and detailed modelling of the wind farm and its collection grid is considered out of the scope. The collection grid is assumed to be AC, as this is the conventional solution. The chosen voltage level is 36 kV, as wind farms built up to now commonly have collection grid voltages around this value. However, in the future higher voltage levels are likely to be chosen in large offshore wind farm like this. A 400 / 36 kV transformer is included in the model, connected directly to the wind farm HVDC terminal. This transformer is directly-grounded on the collection grid (36 kV) side. The collection grid would in reality consist of several radial feeders, but is here modelled in a very simple way based on aggregated wind turbines.

PROJECT NO.
502000064

REPORT NO.
TR A7482

VERSION
1.0

75 of 133

The wind farm is assumed to consist of full power converter interfaced turbines. This means that short circuit capacity is not very much higher than the nominal power. A very simple approach would be to model the wind turbines as a source behind an impedance of size corresponding to the short circuit capacity. This will however not give a good representation of the behaviour of converter interfaced turbines which are more like controllable voltage sources with limited current capability. Instead it is chosen to represent the wind turbines by the back-to-back converter with an AC-voltage source on the wind turbine side of the converter. The wind turbine in itself is not modelled. This is assumed acceptable since the DC-link is decoupling the wind turbine from the wind farm collection grid (although some transients can be transferred over the DC-link). Further, the wind turbine back-to-back converters are modelled by an average (non-switching) model [4.9], so that the output is without harmonics. There are DC-choppers in the DC-links, which are set to be connected when the DC-link voltage becomes higher than 1.2 pu. The intention with the DC-choppers is to absorb excess active power when there is a voltage dip in the collection grid, in order to ensure fault-ride-through capability for the wind turbines.

Rather than modelling each wind turbine separately, aggregated wind turbine models are used. The simplest approach is to model the whole wind farm by one large aggregated wind turbine model. Such a model, shown in Figure 4.3a, has been used in simulations of faults in the HVDC-grid and in the onshore AC-grids. However, for simulations of faults in the wind farm collection grid a bit more detailed model has been used. One branch with 4 wind turbines with cable sections between and an aggregated wind turbine corresponding to 12 turbines is modelled separately. Thus the total number of turbines on this branch is 16. The remaining 184 turbines are represented by an aggregated model, as shown in Figure 4.3b.

PROJECT NO.
502000064

REPORT NO.
TR A7482

VERSION
1.0

76 of 133

Figure 4.3: Wind farm model layouts; (a) one single aggregated wind turbine model, (b) one branch modelled separately and the remaining wind farm represented by one large aggregated wind turbine converter.

For simplicity, the transformers on the wind turbine terminals have ratios 36/36 kV. The DC voltage for the wind turbine converters is 2·36 kV = 72 kV. The wind farm is assumed to consist of 200 turbines rated 5 MW, with each wind turbine converter rated 6.25 MVA. Thus in Figure 4.3 (b), the 4 single turbines are represented by 6.25 MVA converters while the remaining 12 turbines on the same branch are aggregated and represented by a 75 MVA (12·6.25 MVA) back-to-back converter. The rest of the wind farm is represented by a 1150 MVA (184·6.25 MVA) converter. The cable sections are modelled by pi-equivalents, with parameters for a 36 kV PEX cable, as given in Table 4.3. Each cable section is 0.5 km, but with different cross-sections. The largest cable cross-section is used at the beginning of the branch and vice-versa.

Table 4.3 Parameters for 36 kV TSLE cable [4.8]

No.	Type	R [Ω/km]	X [Ω/km]	C_d [μF/km]	C_j [μF/km]	I_{th} [A]	I_k 1s [kA]
1	TSLE 3x1x150 Al / 25	0.206	0.2	0.18	0.18	370	13.5

PROJECT NO.
502000064

REPORT NO.
TR A7482

VERSION
1.0

77 of 133

2	TSLE 3x1x300 Al / 35	0.1	0.18	0.24	0.24	500	27
3	TSLE 3x1x500 Al / 50	0.061	0.17	0.29	0.29	650	45
4	TSLE 3x1x630 Al / 50	0.047	0.16	0.31	0.31	715	56.7

R, *X*: resistance and reactance at 20 ºC; C_d, C_j: equivalent capacitance per phase and phase-to-ground capacitance; I_{th}: maximum continuous operating current; I_k: maximum short circuit current for 1 s

The collection grid has all sources connected via inverters, so it is an AC grid without stiff sources and inertia. This means that one of the converters has to be responsible for controlling the AC voltage amplitude and phase, and this is chosen to be the wind farm HVDC converter. The wind turbine converters have active and reactive power control.

4.5 Bibliography

[4.1]   K.Veum, L. Cameron, D.H. Hernando, M. Korpås, "Roadmap to the deployment of offshore wind energy in the Central and Southern North Sea (2020-2030)", Windspeed Final Roadmap 2011, 26 pages, available from: http://www.windspeed.eu/publications.php

[4.2]   J.M. Roney, "Offshore Wind Development Picking Up Pace", in Plan B Update, Earth Policy Institute, available from: www.earth-policy.org/plan_b_updates/2012/update106

[4.3]   N. Mohan, T. Undeland, W. Robbins, "Power Electronics, Converters, Applications, and Design", Second Edition, John Wiley and Sons, Inc., 1995, ISBN: 0-471-58408-8

[4.4]   Manitoba HVDC Research Centre. PSCAD On-Line Help System

[4.5]   A.B. Fernandes, W.L.A. Neves, E.G. Costa, M.N. Calacanti, "The Effect of the Shunt Conductance on Transmission Line Models", presented at the International Conference on Power System Transients IPST'01, Brasil 2001

[4.6]   ABB, 2012, "Submarine XLPE cables up to 420 kV AC", Available from: www.abb.com/product/db0003db002618/c12573e7003302adc1256bdc00421ed7.aspx

[4.7]   T.M. Haileselassie, "Control of Multi-terminal VSC HVDC Systems", MSc-thesis, Department of Electric Power Engineering, NTNU, Trondheim, Norway 2008, 112 pages

[4.8]   SINTEF Energy Research, "Planleggingsbok for kraftnett" (In Norwegian, translated title: Planning book for power networks, Technical data), 2010

[4.9]   O. Mo, "Average model of PWM converter", SINTEF Energy Research, project memo AN 02.12.103, 2003

PROJECT NO.
502000064

REPORT NO.
TR A7482

VERSION
1.0

78 of 133

5 HVDC converter modelling

This chapter continues the modelling work in the previous chapter with a detailed description of the HVDC system, including control loops and parameter tuning.

Parameters and symbols used in the modelling of the HVDC converters are given in Table 5.1.

Table 5.1 converter modelling parameters

Symbol	Description
IL	Current in HVDC cable, load current
Idc	Current into converter DC-side
Ic	Current into converter DC-side shunt capacitor
RS	Converter AC-side grid filter series resistance
LS	Converter AC-side grid filter series inductance
$e_{a,b,c}$	Converter AC-terminal three-phase voltages
$i_{a,b,c}$	Converter AC-terminal three-phase currents
$v_{a,b,c}$	Converter AC-terminal three-phase voltages after filter

The HVDC terminals are of VSC-type with PWM-switching. Each converter is modelled with two-level topology, as shown in Figure 5.1. In reality converters of such high voltage and power ratings as in this case would have multi-level topology. However, the development of a multi-level converter simulation model was considered outside of the scope of the present project, and remains as future work. The two-level converter will in principle work the same way as a multi-level converter, but will generate larger harmonics. In that way it can be said to represent a worst case when it comes to filtering the output signals in order to get acceptable harmonic levels.

As described in the previous chapter, the wind farm has rated active power of 1000 MW, and 1000 MW can be transmitted in the DC cable. In order to have reactive power capability, the apparent power ratings of the converters are a bit higher, 1250 MVA. All HVDC converters (one located offshore and two onshore) have equal rating.
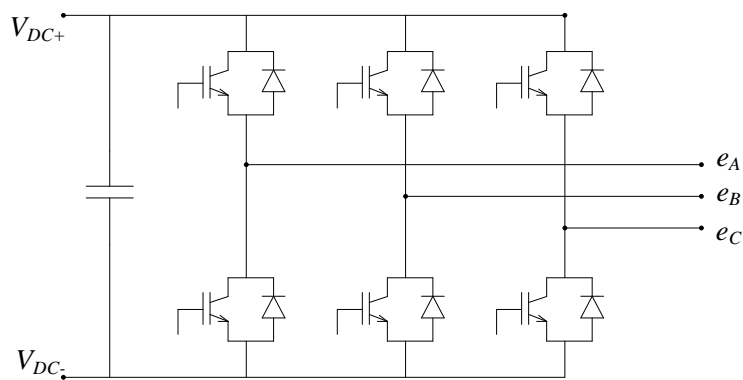
Figure 5.1 Two-level VSC converter

A switching frequency of 2500 Hz is chosen.

PROJECT NO.
502000064

REPORT NO.
TR A7482

VERSION
1.0

79 of 133

This work does not aim at defining an HVDC converter where the topology, filter design and controller parameters are optimized, but rather to develop an adequate model for performing simulation studies of different dynamic cases.

5.1.1 Base values for converter per unit system

Base values for the system are given in eq. (5.1).

$$U_{base} = \frac{\sqrt{2}}{\sqrt{3}} U_{ll,rms,base} \qquad I_{base} = \sqrt{2} \cdot \frac{S_{base}}{\sqrt{3}U_{ll,rms,base}} = \frac{2}{3} \cdot \frac{S_{base}}{U_{base}}$$

$$Z_{base} = \frac{\left(U_{ll,rms,base}\right)^2}{S_{base}} = \frac{U_{base}}{I_{base}} \qquad L_{base} = \frac{Z_{base}}{\omega_{base}} \qquad C_{base} = \frac{1}{\omega_{base}Z_{base}}$$

$$U_{dc,base} = 2\sqrt{2}\frac{U_{ll,rms,base}}{\sqrt{3}} = 2U_{base} \qquad I_{dc,base} = \frac{S_{base}}{U_{dc,base}} = \frac{3}{4}I_{base}$$

$$Z_{dc,base} = \frac{U_{dc,base}}{I_{dc,base}} = \frac{8}{3}Z_{base} \qquad C_{dc,base} = \frac{1}{\omega_{base}Z_{dc,base}} = \frac{3}{8} \cdot \frac{1}{\omega_{base}Z_{base}}$$

(5.1)

It can be noticed that $U_{DC,base}$ for the converter is lower than nominal voltage for the DC transmission of 800 kV.

5.2 Converter AC filter

The PWM generates harmonics in the output voltage and current on the converter AC-side, and the high frequency components needs to be filtered out.

5.2.1 RL filter

The simplest AC-filter is a series RL-filter, as shown on the right side of the VSC in Figure 5.2. Ref. [5.1] suggests a series RL filter with the following values: L_S = 10-25 % of Z_{base}, R_S = 1 % of Z_{base}.
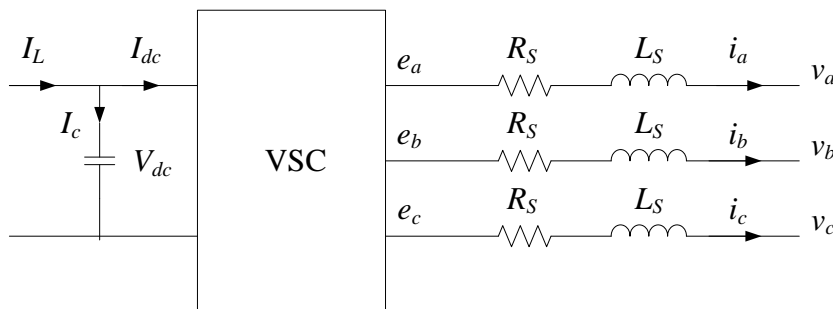
Figure 5.2 Schematics of VSC HVDC terminal

5.2.2 LCL filter

The switched two-level converter with a series RL filter as described in section 5.2.1 generates considerable harmonics. In order to reduce the distortion of the output currents and voltages to

PROJECT NO.
502000064

REPORT NO.
TR A7482

VERSION
1.0

80 of 133

acceptable levels a LCL filter, as shown in Figure 5.3, is introduced. Resistors are included in series with the L- and C-elements to for damping.
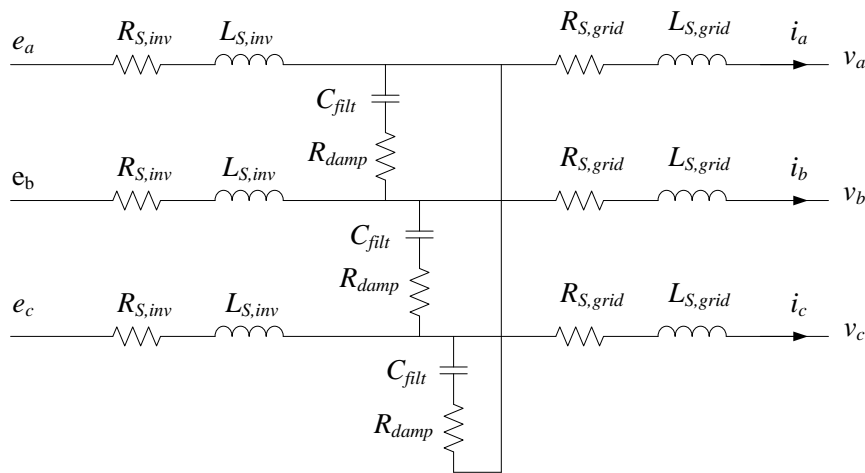
Figure 5.3 LCL filter for grid side of converter

The filter should have a resonance frequency in the range [5.2], [5.3]:

$$10 \cdot f_N < f_{filter,resonance} < 0.5 \cdot f_{switching}$$

$10 \cdot 50 \text{ Hz} = 500 \text{ Hz} < f_{filter,resonance} < 0.5 \cdot 2500 \text{ Hz} = 1250 \text{ Hz}$

In addition the capacitance should be limited to 0.05 pu in order have an acceptable power factor at nominal power. The filter inductance should not be higher than 0.1 pu for low power filters, while for high power applications avoiding saturation is most important. Some resistance is required for passive damping, but it should not be too high to avoid too large losses in the filter [5.2], [5.3].

Meeting all the above described requirements at the same time was not possible, and the filter inductance had to be increased to 0.15 pu. The resulting resonance frequency was about 1225 Hz, which is almost at the upper limit. The LCL-filter parameters are given in Table 5.2.

Table 5.2 LCL filter parameters

$R_{S,inv}$	0.8533 Ω	$R_{S,grid}$	0.4267 Ω	R_S	1.28 Ω	$C_{filt,\Delta}$	0.41447 µF
	0.0067 pu		0.0033 pu		0.01 pu		0.05 pu
$L_{S,inv}$	0.0407 H	$L_{S,grid}$	0.0204 H	L_S	0.0611 H	$R_{damp,\Delta}$	104.5 Ω
	0.0667 pu		0.0333 pu		0.15 pu		0.27 pu

Where $Z_{base,\Delta} = 3 \cdot Z_{base,Y} = 3 \cdot 128 \ \Omega = 384 \ \Omega$.

Ref. [5.3] suggests that the damping resistance should be in the same order of magnitude as the capacitor impedance at the resonance frequency. In [5.4] it suggested that the resistance should be one third of the capacitor impedance at resonance frequency. Following this the damping resistance is calculated as:

$$R_{damp,\Delta} = \frac{1}{3} \cdot \frac{1}{2\pi \cdot 1225 \cdot 0.41447 \cdot 10^{-6}} \Omega = 104.5 \ \Omega \tag{5.2}$$

PROJECT NO.
502000064

REPORT NO.
TR A7482

VERSION
1.0

81 of 133

5.3 Vector-oriented control of converter current

For the design of the current controllers, the shunt capacitor, C_{filt}, is neglected (and the damping resistor, R_{damp}). This is can be done since the LC-part of the filter works primarily to reduce high-frequency harmonics, while the current control primarily works on the lower frequency harmonics [5.3]. Referring to Figure 5.2 and Figure 5.3, the following is assumed: $R_S = R_{S,inv} + R_{S,grid}$, $L_S = L_{S,inv} + L_{S,grid}$.

Based on the schematics shown in Figure 5.2, the following equation can be put up for the AC-side of the VSC. Positive current flow is defined from the converter to the grid.

$$L_S \cdot \frac{d}{dt} \begin{bmatrix} i_A \\ i_B \\ i_C \end{bmatrix} = -R_S \begin{bmatrix} i_A \\ i_B \\ i_C \end{bmatrix} + \begin{bmatrix} e_A - v_A \\ e_B - v_B \\ e_C - v_C \end{bmatrix} \tag{5.3}$$

Transforming the equation to a reference system rotating synchronously with the grid voltage, (Park-transform), and conversion to pu gives [5.5]:

$$\frac{L_s}{\omega_{base}} \frac{d}{dt} \begin{bmatrix} i_d \\ i_q \end{bmatrix} = \begin{bmatrix} -R_s & \omega \cdot L_S \\ -\omega L_S & -R_S \end{bmatrix} \begin{bmatrix} i_d \\ i_q \end{bmatrix} + \begin{bmatrix} e_d - v_d \\ e_q - v_q \end{bmatrix} \tag{5.4}$$

Where ω is the rotational speed [pu/s].

It can be seen that there is a coupling between the d- and q-axes via the term ωL_S. To cancel out the cross-coupling feed-forward should be applied. The converter and the current controller block diagram is drawn in Figure 5.4. The VSC is represented by a time delay T_{conv}, which is half the switching period for the converter [5.1], [5.6]. The current controller is a proportional-integral (PI) controller.
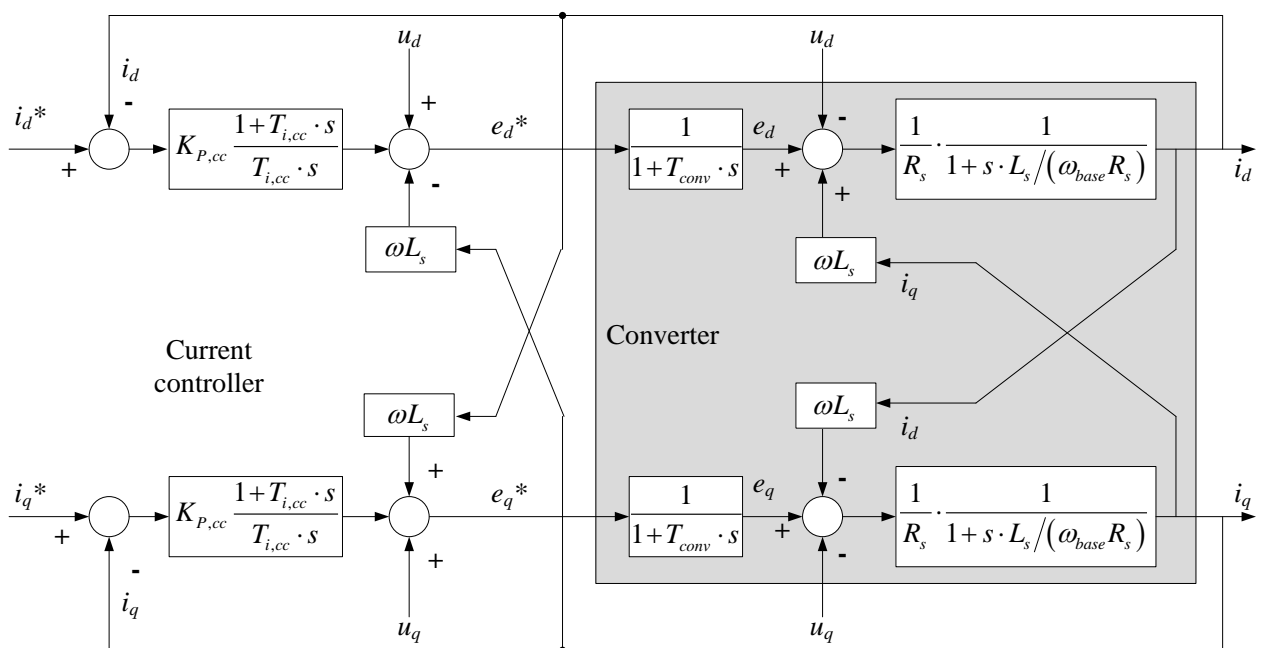
Figure 5.4 Block diagram representation of converter and current controllers

PROJECT NO.
502000064

REPORT NO.
TR A7482

VERSION
1.0

82 of 133

The time delay T_{conv} of the converter could have been taken into account for the feed-forward terms, but have been neglected.

5.4 Outer control loops

The current references $i_d{}^*$, $i_q{}^*$ to the current control loops described in the previous section are output from outer control loops. The d-axis reference can be output from DC-voltage, active power or AC-voltage control loops, and the q-axis reference can be output from reactive power or AC-voltage phase angle control loops.

5.4.1 DC-voltage control

A block diagram with the control loop for the DC-voltage and the inner control loop for i_d shown as $h_{CL,cc}$ is shown in Figure 5.5.

Figure 5.5: Control loop for DC-voltage control

The feed forward term $I_L \cdot U_{dc0}/u_{d0}$ has not been included in the simulation model. The transfer function for the DC-voltage control loop and determination of controller parameters are shown in appendix A.1.3

5.4.2 Active and reactive power control

Control of active and reactive power is based on the following equations:

$$P = u_d i_d$$
$$Q = u_d i_q$$

(5.5)

P will be controlled by an outer loop for the *d*-axis current control, and Q will be controlled via an outer loop for the *q*-axis current control. The open loop transfer function becomes:

$$h_{OL,PQ}(s) = K_{P,PQ} \cdot \frac{1 + T_{i,PQ} \cdot s}{T_{i,PQ} \cdot s} \cdot h_{CL,cc} \cdot u_d = \frac{K_{P,PQ} u_d}{T_{i,PQ}} \cdot \frac{1 + T_{i,PQ} \cdot s}{s\left(1 + T_{eq,c} s + T_{eq,c} T_{conv} s^2\right)}$$

$$\approx \frac{K_{P,PQ} u_d}{T_{i,PQ}} \cdot \frac{1 + T_{i,PQ} \cdot s}{s\left(1 + T_{eq} s\right)}$$

(5.6)

The tuning of these controllers are described in appendix A.1.4.

5.4.3 Control of voltage amplitude and phase angle

As mentioned in section 4.4, the wind farm HVDC converter has to control the voltage in the AC collection grid rather than the power. This is realized by outer control loops for the d- and q-axis voltages, respectively.

The control loops are shown in Figure 5.6.
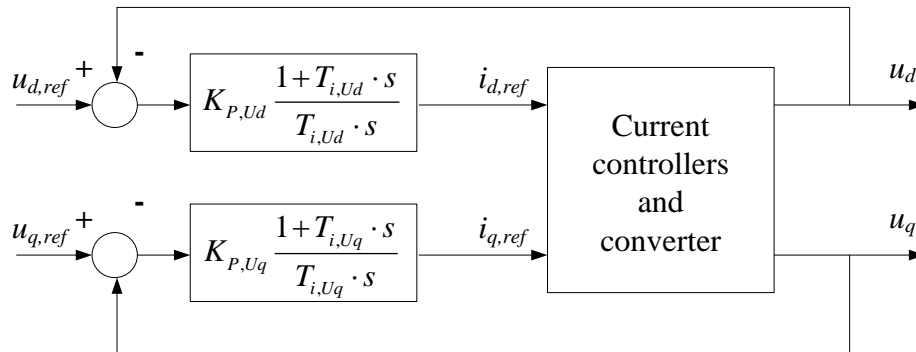
Figure 5.6: Outer control loops for AC-voltage control

No attempt has been done to determine the controller parameters analytically. Instead, this has been done by trial-and-error. Choosing the same parameters as for the PQ-controller gave good response.

5.5 Converter controller parameters

The controller parameters are summarised in Table 5.3.

Table 5.3: Summary of HVDC converter controller parameters

$K_{P,CC}$	3.2229	$K_{P,Udc}$	6.656	$K_{P,PQ}$	1	$K_{P,Udq}$	6.656
$T_{i,CC}$	0.0477	$T_{i,Udc}$	0.0160	T_{i_PQ}	0.0160	$T_{i,Udq}$	0.0160

5.6 Wind turbine converters

The wind turbine converters are modelled with an average converter model with series RL-filters. Filter parameters are chosen as $R_S = 0.01$ pu and $L_S = 0.1$ pu. The single wind turbines are rated 6.25 MVA and the 12 aggregated turbines on the same branch 75 MVA together. The aggregated wind turbine representing the remaining wind farm is rated 1150 MVA. The corresponding filter parameters and DC-link capacitors are given in Table 5.4. Wind farm grid voltage, $U_{AC,WF} = 36$ kV and wind turbine DC-voltage is $U_{DC,WT}=72$ kV. The capacitance is calculated from the time constant and voltage.

Table 5.4: Filter parameters and DC-capacitance value for wind farm converters

S_N [MVA]	6.25	75	1150	1250
R_S [Ω]	2.0736	0.1728	0.01127	0.01037
L_S [L]	0.066	0.0055	0.0003587	0.00033
C_{dc} [µF]	18.52	222.22	3407.41	3703.70

PROJECT NO.
502000064

REPORT NO.
TR A7482

VERSION
1.0

84 of 133

The converters are controlled the same way as the HVDC converter, with inner current controller loops and outer control loops for control of P and Q. Parameters are summarised in Table 5.5.

**Table 5.5: Summary of wind farm converter controller parameters**

$K_{P,CC}$	2.1486	$K_{P,PQ}$	1	$K_{P,Udq}$	6.656
$T_{i,CC}$	0.0318	T_{i_PQ}	0.016	$T_{i,Udq}$	0.0160

5.7 Power flow control

The three-terminal VSC HVDC network was shown in Figure 4.1 The converters in country 1 and 2 are named $C1$ and $C2$, while the converter in the offshore wind farm is named CWf. As described in section 5.4, the active and reactive power of each VSC can be controlled independently. The outer control loop for the active power current component (d-axis current) can be implemented with different control objectives [5.1],[5.7]:

- Constant active power
- Constant DC-voltage
- DC-voltage droop
- Constant AC voltage

The block diagram for DC-voltage droop is shown in Figure 5.7.
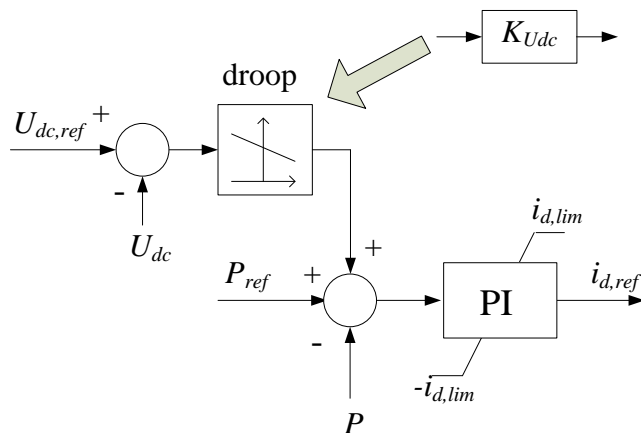
Figure 5.7: Block diagram for DC-voltage droop control.

This control has large impact on the behaviour of the HVDC link during a disturbance in one of the onshore AC-grids. A fault on the AC-side of the converter which is controlling the DC-voltage is critical if the other terminal(s) have constant active power control. This would lead to uncontrolled increase or decrease of the DC-voltage. To avoid this, DC-voltage droop is implemented. Then the active power set-point of the remaining converter(s) will be adjusted up or down according to the deviation of the DC-voltage, and thus contribute to control of the DC-voltage. In the case study, converter $C1$ is set to control the DC-voltage (constant DC-voltage control). DC-voltage droop has been implemented in converter $C2$, and this provides some fault-ride-through capability for the HVDC-system to faults on the AC-side in country 1.

Summarized, the converters in the case study are controlled in different ways:

- The country 1 converter ($C1$) is set to control the DC-side voltage and the AC-side reactive power. This converter then works as a slack-bus for the power flow in the HVDC system.

PROJECT NO.
502000064

REPORT NO.
TR A7482

VERSION
1.0

85 of 133

- The country 2 converter (*C2*) controls the AC-side active and reactive power. DC-voltage droop is implemented on the active power controller. The controller set-points can be determined by a TSO in a control centre.
- The wind farm converter (*CWf*) is controlling the AC-side (i.e. wind farm collection grid) voltage magnitude and phase angle. The active power from the wind turbines are passed through the converter to the HVDC grid.

In terms of active power control this system can operate without any communication. However it is assumed that communication would be desirable in a real case to adjust the active power set-point of *C2* to the actual wind power generation level. Communication with country 1 is not needed. If two or more terminals have active power control some coordination would be required, and there would be need for communication. With DC-voltage droop the need for communication can be avoided.

The control of reactive power is a local problem on the AC-side of each HVDC terminal. The need for reactive power depends on the impedance and voltage in the AC grid, and alternatively the AC-voltage could be controlled instead of the reactive power. In this work however the mainland AC-grids have not been modelled in detail, and reactive power control with a constant set-point close or equal to 0 is assumed sufficient.

5.7.1 DC-voltage droop

The DC-voltage droop R_{Udc} in percent is given by:

$$R_{Udc}\left[\%\right] = \frac{\Delta U_{dc}\left[\%\right]}{\Delta P\left[\%\right]} \cdot 100 \tag{5.7}$$

As an example, 10 % droop then means that a 10 % deviation in DC-voltage causes a 100 % change in the active power output of the converter.

The converter control is implemented in p.u., based on the apparent power rating, and a 100 % change in active power corresponds to 0.8 p.u. change. In the simulation model the droop is implemented as a constant K_{Udc}, which is multiplied with $U_{dc,ref} - U_{dc,measured}$ shown in Figure 5.7.

$$K_{Udc}\left[p.u.\right] = \frac{100}{R_{Udc}\left[\%\right]} \tag{5.8}$$

With $K_{Udc} = -8$, a 0.1 pu change in DC-voltage causes a 0.8 pu change in active power output. With $K_{Udc} = -4$, a 0.2 pu change in DC-voltage causes a 0.8 pu change in active power output.

With droop implemented, the *C2*-converter contributes to the DC-voltage control. With a fault on the AC-side of converter *C1*, the active power set-point of *C2* should be changed as much as possible to support the DC-voltage. Then a small droop is desirable. However, a smaller droop means higher sensitivity also to small deviations in the DC-voltage, for instance due to voltage drop in the DC-cables. This leads to a steady-state deviation from the active power set-point in *C2*. Figure 5.8 shows simulation results when the wind farm was generating about 1 pu active power, the active power set-point of *C2* was 0, and a three-phase short circuit occurred at the AC-side of *C1* at 2.5 s.
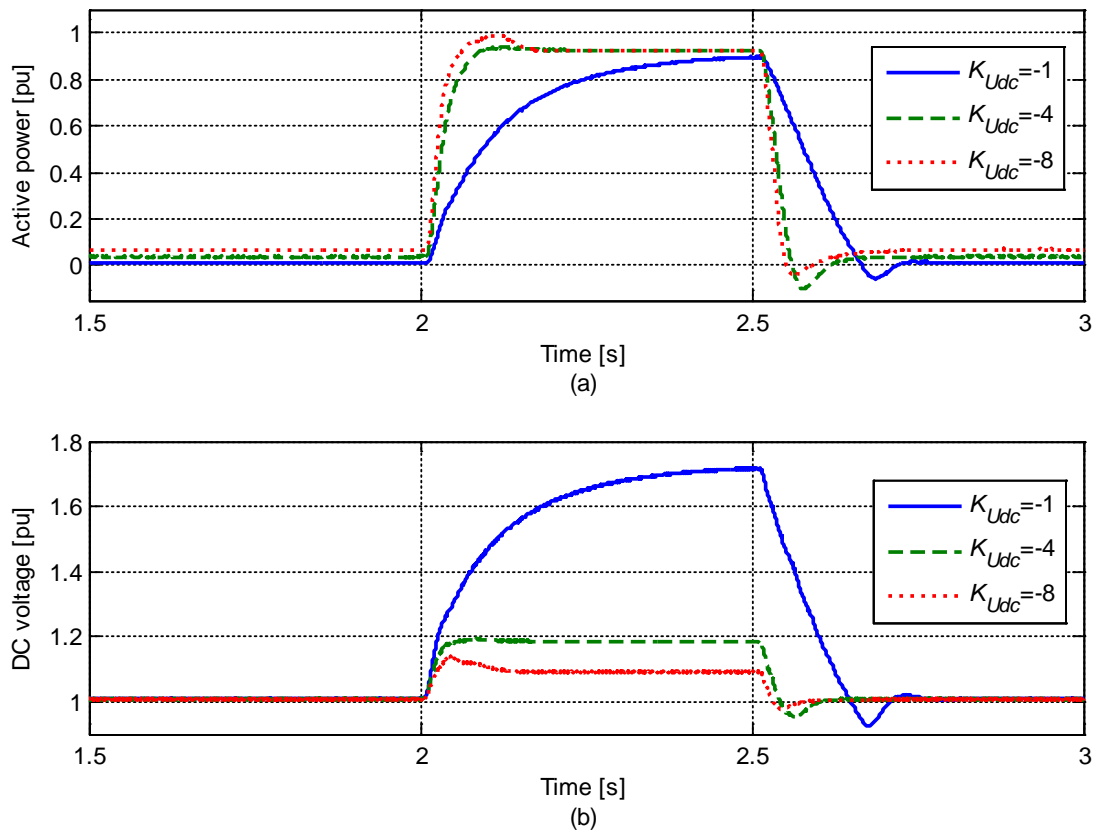
Figure 5.8: Response to short-circuit on AC-side; (a) active power, measured on grid side of converter filter and (b) DC-voltage

Positive direction of power flow is from the converter DC- to AC-side. pu-base for active power plot is 1000 MW. In steady-state the active power in converter $C2$ is a bit higher than the set-point value of zero because the DC-voltage is slightly higher than 1 pu. When the fault occurs, the active power through converter $C1$ is reduced almost to zero, while the active power through $C2$ is increased correspondingly to about 1 pu.

A smaller droop R_{Udc} and corresponding larger K_{Udc} gives a smaller increase in the DC-voltage during the fault, but larger steady-state deviation from the set-point of zero for active power in $C2$. Based on the plots, K_{Udc} is set to -4, assuming that the DC-system can withstand a 20 % overvoltage for a short period. The case where the active power in converter $C2$ has to be increased from 0 to 1 pu when the short-circuit occurs is worst case when it comes to DC-voltage increase. In other cases the voltage change will be smaller.

A dead band can be implemented on the droop, in order to avoid steady-state error in the active power at small deviations in voltage level. Then a smaller K_{Udc} could be chosen without the drawback of steady-state error in normal operation.

5.8 Bibliography

[5.1]   T.M. Haileselassie, "Control of Multi-terminal VSC HVDC Systems", MSc-thesis, Department of Electric Power Engineering, NTNU, Trondheim, Norway 2008, 122 pages

[5.2]   A. Julean, "Active damping of LCL filter resonance in grid connected applications", Aalborg University, Denmark, 2009, 83 pages

[5.3] M. Liserre, F. Blaabjerg, S. Hansen, "Design and control of an LCL-filter based three-phase active rectifier", IEEE Transactions on Industry Applications, Vol. 41, 2005, p. 1281-1291

[5.4] S.V. Araujo, A. Engler, B. Sahan, F.L.M. Antunes, "LCL Filter design for grid-connected NPC inverters in offshore wind turbine", The 7th International Conference on Power Electronics, Daegu, Korea, 2007

[5.5] C. Schauder, H. Mehta, "Vector analysis and control of advanced static VAR compensators", IEE Proceedings-C, Vol. 140, 193, p. 299-306

[5.6] C. Bajracharya, "Control of VSC-HVDC for wind power", MSc-thesis, Department of Electric Power Engineering, NTNU, Trondheim, Norway, 2008

[5.7] J. Beerten, R. Belmans. "Modeling and control of Multi-terminal VSC HVDC systems", Energy Procedia 24, 2012, p. 123-130

6 Dynamic analyses of three-terminal HVDC grid connected offshore wind farm

An offshore wind farm with three-terminal HVDC grid connection has been modelled in PSCAD. The modelling was described Chapter 5. The developed model is applied in this Chapter for investigating different fault events through simulations. Emphasis is on on fault detection and fault-ride-through capability, and short circuits and ground faults in the wind farm collection grid, in the DC transmission grid and on AC-sides of the two onshore HVDC terminals are considered.

The simulation results to be presented demonstrate that the HVDC-transmission system can operate through faults in the onshore AC grids if the HVDC terminals have either DC-voltage control and/or active power control with DC-voltage droop.

6.1 Dynamic simulation cases

An offshore wind farm with three-terminal HVDC grid connection has been modelled in PSCAD, and the system is illustrated by Figure 6.1. The modelling has been described in detail in the previous Chapter.

Figure 6.1 Offshore wind farm with three-terminal HVDC connection to the mainland grids.

The developed model will be used for investigating different fault events through simulations. Short circuits and ground faults in the wind farm collection grid, in the DC transmission grid and on AC-sides of the two onshore HVDC terminals will be considered. Focus is on methods and criteria for detection of the faults, and on fault-ride-through capability. Both HVDC- and wind farm collection grid consist of subsea cables. Phase-to-phase short circuits can be expected to occur much less frequent on subsea cables than overhead lines, and ground faults are probably the most likely fault event. Phase-to-phase faults are however more severe, and must still be considered. Thus fast detection and disconnection of all types of faults are very important.

PROJECT NO.
502000064

REPORT NO.
TR A7482

VERSION
1.0

89 of 133

A main advantage with DC- compared to AC-grids is generally lower active power losses and no reactive power losses. The relatively lower grid impedance however causes voltage drops due to faults to be larger and spread out faster than in AC-grids. This may disturb the operation of HVDC converters not directly connected to the faulted branch. Therefore the DC breakers must be faster than the AC breakers used today [6.2]. In the future, with the availability of sufficiently fast DC breakers with acceptable loss levels, the fault clearance strategy can be the same for a DC grid as for a meshed AC grid.

6.1.1 Adaption of model detail level for different studies

For the different case studies, some adaptions of the simulation model will be done. A main reason for this is to avoid unnecessarily complex models and correspondingly long simulation times.

- For simulations of onshore grid faults and faults in the HVDC-grid a three-terminal HVDC model will be used. The third terminal is essential when studying fault-ride-through capability. The wind farm is represented by a single aggregated wind turbine converter model in this case.
- For simulations of wind farm grid faults a model with two HVDC-terminals will be used, since the HVDC grid is not of main interest in this case. This allows for some more details in the modelling of the wind farm collection grid.

6.2 Onshore Side Grid Faults

Detection and disconnection of faults in the mainland AC-grids are assumed to be handled by conventional protection and AC-breakers, and will not be studied in this work. Instead the dynamic responses of the HVDC-network and the wind farm grid to such faults will be investigated. When there is a voltage dip on the AC-side of an HVDC-converter, the amount of power that can be delivered to the AC-grid is limited. This can lead to overvoltage on the DC-side. With a three-terminal HVDC-grid, the power can instead be delivered through the healthy terminal, and the overvoltage can possibly be avoided. Thus it is expected that the connection to two different countries will have a stabilizing effect, helping the HVDC-network to ride-through AC-side faults.

Figure 6.2 shows the response of a three-phase short circuit on the AC-side of converter $C2$. The wind farm is generating about 1000 MW, and the active power reference for converter $C2$ is also 1000 MW. This represents a worst case since converter $C1$ has to change the power output from 0 to about 1000 MW when the short circuit occurs.

PROJECT NO.
502000064

REPORT NO.
TR A7482

VERSION
1.0

90 of 133
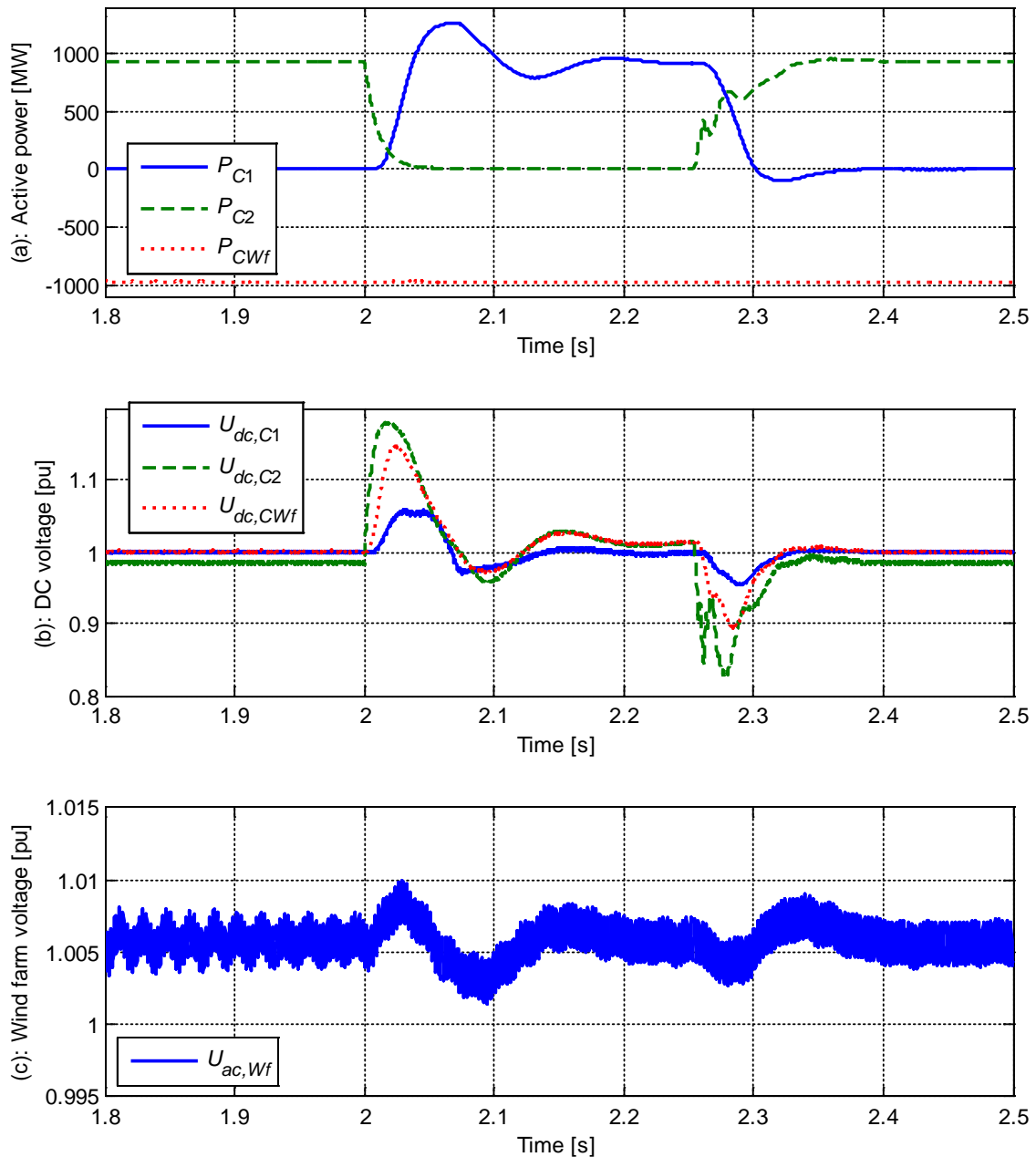
Figure 6.2 Response to three-phase short circuit on converter *C*2 AC-side. *P*$_{ref,C2}$=1000 MW

Plot (a) shows that the active power through converter *C*1 is increased when the active power through *C*2 is reduced to zero due to the short circuit. Therefore the active power through the wind farm converter terminal, P$_{Cwf}$, is kept constant during the fault, and the disturbance in the wind farm voltage is negligible, as seen in plot (c). The DC-system operates through this fault with relatively small oscillations in the DC-voltage.

The response of a three-phase short circuit on the AC-side of converter *C*1 is shown in Figure 6.3. The wind farm is generating about 1000 MW, and the active power reference for converter *C*2 is also 0 MW.

PROJECT NO.
502000064

REPORT NO.
TR A7482

VERSION
1.0

91 of 133
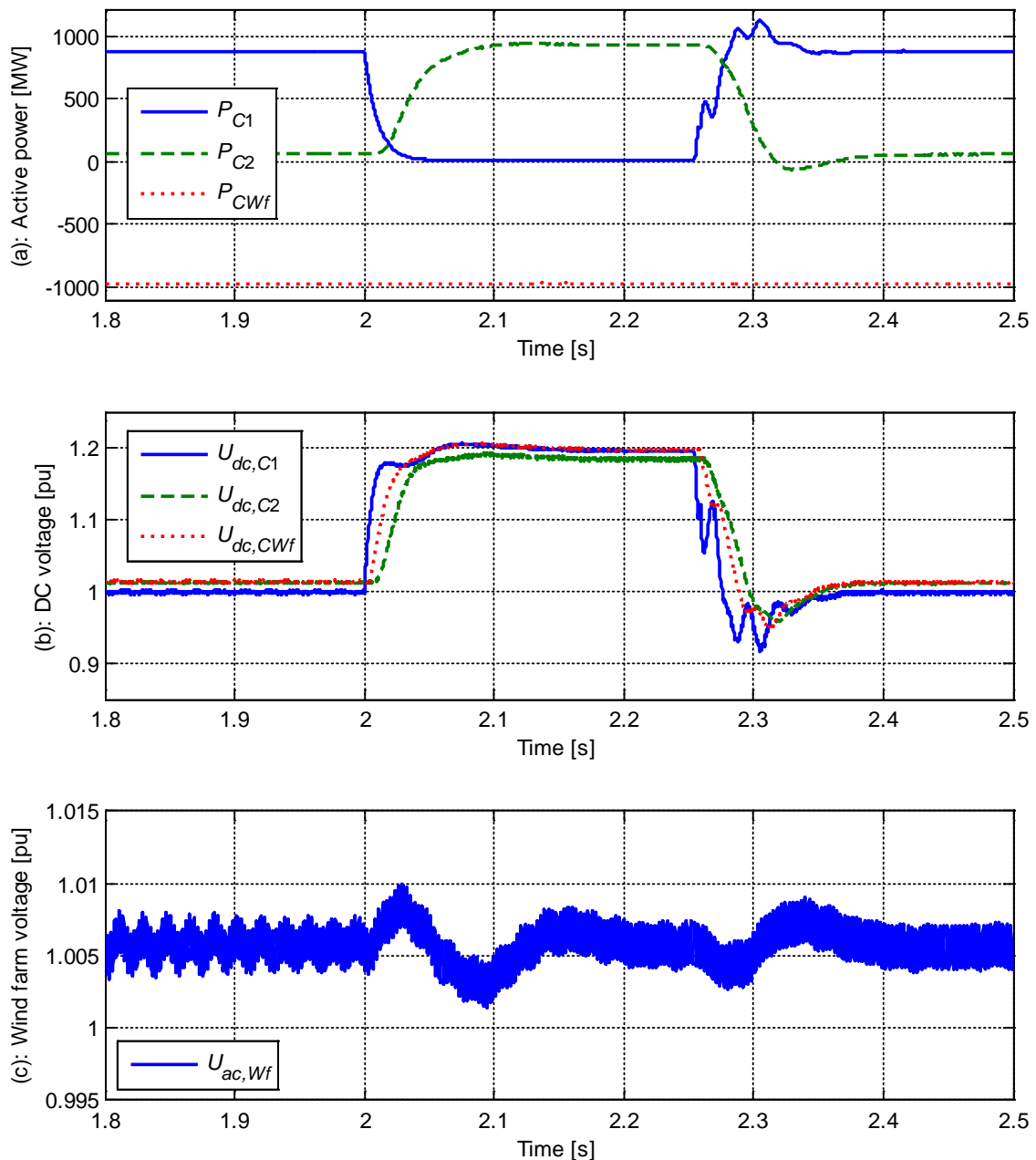
Figure 6.3 Response to three-phase short circuit on converter *C*1 AC-side. *P*_{ref,C2} = 0 MW. (a) Active power, (b) DC-voltage, (c) voltage in wind farm collection grid

The droop of the active power controller of converter *C*2 has been chosen so that a 0.2 pu change of DC voltage leads to a 0.8 pu (1000 MW/1250 MVA = 0.8) change of the active power. As seen in plot (a), converter *C*2 changes the power output from 0 to about 1000 MW when the short circuit occurs in country 1, and the power flow through converter *C*1 is reduced to zero. The active power delivered through the wind farm HVDC terminal is not disturbed by the short circuit, and therefore only a negligible disturbance is seen in the collection grid voltage in plot (c). The DC-voltage increases to 1.2 pu during the short circuit due to the chosen droop setting. The very large and sudden change of the active power output of terminal *C*2 might not be desirable for the AC-grid, so in a real case the impact on the grid should be investigated.

PROJECT NO.
502000064

REPORT NO.
TR A7482

VERSION
1.0

92 of 133

The plots show that the DC-transmission system can operate through onshore AC-side faults if the HVDC terminals have either DC-voltage control or active power control with DC-voltage droop. The short circuits cause negligible fluctuations in the wind farm voltage, and are therefore assumed to also have negligible impact on operation of the wind turbines.

Only results for symmetrical faults were shown here. The DC-system can operate through unsymmetrical faults in the same way. The reduction in active power through the converter close to the fault is less for a unsymmetrical fault, and these faults are therefore less severe for the system than three-phase short circuits. However, more oscillations are seen in active power and DC-voltage during the unsymmetrical condition.

In the same way as with a DC-side fault, the IGBTs will block when an overcurrent is detected due to a fault on the AC side. When the IGBTs are blocked no fault current will flow through the anti-parallel diodes, because the fault current is directed in the backward direction of the diodes. Simulation results however showed that the converter current with a fault on the AC-side (on grid-side of converter filter) did no cause a fault current large enough to block the IGBTs. (Peak current was about 3 kA, while the overcurrent protection was set to block the IGBTs at 4 kA).

6.3 Dynamic events in HVDC grid

This section deals with dynamic events in the HVDC transmission grid. First, system responses to some large load steps are studied. Then faults on the HVDC transmission cables are investigated.

When step changes in the load occur, the HVDC converters have to go to a new steady-state operating point after some transients. Step changes in the load are normal events which the HVDC-system has to handle without getting instable or without tripping the protection. A diagram showing the currents and voltages on the DC-sides of the three terminals is shown in Figure 6.4.
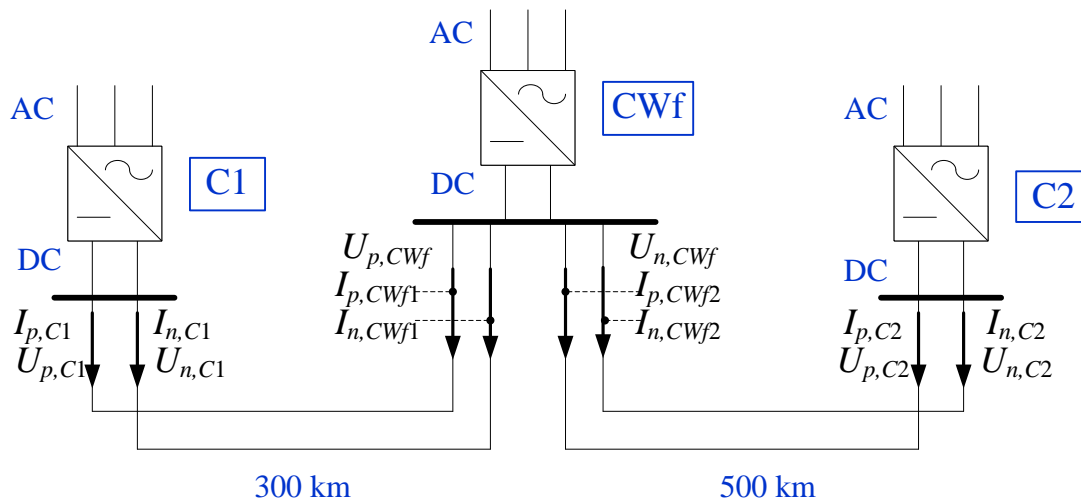
Figure 6.4 Diagram for study of DC-grid dynamic events

Figure 6.5 shows the response when the wind farm is generating nominal power and the active power reference in converter C2 is increased from zero to nominal power. This was found to be worst case regarding current increase and voltage dips.

PROJECT NO.
502000064

REPORT NO.
TR A7482

VERSION
1.0

93 of 133
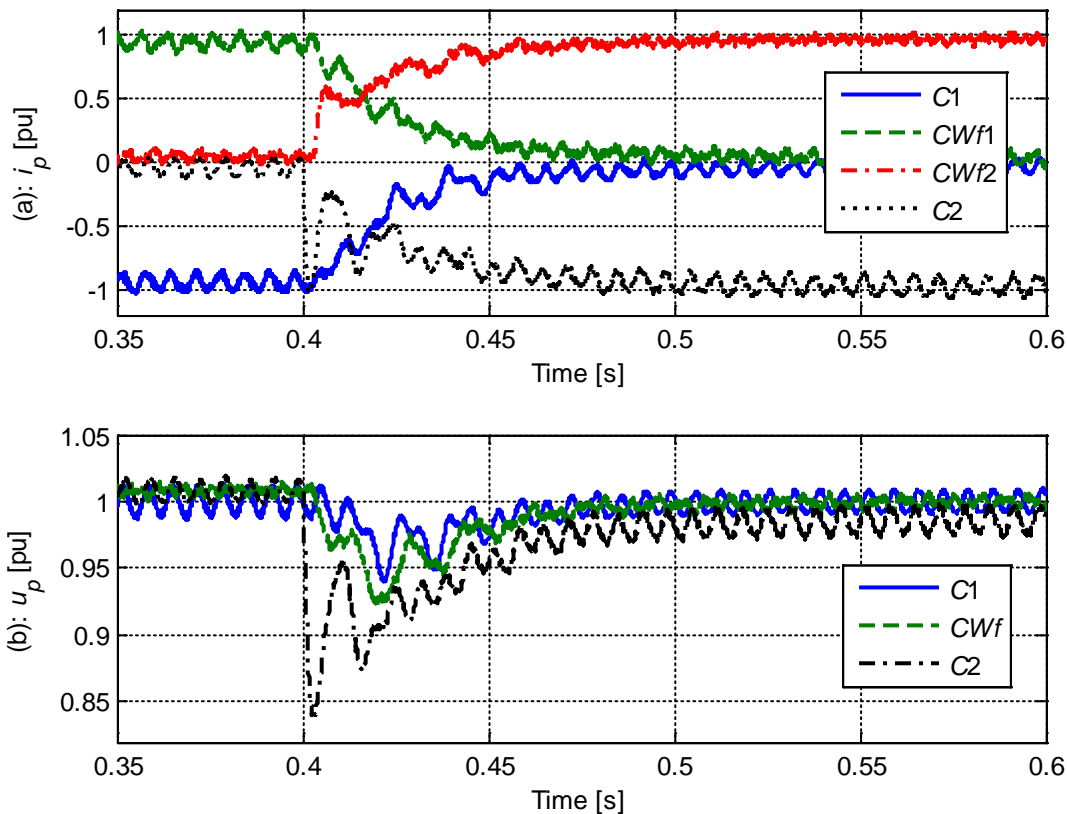
Figure 6.5 Response with step change in wind power production. $P_{ref,CW}$=**1000 MW.** $P_{ref,C2}$**:**
0→1000 MW I_{base}=**1000/800 kA. (a) Positive phase currents and (b) positive phase voltages**

Fast detection and disconnection of faults within the HVDC-link is important to maintain stable operation of the wind farm. A short circuit on one of the DC transmission cables is very critical, as it would lead to large capacitive discharge currents. Such faults are likely to be permanent, but the three-terminal solution allows for continued power transmission between two of the terminals despite of a fault. Due to the low impedance in the DC-cables, the voltage drop is spread out very fast. It is therefore important to detect and clear such faults very fast to prevent instability and further damage of equipment [6.3]. Compared to AC-grids, the critical clearing time is typically much shorter in DC-grids, which means that fast DC-breakers are required in multi-terminal DC-grids.

The VSC is made up of IGBT-switches. In real installations, the current ratings would be chosen according to nominal power and probably some overload current capability [6.4], [6.5]. A short-circuit somewhere in the system may lead to very high converter currents, which can damage the IGBT in short time. IGBTs therefore normally have overcurrent protection for fast blocking of the device when the current exceeds the maximum value. Peak current through a switch at nominal apparent power in the 1250 MVA wind farm case study is:

$$\hat{I}_N = \frac{\sqrt{2} \cdot S_N}{\sqrt{3} \cdot U_{AC,rms}} = \frac{\sqrt{2} \cdot 1250 \, MVA}{\sqrt{3} \cdot 400 \, kV} = 2.55 \, kA \tag{6.1}$$

Including some margin, the overcurrent protection is set to block the IGBTs at a current level of 4 kA.

PROJECT NO.
502000064

REPORT NO.
TR A7482

VERSION
1.0

94 of 133

6.3.1 Phase-to-phase short circuits

As starting point for the analyses of DC-faults phase-to-phase faults are studied. Although such faults are not very likely to happen on the subsea cables, the consequences are large. Equivalent circuits as shown in Figure 6.6 [6.6] can be used to study the fault current path for the different time periods of a short circuit. Immediately after the fault has occurred the DC-capacitor on the converter terminals is discharged, (i). The magnitude and steepness of the first current peak is determined by the DC-voltage and the cable resistance and inductance. In the next phase the capacitor voltage is zero, and the cable is discharged through the anti-parallel diodes in the converter bridge (ii). If a fault occurs on the DC-side of the converter and an overcurrent is detected, the IGBT switches can be blocked for self-protection [6.4]. However, the converter anti-parallel diodes will continue conducting current and the VSCs will act as rectifier bridges, and the fault will be feed from the AC-side via the diodes [6.6],[6.7]. The initial diode current can be very large, because the current in the cable inductor cannot change instantaneously when the DC-capacitor voltage goes to zero. Finally, in the third phase the fault is fed from the AC-grid through the diodes, (iii). In this phase the current depends on the short circuit capacity of the grid, the filter impedance, the DC-cable impedance and fault resistance.
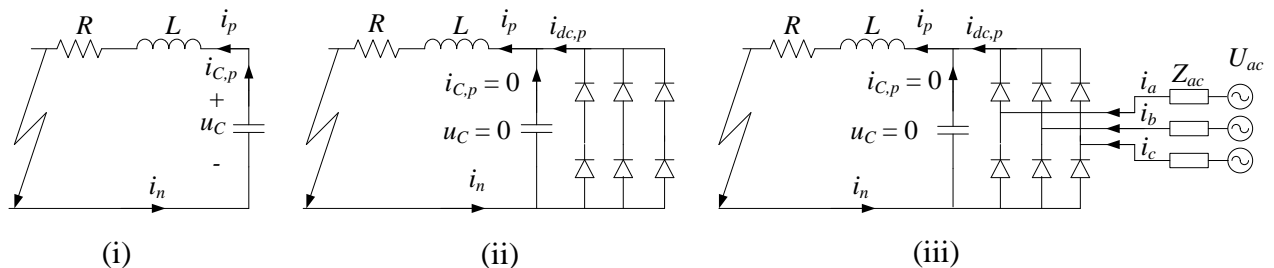
Figure 6.6 Equivalent circuits for fault on DC-side during: (i) capacitor discharge phase, (ii) freewheel diode phase, (iii) grid feeding phase.

Figure 6.7 shows fault currents during for some example phase-to-phase short circuits. Immediately after the fault occurs the DC-cable current i_p equals the capacitor current $i_{C,p}$. When the capacitor has been discharged and $i_{C,p}$ goes to zero, the DC-cable current equals the current fed via the diodes, $i_{dc,p}$. The distance from the converter terminal to the fault location is 1 and 10 km, and a longer distance means larger R and L in between the fault location and the HVDC terminal. The currents are shown in pu based on the converter rating, 1250 MVA. Thus at nominal active power in the DC-cable the current should be 0.8 pu.

PROJECT NO.
502000064

REPORT NO.
TR A7482

VERSION
1.0

95 of 133
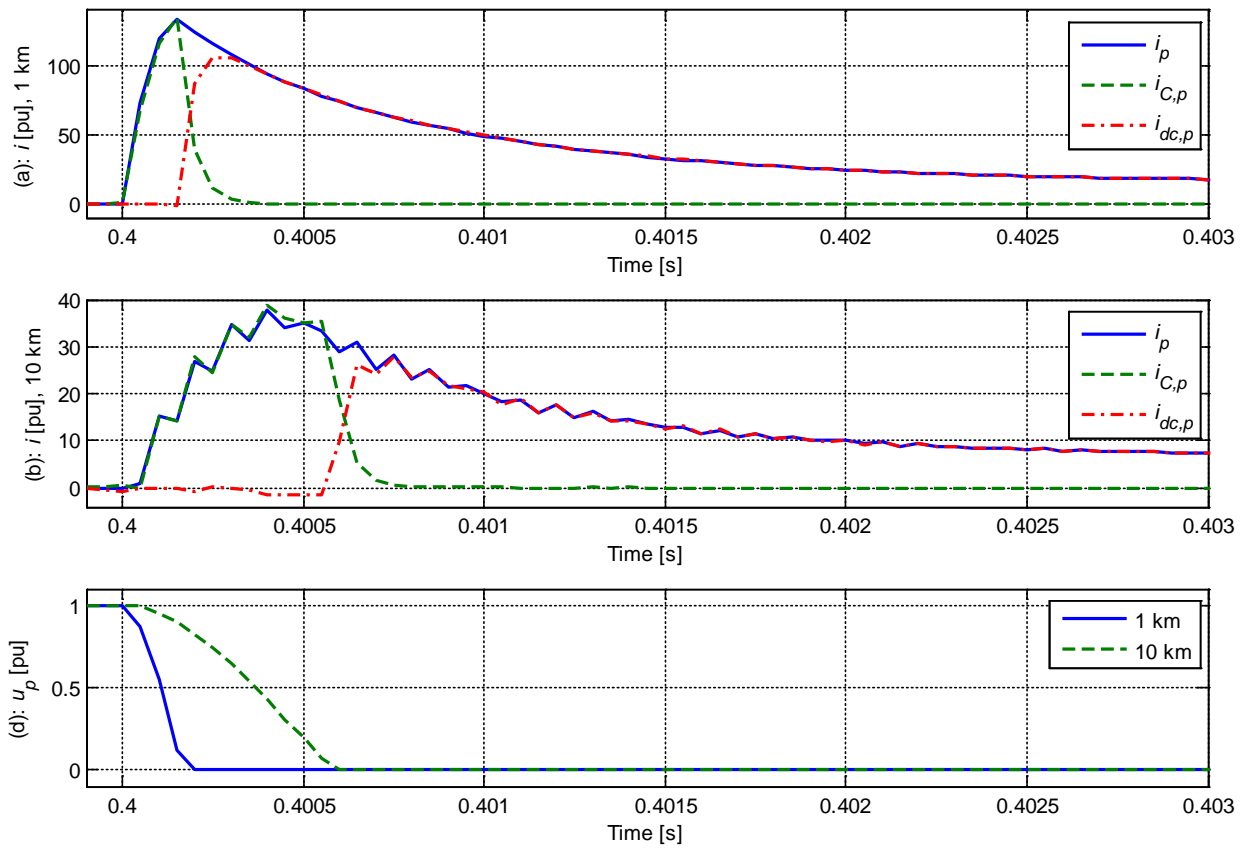
Figure 6.7 Current and voltage responses to phase-to-phase short circuits 1 and 10 km from the converter terminals on DC-side. R_f=0.01 Ω. I_{base}=1250/800 kA.

The plots show that the steepness and amplitude of the fault current depends very much on the length of cable between the converter and the fault location. For phase-to-phase faults located 1 and 10 km from the converter terminal, the maximum current through the diodes ($i_{dc,p}$) are about 100 pu and 27 pu respectively. These very large currents are much more than the diodes can withstand, and will probably damage the diodes. A short-circuit 100 km away from the converter terminal was also simulated, and in this case there was no large initial current through the diodes, but only a slow increase towards the steady-state fault current.

The fault current approaches the same final "steady-state" value independent on the distance to the fault location. This final fault current value depends on the short-circuit capacity of the AC-grid and the filter impedance. In this case study the AC-grids in the two countries have short-circuit capacities of 5000 MW and short-circuit impedances of (5.6 + j31.5) Ω. The filter series impedance is (1.3 + j19.2) Ω. The total short-circuit impedance on the AC-side then becomes 15.2 Ω. Cable resistance and possible fault resistance (more significant for phase-to-ground faults) come in addition. The steady-state peak current through the diode with a short circuit at the DC-terminals of the converter can be calculated from:

$$\left|i_p\right| = \frac{\sqrt{2} \cdot \left|U_{AC}\right|}{\sqrt{3} \cdot \left|Z_{AC}\right|} = \frac{\sqrt{2} \cdot 400\,kV}{\sqrt{3} \cdot 51.2\,\Omega} = 6.3\,kA = 6.3\,kA \cdot \frac{800\,kV}{1250\,MVA} = 4.1\,pu$$

PROJECT NO.
502000064

REPORT NO.
TR A7482

VERSION
1.0

96 of 133

6.3.1.1 Fault detection

Figure 6.8 shows current and voltage responses to phase-to-phase faults 250 km and 5 km respectively from the HVDC terminal in country 2 (*C*2), respectively.
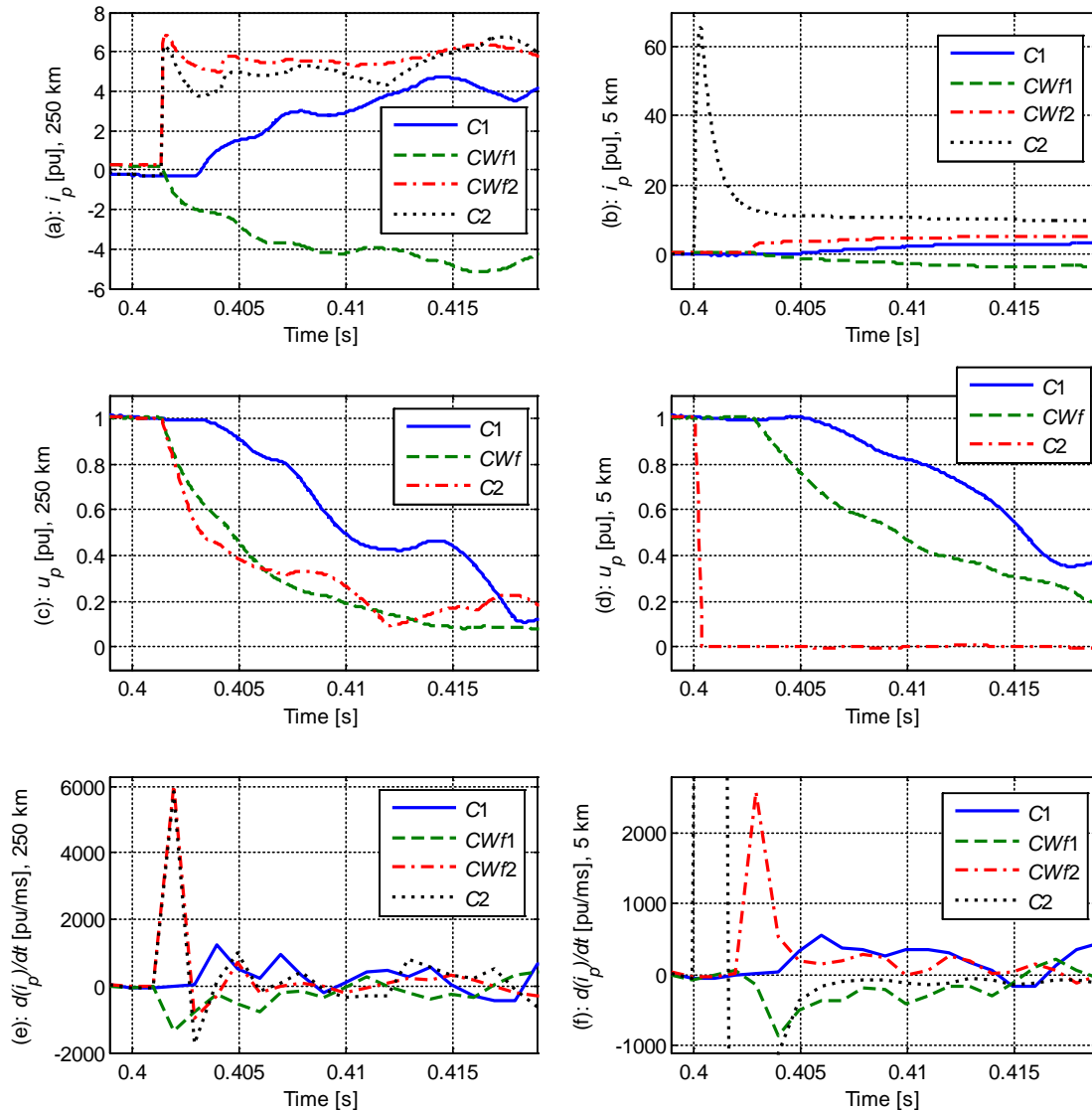
Figure 6.8 Positive phase current, -voltage and current derivative with phase-to-phase short circuit (a), (c) and (e): 250 km from converter *CWf* and *C*2. (b), (d) and (f): 495 km from converter *CWf* and 5 km from *C*2. I$_{base}$=1000/800 kA.

It can be seen from (a) and (b) that the fault current from the wind farm converter terminal towards country 1 ($i_{p,CWf1}$) is negative, while the fault current towards country 2 ($i_{p,CWf2}$) is positive. Based on this it can be concluded that the fault was located between the wind farm and country 2 HVDC terminals.

The maximum fault current and voltage drop seen at terminal *C*1 are not significantly smaller than at *CWf*. Therefore it cannot be clearly concluded based on local measurements at *C*1 that the fault is not located between *C*1 and *CWf*. However, the rate-of-change of current on each end of the faulted branch ($i_{p,C2}$ and $i_{p,CWf2}$) are significantly larger than at the ends of the healthy branch ($i_{p,C1}$ and $i_{p,CWf1}$). Thus criteria for detection of fault can be rate-of-change of current above a certain level, together with the decrease of voltage. For the fault 250 km from *C*2 (e), the maximum current derivative in terminal

PROJECT NO.
502000064

REPORT NO.
TR A7482

VERSION
1.0

97 of 133

$C1$ is 1200 pu/ms. For the fault 5 km from $C2$ (f) the maximum current derivative is very large, and the peak value is not shown. The derivative of the current from the wind farm terminal towards $C2$ is 2600 pu/ms. Thus a current derivative of 1200 pu/ms should not be lead to opening of the local circuit breaker, while a current derivative of 2600 pu/ms should be interpreted as a fault and lead to opening of the local breaker.

6.3.2 Phase-to-ground short-circuits

Although phase-to-phase faults are the most serious, phase-to-ground faults are much more likely to occur, and are therefore important to study. Figure 6.9 shows the current and voltage response on converter $C1$ terminals with positive-phase-to-ground faults 1 and 10 km from the converter terminal. The fault resistance is set to 0.01 Ω. Compared to the cases with phase-to-phase short circuits, no sharp increase of the current through the converter diodes, $i_{dc,p}$, is seen, but rather a more slow increase towards the steady-state fault current (similar to the phase-to-phase fault 100 km from the converter). Therefore a phase-to-ground fault appears less critical for the converter than a phase-to-phase fault. Still, very large capacitor discharge currents will flow to the fault location, which can be harmful.
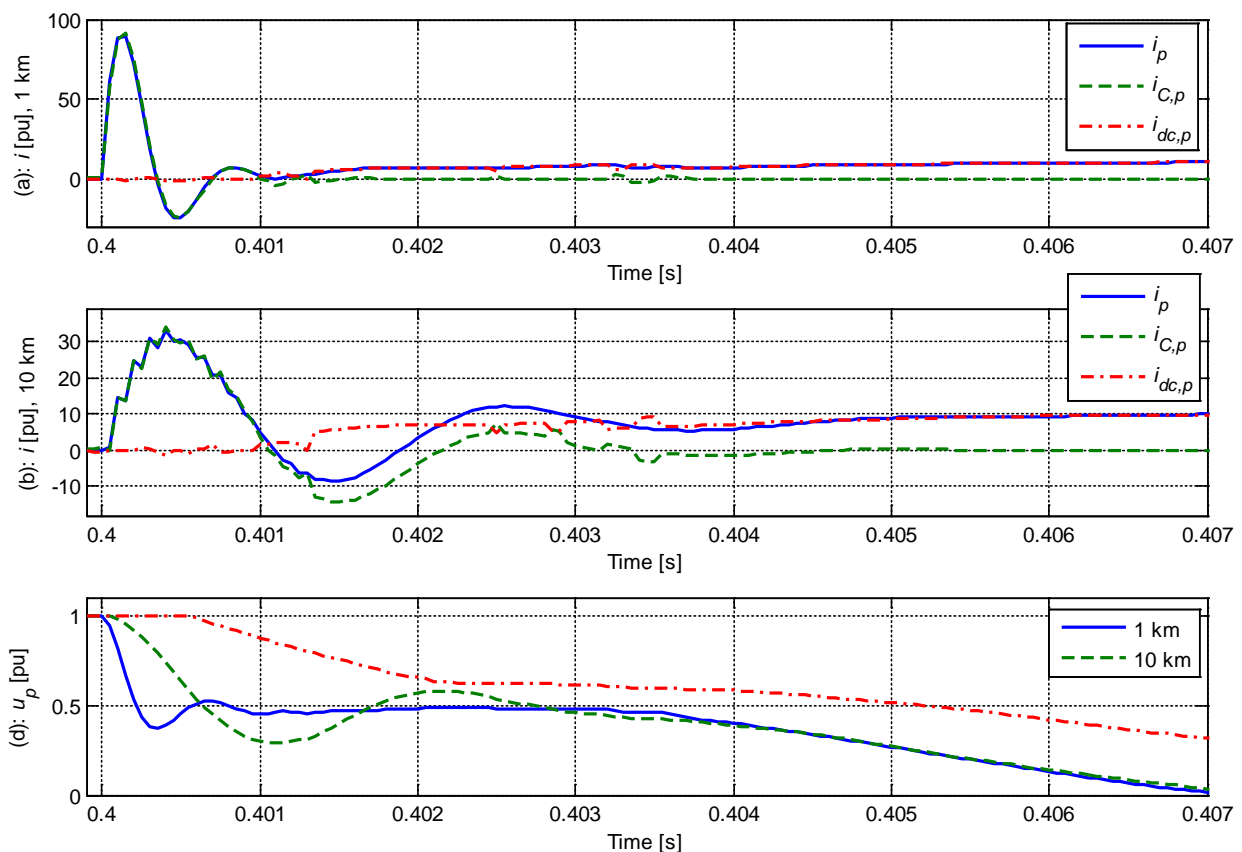
Figure 6.9 Response to positive phase-to-ground short circuits 1 and 10 km from the converter terminal. Current and voltage measured at converter terminals. R_f=0.01 Ω. I_{base}=1250/800 kA.

As for the phase-to-phase fault, the fault current approaches the same final "steady-state" value independent on the distance to the fault location. This final fault current value depends, among others, on the fault resistance and the transformer grounding. The equivalent circuit in Figure 6.10 can be used to calculate the fault current with a phase-to-ground fault at the converter DC-terminals. The transformer is Y-Δ connected, and the Y on the converter side with a very low resistance (1e^{-6} Ω) from the neutral-point to ground.

PROJECT NO.
502000064

REPORT NO.
TR A7482

VERSION
1.0

98 of 133
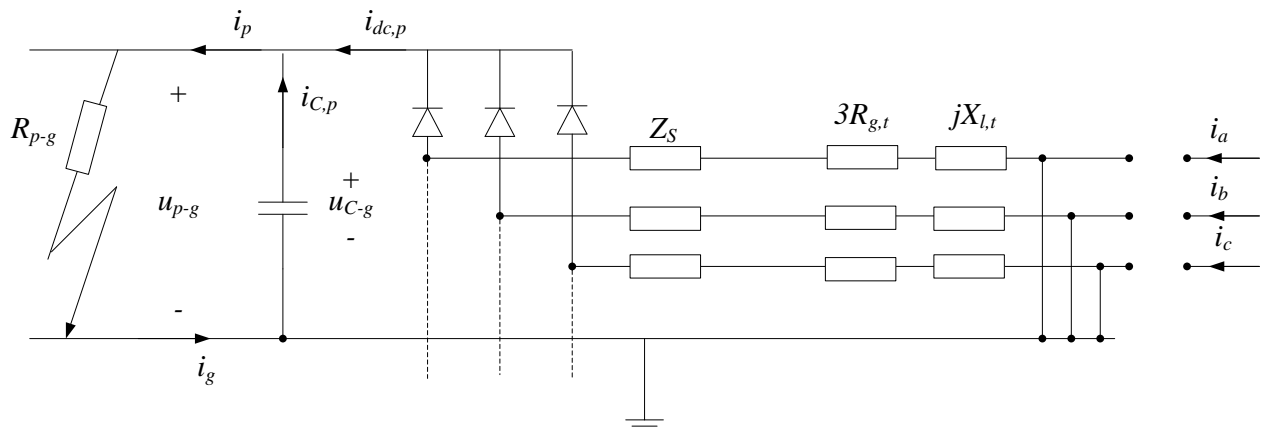
Figure 6.10 Equivalent circuit for steady-state earth fault current calculation

Where R_{p-g} is the fault resistance, Z_S is the converter filter impedance, $R_{g,t}$ is the transformer neutral point resistance and $X_{l,t}$ is the transformer leakage reactance.

$$\left|i_g\right| = \frac{\left|u_{p-g}\right|}{\left|R_{p-g} + Z_S + 3 \cdot R_{g,t} + jX_{l,t}\right|} = \frac{400\,kV}{\left|1 + 1.28 + j19.2 + 3 \cdot 1e^{-6} + j6.4\right|\Omega}$$

$$= \frac{400\,kV}{25.7\,\Omega} = 15\,kA = 15\,kA \cdot \frac{800\,kV}{1250\,MVA} \approx 10\ pu$$

The steady-state fault current of about 10 pu is probably large enough to damage the diodes, and the fault should be disconnected fast enough to prevent damage. As seen in Figure 6.9 this means that disconnection within a few milliseconds is required, which is very fast.

With a larger neutral point resistance, the fault current will be smaller. Figure 6.10 shows that the earth fault cannot be fed from the grid side of the AC-transformer with the Y-Δ connection. However, if the transformer was Y-Y connected, the earth fault would be fed from the AC-grid. Thus the grounding in the AC-grid determines the size of the steady-state earth fault current in the DC-grid. The low impedance grounding is positive for the HVDC-system, which would be "floating" without grounding on one its AC-sides.

6.3.2.1 Fault detection

Figure 6.11 shows current and voltage responses to positive-phase-to-ground fault 250 km and 5 km from the HVDC terminal in country 2 (*C2*).

PROJECT NO.
502000064

REPORT NO.
TR A7482

VERSION
1.0

99 of 133
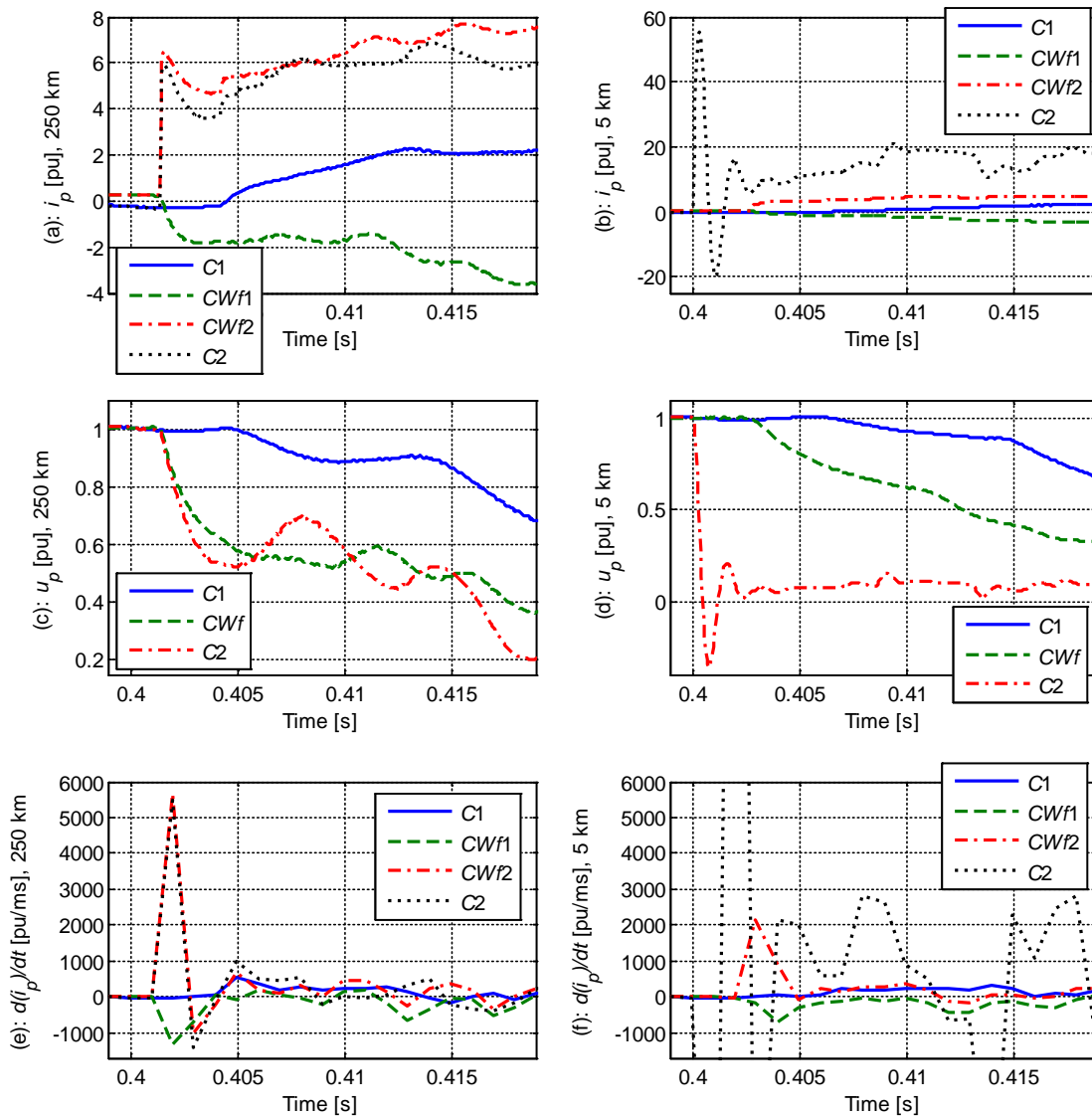
Figure 6.11 Positive phase current, -voltage and current derivative with positive phase-to-ground fault (a), (c) and (e): 250 km from converter *CWf* and *C*2. (b), (d) and (f): 495 km from converter *CWf* and 5 km from *C*2. 1000/800 kA.

Plots (a) and (b) show that the fault current from the wind farm converter terminal towards country 1 ($i_{p,CWf1}$) is negative, while the fault current towards country 2 ($i_{p,CWf2}$) is positive, similar to the phase-to-phase fault cases. The positive current indicates the faulted branch.

In this case there is some difference between the currents through terminal *C*1 and from *CWf* towards *C*1, and the current level could possibly be utilized for fault detection. However, as for the phase-to-phase faults, rate-of-change of current is a safer criterion for detection, together with the voltage drop. The rate-of-change of current on each end of the faulted branch ($i_{p,C2}$ and $i_{p,CWf2}$) are significantly larger than at the ends of the healthy branch ($i_{p,C1}$ and $i_{p,CWf1}$). For the fault 250 km from *C*2 (e) the maximum current derivative in terminal *C*1 is 550 pu/ms, which should not be seen as a fault an lead to opening of the breaker. With a fault 5 km from *C*2 (f) the maximum derivative of the current from the wind farm terminal towards *C*2 is 2200 pu/ms, and this should lead to breaker opening. Based on the results shown in Figure 6.8 and Figure 6.11 the criterion for detection should be a rate-of-change of current somewhere between 1200 and 2200 pu/ms. The rate-of-change of current and voltage drop

due to load changes are much smaller than for fault events as was seen for the most severe load step in Figure 6.5, and will not be mistaken for a fault.

6.3.3 Fault-ride-through capability with a DC-transmission fault

One advantage with having a multi-terminal topology is that the transmission system has redundancy. Thus, if there is a fault on one of the transmission branches, the remaining healthy part of the system can continue operation. This chapter studies the response of the system to different faults on the DC-transmission cables, in order to investigate if the remaining system can ride-through the fault and continue stable operation during and after the fault. The cable faults are assumed to be permanent, so that the faulted line section has to be disconnected and the system will operate as a two-terminal system after disconnection.

Figure 6.12 shows the active power (a) and DC-voltages (b) at the three terminals, in addition to the voltages in the wind farm collection grid and wind turbine generator DC-link (c) before and during a fault, and after disconnection of the faulted branch. The fault is a positive-phase to ground fault 5 km from CWf and 295 km from $C2$. In this case, the wind farm was modelled as a single back-to-back converter with rating 1250 MVA. $U_{DC,Wtg}$ in plot (c) is the voltage in the back-to-back converter DC-link. Before the fault occurrence, the wind farm is generating constant and close to nominal power (1000 MW), and all the generated power is delivered to terminal $C2$ while the power through terminal $C1$ is approximately zero. This is a worst case since the active power through $C1$ has to be changed from zero to nominal after the fault.
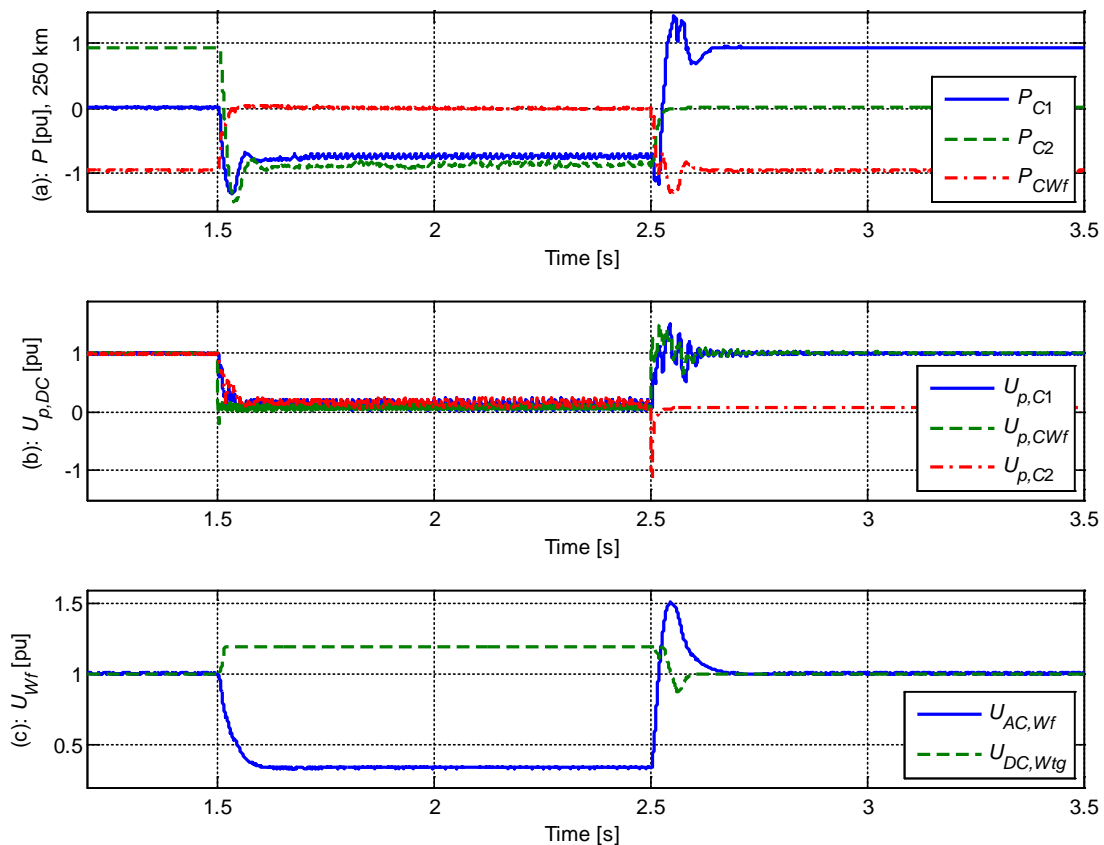
Figure 6.12 Response to positive-phase-to-ground fault between $C2$ and CWf, 5 km from CWf, at 1.5 s. Disconnection at 2.5 s. (a): Active power (P_{base}=1000 MW), (b): Positive phase DC-voltage, (c): wind farm collection grid AC-voltage and wind turbine DC-link voltage

The faulted section was in this case disconnected after 1 s., however the system remained stable for longer disconnection times. As seen from the plots, the system goes to a new stable operating point after the fault and disconnection of the faulted branch. In the post-fault state all power generated in the wind farm is transferred to terminal 1. The fault creates a voltage dip in the wind farm collection grid, and the generated power from the wind farm cannot be delivered to the grid. The excess power is therefore consumed by the DC-chopper, and the wind turbine DC-link voltage increases to 1.2 pu during the fault. The fault-ride-through capability is thus due to the action of the DC-chopper and the DC-voltage control of HVDC-terminal $C1$, which quickly adjusts the power through the terminal. The results with phase-to-phase faults, or faults closer to terminal $C2$ are similar, i.e. the disconnection of the faulted branch could take more than 1 s.

Figure 6.13 shows the response to a positive-phase-to-ground fault on the cable between the HVDC-terminals CWf and $C1$. The fault is located 5 km from CWf and 295 km from $C1$. As in the previous case the wind farm is generating close to nominal active power, but the power through terminal $C2$ is zero, and thus all power is delivered through terminal $C1$ before the fault occurs. In this case the faulted branch had to be disconnected within 15 ms in order to avoid instability.
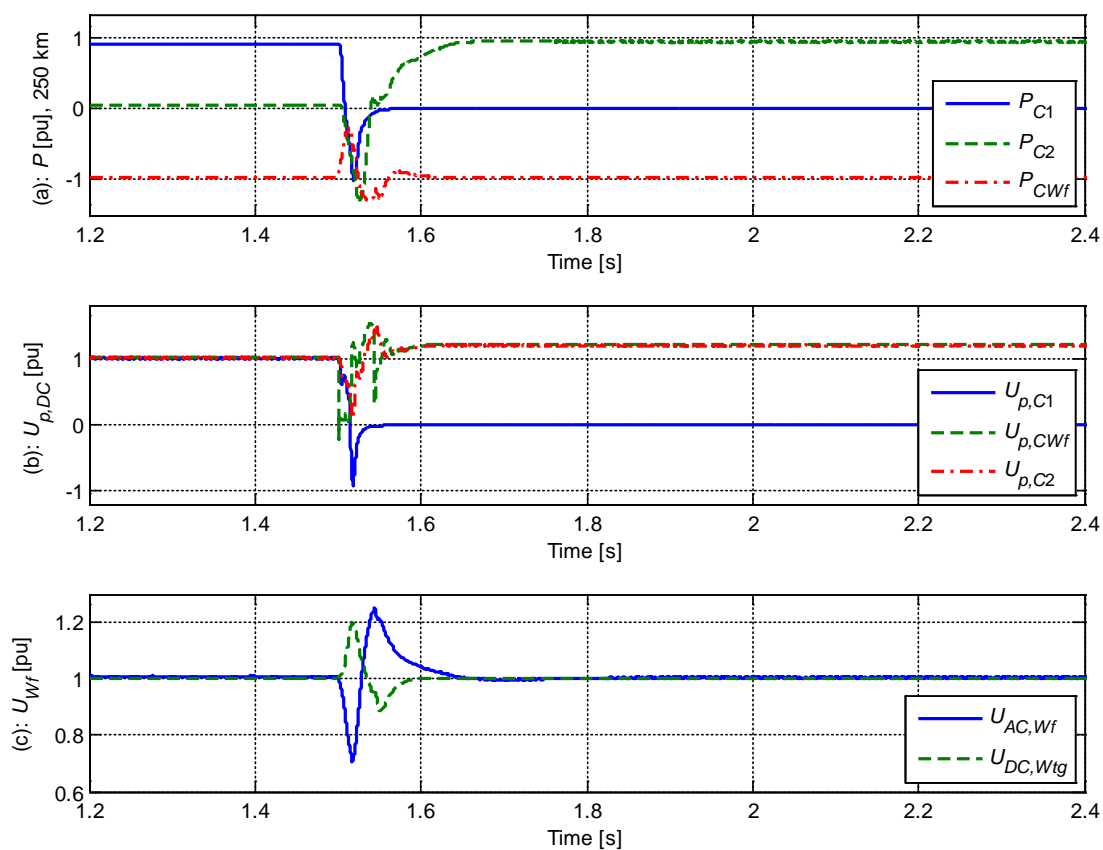
Figure 6.13 Response to positive-phase-to-ground fault between $C1$ and CWf, 5 km from to CWf, at 1.5 s. Disconnected at 1.515 s. (a): Active power (P_{base}=1000 MW), (b): Positive phase DC-voltage, (c): wind farm collection grid AC-voltage and wind turbine DC-link voltage

With a phase-to-phase fault in the same location, the faulted branch had to be disconnected within 8 ms in order to avoid instability for the remaining grid. If the fault was located 5 km from terminal $C1$ a phase-to-ground and phase-to-phase fault had to be disconnected within 32 ms. and 17 ms., respectively. Thus a fault close to the wind farm HVDC-terminal is more critical than a fault close to the terminal $C1$ regarding transient stability. Also, a phase-to-phase fault is more critical than a phase-to-ground fault.

PROJECT NO.
502000064

REPORT NO.
TR A7482

VERSION
1.0

102 of 133

However, the case where all the power from the wind farm is flowing through terminal *C*2 instead of *C*1 in the pre-fault state appears more critical than the case shown in Figure 6.13. The faulted branch then has to be disconnected within 12 ms instead of 15 ms.

Generally, the critical clearing times are much shorter for faults on the branch between *C*1 and *CWf* than for faults on the branch between *C*2 and *CWf*. A major difference between the two cases is that terminal *C*1 has constant DC-voltage control, while terminal *C*2 has active power control with DC-voltage droop. Thus it appears to be much more critical to lose the terminal with constant DC-voltage control than the terminal with DC-voltage droop. Faults close to the wind farm HVDC terminal (*CWf*) are more critical than faults close to terminals *C*1 and *C*2, which is as expected since faults close to *CWf* will have the largest impact on the whole DC-transmission grid. Also, *CWf* is controlling the wind farm collection grid voltage, and with a large voltage drop on its DC-side it might not be able to maintain this control. In addition, it is found that phase-to-phase faults are more critical than phase-to-ground faults, which is also expected since phase-to-phase faults cause the largest voltage drops.

In order for the system to ride-through faults in the DC-grid without interruption of operation, DC-breakers are required. If the fault is located on the branch between terminals *C*1 and *CWf*, the DC-breakers have to be very fast (disconnection within 8–32 ms for the cases discussed above). As a comparison, ABBs hybrid DC-breaker for high power applications can break currents within 5 ms [6.8]. However, this technology is still very new. As seen in chapters 6.3.1 and 6.3.2, HVDC grid faults close to the converter stations need to be disconnected very fast in order to prevent damage in the anti-parallel diodes. For phase-to-phase faults the required disconnection times were less than 1 ms for the worst cases, while the phase-to-ground faults should be disconnected within a few ms. Thus it appears very difficult to manage fast enough disconnection in these cases.

6.4 Fault-ride-through capability during collection grid faults

This section deals with responses to faults within the wind farm AC collection grid. The wind farm collection grid differs from conventional AC-grids as all sources are connected via power electronics converters, and thus the dynamic characteristics are governed by the converters and corresponding controllers. The short circuit current capacity in such a grid is very limited since the short circuit current capability of a converter is generally only slightly larger than the nominal current. In addition the grid is lacking inertia, making fast frequency fluctuations possible.

As the focus here is on the AC-collection grid and wind turbine responses, the HVDC-grid is modelled as a two-terminal connection. The wind farm was modelled with one branch with 16 wind turbines, where 4 of them were modelled separately with rating 6.25 MVA each and 12 were modelled as one aggregated wind turbine of rating 75 MVA. The remaining wind farm was modelled as one large aggregated wind turbine rated 1150 MVA (920 MW).

The responses to three-phase, two-phase and phase-to-ground short circuits in the collection grid are shown in Figure 6.15 to Figure 6.17. In all cases, the short circuit was located on the terminals of wind turbine 1, 0.5 km from the wind farm HVDC terminal. The fault durations were 100 ms. The fault location and the measurement points for the following figures are shown (with red) in Figure 6.14.

PROJECT NO.
502000064

REPORT NO.
TR A7482

VERSION
1.0

103 of 133
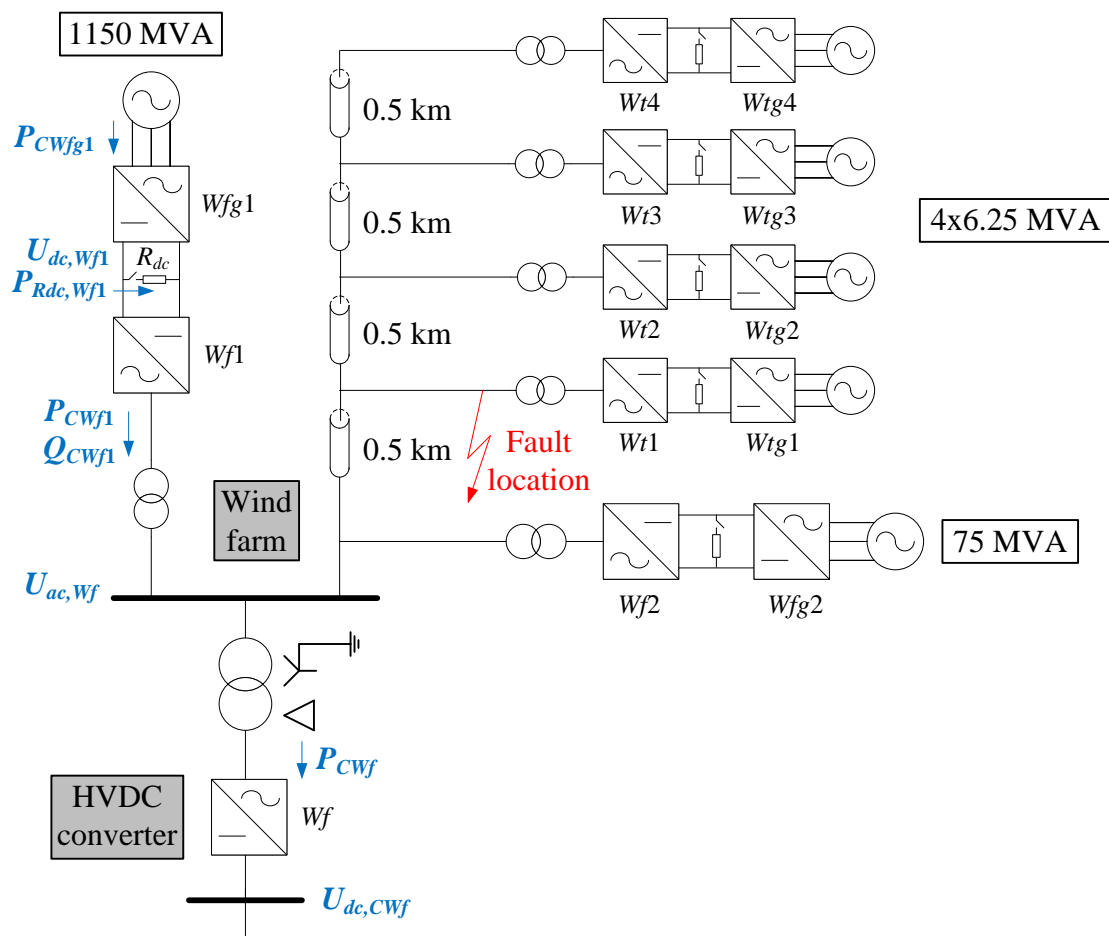
Figure 6.14 Wind farm collection grid with fault location and measurement points

The plot legends in Figure 6.15 and Figure 6.17 thus refer to the following:

- Plot (a): Collection grid AC-voltage ($U_{ac,wf}$). Active and reactive power delivered to the collection grid from the large aggregated 1150 MVA wind turbine (P_{QWf1}, Q_{CWf1}).
- Plot (b): Active power into 1150 MVA wind turbine on turbine-side (P_{CWfg1}). DC-voltage ($U_{dc,Wf1}$) and active power consumption in DC-chopper ($P_{Rdc,Wf1}$) of the same wind turbine.
- Plot (c): DC voltage ($U_{dc,CWf}$) and active power into wind farm HVDC-terminal (P_{CWf})

In the plots the pu-base for active and reactive power of the large aggregated wind turbine of rating 1150 MVA is chosen equal to the nominal active power: 920 MW.

All wind turbines are generating nominal active power, while the reactive power is set to zero.

PROJECT NO.
502000064

REPORT NO.
TR A7482

VERSION
1.0

104 of 133

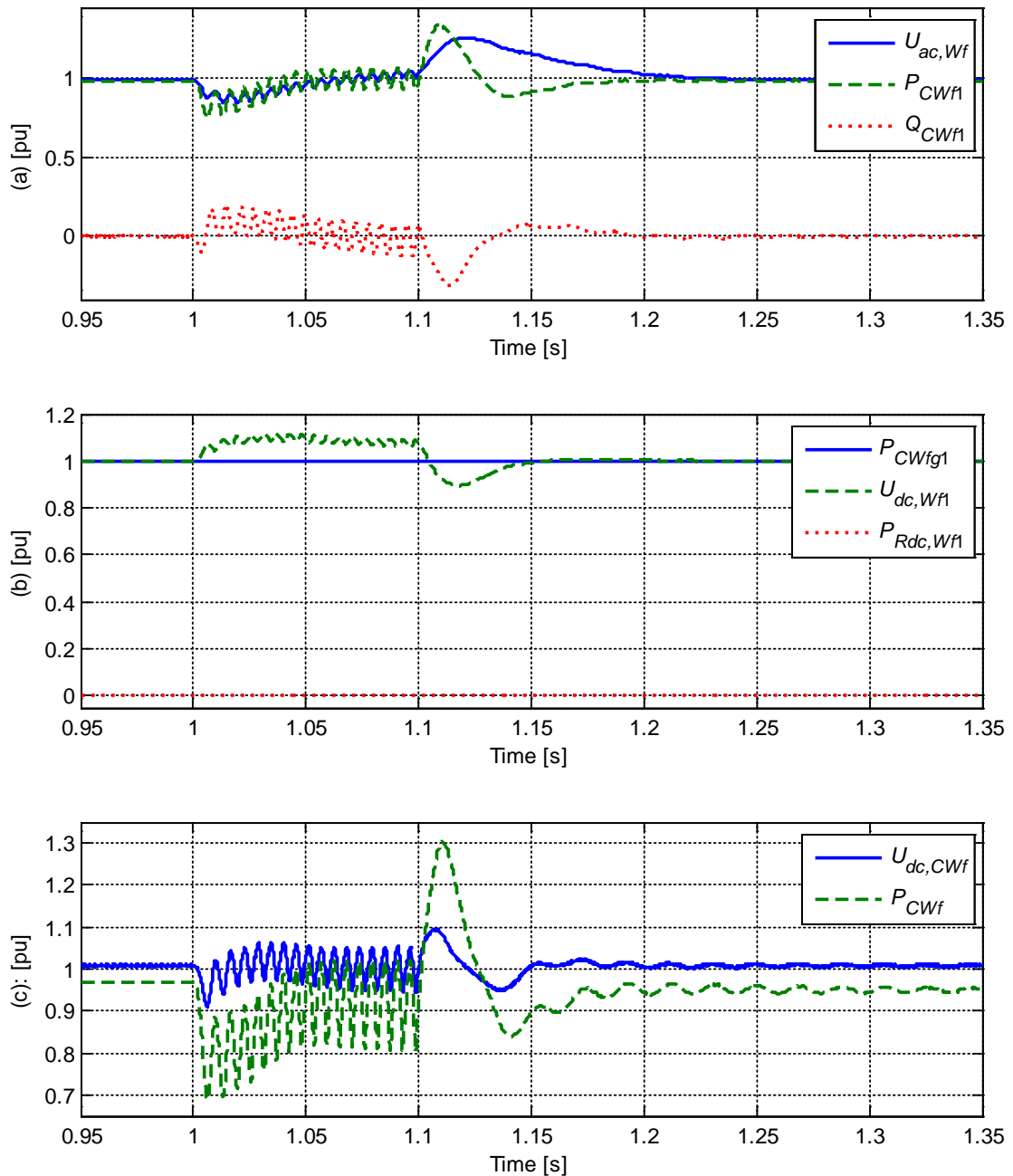## 6.4.1 Three-phase short circuit
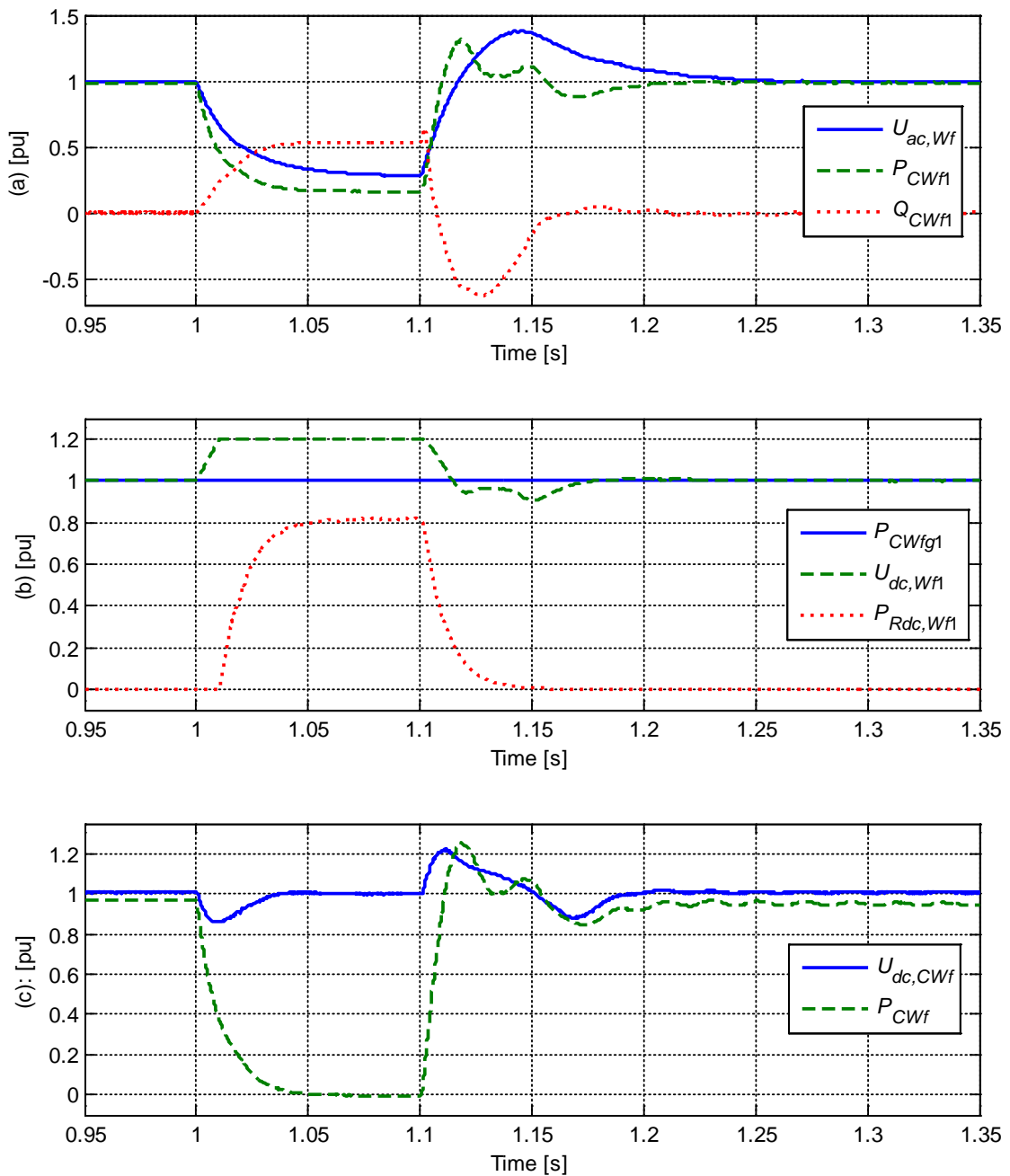
Figure 6.15 Response to a three-phase short circuit in the wind farm AC collection grid, 0.5 km from the wind farm HVDC terminal.

Plot (a) shows that the collection grid voltage drops down to about 0.28 pu during the three-phase short-circuit. This leads to a reduction of the active power delivered from the wind turbine goes down from 1 pu to 0.16 pu. The reactive power increases from zero to 0.53 pu. When the active power output is reduced there will be surplus of energy in the DC-link, since the power delivered from the wind turbine is not reduced, but cannot be delivered to the grid. This leads to an increase of the DC-link voltage, as seen in plot (b). When this voltage reaches 1.2 pu, the DC-resistor is connected and is consuming the surplus energy, preventing the voltage to increase above 1.2 pu. The active power into wind turbine side converter is not disturbed by the fault on the grid side. Plot (c) shows that the power

PROJECT NO.
502000064

REPORT NO.
TR A7482

VERSION
1.0

105 of 133

delivered to the wind farm HVDC converter goes down to zero during the dip. Some relatively small disturbances are seen in the HVDC voltage.
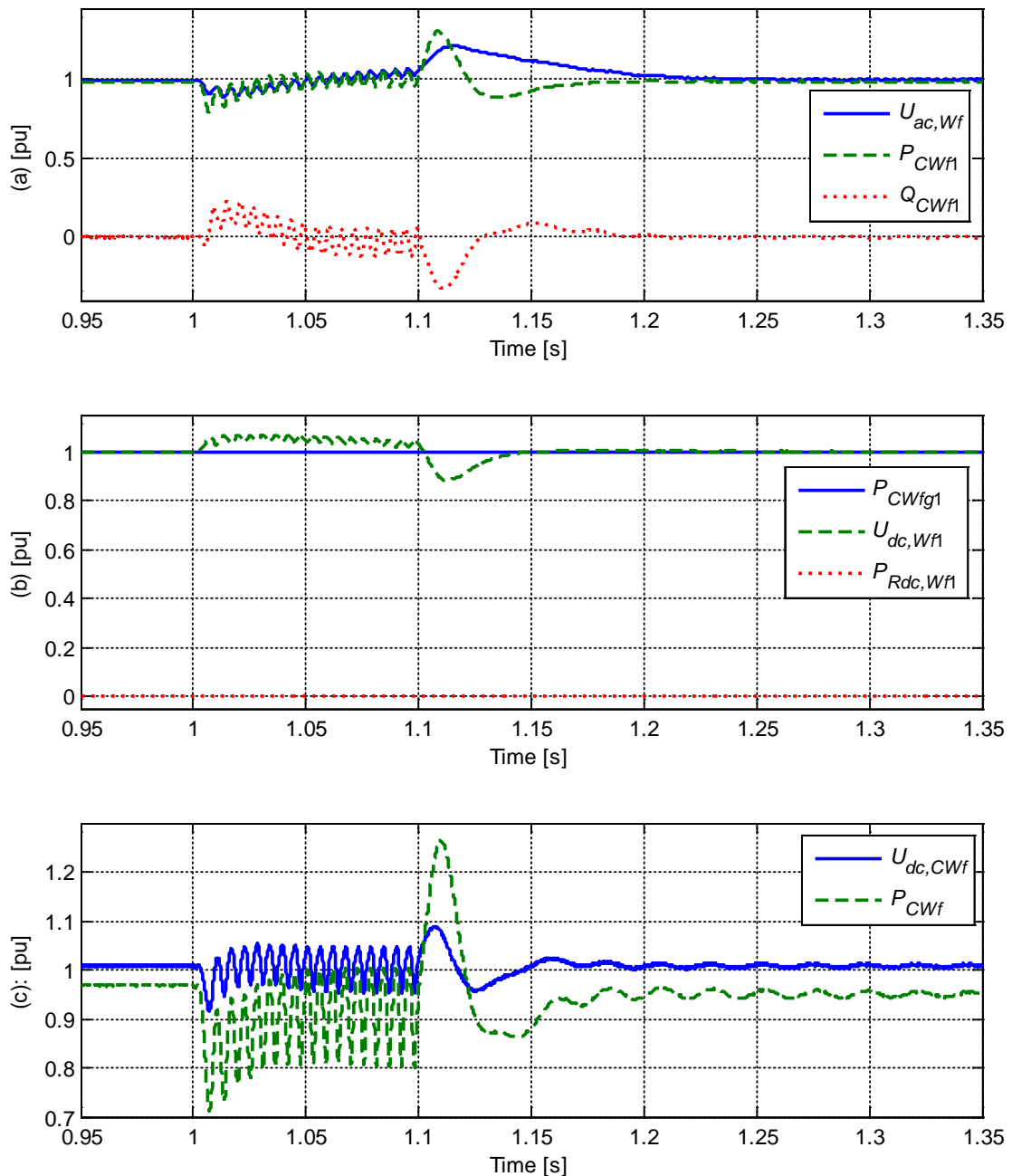
6.4.2 Two-phase short-circuit

Figure 6.16 Response to a two-phase short circuit in the wind farm AC collection grid, 0.5 km from wind farm HVDC terminal.

From plot (a) it can be seen that the collection grid voltage drops down to about 0.85 pu during the two-phase short-circuit, causing a similar reduction in the active power output. The reactive power output increases slightly. Oscillations are seen during the short-circuit, and these are due to the presence of negative sequence components. The active power delivered to the converter from the wind turbine side is not affected by the short-circuit, as seen in plot (b). Since the active power delivered to

the grid is reduced, the DC-link voltage is increased, up to about 1.1 pu. This is not enough to activate the DC-chopper. Plot (c) shows some oscillations in the HVDC-voltage at the wind farm terminal, which is caused by the disturbance in the power delivered from the wind farm to the HVDC-transmission grid.

6.4.3 Single phase-to-ground short-circuit

Figure 6.17 Response to a single-phase-to-ground short circuit in the wind farm AC collection grid, 0.5 km from wind farm HVDC terminal.

The response to the single-phase-to-ground fault is quite similar to that of the two-phase short-circuit, but slightly less severe. The collection grid voltage drops down to about 0.9 pu during the fault, which

leads to a small reduction in the active power output of the wind turbine converter and a small increase in the reactive power. The reduction of the active power output leads to an increase of the DC-link voltage up to about 1.05 pu, which is not enough to connect the DC-chopper. The fault causes oscillations in the HVDC-transmission voltage, but these are relatively small as seen in plot (c). Both negative- and zero- sequence components are present during the single-phase fault, and similar oscillations as for the two-phase short-circuit are seen.

The size of the single-phase to ground fault current depends on the grounding of the collection grid. In this case the main wind farm transformer connected to the HVDC-terminal was grounded through a very small (1 μΩ) resistance, so the collection grid is in reality directly grounded. This type of grounding gives the largest possible fault current, and the advantage is that fault detection becomes easier. What has not been considered in the simulation is the impedance in the ground-path between the fault location and the transformer neutral, whether the current goes in the real ground or in a separate ground conductor. This impedance will reduce the fault current.

6.4.4 Discussion of results

The three-phase short-circuit is seen to be the most severe; however the two-phase and single phase faults causes oscillations due the presence of negative sequence components. The wind turbine returns to normal operation after all three faults. In this case the fault-ride-through capability is determined by the converter characteristics, and not by the inertia as for a conventional generator directly connected to the grid. Due to the chopper-resistor in the DC-link, the wind turbine is transient stable despite of lacking inertia on the grid side.

Wind turbine converters can be controlled to have different types of behaviour during voltage dips. In this case reactive power control with a constant set-point of zero was applied. Other strategies could be chosen for the control of reactive power in order to maximize the voltage support during voltage dips, which is commonly required by grid codes in order help recovering the grid voltage. The simplest would be to apply voltage control instead of reactive power control. This requires an additional control loop where the output of the voltage controller will be input to the reactive power controller. Another solution is to apply a different strategy when the grid voltage goes below a certain value than in normal operation. When the wind turbine is generating nominal active power, there is little reactive current capability available in the converter. Therefore such a strategy could give priority to reactive power, and reduce the active power output to zero during the dip. Then the total current capability of the converter can be used for generating reactive power. This type of fault-ride-through strategy was not implemented in the model used in this work. Such a control strategy anyhow relies on having a chopper-controlled resistor in the DC-link, which has been implemented.

6.5 Short-circuit protection in the wind farm collection grid

Faults should be detected and disconnected fast enough so that the wind turbines can operate through the faults without disconnection. In Figure 6.15 to Figure 6.17 above the faulted branch was disconnected after 100 ms, and the system remained stable during and after the faults.

Distance protection is the most common main short-circuit protection of transmission lines and cables, as well as for meshed distribution networks [6.9]. Therefore it is interesting to investigate the possibility to use this type of protection for fault detection in the wind farm collection grid. Due to the power electronics converters, the grid has lower short-circuit current levels than conventional grids. Numerical distance relays can have different characteristics, but the basic principle for detection is that the impedance seen by the relay changes from a large value during normal operation to a small value when there is a fault in the grid. In addition the impedance is generally resistive during normal operation (reflecting the load impedance) and relatively more reactive during fault (reflecting the line/cable impedance).

PROJECT NO.
502000064

REPORT NO.
TR A7482

VERSION
1.0

108 of 133

Figure 6.19 shows impedance values seen by the distance relay located at the beginning of the collection grid branch with 16 wind turbines for three-phase and two-phase short-circuits at two different locations. All turbines are generating nominal active power. The fault locations and the measurement point for the relay are shown in Figure 6.18.
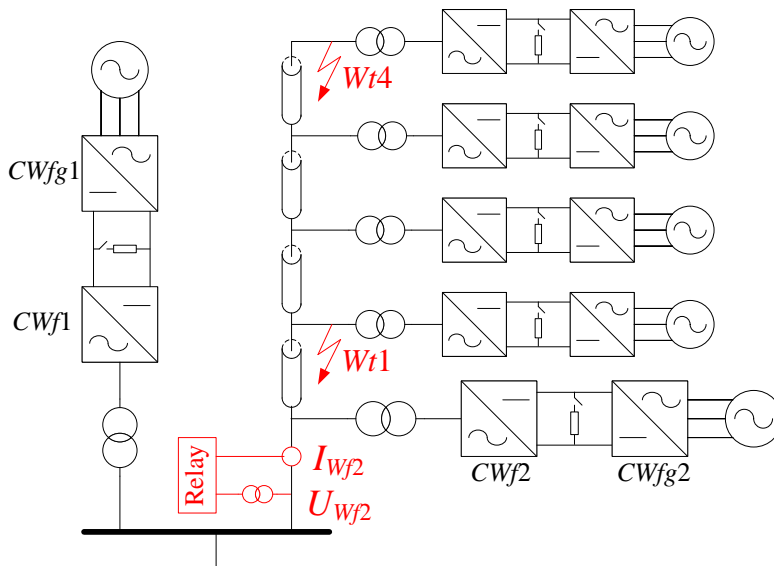

Figure 6.18 Fault locations ($Wt1$, $Wt4$) and "measurement" point (I_{Wf2}, U_{Wf2}) for distance relay corresponding to plots in Figure 6.19

The impedances are calculated from:

$$R_{ab,Wf2} + jX_{ab,Wf2} = \frac{U_{a,Wf2} - U_{b,Wf2}}{I_{a,Wf2} - I_{b,Wf2}}$$

(6.2)

Where subscripts a and b refers to phase a and phase b.

For a three-phase short-circuit, any pair of phase quantities can be used to calculate the impedance (ab, bc, ca), while for a two-phase short-circuit the two faulted phases will give the correct impedance. In the case shown here, the two-phase short-circuit was between phase a and b.

PROJECT NO.
502000064

REPORT NO.
TR A7482

VERSION
1.0

109 of 133
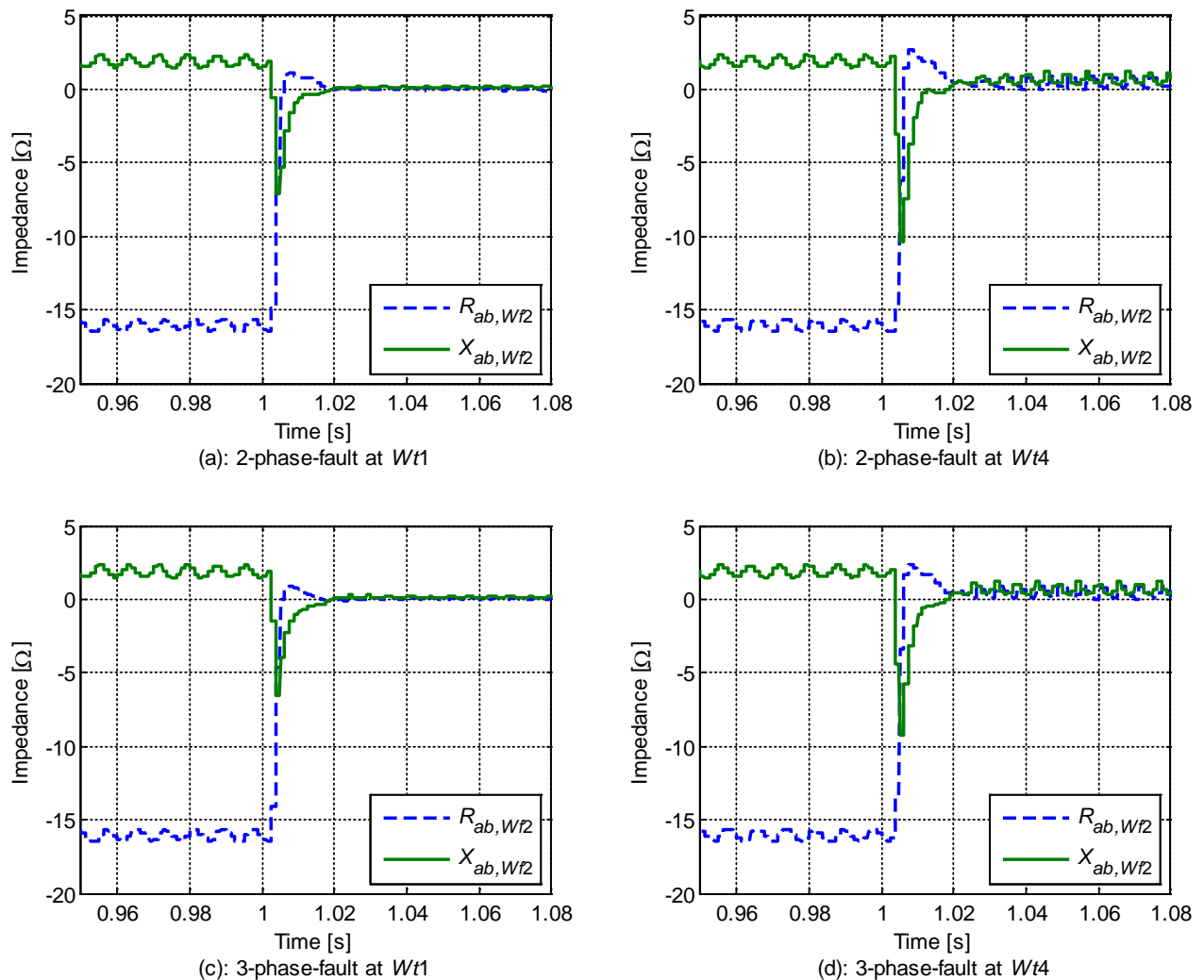
Figure 6.19 Impedances seen from distance relay at the beginning of the single branch of the wind farm collection grid during three-phase- and two-phase- faults at *Wt*1 and *Wt*4 terminals.

During normal operation the relay sees an impedance of $Z_{ab,Wf2} \approx -16 + j2\ \Omega = 16.1 e^{j172.9°}\ \Omega$. The resistance is negative, since positive direction for current measurement for the relay is from the HVDC-terminal towards the wind turbines, while the power flow is in the opposite direction. During the faults close to turbine *Wt*1 the impedance goes to approximately zero, while during the faults close to *Wt*4 the impedance is slightly larger, about $Z_{ab,Wf2} \approx 0.4 + j0.8\ \Omega = 0.9 e^{j63.4°}\ \Omega$. There is little difference between the two-phase and three-phase short-circuit cases. The difference between the impedance in normal and faulted operation is sufficient to allow for fault detection.

Even though the overcurrent capability of the converters is limited, the current through the relay during short-circuit will be significantly larger than during normal operation. This is because the total installed capacity on the faulted branch is much smaller than the total capacity of the wind farm, and during a fault, current will flow from the neighbouring un-faulted branch(es) to the fault. The sum of these currents will be significantly larger in magnitude than that floating from the branch to the HVDC-terminal in normal operation. In the example case there was 16 wind turbines on the faulted branch, while the total number of turbines in the wind farm is 200, i.e. only 0.08 of the installed capacity is connected to the faulted branch. If a larger share of the wind turbines were connected to the faulted branch, the difference between normal and faulted states would be less.

In order to illustrate which parameters that impact on the impedance seen by the relay, four different cases are shown in Figure 6.20. Impedances before and during three-phase short-circuits at wind turbine $Wt4$ terminals are shown. All wind turbines are generating nominal power, except in plot (a), where all are generating 10 % of nominal power. In plot (b) the length of each cable section is extended from 0.5 km to 2 km, and thus the total distance to $Wt4$ becomes 8 km. In plot (c) the rating of the two aggregated wind turbine converters have been changed. It is assumed that the wind farm has two branches with 100 turbines on each, so that the total converter rating on each branch is 625 MVA. Plot (d) shows results with a larger fault resistance, 10 Ω.
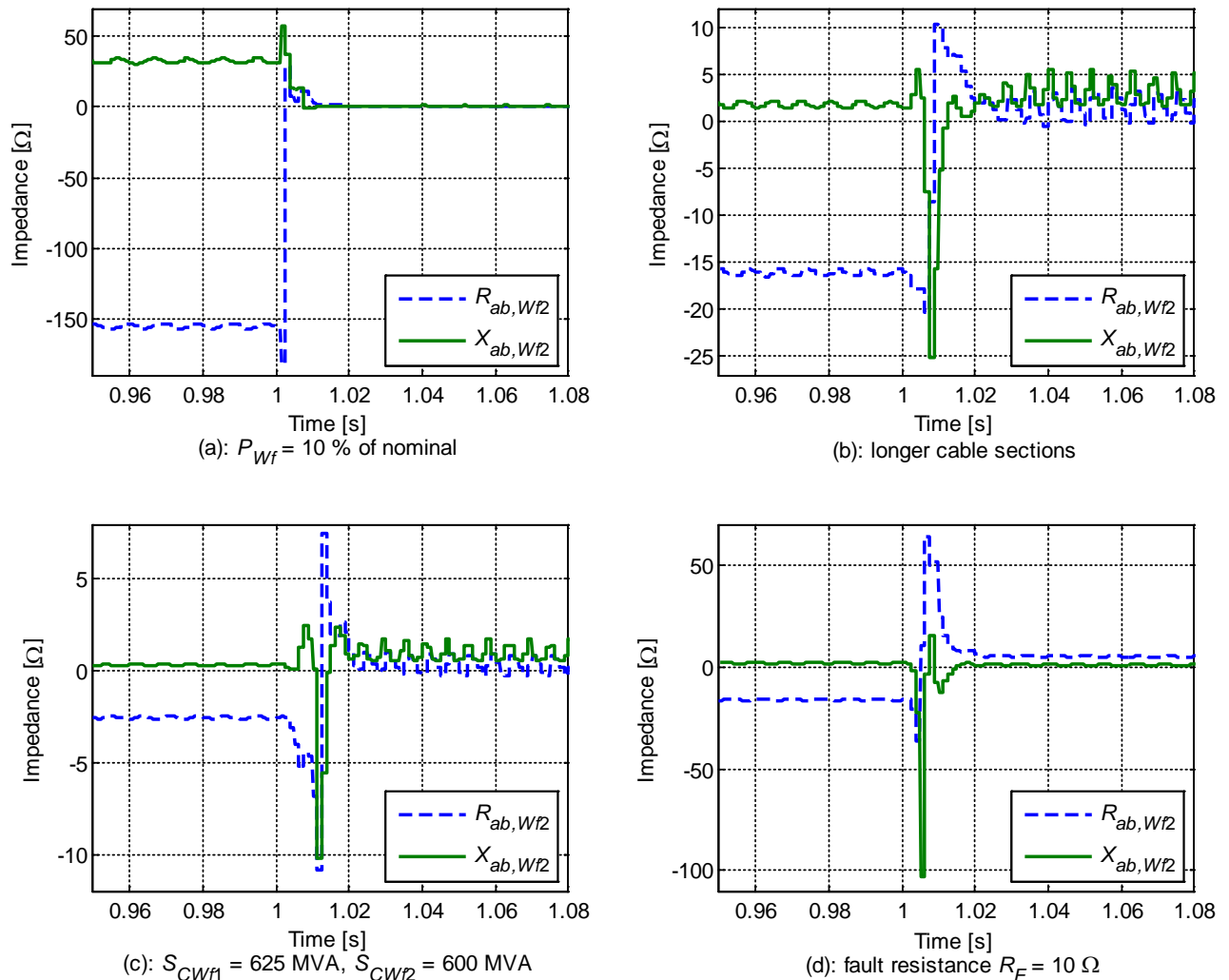
Figure 6.20 Impedances seen from distance relay at the beginning of the single branch during three-phase faults at $Wt4$ terminals. (a) Active power generation in wind farm 10 % of nominal, (b) 2 km cable sections, total 8 km (c) 100 wind turbines on each branch (d) large fault resistance

The high load case, i.e. all wind turbines are generating nominal active power, gives the smallest impedance in normal operation. As seen in plot (a), if the production level is lower, the impedance will be higher, and the difference between normal and faulted operation will also be larger. Therefore the case with nominal production is the most relevant to study.

In plots (b) and (d) the impedance in the pre-fault state is equal to that in Figure 6.19 above. In the case with 8 km to the fault location, the impedance becomes approximately $Z_{ab,Wf2} \approx 1.5 + j3.4$ Ω = $3.7e^{j66.2°}$ Ω during fault. This is 3-4 times larger than in the initial case with 0.5 km cable sections.

PROJECT NO.
502000064

REPORT NO.
TR A7482

VERSION
1.0

111 of 133

Thus with a longer distance from the relay to the fault the relay sees a larger impedance during fault. In this case there is still significant difference between normal and faulted state, and the fault can be detected. However, problems with detection could occur in case of very long feeders/branches.

In plot (c), the impedance in the pre-fault state is significantly reduced compared to the base-case, since much production is connected to the branch where the relay is located. The impedance is changing from $Z_{ab,Wf2} \approx$ -2.5 + j0.3 Ω = 2.5$e^{j173.2°}$ Ω to $Z_{ab,Wf2} \approx$ 0.3 + j1.1 Ω = 1.1$e^{j74.7°}$ Ω due to the fault. In this case there is little difference between the pre-fault and faulted state, and detection of the fault can be difficult. Detection based on the resistance value is however possible. If the fault resistance is large, detection could still be difficult. In plot (d) the fault resistance was 10 Ω, and this resulted in an impedance of $Z_{ab,Wf2} \approx$ 5 + j1 Ω = 5.1$e^{j11.3°}$ Ω during fault. A very high fault resistance is however most likely when the fault involves ground.

Summarized, distance protection seems to be suited for the type of grid studied. Studies with a sufficient detail level is however necessary to draw safe conclusions for each specific grid. A too simple model of the wind farm can lead to wrong conclusions. There could be problems with fault detection using distance relays in smaller wind farms with converter interfaced turbines. The solution would then be to use differential protection.

6.6 Summary

Simulations of faults in the onshore AC grids showed that the HVDC-transmission system can operate through such faults if the HVDC terminals have either DC-voltage control or active power control with DC-voltage droop. The short circuits caused very small disturbances in the wind farm voltage, and are therefore assumed to also have negligible impact on operation of the wind turbines. The proportional gain of the droop controller determines the sensitivity to changes in the DC-voltage. In the simulated cases, the controllers were tuned so that 0.2 pu change in DC-voltage caused 1.0 pu change in the active power reference for the controller, but other settings could be chosen. Also, no limit was put on the rate-of-change of the active power reference, and thus the response time was determined by the response time of the converter and corresponding control loops for d-axis current and active power. The very large and sudden change of the active power output of the HVDC-terminal connected to the healthy AC-grid might have negative consequences for the AC-grid. Therefore other solutions where the active power output of the wind farm is reduced during the dip could be better alternatives for providing fault-ride-through. Such solutions include having a chopper controlled resistor connected to the HVDC-grid [6.10], temporary reduction of the voltage magnitude or slight increase of the frequency in the wind farm collection grid [6.11]. These methods have however not been tested in this work.

Critical clearing times to assure fault-ride-through for the healthy part of the system for different faults in the HVDC-grid were investigated. Generally, faults close to the terminal with constant DC-voltage control lead to much shorter critical clearing times than faults close to the terminal with DC-voltage droop. In addition, faults close to the wind farm HVDC terminal were more critical than faults close to the two mainland terminals. This is not unexpected, since such faults will have the largest impact on both branches at the same time. Also, the wind farm HVDC converter is responsible for controlling the wind farm collection grid voltage, and with a large voltage drop on its DC-side the converter might not be able to maintain the control. Phase-to-phase faults were found to be more critical than phase-to-ground faults, which is expected since phase-to-phase faults cause the largest voltage drops. In order to assure fault ride-through of the un-faulted parts of the system, DC-breakers are required. For faults located on the branch between the wind farm HVDC-terminal and the terminal with constant DC-voltage control, the required disconnection time was found to be as short as 8-32 ms. This means that semiconductor based or hybrid breakers have to be used. As a comparison, ABBs hybrid DC-breaker for high power applications can break currents within 5 ms [6.8]. However, this technology is still very new and lacking experience from practical applications. Another issue is that faults close to the converter stations were seen to cause very large currents in the anti-parallel diodes of the

PROJECT NO.
502000064

REPORT NO.
TR A7482

VERSION
1.0

112 of 133

semiconductor switches. To prevent damage the required disconnection times for phase-to-phase faults were found to be less than 1 ms for the worst cases, and a few milliseconds for phase-to-ground faults. This appears very difficult to manage in practice. However, with other topologies, especially the modular multilevel converter (MMC), the large current due to discharge of the capacitor in the phase-to-phase fault cases could probably be avoided. For the phase-to-ground fault a larger grounding impedance could reduce the steady-state fault current. These matters could be topics of further research.

Three-phase, two-phase and single-phase-to-ground short-circuits in the wind farm AC-collection grid were investigated. The three-phase fault is naturally the most severe, however the two-phase and single phase faults cause oscillations in currents and voltages due the presence of negative sequence components. The wind turbines returned to normal operation after all simulated fault cases. With faults in the wind farm grid the fault-ride-through capability is determined by the wind turbine converter characteristics, rather than the generator inertias as in a conventional grid. The wind turbine converters were implemented with chopper-controlled resistors in their DC-links, which is a common solution [6.10]. These consume excess energy which cannot be delivered to the grid during voltage dips, so that overvoltages in the DC-links are avoided. The wind turbines can then operate undisturbed through the grid faults. Grid codes commonly require wind turbines to provide reactive power to the grid during voltage dips in order help recover the grid voltage [6.12]. To achieve this, the control can give priority to reactive power, and reduce the active power output to zero when the grid voltage goes below a certain value. Then the total current capability of the converter can be used for generating reactive power during the dip. This type of fault-ride-through strategy was not implemented in the model used in this work. Such a control strategy anyhow relies on having a chopper in the DC-link, which has been implemented.

Distance protection appears suited for use in the wind farm collection grid, despite the low short-circuit levels of the converter interfaced generators. However, there could potentially be problems with this type of protection in smaller wind farms with converter interfaced turbines. The solution would then be to use differential protection.

6.7 Bibliography

[6.1]   Jorun I. Marvik, AN 13.12.30 "Three-terminal HVDC case study specification and modelling". Project memo, SINTEF Energy Research, 2013 (Internal memo).

[6.2]   M. Callavik, A. Blomberg, J. Häfner, B. Jacobson, "The Hybrid HVDC Breaker. An innovation breakthrough enabling reliable HVDC grids", ABB Grid Systems, White Paper, 2012. Accessible from http://new.abb.com/about/hvdc-grid.

[6.3]   J. Yang, J.E. Fletcher, J. O'Reilly, "Short-Circuit and Ground Faults Analyses and Location in VSC-Based DC Network Cables", IEEE Transactions on Industrial Electronics, Vol. 59, No. 10, Oct. 2012, p. 3827-3837

[6.4]   M.E. Baran, N.R. Mahajan, "Overcurrent Protection on Voltage-Source-Converter-Based Multiterminal DC Distribution Systems", IEEE Transactions on Power Delivery, Vol. 22, No. 1, Jan. 2007, p. 406-412

[6.5]   R.S. Chokhawala, J. Catt, L. Kiraly, "A Discussion on IGBT Short-Circuit Behaviour and Fault Protection Schemes", IEEE Transactions on Industry Applications, Vol. 31, No. 2, 1995, p. 256-263

[6.6]   J. Yang, J.E. Fletcher, J. O'Reilly, "Multiterminal DC Wind Farm Collection Grid Internal Fault Analysis and Protection Design", IEEE Transactions on Power Delivery, Vol. 25, No. 4. Oct. 2010, p. 2308-2318

[6.7]   L. Tang, B.-T. Ooi, "Protection of VSC-Multi-Terminal HVDC against DC Faults", IEEE 33rd Annual Power Electronics Specialists Conference, 2002, Vol. 2, p. 719-724

[6.8]   ABB web page, http://new.abb.com/about/hvdc-grid, accessed May 3rd 2013.

[6.9]   G. Ziegler, Numerical Distance Protection. Principles and Application. 3rd edition, 2008. Publicis KommunikationsAgentur GmbH, GWA, Erlangen, Germany. ISBN 978-3-89578-318-0

PROJECT NO.
502000064

REPORT NO.
TR A7482

VERSION
1.0

113 of 133

[6.10] S.K. Chaudhary, R. Teodorescu, P. Rodriguez, P.C. Kjar. "Chopper controlled resistors in VSC-HVDC transmission for WPP with full-scale converters", IEEE PES/IAS Conference on Sustainable Alternative Energy, 2009, 8 pages.

[6.11] C. Feltes, H. Wrede, F.W. Koch, I. Erlich, "Enhanced Fault Ride-Through Method for Wind Farms Connected to the Grid Through VSC-based HVDC Transmission", IEEE Transactions on Power Systems, vol. 24, no. 3, pp 1537-1545, 2009

[6.12] ENTSO-E, "Network Code for Requirements for Grid Connection Applicable to all Generators", June 2012. Available from: www.entsoe.eu/major-projects/network-code-development/requirements-for-generators/

PROJECT NO.
502000064

REPORT NO.
TR A7482

VERSION
1.0

114 of 133

A HVDC converter modeling

A.1 Determination of controller parameters

A.1.1 Transfer function for current control loop

The resulting open-loop transfer function included the PI-controller becomes:

$$h_{OL,cc}(s) = K_{P,cc} \frac{1 + T_{i,cc} \cdot s}{T_{i,cc} \cdot s} \cdot \frac{1}{1 + T_{conv} \cdot s} \cdot \frac{1}{R_S} \cdot \frac{1}{1 + T_S \cdot s} \tag{A.1}$$

The transfer function has two poles:

- one at $T_{conv} = 1/(2 \cdot f_s) = 1/(2 \cdot 2500)$ s $= 0.0002$s, where f_s is the converter switching frequency
- one at $T_S = L_S/(\omega_{base} \cdot R_S) = 0.10/(0.01 \cdot 2 \cdot \pi \cdot 50)$ s $= 0.03183$ s

The controller can be tuned using the magnitude (modulus) optimum criteria. Then the first step is to choose the integral time constant $T_{i,cc}$ so that the largest pole is cancelled out: $T_{i,cc} = T_S$.

This results in the following open-loop (OL) and closed-loop (CL) transfer functions respectively:

$$h_{OL,cc}(s) = \frac{K_{P,cc}}{T_S R_S} \cdot \frac{1}{s(1 + T_{conv}s)} \tag{A.2}$$

$$h_{CL,cc} = \frac{h_{OL,cc}}{1 + h_{OL,cc}} = \frac{K_{P,cc}}{T_S R_S T_{conv} \cdot s^2 + T_S R_S \cdot s + K_{P,cc}} \tag{A.3}$$

In the literature $K_{P,cc}$ is chosen as: $K_{P,cc} = \dfrac{T_S R_S}{2T_{conv}}$

The band-width can be increased by increasing $K_{P,cc}$, by a constant n_{cc}:

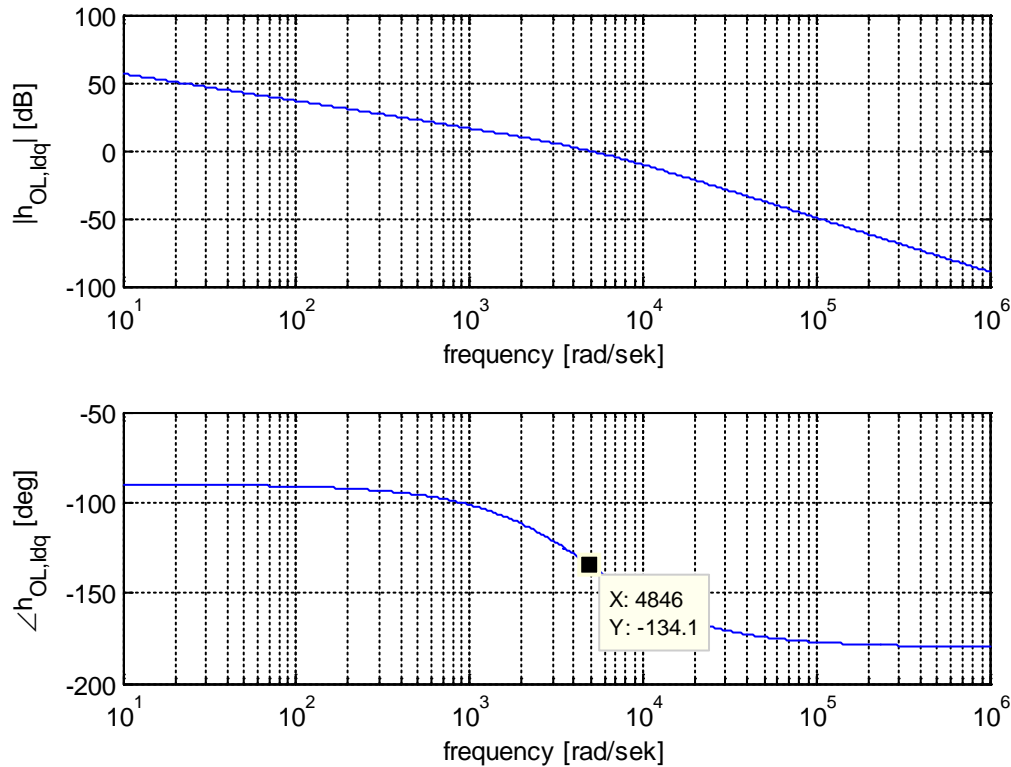$$K_{P,cc} = n_{cc} \frac{T_S R_S}{2T_{conv}} \tag{A.4}$$

Inserting (A.4) into (A.2) and (A.3) results in the following OL and CL transfer functions:

$$h_{OL,cc}(s) = \frac{n_{cc}}{2T_{conv}} \cdot \frac{1}{s(1 + T_{conv}s)} \tag{A.5}$$

$$h_{CL,cc}(s) = \frac{n_{cc}}{n_{cc} + 2T_{conv}s(1 + T_{conv}s)} = \frac{1}{1 + T_{eq,c}s + T_{eq,c}T_{conv}s^2} \tag{A.6}$$

Where $T_{eq,c} = \dfrac{2T_{conv}}{n_{cc}}$

Bode plot of the open-loop transfer functions is shown in Figure A.1 for $n_{cc} = 2.7$:

Figure A.1: Open loop transfer function for the current control loops, $n_{cc} = 2.7$

The cross-over frequency ω_c is about 4846 rad/s, and this corresponds to the bandwidth. The phase margin is then about 46°, which is an acceptable stability margin.

A.1.2 Linearized control of DC-voltage (outer loop)

The control of the DC voltage is implemented by cascade-control, with a DC-voltage control loop outside of the d-axis current control loop. If losses in the converter are neglected, the active power on the DC-side equals the active power on the AC-side:

$$U_{DC}I_{DC} = \frac{3}{2}\left(u_D i_D + u_Q i_Q\right) = \frac{3}{2}u_D i_D \tag{A.7}$$

And in pu:

$$U_{dc} \cdot I_{dc} = u_d \cdot i_d \quad \Rightarrow I_{dc} = \frac{u_d \cdot i_d}{U_{dc}} \tag{A.8}$$

Capital letter in the subscript means SI-unit values (A, V), while small letters in the subscript means pu-values.

The current in the DC link capacitor is:

$$I_C = C'\frac{dU_{DC}}{dt} \quad \Rightarrow I_c = \frac{C}{\omega_{base}} \cdot \frac{dU_{dc}}{dt} \tag{A.9}$$

PROJECT NO.
502000064

REPORT NO.
TR A7482

VERSION
1.0

116 of 133

For the DC-side, the following equation can be put up:

$$I_L = I_c + I_{dc} = \frac{C}{\omega_{base}} \frac{dU_{dc}}{dt} + \frac{u_d i_d}{U_{dc}} \tag{A.10}$$

The equation can be written as a Taylor series around an equilibrium point, with $U_{dc} = U_{dc,0}$, $u_d = u_{d,0}$, $i_d = i_{d,0}$ and $I_L = I_{L,0}$. Only the first order term is taken into the account, as the higher order terms are assumed close to zero.

$$\frac{C}{\omega_{base}} \frac{dU_{dc}}{dt} \approx \frac{u_{d0} i_{d0}}{U_{dc0}^2} U_{dc} - \frac{i_{d0}}{U_{dc0}} u_d - \frac{u_{d0}}{U_{dc0}} i_d + I_L$$

$$\Rightarrow U_{dc} = \frac{\omega_{base}}{Cs} \left(\frac{u_{d0} i_{d0}}{U_{dc0}^2} U_{dc} - \frac{i_{d0}}{U_{dc0}} u_d - \frac{u_{d0}}{U_{dc0}} i_d + I_L \right) \tag{A.11}$$

A block diagram showing the relation from eq. (A.11) is shown in Figure A.2. The feedback term from V_{dc} and the input proportional to v_d are considered as disturbances which are neglected in the further work. It is assumed that $u_{dc,0} = 1$ pu and likewise $u_d \approx u_{d0} \approx 1$ pu, and thus the two terms can be assumed to approximately cancel each other out.
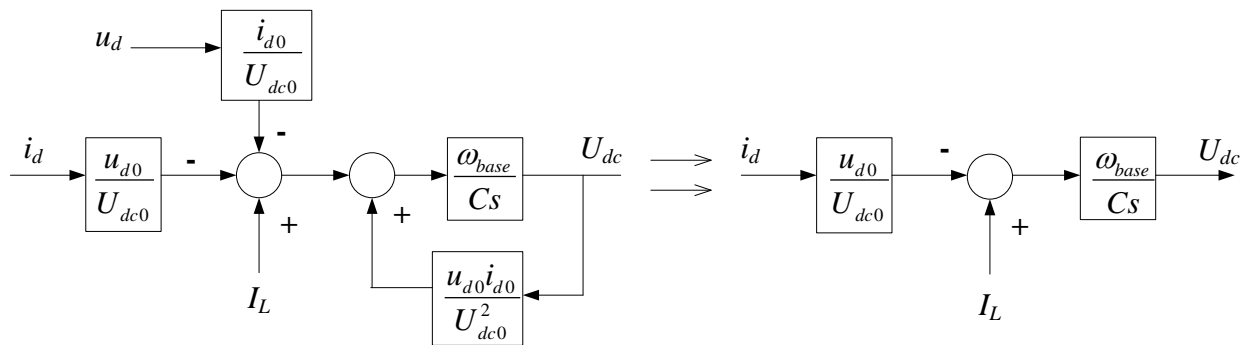
Figure A.2: Block diagram representation of relation between i_d and U_{dc}, simplified relation shown to the right.

Feed-forward can be used to reduce the impact of slow dynamic response in a cascade control system. Assuming that the current in the DC-capacitor is zero, $I_L = I_{dc}$. The feed-forward (f-f) term for i_d then becomes:

$$i_d^{f-f} = \frac{U_{dc}}{u_d} I_L \tag{A.12}$$

The resulting control loop including the current control was shown in Figure 5.5. One question is if the capacitance in the cable should be included in the DC-link tuning. For now, only the shunt capacitor on the converter terminal is included.

A.1.3 Transfer function of U_{dc}-control loop

The open-loop transfer function becomes:

PROJECT NO.
502000064

REPORT NO.
TR A7482

VERSION
1.0

117 of 133

$$h_{OL,Udc}(s) = K_{P,Udc} \cdot \frac{1 + T_{i,Udc} \cdot s}{T_{i,Udc} \cdot s} \cdot h_{CL,cc} \cdot \frac{1}{T_C \cdot s}$$

$$= \frac{K_{P,Udc}}{T_{i,Udc} \cdot T_C} \cdot \frac{1 + T_{i,Udc} \cdot s}{s^2\left(1 + T_{eq,c}s + T_{eq,c}T_{conv}s^2\right)} \approx \frac{K_{P,Udc}}{T_{i,Udc} \cdot T_C} \cdot \frac{1 + T_{i,Udc} \cdot s}{s^2\left(1 + T_{eq,c} \cdot s\right)} \qquad (A.13)$$

Where: $T_C = \dfrac{C}{\omega_{base}}$

The capacitance on the DC side is uncertain, but for now only the shunt capacitor on the dc-terminals of the converter is included in T_C, while the cable capacitance is neglected.

A common practice in the tuning of the outer control loop is to neglect the second order term in the closed loop transfer function for the inner current control loops so that only one time constant remains; T_{conv}. Then the outer controller can be tuned according to the so-called symmetrical optimum. The cross-over frequency ω_c corresponds to the maximum phase margin:

$$\frac{d}{d\omega}\left(\angle h_{OL,Udc}(j\omega_c)\right) = 0 \;\Rightarrow\; \omega_c = \frac{1}{\sqrt{T_{i,Udc}T_{eq,c}}} \qquad (A.14)$$
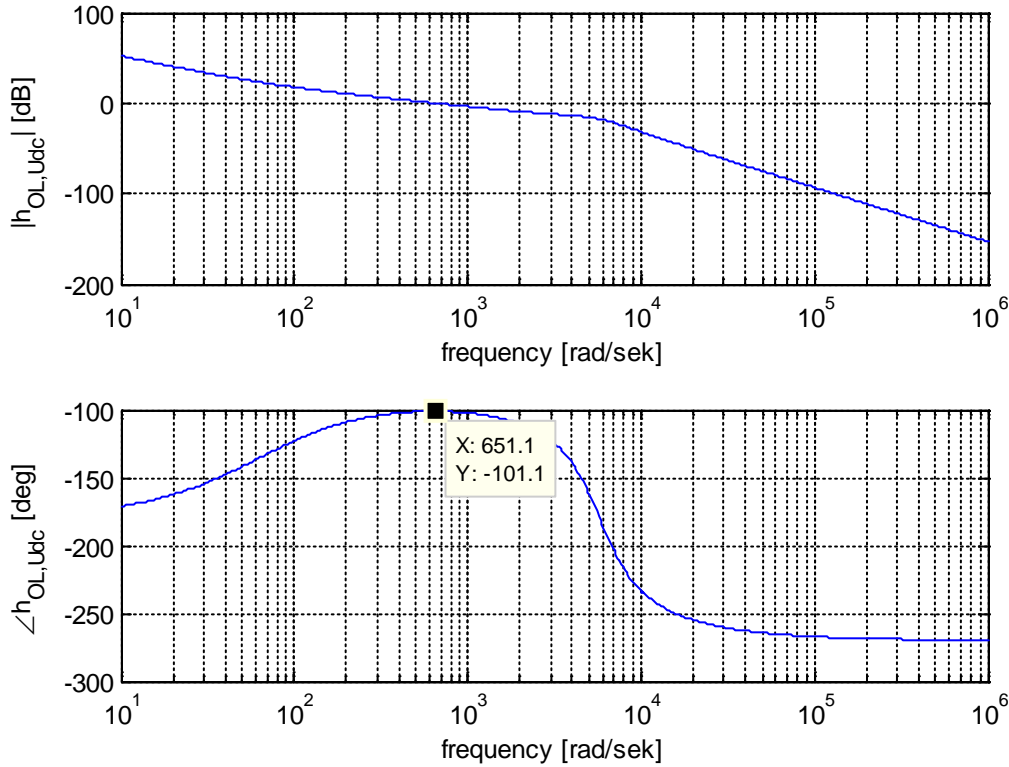
The proportional constant is found by setting the absolute value of the transfer function at the cross-over frequency equal to 1:

$$\left|h_{OL,Udc}(j\omega_c)\right| = 1 \;\Rightarrow\; K_{P,Udc} = T_{i,Udc}T_C\omega_c^2\sqrt{\frac{1 + \omega_c^2 T_{eq,c}^2}{1 + \omega_c^2 T_{i,Udc}^2}} = T_C\sqrt{\frac{1}{T_{i,Udc} \cdot T_{eq,c}}} \qquad (A.15)$$

The integral time-constant is a function of the phase margin $\Phi_{OL,Udc}$:

$$T_{i,Udc} = T_{eq,c}\frac{\left(1 + \sin\left(\Phi_{OL,Udc}\right)\right)}{\left(1 - \sin\left(\Phi_{OL,Udc}\right)\right)} \qquad (A.16)$$

The cross-over frequency should be about 1 decade lower for the outer voltage control loop than the inner loop current control loop (which was 4846 rad/s). A phase margin $\Phi_{OL,Udc} = 79°$ gives a cross-over frequency of approximately 650 rad/s, which is less than 1 decade below that of the current control loop. However, this can still be acceptable as the phase margin is large. The corresponding bode plot is shown in Figure A.3. The resulting controller parameters are $K_{P,Udc} = 6.656$ and $T_{i,Udc} = 0.016$.

PROJECT NO.
502000064

REPORT NO.
TR A7482

VERSION
1.0

118 of 133

Figure A.3: Open loop transfer function for the DC-voltage control loop

A.1.4 Control of active and reactive power

It is attempted to tune these controllers using symmetrical optimum, as for the dc-voltage controller. Again, the cross-over frequency ω_c corresponds to the maximum phase margin:

$$\frac{d}{d\omega}\left(\angle h_{OL,PQ}\left(j\omega_c\right)\right) = 0 \quad \Rightarrow \omega_c = \frac{1}{\sqrt{T_{eq}T_{i,PQ}}} \tag{A.17}$$

The proportional constant is found by setting the absolute value of the transfer function at the cross-over frequency equal to 1:

$$\left|h_{OL,PQ}\left(j\omega_c\right)\right| = 1 \quad \Rightarrow K_{P,PQ} = \frac{\omega_c T_{i,PQ}}{v_d}\sqrt{\frac{1+\omega_c^2 T_{eq}^2}{1+\omega_c^2 T_{i,PQ}^2}} = \frac{1}{v_d} \tag{A.18}$$

Where v_d is assumed constant and equal to 1 pu.

The integral time-constant is a function of the phase margin $\Phi_{OL,PQ}$:

$$T_{i,PQ} = T_{eq}\frac{\left(1+\cos\left(\Phi_{OL,PQ}\right)\right)}{\left(1-\cos\left(\Phi_{OL,PQ}\right)\right)} \tag{A.19}$$

As for the U_{dc}-controller, the cross-over frequency should be lower than for the inner current control loop.

PROJECT NO.
502000064

REPORT NO.
TR A7482

VERSION
1.0

119 of 133

A phase margin $\Phi_{OL,PQ} = 169°$ gives a cross-over frequency of approximately 650 rad/s, which is acceptable as the phase margin is very large. The corresponding bode plot is shown in Figure A.4. The resulting controller parameters are $K_{P,PQ} = 1$ and $T_{i,Udc} = 0.016$.
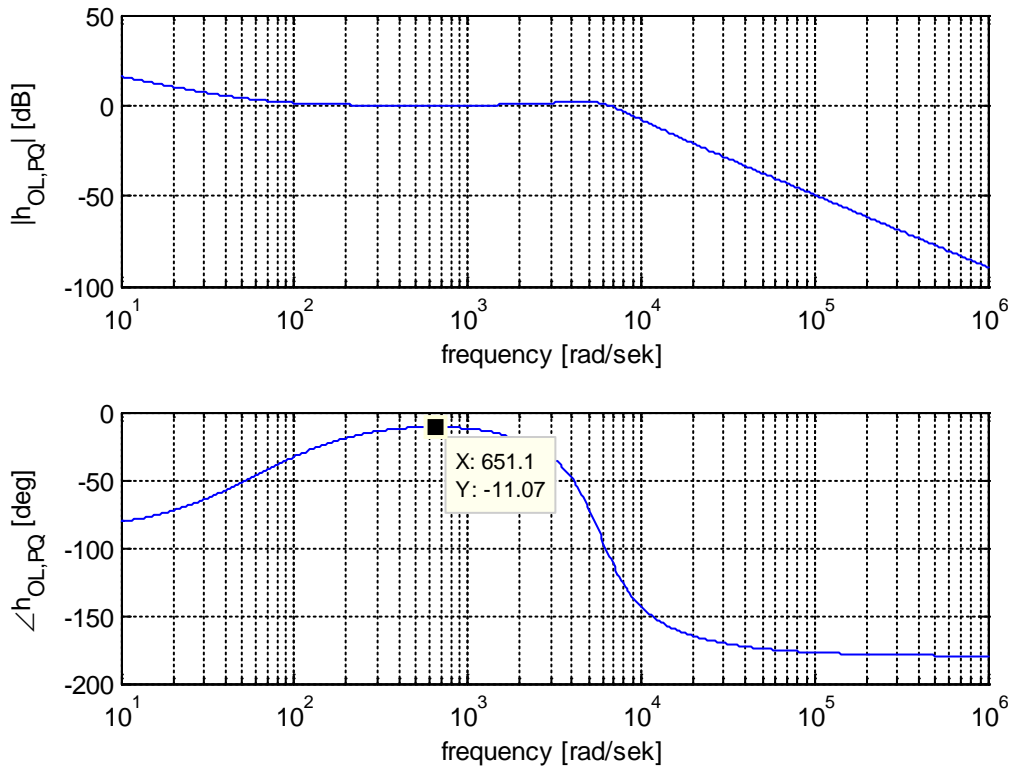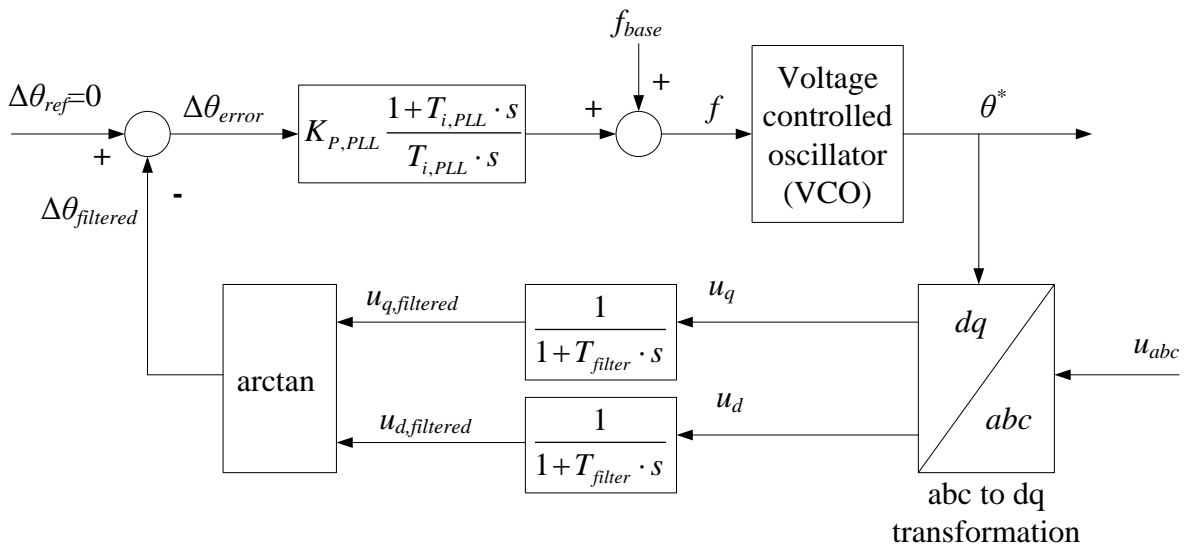

Figure A.4: Bode plot for open-loop transfer function for *P* and *Q* control

A.2 Synchronous reference frame phase locked loop

The block diagram for the PLL is as shown in Figure A.5.

PROJECT NO.
502000064

REPORT NO.
TR A7482

VERSION
1.0

120 of 133

Figure A.5: block diagram for PLL

The *d*-axis is aligned with the grid voltage vector. A deviation between the *dq* synchronous reference frame and the phase angle of the voltage vector will results in a non-zero *q*-axis voltage component. The PI-controller of the PLL can be tuned by symmetrical optimum.

A.3 Test simulation for validation of three-terminal HVDC-model

As an initial test the system responses to steps in the active power flow have been investigated through simulations.

A.3.1 Case 1: positive active power reference for converter *C*2

In this case the wind farm is generating constant power of 1000 MW, while the active power reference for converter *C*2 is increased in steps from 0 to 1000 MW, as shown in Figure A.6. The response in the DC-voltage is shown in Figure A.7.
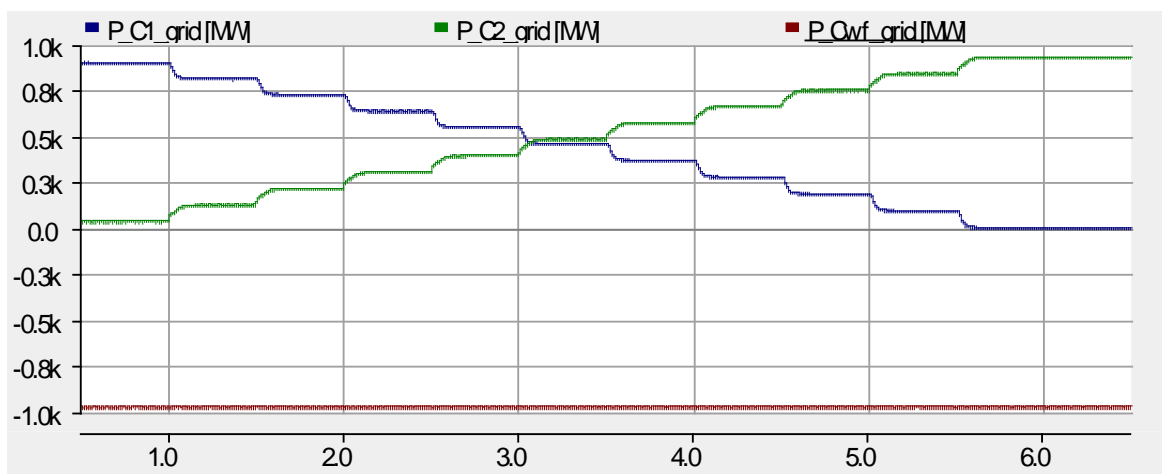
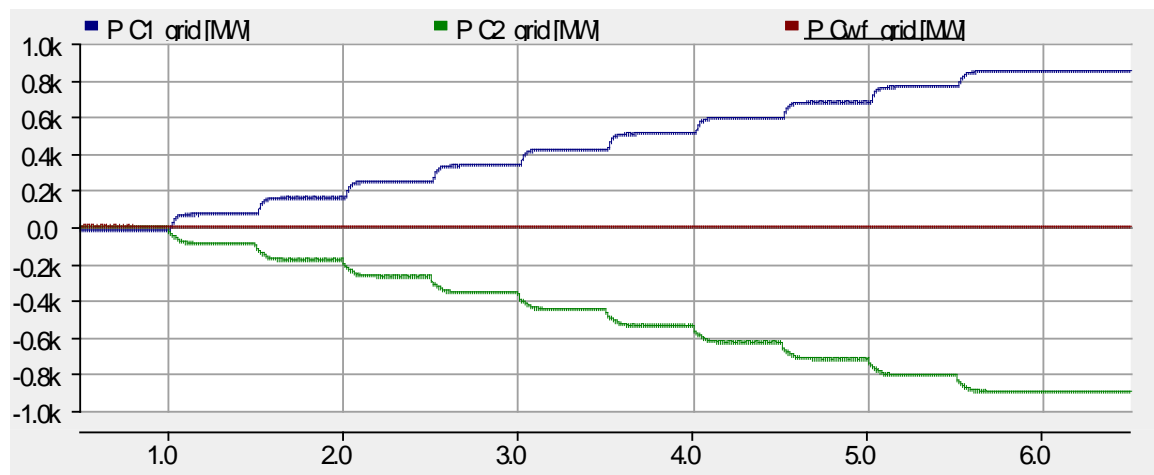**Figure A.6: Active power on AC-grid side of converters *C*1, *C*2 and *CWf***

PROJECT NO.
502000064

REPORT NO.
TR A7482

VERSION
1.0

121 of 133
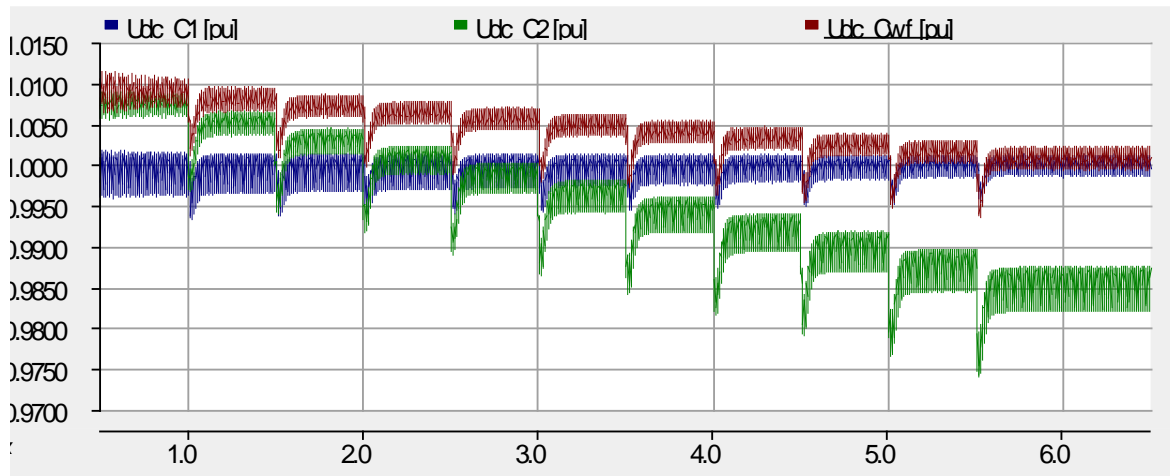
Figure A.7: Voltage on DC-terminals of converters *C*1, *C*2 and *CWf*.

The system operates stable for all active power levels. Terminal *C*1 has DC-voltage control, and thus the voltage is kept constant.

A.3.2 Case 2: negative active power reference for converter *C*2

The wind farm is generating zero active power while the active power reference for converter C2 is stepped down from zero to –1000 MW, as shown in Figure A.8. The corresponding DC-voltage responses are shown in Figure A.9.

As seen, the system operates stable through the step changes in active power reference.

Figure A.8: Active power on AC-grid side of converters *C*1, *C*2 and *CWf*

PROJECT NO.
502000064

REPORT NO.
TR A7482

VERSION
1.0

122 of 133
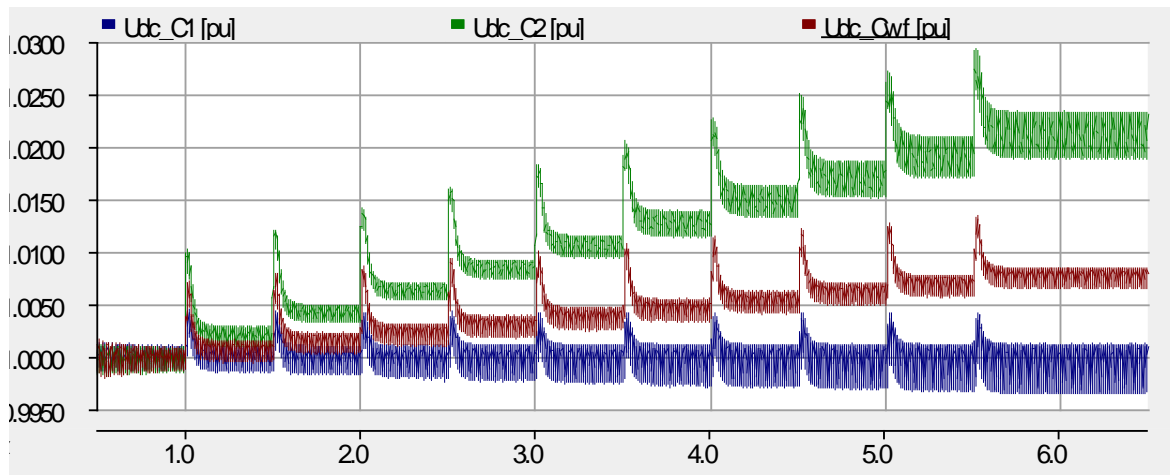
Figure A.9 Voltage on DC terminals of converter *C*1, *C*2 and *CWf*.

PROJECT NO.
502000064

REPORT NO.
TR A7482

VERSION
1.0

123 of 133

B Economic assessment of grid connection alternatives

This subsection analyzes the investment costs and makes efficiency estimations of four different transmission architectures. On the one hand transmission architectures with a medium voltage AC collector grid, that is HVAC (figure B.1(a)) and HVDC VSC (figure B.1(b)) are considered. On the other hand, transmission systems with a medium voltage DC collector system are also analyzed. Related to the latter, parallel connection of wind turbines to a unique offshore platform (figure B.2(a)) and series connection of two wind turbines without an offshore platform (figure B.2(b)) are studied. The voltage levels of the transmission and collector systems of each architecture can be found in the figures. It is important to highlight that for the architecture with series connection of two wind turbines a ±80 kV bipolar configuration has been considered. At this voltage level a power up to 450 MW can be transmitted with just one cable using to the current state of the art cable technology. Thus, for this power level, it is not necessary to use an offshore substation. Under this configuration each wind turbine should allocate an 80 kV DC output that, according to some wind turbine manufacturers consulted, could be feasible in terms of isolation and space requirements.
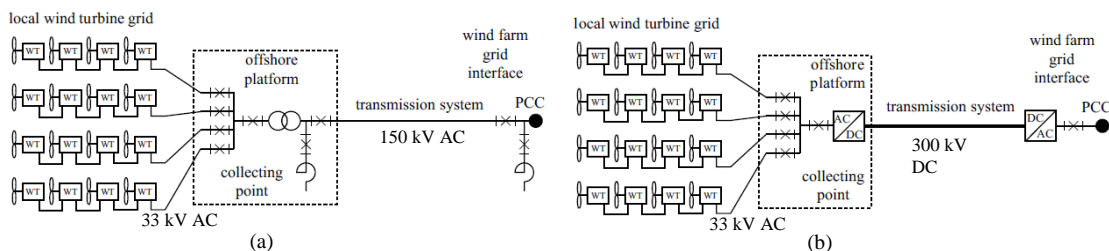
Figure B.1. (a) HVAC wind farm layout; (b) HVDC VSC wind farm layout. Courtesy of [B.1].
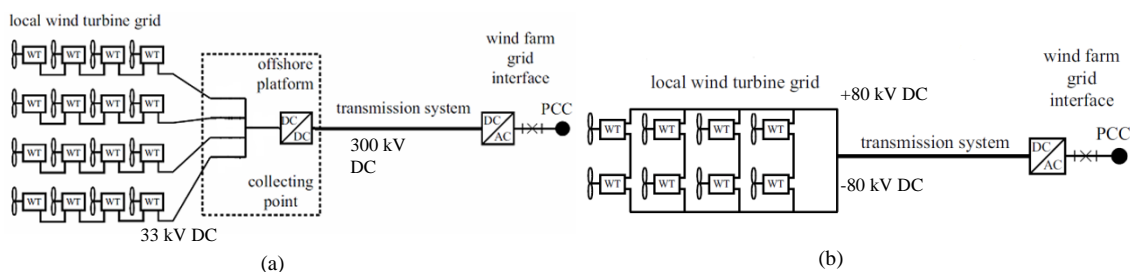

Figure B.2. (a) DC collector system. Parallel connection; (b) DC collector system. Series connection. Courtesy of [B.1].

Figure B.3 (a) and B.3 (b) show a cost analysis for a 495 MW offshore wind farm located at 50 and 100 km from the coast line, respectively. A description on the input data used for this analysis can be found in subsection B.1. The analysis shows the cost in p.u. of the main transmission components. It includes the cost of the collector system, the transmission cable, the offshore platform, the AC/DC or DC/DC and DC/AC power converters, the transformers and the global cost for different transmission technologies. Similarly, figure B.4 (a) and B.4 (b) show the losses in p.u. for similar wind farms. The procedure followed for the estimation of the losses is described in subsection B.2. The contribution to the losses of the wind turbine power converters, transmission and collector cables, transformers and the AC/DC, DC/DC and DC/AC HVDC VSC converters are broken down for different transmission technologies. Based on this study the following conclusions can be drawn:

- Those topologies including a DC collector grid have better efficiency and lower cost than the conventional HVDC VSC transmission architecture. This is mainly due to the lower cost and losses of the DC cables.

PROJECT NO.
502000064

REPORT NO.
TR A7482

VERSION
1.0

124 of 133

- When the distance up to the grid connection point is around 100 km both, the conventional HVDC VSC and the transmission architectures with a medium voltage DC collector grid, have better efficiency and lower cost than the HVAC systems.
- The transmission architecture without the offshore platform is the one with lowest losses and cost. According to the previous results this topology is advantageous in terms of efficiency and costs with regard to the HVAC systems even when the distance to the connection point decreases up to 50 km.

Therefore, according to these conclusions, it seems interesting to develop a medium voltage DC/DC converter that allows tapping the wind turbines to a DC collector system.

(a)

(b)
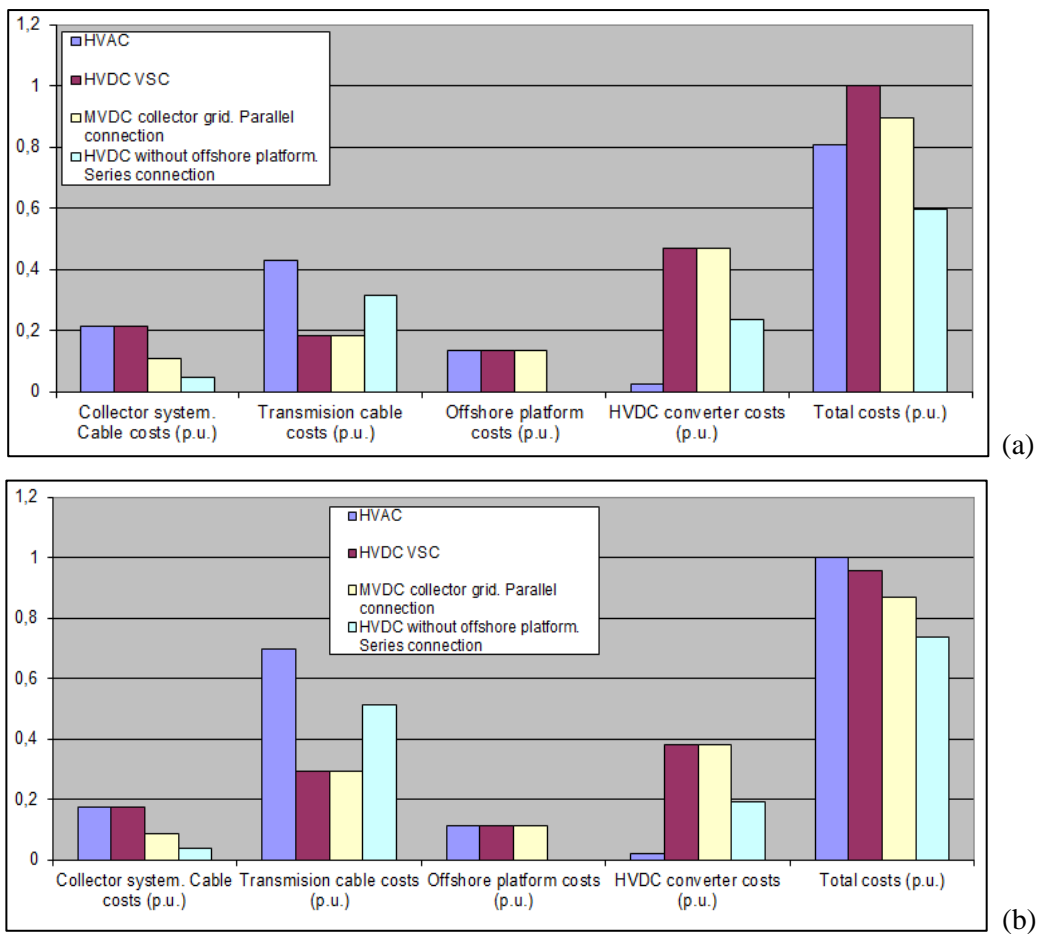
Figure B.3. Cost break down of different transmission technologies for a 495 MW offshore wind farm: (a) 50 km; (b) 100 km.

PROJECT NO.
502000064

REPORT NO.
TR A7482

VERSION
1.0

125 of 133

(a)

(b)
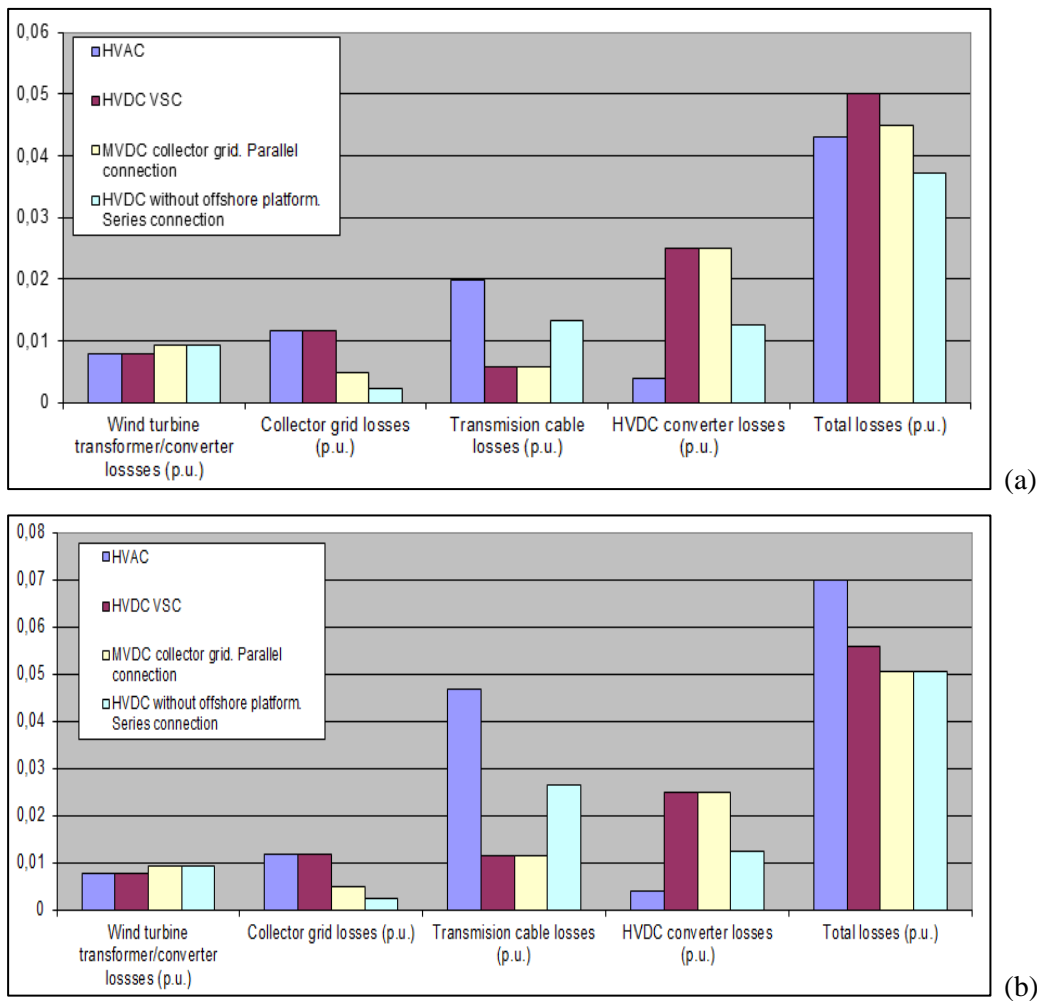
Figure B.4. Losses break down in p.u. of different transmission technologies for a 495 MW offshore wind farm : (a) 50 km; (b) 100 km.

B.1 Input data for cost estimations

The wind farms analyzed in the previous section are constituted by 110 4.5 MW wind turbines. The separation between wind turbines has been fixed to 7 times the turbine diameter. Turbines are clustered forming groups of up to 10 units.

Most of the input data necessary for cost estimations have been obtained from the costs models presented in [B.1]. These models have been taken as a reference in latter research activities [B.2]-[B.4] and some of the data have also been supported by ABB. Therefore they are considered reliable. The cost models introduced in [B.1] are given in SEK. They have been converted into €for comparison purposes. A conversion rate of 0.12€SEK has been considered.

1. The AC cable cost model proposed in [B.1] is given by equation (B.1). This model considers that the cost of the AC cables increases exponentially with the rated power.

$$C_{AC} = A_p + B_p e^{\left(\frac{C_p S_n}{10^8}\right)} \quad \text{(B.1)}$$

where C_{AC} is the cost of the AC cable in SEK/km, S_n is the AC cable rated power in VA and A_p, B_p and C_p are the model constants given in table B.1 for different rated voltages.

PROJECT NO.
502000064

REPORT NO.
TR A7482

VERSION
1.0

126 of 133

Table B.1. Model constants for AC cable estimation costs.

Rated voltage (kV)	A_p [10^6]	B_p [10^6]	C_p
22	0.284	0.583	6.15
33	0.411	0.596	4.1
45	0.516	0.612	3
66	0.688	0.625	2.05
132	1.971	0.209	1.66
220	3.181	0.11	1.16

2. The DC cable cost model proposed in [B.1] is given by equation (B.2). In this case the cost of the cables increases linearly with the rated power.

$$C_{DC} = A_p + B_p P_n \qquad (B.2)$$

where C_{DC} is the cost of the DC cable in SEK/km, P_n is the DC cable rated power in W and A_p and B_p are the model constants given in table B.2 for different rated voltages.

Table B.2. Model constants for DC cable estimation costs.

Rated voltage (kV)	A_p [10^6]	B_p
5	- 0.346	0.408
40	-0.314	0.0618
160	-0.1	0.0164
230	0.079	0.012
300	0.286	0.00969

3. An installation cost of 100 000 €/km has been considered for a three-phase AC cable according to [B.4]. For DC cables the estimated installation cost is 200 000 €/km. This estimation has been made under the assumption that it is necessary to install two independent cables for a bipolar system and only one cable can be installed each time.

4. The data given in [B.4] has been considered for the transformer cost estimation since it suits better the power range of the proposed case study than the data presented in [B.1]. The cost of the transformer is given by equation (B.3).

$$C_{Trans} = 0.03327 S_n^{0.7513} \qquad (B.3)$$

where C_{Trans} is the cost of the transformer in M€ and S_n is the rated power of the transformer in MVA.

PROJECT NO.
502000064

REPORT NO.
TR A7482

VERSION
1.0

127 of 133

5. The cost of the reactive compensating inductors is considered to be 2/3 of the cost of a similar rated transformer in accordance with data given in [B.1] and [B.4].

6. Two different models to estimate the cost of the switchgear depending on the switchgear location are proposed in [B.1]. Both models assume a linear increase of the cost of the switchgear with the rated voltage.

   For the switchgears located in the offshore platform the costs are given by equation (B.4).

$$C_{\text{SG\_OS}} = 320 \cdot 10^3 + 6V_n \qquad \text{(B.4)}$$

where C_{SG_OS} is the cost in SEK of the switchgear placed in the offshore substation and V_n is the switchgear rated voltage in V.

   For the switchgears used in the offshore wind turbine the cost model is given by equation (B.5).

$$C_{\text{SG\_OWT}} = 100.33 \cdot 10^3 + 2.8726V_n \quad \text{(B.5)}$$

where C_{SG_OWT} is the cost in SEK of the switchgear used inside the wind turbines and V_n is the switchgear rated voltage in V.

7. An estimated cost of 0.11€/VA has been assumed for all the converters involved on the transmission architectures regardless the rated power and the topology used. This cost seems to be in accordance with [B.1], [B.4] and supported by ABB in a technical report [B.5].

8. Finally, (B.6) gives the cost model estimated for the structure of the offshore platform according to [B.1].

$$C_{\text{OP}} = 20 \cdot 10^6 + 0.7P_n \qquad \text{(B.6)}$$

where C_{OP} is the cost in SEK of the offshore platform structure and P_n is the rated power of the offshore wind farm connected to the offshore platform in W.

B.2 Methodology to estimate the electrical losses

To assess the losses of the transmission architectures, individual losses of each component has to be estimated. The total losses can be calculated using expression (B.7).

$$P_{\text{L}} = P_{L\_CS} + P_{L\_OS} + P_{L\_TS} + P_{L\_S} \qquad \text{(B.7)}$$

Where P_L are the total power losses of the transmission architecture, P_{L_CS} are the power losses of the collector system, P_{L_OS} are the power losses of the transformer and/or the converter inside the offshore substation, P_{L_TS} are the power losses of the transmission system and P_{L_S} are the power losses of the onshore substation in case it is required.

The power losses P_L depend on the instantaneous power that the offshore wind farm is producing at any instant. Therefore, to calculate the total energy loss over a year, it is necessary to estimate the power distribution of the wind farm. In order to assess the power distribution it is necessary to know the power curve of the wind turbines, usually disclosed by the manufacturers in their turbine datasheets, and the wind conditions of a given site.

It is widely accepted that, in the absence of specific wind measurements, the wind conditions of an offshore site can be well described by the Rayleigh probability density function. This function allows estimating the number of hours per year that the wind is blowing under a certain speed value when the average wind speed of the site is the only parameter known. For the case study analyzed in this section a site with an average wind speed of 7.5 m/s has been considered.

PROJECT NO.
502000064

REPORT NO.
TR A7482

VERSION
1.0

128 of 133

In order to estimate the power distribution of a wind farm over a year, the wind speed operating range of the turbines can be discretized in small wind speed intervals. Then, using the Rayleigh probability density function, it is possible to estimate the number of hours per year the wind speed is going to be within the specific interval limits. Finally using the power curve of the turbine, the output power of the turbine for each specific interval can be calculated.

In the proposed case study the cut-in and cut-out speeds of the wind turbines are 2.5 m/s and 25 m/s respectively and the pitch control limits the wind turbine output power to 4.5 MW once the wind speed is above 12 m/s. The wind speed operating range has been discretized into eleven speed intervals of 1m/s each. Under these assumptions the power distribution of one wind turbine is shown in table B.3.

Data presented in table B.3 allows estimating the wind farm energy produced on a yearly basis assuming an availability of 100%. The energy produced yearly E is given by expression (B.8).

$$E = N_t \sum_{i=1}^{11} P_i H_i \qquad \text{(B.8)}$$

where N_t is the number of turbines in the wind farm, P_i is the output power of one turbine when the wind speed is within the $[x_i, y_i]$ interval and H_i is the number of hours the wind speed is within the $[x_i, y_i]$ speed interval. i varies from 1 to 11 because, according to the data disclosed in table B.3, the wind speed operating range of the wind turbines has been discretized in eleven wind speed intervals.

Table B.3. Wind turbine power distribution over a year.

Wind speed intervals (m/s)	Wind turbine output power P_i (kW)	H_i/H_{year} (*)
[2.5, 3.5]	54.8	0.079
[3.5, 4.5]	175	0.0948
[4.5, 5.5]	382.6	0.1034
[5.5, 6.5]	710.3	0.1051
[6.5, 7.5]	1171.6	0.1008
[7.5, 8.5]	1779.6	0.0918
[8.5, 9.5]	2535.9	0.0799
[9.5, 10.5]	3470.2	0.0666
[10.5, 11.5]	4251.7	0.0533
[11.5, 12.5]	4500	0.0411
[12.5, 25]	4500	0.0937

(*) H_i is the number of hours per year the wind speed is within the specific interval limits; H_{year} is the total number of hours in a year.

Data presented in table B.3 also allows calculating the total energy losses over a year. The power losses P_{Li} of the transmission architecture can be estimated according to (B.7) for each wind speed interval. Then the energy losses E_L can be calculated according to (B.9).

$$E_L = N_t \sum_{i=1}^{11} P_{Li} H_i \qquad \text{(B.9)}$$

The ratio E_L/E gives the estimation of the total energy losses in per unit shown in Fig. B.4.

PROJECT NO.
502000064

REPORT NO.
TR A7482

VERSION
1.0

129 of 133

According to (B.9) and (B.7) assessing the energy losses requires to calculate the power losses of the components forming the transmission system. That is, it is necessary to calculate the collector and transmission system losses and the losses in the transformers and power electronics. The formulation and data used to calculate these losses are described below.

B.2.1 Losses in the collector system

The losses in the collector system can be determined according to (B.10).

$$P_{L\_CS} = N_C l_1 \frac{P_{out}^2}{P_N^2} P_l \sum_{j=1}^{N} j^2 + N_C l_2 N^2 \frac{P_{out}^2}{P_N^2} P_l \qquad \text{(B.10)}$$

where N_c is the number of clusters of the collector system, l_1 is the distance between wind turbines, P_{out} is the output power of a wind turbine, P_N is the nominal power of the cable, P_l are the power losses of the cable at full load, N is the number of turbines in each cluster and l_2 is the average distance from the last wind turbine in the cluster to the offshore substation.

In the case study analyzed here, the wind farm is composed by eleven (N_C=11) clusters of ten (N=10) turbines each and the distance between turbines has been fixed to seven times the turbine diameter. In those transmission architectures with an AC collector system, a three-phase AC copper cable with a conductor area of 800 mm^2 and a rated voltage of 33 kV has been selected for inter-turbine connections. According to the manufacturer information [B.6], the rated power of the cable is P_N=47.9 MVA and the cable losses at full load are P_l=107.1 W/m. The resistance dependence with the internal conductor temperature has not been considered in the current study.

In case of a DC collector system no information about the cable losses at full load has been found. Therefore the DC resistance has been estimated according to (B.11).

$$R_{DC\_20} = \rho_{Cu} \frac{1}{S_{cond}} \text{ ohm/km} \qquad \text{(B.11)}$$

where R_{DC_20} is the DC resistance at 20 ℃, ρ_{Cu} is the cooper resistivity at 20 ℃ and S_{cond} is the conductor section. The dependence of DC the resistance with the conductor temperature t for a copper cable can be estimated according to (B.12).

$$R_{DC\_t} = R_{DC\_20}[1 + 0.00393(t - 20)] \qquad \text{(B.12)}$$

Finally, the cable losses at full load are given in (B.13).

$$P_l = i_{rated}^2 R_{DC\_90} \qquad \text{(B.13)}$$

where i_{rated} is the rated current of the DC cable and R_{DC_90} is the DC resistance when the cable is carrying its rated current (typically the operating temperature of a XLPE cable at its rated current is 90 ℃).

B.2.2 Losses in the transmission system

The losses in DC transmission systems can be calculated using expression (B.13).

However for the HVAC transmission architecture the calculation of the transmission losses is a more complicated procedure. This is mainly because the current and voltage profile inside the cable are not constant due to the parasitic inductance and capacitance of the cable. This makes complicated the analytical calculation of the transmission losses. To perform this calculation a digital simulator with a distributed transmission line model has been used. The input data necessary for this model are the inductance, the capacitance, the AC resistance and the dielectric loss resistance per unit of length and the length of the cable. The first two parameters are usually disclosed in the AC cable datasheets [B.7]. The dielectric resistance R_D can be estimated according to (B.14).

PROJECT NO.
502000064

REPORT NO.
TR A7482

VERSION
1.0

130 of 133

$$R_D = \frac{1}{\omega C \tan\delta} \text{ ohm/km} \qquad (B.14)$$

where ω is the angular frequency of the AC voltage, C is the capacitance per unit of length of the cable and $\tan \delta$ is the dielectric power loss factor.

The AC resistance of the cable is comprised of the following contributions:

- Ohmic conductor resistance
- Losses due to skin and proximity effects in the conductor
- Losses in the metallic sheath and armour (especially important where the cables are ground bounded at both ends)

The contribution of the first two terms to the total AC resistance of the cable can be calculated using expression (B.15).

$$R_{cond\_ac} = R_{DC\_t}(1 + y_s + y_p) \text{ ohm/km} \qquad (B.15)$$

where R_{cond_ac} is the AC conductor resistance per unit of length, R_{DC_t} is the conductor DC resistance at temperature t calculated by means of (B.12), y_s is the skin effect contribution to the AC losses and y_p is proximity effect contribution to the AC losses considering a three-core cable. According to [B.7]-[B10] these contributions can be determined using the following expressions:

$$y_s = \frac{X_S^4}{192 + 0.8X_S^4} \qquad (B.16)$$

$$X_S^2 = \frac{8\pi f K_S 10^{-7}}{R_{DC\_90}} \qquad (B.17)$$

$$y_p = y_p'[0.312\left(\frac{d_{cond}}{s}\right)^2 + \frac{1.18}{y_p' + 0.27}] \qquad (B.18)$$

$$y_p' = \frac{X_p^4}{192 + 0.8X_p^4} \qquad (B.19)$$

$$X_p^2 = \frac{8\pi f K_p 10^{-7}}{R_{DC\_90}} \qquad (B.20)$$

$$s = \frac{70}{196} d_{cab} \qquad (B.21)$$

where f is the AC voltage frequency, K_s and K_p are constants for cable types that can be estimated according to IEC287 [B.8], R_{DC_90} is the DC conductor resistance at 90 ºC, s is the distance between conductor centres in a cable, d_{cond} is the conductor diameter and d_{cab} is the cable outer diameter.

In order to assess the total AC resistance per unit of length, the sheath and armour contributions should be considered. The total AC resistance R_{ac} can be calculated using (B.22).

$$R_{ac} = R_{cond\_ac}(1 + \lambda_1' + \lambda_2') \qquad (B.22)$$

where λ_1' and λ_2' accounts for the sheath and armour contributions to the total losses. According to [B.7]-[B.10], this contribution can be calculated using (B.23)-(B.34)

$$\lambda_1' = 1.7 \frac{R_{she\_90}}{R_{cond\_ac\_90}} \frac{1}{1 + \left(\frac{R_{she\_90}}{X_{she}}\right)^2} \qquad (B.23)$$

$$R_{she\_90} = R_{she_{20}}(1 + \alpha_{she}70) \qquad (B.24)$$

$$R_{she\_20} = \rho_{she} \frac{1}{S_{she}} \qquad (B.25)$$

$$S_{she} = \pi d_{she} e_{she} \qquad (B.26)$$

$$d_{she} = d_{over} + \frac{e_{she}}{2} \qquad (B.27)$$

PROJECT NO.
502000064

REPORT NO.
TR A7482

VERSION
1.0

131 of 133

$$X_{she} = 4\pi f \ln\left(\frac{2S}{d_{she}}\right) \tag{B.28}$$

$$\lambda_2' = \lambda_2(1 - \lambda_1') \tag{B.29}$$

$$\lambda_2 = 1.23 \frac{R_{arm\_90}}{R_{cond\_ac\_90}} \left(\frac{2c}{d_{arm}}\right)^2 \frac{1}{1 + \left(\frac{2.77\,10^6 R_{arm\_90}}{\omega}\right)^2} \tag{B.30}$$

$$R_{arm\_90} = R_{arm\_20}(1 + \alpha_{arm}70) \tag{B.31}$$

$$R_{arm\_20} = \rho_{arm}\frac{1}{S_{arm}} \tag{B.32}$$

$$d_{arm} = \frac{183.5}{196}d_{cab} \tag{B.33}$$

$$S_{arm} = \frac{2087}{196}d_{cab} \tag{B.34}$$

where R_{she_90} and R_{she_20} are the sheath resistance per length unit at 90 ºC and 20 ºC respectively, $R_{cond\_ac\_90}$ is the AC conductor resistance per length unit at 90 ºC, X_{she} is the sheath reactance, α_{she} is the sheath coefficient of resistance variation with the temperature, ρ_{she} is the sheath resistivity, S_{she} is the sheath cross section, d_{she} is the average sheath diameter, e_{she} is the sheath thickness, d_{over} is the diameter over insulation, R_{arm_90} and R_{arm_20} are the armour resistance per length unit at 90 ºC and 20 ºC respectively, c is the distance between the conductor and the cable centre, d_{arm} is the average armour diameter, α_{arm} is the armour coefficient of resistance variation with the temperature, ρ_{arm} is the armour resistivity, S_{arm} is the armour cross section and d_{cab} is the cable outer diameter.

B.2.3 Losses in the offshore and offshore substation.

The main foci of losses in the substations are the converters and transformers. The converter losses depend basically on the converter topology, power factor, modulation index and operating power. In order to get an accurate estimation of the converter losses it is necessary to make detailed converter models in a simulation platform. It is difficult to estimate the losses analytically. However, for a fast engineering estimation, supposing modular multilevel converters are used, the converter losses are considered to be near 1%.

The losses in the transformers P_{l_trans} can be estimated according to (B.35).

$$P_{l\_trans} = P_{nl\_trans} + P_{l\_trans}\frac{P^2}{P_{rated}^2} \tag{B.35}$$

Where P_{nl_trans} are the transformer core losses, P_{l_trans} are the copper losses, P_{rated} is the transformer rated power and P in the input power. Reference values for the core and copper losses in 50 Hz transformers are usually disclosed in the technical datasheets. However it is not easy to find information for high frequency transformers with the rated power required for these applications. Valuable reference information to estimate losses for high and low frequency transformers is disclosed in [B.11].

B.3 Bibliography

[B.1] S. Lundberg, "Performance comparison of wind park configurations," *Dept. Electric Power Engineering, Chalmers University of Technology, Tech. Rep.*, 2003.

[B.2] P. Bresesti, W. L. Kling, R. L. Hendriks, and R. Vailati, \HVDC connection of offshore wind farms to the transmission system," *IEEE Transactions on Energy Conversion*, vol. 22, no. 1, pp. 37-43, 2007.

PROJECT NO.
502000064

REPORT NO.
TR A7482

VERSION
1.0

132 of 133

[B.3] T. Ackermann, N. Barberis Negra, J. Todorovic, and L. Lazaridis, "Evaluation of electrical transmission concepts for large o_shore wind farms," *Copenhagen Offshore Wind*, October 2005.

[B.4] L.P. Lazaridis, "Economic Comparison of HVAC and HVDC Solutions for Large Offshore Wind Farms under Special Consideration of Reliability," Masther's thesis, Department of Electrical Engineering, KTH, 2005.

[B.5] ABB, "Middletown – Norwalk Transmission Project – Technical Description of VSC HVDC Converter and Cable Technology," Prepared for Northeast Utilities, ABB Power Technologies AB, Ludvika, Sweden, October 2004

[B.6] ABB, "Submarine cables for inter-turbine connections," ABB technical sheet.

[B.7] A. Madariaga, "Methodology to Evaluate Offshore Wind Power Plant Electric Topologies,"Phd. Thesis, Electrical Engineering Department, UPV/EHU, Nov. 2012.

[B.8] UNE 21144 Electric cables - Calculation of the current rating (corresponds to IEC 287), Std.

[B.9] UNE-EN 60228 Conductors of insulated cables (corresponds to IEC 60228), Std.

[B.10] UNE 211435 Guidance on the selection of distribution cables for rated voltages up to and including 0,6/1kV, Std.

[B.11] S. Meier, P. C. Kjaer, "Benchmark of Annual Energy Production for Different Wind Farm Topologies," *36th Annual Power Electronics Specialists Conference, PESC'2005*, Recfe, Brazil, June 2005.